The Dissertation Committee for Eduardo Gildin
certifies that this is the approved version of the following dissertation:

Model and Controller Reduction of Large-Scale Structures Based on Projection Methods

Committee:

Robert H. Bishop, Supervisor

David G. Hull

Maruthi R. Akella

Raul G. Longoria

Athanasios C. Antoulas

Model and Controller Reduction of Large-Scale Structures Based on Projection Methods

by

Eduardo Gildin, B.S.; M.S.

DISSERTATION

Presented to the Faculty of the Graduate School of

The University of Texas at Austin

in Partial Fulfillment

of the Requirements

for the Degree of

DOCTOR OF PHILOSOPHY

THE UNIVERSITY OF TEXAS AT AUSTIN

August 2006

To my family

Acknowledgments

Many people have participated in this great endeavor. First, and foremost, I would like to acknowledge my advisor, Dr. Robert H. Bishop, for his invaluable support, advice and patience in all stages of this work. I would like to thank him for giving me the opportunity and freedom of teaching several classes in the Aerospace Engineering and Engineering Mechanics Department at UT and for allowing me to help in the development of the Controls Lab and its introduction to the undergraduate curriculum. I have learned a lot as the course's first instructor!

Furthermore, I would like to thank Dr. Bishop for introducing me to Dr. Antoulas from Rice University. This dissertation would not be possible without him. I would like to thank Dr. Antoulas for proposing this dissertation's topic and for introducing me to the area of model reduction. Dr. Antoulas has guided me throughout the entire research and has been a "second advisor" in this journey. All the trips to Houston, mainly in the last semester, when I attended his class at Rice, have proven to be all worth it.

I would like to thank Dr. Hull for being part of my dissertation's committee and for believing that I could do a good job teaching the Flight Dynamics Lab. I would like to thank Dr. Akella and Dr. Longoria for being part of my committee and for being such good teachers in their classes.

I would like to thank Dr. Sorensen at the CAAM Department at Rice University for his time spent teaching me concepts in Numerical Linear Algebra and for accepting me as part of his research project.

I am indebted to my family, especially to my parents, Jacob and Raquel, for their support, love, positive thinking and all the great values that they have shown to be worth it. My sister and brother, Fernanda and Andre, together with their respective spouses have also a special place in this dissertation with their endless questions about my graduation date.

The gratitude that I hold to my in-laws is incalculable. I thank them for all the support and patience and for always believing that we could make it through the difficult stages. Their constant trips to Austin have helped me to take a little break from the hard work.

I would like to thank all my former students who have shown my teaching's strengths and weaknesses through the course-instructor surveys. Their evaluation helped me improve my teaching skills. I wish to express my gratitude to the staff and my colleagues of the ASE-EM Department for all the help and advice during those years.

Finally, the hardest part of this dissertation has arrived. I could write another two hundred pages simply to acknowledge my wife Suzana on how much I appreciate her love, support and patience with all those years of unknown future. I thank her for the support of the countless hours spent working on this dissertation that could have been happily spent with my family. Her

decision to not let me give up has helped me through the difficult moments, but also has shown how important it is to achieve our goals. She has given me an incredible family. Though my three year old son Daniel has not participated directly in this dissertation, his smile during this time will always be in my memory.

Model and Controller Reduction of Large-Scale Structures Based on Projection Methods

Publication No. ______________

Eduardo Gildin, Ph.D.
The University of Texas at Austin, 2006

Supervisor: Robert H. Bishop

The design of low-order controllers for high-order plants is a challenging problem theoretically as well as from a computational point of view. Frequently, robust controller design techniques result in high-order controllers. It is then interesting to achieve reduced-order models and controllers while maintaining robustness properties. Controller designed for large structures based on models obtained by finite element techniques yield large state-space dimensions. In this case, problems related to storage, accuracy and computational speed may arise. Thus, model reduction methods capable of addressing controller reduction problems are of primary importance to allow the practical applicability of advanced controller design methods for high-order systems.

A challenging large-scale control problem that has emerged recently is the protection of civil structures, such as high-rise buildings and long-span bridges, from dynamic loadings such as earthquakes, high wind, heavy traffic,

and deliberate attacks. Even though significant effort has been spent in the application of control theory to the design of civil structures in order increase their safety and reliability, several challenging issues are open problems for real-time implementation.

This dissertation addresses with the development of methodologies for controller reduction for real-time implementation in seismic protection of civil structures using projection methods. Three classes of schemes are analyzed for model and controller reduction: nodal truncation, singular value decomposition methods and Krylov-based methods. A family of benchmark problems for structural control are used as a framework for a comparative study of model and controller reduction techniques. It is shown that classical model and controller reduction techniques, such as balanced truncation, modal truncation and moment matching by Krylov techniques, yield reduced-order controllers that do not guarantee stability of the closed-loop system, that is, the reduced-order controller implemented with the full-order plant.

A controller reduction approach is proposed such that to guarantee closed-loop stability. It is based on the concept of dissipativity (or positivity) of linear dynamical systems. Utilizing passivity preserving model reduction together with dissipative-LQG controllers, effective low-order optimal controllers are obtained. Results are shown through simulations.

Table of Contents

List of Tables

List of Figures

Chapter 1

Introduction

1.1 Approaches to Model Reduction

The design of low-order controllers for high-order plants is a challenging problem, both theoretically as well as from a computational point of view. Designs for control of large structures are often based on mathematical models constructed by finite element techniques together with experimental data, and so frequently, they yield large state-space dimensions (on the order of tens of thousands to millions) upon discretization. Advanced controller design methods such as LQG/LTR loop-shaping, H_2/H_∞ control design, μ-synthesis and linear matrix inequalities (LMIs) typically produce controllers with orders comparable to the order of the plant. Highly accurate models desired for feedback control often lead to high-order controllers. These high-order controllers are not practical for real-time applications. It is an important problem to consider how to achieve reduced-order models and controllers while maintaining the desired performance during real-time implementation.

Applying classical design methodologies to complex systems relies on the *ad hoc* design process of introducing controllers in various locations, as the performance with the control system is assessed. This process necessarily relies on the level of experience and capability of the designer, sometimes leading to good results but often not. The complexities of the system may be inadvertently overlooked. As a result, a more difficult control design problem (from a mathematical and computational point of view) is to consider a structured and theoretically-based modern control design methodology which addresses problems related to storage, accuracy, and computational speed [8]. In general, however, the order of these modern controllers tends to be too high for practical use. For many reasons, simple controllers are preferred over complex ones [86]. Thus, model reduction methods capable of addressing controller reduction problems are of primary importance to allow the practical applicability of modern controller design methods for high-order systems. As sensor networks and embedded processors proliferate our environment, technologies for such approximations and real-time control emerge as a major technical challenge [5].

A challenging large-scale control problem that has emerged recently is the protection of civil structures, such as high-rise buildings and long-span bridges, from dynamic loadings such as earthquakes, high wind, heavy traffic, and deliberate attacks. Even though significant effort has been expended on the application of control theory to the design of civil structures (see [100], [20]) in order to increase safety and reliability, several challenging issues are yet to be successfully addressed for real-time implementation. The control of civil structures using passive, active or semi-active techniques has reached the stage of full-scale implementations [19]. More than fifty installations in building structures and bridges have been subjected to actual wind forces and earthquake inputs [19]. However, with the increasing complexity of the available finite element models, model reduction has to be performed to reduce the problem to a feasible number of degrees of freedom (DOF) so that design and simulation of the control system can be accomplished in a reasonable time and so that practical low-order controllers can be applied to real-time implementations.

Model and controller reduction for large-scale structures have not yet been addressed in the building control literature. Usually, the low-order structural models for building control are obtained by standard model reduction techniques, such as modal reduction, balanced truncation and static condensation [24]. However, those techniques do not address the issue of controller design in a closed-loop framework, where destabilizing reduced-order controllers are often obtained. In such cases, by means of trial-and-error, stabilizing reduced-order controllers may be achieved. Thus, model and controller design techniques that guarantee stabilizing reduced-order controllers when they are implemented on the actual structure become important factors for the success of building control.

The model and controller reduction methods can be divided into two different classes [2]: *Direct* and *Indirect*. Figure 1.1 shows the direct method design from a high-order plant to a low-order controller. With direct methods, the parameters defining a low-order controller are computed by employing an optimization technique. With indirect methods, two design pathways are possible. A high-order controller can first be designed, and then a procedure can be used to reduce the controller complexity. In Figure 1.1, this pathway is illustrated in the upper right. Following a different procedure, a reduced-order plant can be found prior to the controller design, and then a reduced-order controller is designed for the reduced-order plant. In Figure 1.1, this pathway is illustrated in the lower left. There are many issues that arise with the indirect approach. In the overall design process, the plant model approximation is carried out at an early step of the design process, without the benefit of pertinent information about the low-order controller. As discussed in [33, 34], a good approximation of the plant requires knowledge of the controller. It is important to understand that the problem of controller reduction (closed-loop) is distinct from the problem of model reduction (open-loop), since it is after all, closed-loop performance that should be approximated. Recently, Antoulas, *et al.* [8, 50] proposed a method for incorporating closed-loop system information into the plant and controller reduction process for large-scale systems, using rational interpolation through the poles of the large-scale closed-loop system and the large-scale controller.

Most computational methods currently employed for controller reduction [125] cannot effectively handle very large-scale problems that exhibit some sparsity. They frequently involve the solution of Riccati equations and linear matrix inequalities (LMI) in the controller reduction process. It is known that current methods exhibit computational cost associated with the algorithms on the order $\mathcal{O}(n^3) - \mathcal{O}(n^6)$ operations, where n is the number of states, thus

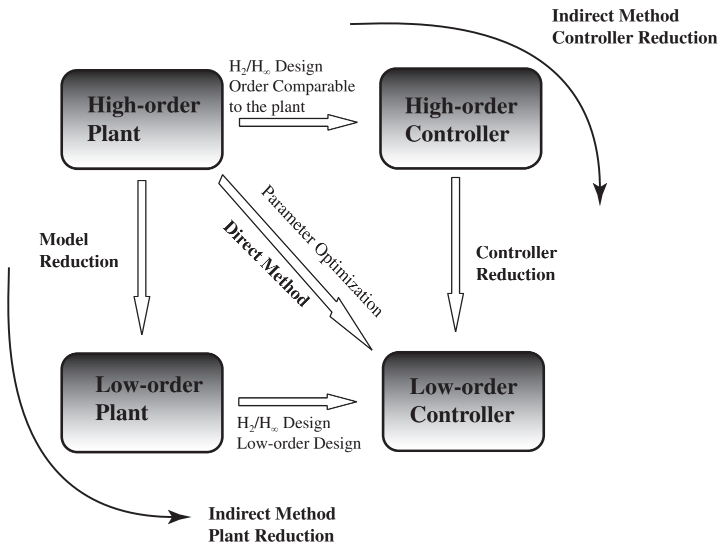

Figure 1.1: Direct and Indirect Approaches for Controller Reduction (Adapted from [2]).

becoming impractical for large-scale applications [8, 41, 90]. A systematic way for reducing the order of large-scale controllers using a reasonable amount of computational effort and storage, that is, involving efficient algorithms, would yield controllers feasible for real-time implementations.

1.2 Control of Structures: Building Control Problem

Recent devastating events around the world have raised awareness of the importance of understanding the way in which civil engineering structures respond during dynamic events. One of the main challenges in structural engineering is to develop innovative design concepts to better protect civil structures from earthquakes, strong winds and direct attacks. With the improvements in construction techniques, an increase in height for civil structures has been seen in practice. This brings up very interesting problems related to the comfort sensations of its occupants due to high accelerations and displacements and structural safety due to external disturbances.

Buildings and other physical structures have traditionally relied on their strength and the use of passive devices, such as base isolation schemes, to dissipate energy under severe dynamic loading [100]. However, in recent years, the field of active (or semi-active) control of civil structures has emerged as a way to enhance the capability of dealing with natural and man-made hazards [101].

The first full-scale application of active control to a building was accomplished by the Kajima Corporation in 1989 [100]. The Kyobashi Seiwa building, as shown in Fig. 1.2, is an eleven-story building in Tokyo, Japan, having two Active-Mass Dampers (AMDs) for controlling the structure. The primary AMD is employed to control transverse motion, while a smaller secondary AMD is employed to reduce torsional motion. Since 1989, several advances have been made in the application of feedback control for civil structures. Research has been conducted in the application of control strategies for linear and nonlinear building models [29, 32, 65]. Jansen ([65] and references therein) analyzed the use of LQG/H_2 control for the active control of buildings, as well as Lyapunov-based schemes, bang-bang, and clipped-optimal control strategies for semi-active control of buildings. Also, the possibility of using a combination of passive and active control strategies, the so-called hybrid con-

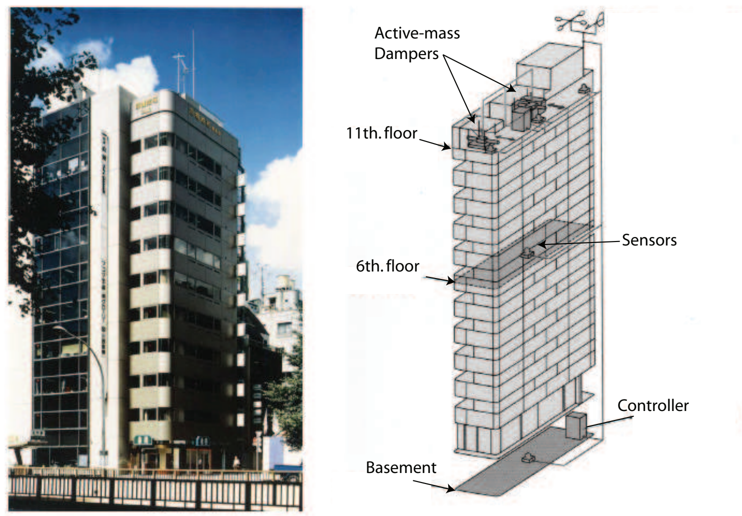

Figure 1.2: Kyobashi Seiwa Building with AMD Installation [100].

trol, has been successfully investigated. To date, there have been over forty buildings and ten bridges that have employed feedback control strategies in full-scale implementation [19, 101]. Most of these full-scale systems have been subjected to actual wind forces and ground motions. Significant improvements in the response of the structures to external disturbances has been observed together with model and controller validations [19].

One of the disadvantages of the active and hybrid control strategies is that they depend on external power, which may not be available during seismic events when the main power to the structure may fail. Also, they rely on hydraulic actuators, which require large amount of power to function. Semi-active control strategies on the other hand, such as variable-orifice dampers, variable friction dampers and controllable fluid dampers are particularly promising in addressing many of these issues. They combine the best features of both passive and active control systems and offer the greatest reliability for civil protection. This is due to the fact that they can operate on battery power, and at the same time guarantee to stabilize the structure since they do not add energy to the system. The Kajima Technical Research Institute, as shown in Fig. 1.3, was the first full-scale building structure to be implemented with semi-active control devices in 1990 [101]. As seen in Fig. 1.3, semi-active hydraulic dampers are installed inside the walls on both sides of the building to enable it to be used as a disaster relief base in post-earthquake situations.

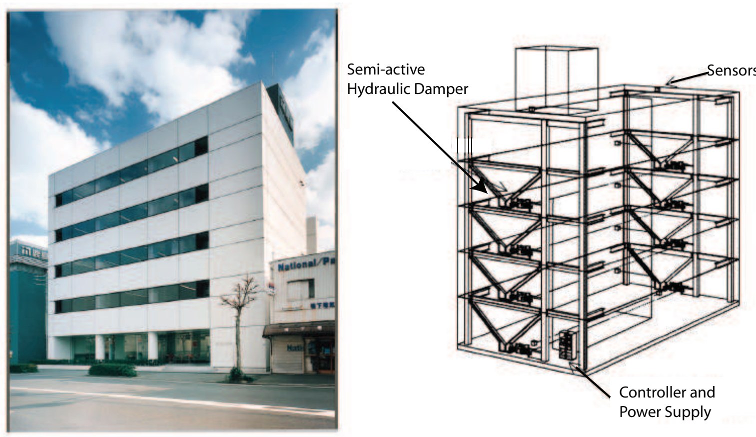

Figure 1.3: Semi-active hydraulic dampers installed in the Kajima Shizuoka Building [100].

Although several full-scale implementations have been accomplished, there is a general lack of research on the application of model and controller reduction for building control. Indeed, the most challenging aspect of active control research in civil engineering is the fact that it involves large-scale models (often above one million degrees-of-freedom), and it comprises the knowledge of diverse disciplines, such as computer science, systems and control theory, structural dynamics, materials science and earthquake engineering.

1.3 Problem Overview and Dissertation Goals

This dissertation addresses the development of efficient algorithms for reducing the order of large-scale building models and/or feedback controllers in a closed-loop framework for real-time implementation. The aim is to achieve reduced-order controllers that are guaranteed to stabilize the closed-loop system when implemented in a closed-loop framework using the original building structure as the large-scale plant.

To this end, one considers the feedback control loop as depicted in Fig. 1.4. Given a large-scale dynamical system or plant, $\mathbf{G}(s)$, with state-space representation

$$\mathbf{\Sigma} : \left\{ \begin{array}{l} \dot{\mathbf{x}}(t) = \mathbf{A}\mathbf{x}(t) + \mathbf{B}\mathbf{u}(t) \\ \mathbf{y}(t) = \mathbf{C}\mathbf{x}(t) + \mathbf{D}\mathbf{u}(t) \end{array} \right. \Leftrightarrow \mathbf{\Sigma} = \left[\begin{array}{c|c} \mathbf{A} & \mathbf{B} \\ \hline \mathbf{C} & \mathbf{D} \end{array} \right] \in \mathbb{R}^{(n+p)\times(n+m)}, \tag{1.1}$$

and a stabilizing high-order controller $\mathbf{K}(s)$, with closed-loop performance index defined as $\mathcal{J}\left(\mathbf{G}(s), \mathbf{K}(s)\right)$, one seeks a low-order controller $\mathbf{K}_r(s)$, with $r \ll n$, such that $\left(\mathbf{G}(s), \mathbf{K}_r(s)\right)$ is a stable closed-loop system and $\mathcal{J}\left(\mathbf{G}(s), \mathbf{K}(s)\right) \approx \mathcal{J}\left(\mathbf{G}(s), \mathbf{K}_r(s)\right)$.

The unifying feature of all model and controller reduction techniques presented here is that they are obtained by means of a *projection*. The defini-

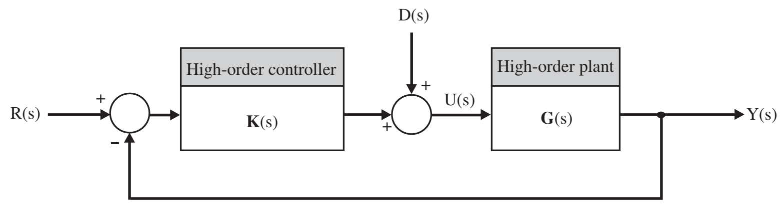

Figure 1.4: Feedback configuration.

tion of a projector is given in Chapter 2. The idea is to construct the projector $\mathbf{\Pi} = \mathbf{V}\mathbf{W}^{\mathbf{T}}$ where $\mathbf{V}, \mathbf{W}^T \in \mathbb{R}^{n\times r}$ with $\mathbf{W}^{\mathbf{T}}\mathbf{V} = \mathbf{I_r}$, where $\mathbf{I}_r$ is the identity matrix of size r, such that the reduced-order model can be obtained as

$$\dot{\mathbf{x}}_{\mathbf{r}}(t) = \underbrace{\mathbf{W}^{\mathbf{T}}\mathbf{A}\mathbf{V}}_{:=\mathbf{A_r}}\mathbf{x_r}(t) + \underbrace{\mathbf{W}^{\mathbf{T}}\mathbf{B}}_{:=\mathbf{B_r}}\mathbf{u}(t) \quad \mathbf{y_r}(t) = \underbrace{\mathbf{C}\mathbf{V}}_{:=\mathbf{C_r}}\mathbf{x_r}(t) + \underbrace{\mathbf{D}}_{:=\mathbf{D_r}}\mathbf{u}(t), \qquad (1.2)$$

where $\mathbf{A}_r \in \mathbb{R}^{r\times r}$, $\mathbf{B}_r \in \mathbb{R}^{r\times m}$, $\mathbf{C}_r \in \mathbb{R}^{p\times r}$ and $\mathbf{D}_r \in \mathbb{R}^{p\times m}$. This process applies to the controller and to the closed-loop system as well.

Also, for an efficient reduction algorithm, one has to guarantee that:

i. the dimension of the reduced-order model is $r \ll n$;

ii. the behavior of the reduced-order model approximates the original with certain accuracy, i.e., there is a small error bound on $\|\mathbf{y}(t)-\mathbf{y_r}(t)\|_{\mathcal{H}_2,\mathcal{H}_\infty}$; and

iii. the model reduction procedure is computationally stable and efficient.

In the next chapters, several model and controller reduction techniques will be presented in a projection framework. They are classified according to the scheme used to approximate its model.

1.3.1 Model Reduction Schemes

In a projection framework one can distinguish three families of model reduction techniques([8]): (1) nodal truncation; (2) singular value decomposition (SVD)-based methods; and (3) Krylov-based or moment matching methods. Roughly speaking, nodal truncation, such as Guyan reduction, is based on a rather rough approximation, where nodes, originating from finite element methods, are truncated according to their static or dynamic influence directly on the mass and stiffness matrices of the structure [93]. Nodal truncation involves almost no computational cost for small to medium systems, and often yields satisfactory solutions for systems that involve low frequency content. The SVD family, such as balanced truncation and its variants, relies on dense matrix factorizations for state-space truncation and preserves important theoretical properties of the original system, such as stability, together with a measure of the approximation error. However, they are not suited for large-scale systems [8]. Finally, the Krylov methods based on moment matching rely only on matrix vector multiplications, yielding numerically efficient algorithms for large-scale applications, but they lack good theoretical properties [8].

As will be seen in later chapters, the standard reduction approach used in the industry for structural dynamic problems is modal truncation. The justification is that higher modes generally have much less influence in the total response of the system. However, the computational cost of modal truncation becomes prohibitive for large-scale systems, due to the costly computation of associated eigensolutions.

1.3.2 Second-order Model Reduction

In structural dynamics analysis, the dynamic equations of equilibrium are generally represented as a set of linear second-order differential equations

$$\mathbf{M}\ddot{\mathbf{x}}(t) + \mathbf{D}_a\dot{\mathbf{x}}(t) + \mathbf{K}\mathbf{x}(t) = \mathbf{B}\mathbf{u}(t) \tag{1.3}$$

$$\mathbf{y}(t) = \mathbf{C}_0\mathbf{x}(t) + \mathbf{C}_1\dot{\mathbf{x}}(t) + \mathbf{D}\mathbf{u}(t) \tag{1.4}$$

with $\mathbf{M}, \mathbf{D}_a, \mathbf{K} \in \mathbb{R}^{n\times n}, \mathbf{B} \in \mathbb{R}^{n\times m}$, $\mathbf{C} = [\mathbf{C}_0 \quad \mathbf{C}_1] \in \mathbb{R}^{p\times 2n}$, and $\mathbf{D} \in \mathbb{R}^{p\times m}$. They are, respectively, the mass, damping, stiffness, input, output matrices, and feedforward term of the full-order model. Here, t is the time variable, $\mathbf{x}(t) \in \mathbb{R}^n$ is the state vector and n is the full degrees-of-freedom (DOFs), $\mathbf{u}(t) \in \mathbb{R}^m$ is the input excitation force vector, and $\mathbf{y}(t) \in \mathbb{R}^p$ is the output measurement vector. In general, finite element computer codes, such as NASTRAN [23], ANSYS [59], and SAP2000 [60], provide the model in a second-order framework.

One can take Eq. (1.3) and collapse to a first-order differential equation as in Eq. (1.1), and then obtain a reduced-order model as in Eq. (1.2). However, there is no guarantee that the resulting reduced-order model will have the same second-order structure as the original model. Because second-order models have important physical meaning (mass, spring and dampers), it is interesting to consider model reduction techniques that preserve the second-order structure of the original system [105, 114]. In this manner, one would like to obtain a reduced-order model as

$$\mathbf{M}_r\ddot{\mathbf{x}}_r(t) + \mathbf{D}_{a_r}\dot{\mathbf{x}}_r(t) + \mathbf{K}_r\mathbf{x}_r(t) = \mathbf{B}_{\mathbf{s}r}\mathbf{u}(t) \tag{1.5}$$

$$\mathbf{y}_r(t) = \mathbf{C}_{\mathbf{0}r}\mathbf{x}_r(t) + \mathbf{C}_{\mathbf{1}r}\dot{\mathbf{x}}_r(t) + \mathbf{D}_r\mathbf{u}(t) \tag{1.6}$$

with $\mathbf{M}_r, \mathbf{D}_{a_r}, \mathbf{K}_r \in \mathbb{R}^{r\times n}, \mathbf{B}_{\mathbf{s}r} \in \mathbb{R}^{r\times m}$, $\mathbf{C}_{0_r} \in \mathbb{R}^{p\times r}, \mathbf{C}_{1_r} \in \mathbb{R}^{p\times r}$, and $\mathbf{D}_r \in \mathbb{R}^{p\times m}$, with $r \ll n$. This will be called *structure preserving* model reduction throughout this dissertation.

1.4 Historical Overview

The development of the support theory relevant to this research proceeds along independent paths. The first path encompasses *large-scale approximation systems* represented by the eigenvalue problem and model order reduction methods. The second path incorporates *controller synthesis* and employs advanced control design methods, such H_2/H_∞ applied to controller reduction. The third path is that of *structural modeling and control* applied to building control.

In the literature on computational methods in linear algebra, much emphasis is placed on methods for solving standard linear algebra problems involving large sparse matrix operators [41, 97]. The non-symmetric Lanczos algorithm was originally proposed by Lanczos in 1950 [75] as an oblique projection method for computation of eigenvalues of symmetric and nonsymmetric matrices. The idea was to reduce the general matrix to a tridiagonal form from which the eigenvalues could be easily computed [11]. In the same manner, Arnoldi [10] proposed an orthogonal projection method as a means of reducing a dense matrix to the Hessenberg form to accurately approximate some eigenvalues of the original matrix. For an extensive treatment of the Lanczos Algorithm, the reader should refer to [55, 56]. In [90], a Linear Fractional Transformation (LFT) method was developed in order to obtain a tridiagonal realization of a model in terms of a number of “small” Lanczos algorithms.

The first mathematical connection between the Lanczos algorithm and model reduction was shown in [43]. It was shown that partial realizations could be generated through the Lanczos process. Villemagne and Skelton [117] have shown that adaptations to the Krylov subspaces could be performed in order to generate Padé approximations. Applications of the moment matching results were utilized in the structural dynamics field as a model reduction technique for flexible structures [112] and MIMO systems [73, 74]. However, as studied in [36], model reduction methods, such as partial realizations (i.e, expansion of the frequency response about $s = \infty$), and Padé approximation (i.e, expansion about $s = 0$), are not acceptable in all applications. To circumvent this difficulty, a multi-point Padé approximant was developed, and is known as rational interpolation in the literature [47, 48, 94–96]. In the rational interpolation problem [1, 6], one has to solve a system of equations involving a Loewner matrix, yielding a reduced-order model whose transfer function interpolates the value and subsequent derivatives of the original transfer function model at multiple frequencies. Several algorithms have been developed for a practical computational approach to rational interpolation (see [37, 48, 96] and references therein).

One of the drawbacks of rational interpolation in model reduction is the selection of the interpolation points [46]. The location of the interpolation points and the number of moments matched dictates the accuracy of the reduced-order model. In [51], a method related to an error bound for the Lanczos procedure was suggested in order to choose the interpolation points.

Model reduction using Krylov subspaces in control system design was used in [14]. Related to this work is [15], which uses Krylov subspace methods to obtain bases for the controllability and observability subspaces, such that the coefficients generated during the Lanczos process could be used to compute a minimal realization of a linear dynamical system. Much of the recent work on this subject is in the area of error analysis [63, 64] and stability and passivity retention [47].

Most of the problems related to controller reduction are frequently formulated as frequency-weighted model reduction problems, where the frequency weights are chosen to enforce closed-loop stability and an acceptable performance degradation when the low-order controller is used instead of the original high-order controller [115], [3]. Even though good theoretical results using $\mathcal{H}_\infty$ controller reduction have been reported in the literature [125], there remains a lack of methods for large-scale systems. As will be seen later, the solutions of Lyapunov, Riccati and LMI equations are not well-suited for large-scale systems.

1.5 Contributions of the Dissertation

To date, the issue of stability of reduced-order controllers in a closed-loop framework for large-scale systems has not been addressed in the literature. Several algorithms have been proposed to obtain reduced-order controllers that minimize the $\mathcal{H}_\infty$-norm of the closed-loop system. They rely on the solution of either linear matrix inequalities (LMI) or Riccati-like equations. However, the computational cost associated with their solutions becomes impractical for large-scale systems.

This dissertation develops efficient algorithms for controller reduction in a closed-loop framework applied to large-scale structures. Particularly, it addresses the problem of reduced-order controllers applied to building control. Controller design for civil structures has been based on reduced-order models obtained by either modal or balanced truncation, i.e, they are based on open-loop controller reduction. Issues related to stability of the closed-loop systems have not been addressed. Furthermore, computational efforts related to model and controller reduction for large scale-systems have not been reported in the literature.

To this end, the contributions of this dissertation are:

1. Development of a solution to the problem of closed-loop stability of a reduced-order controller, when implemented with the original plant. The main contribution is a solution to the Positive Real Lemma applied to flexible structures, which plays an important role in the development of

passive controllers.

2. Development of a new scheme to obtain reduced-order controllers applied to large-scale structures using efficient algorithms;

3. Implementation of model and controller order reduction schemes for the building control problem, and assessment of the related performances, and issues related to large-scale implementations and stability; and

4. Illustration and comparison of several feedback control strategies, actuation and sensor schemes applied to the building control problem.

1.6 Outline of the Dissertation

We conclude this introduction with a summary of each of the remaining chapters.

Chapter 2: This chapter covers the basic material used for the development of model reduction schemes. Pertinent results from linear algebra, such as the singular value decomposition, projection and Krylov subspaces are introduced. Also, connections to well-known results from linear systems are described and relevant norm definitions are stated.

Chapter 3: This chapter develops model reduction techniques based on the SVD methods. It is shown how to obtain reduced-order models based on the so-called *Balanced Techniques*. Also, the problem of closed-loop controller reduction is addressed. Examples of model and controller reduction are developed.

Chapter 4: This chapter introduces the field of rational interpolation and the rational Krylov algorithms for model and controller reduction. An example is studied to assess the differences of approximating the moments of the system at different points in the complex plane. Efficient algorithms, such as Lanczos and Arnoldi are derived, and its applications to multi-input, multi-output model and controller reduction is achieved. An algorithm for controller reduction is tested in several examples.

Chapter 5: This chapter solves the problem of controller design and closed-loop controller reduction that guarantee closed-loop stability. First, the notion of passivity and positive realness of linear systems are introduced. Then, it is shown how to construct models and controllers that guarantee the closed-loop stability. Finally, the passivity-preserving model reduction is developed and the application to the controller reduction problem is discussed.

Chapter 6: This chapter describes the existing approaches to building control. Mathematical models of active and semi-active actuators are derived and implementations for building control are shown through examples. Several control strategies are employed to vibration mitigation due to earthquake inputs. Finally, a family of benchmark problems in building control is defined.

Chapter 7: This chapter presents the application of several model reduction techniques applied to the family of benchmark problems. Also, some of the current industrial techniques used for model reduction are discussed.

Chapter 8: The issue of controller reduction for the building control problem is addressed in this chapter. A new scheme that guarantees a stabilizing reduced-order controller is proposed, and its performance is assessed in comparison to techniques presented in previous chapters.

Chapter 9: In this chapter, a summary of the results is provided, together with ideas to be explored in future work.

Chapter 2

Mathematical Preliminaries

Relevant definitions and facts from linear systems analysis and linear algebra required in the development of this dissertation are presented here. Model reduction will be achieved by projection applied to linear time-invariant (LTI) dynamical systems. Metrics to quantify the reduced-order models will be required using different matrix norms. Therefore, concepts such as singular value decomposition (SVD), projectors, Krylov subspaces, matrix norms, and dynamical systems will be briefly described. This description will follow mainly [8], [98], [97] and [41].

2.1 The Singular Value Decomposition: SVD

Every matrix $\mathbf{A} \in \mathbb{R}^{n\times m}$ can be decomposed as a product of unitary and diagonal matrices as:

$$\mathbf{A} = \mathbf{U}\boldsymbol{\Sigma}_d\mathbf{V}^* \in \mathbb{R}^{n\times m} \tag{2.1}$$

where $\mathbf{U}$ and $\mathbf{V}$ are unitary matrices (orthogonal) represented by

$$\mathbf{U} = \begin{bmatrix}\mathbf{u}_1, & \mathbf{u}_2, & \cdots, \mathbf{u}_m\end{bmatrix} \in \mathbb{C}^{m\times m}$$

$$\mathbf{V} = \begin{bmatrix}\mathbf{v}_1, & \mathbf{v}_2, & \cdots, \mathbf{v}_n\end{bmatrix} \in \mathbb{C}^{n\times n}$$

and $\mathbf{\Sigma}_d$ is a diagonal matrix given by

$$\mathbf{\Sigma}_d = \begin{bmatrix} \mathbf{\Sigma_1} & \mathbf{0} \\ \mathbf{0} & \mathbf{0} \end{bmatrix},$$

where $\mathbf{\Sigma_1} = diag(\sigma_1, \cdots, \sigma_n) \in \mathbb{R}^{n \times n}$ is diagonal with nonnegative diagonal entries called *singular values*: $\sigma_i = \sqrt{\lambda_i\left(\mathbf{A}^*\mathbf{A}\right)} \geq \sigma_{i+1}$ and $\lambda_i(\cdot)$ represents the i^{th} eigenvalue of the matrix $\mathbf{A}^*\mathbf{A}$. Also, a *dyadic decomposition* of $\mathbf{A}$ is given by

$$\mathbf{A} = \sigma_1 \mathbf{u}_1 \mathbf{v}_1^* + \sigma_2 \mathbf{u}_2 \mathbf{v}_2^* + \cdots + \sigma_n \mathbf{u}_n \mathbf{v}_n^*.$$

2.2 Linear Dynamical Systems

This section presents the necessary background on linear time-invariant (LTI) dynamical systems in the continuous-time framework. For the discrete time, refer to [8], [68] and references therein. Consider the continuous-time LTI system in state-space:

$$\mathbf{\Sigma} : \begin{cases} \dot{\mathbf{x}}(t) = \mathbf{A}\mathbf{x}(t) + \mathbf{B}\mathbf{u}(t) \\ \mathbf{y}(t) = \mathbf{C}\mathbf{x}(t) + \mathbf{D}\mathbf{u}(t) \end{cases} \Leftrightarrow \mathbf{\Sigma} = \left[\begin{array}{c|c} \mathbf{A} & \mathbf{B} \\ \hline \mathbf{C} & \mathbf{D} \end{array}\right] \in \mathbb{R}^{(n+p)\times(n+m)}. \tag{2.2}$$

One can define for the system $\mathbf{\Sigma}$, a convolution operator $\mathcal{S}$ with kernel $\mathbf{H}(t)$ from $\mathbf{u}(t)$ to $\mathbf{y}(t)$ as

$$\mathcal{S} : \mathbf{u}(t) \mapsto \mathbf{y}(t) = \mathbf{H} * \mathbf{u} = \int_{-\infty}^{\infty} \mathbf{H}(t-\tau)\mathbf{u}(\tau)d\tau \tag{2.3}$$

where $\mathbf{H}(t)$ is called the *impulse response matrix* of $\mathbf{\Sigma}$. It can be shown that the Laplace transform, $\mathbf{H}(s)$ of the impulse response $\mathbf{H}(t)$, is given by

$$\mathbf{H}(s) := \mathcal{L}(\mathbf{H})(s) := \int_{0}^{\infty} \mathbf{H}(t)e^{-st}dt = \mathbf{C}(s\mathbf{I} - \mathbf{A})^{-1}\mathbf{B} + \mathbf{D} \tag{2.4}$$

and $\mathbf{H}(s)$ is called the transfer function matrix of $\mathbf{\Sigma}$. Two important fundamental concepts are discussed next. They are the reachability (controllability) and reconstructability (observability) of $\mathbf{\Sigma}$.

Definition 2.2.1. Controllability: Given the dynamical system $\mathbf{\Sigma}$, the system is called controllable if starting from zero initial state, any state can be reached via a suitable control within finite time. In other words, there exists $\mathbf{u}(t) \leq \infty$, such that, starting from $\mathbf{x}(t_0) = \mathbf{0}$, any desired state $\mathbf{x}(t)$ at a finite time t can be reached. It can be shown that the LTI dynamical system, $\mathbf{\Sigma}$, defined as in Eq. (2.2), is controllable if and only if its reachability (controllability) matrix, $\mathcal{R}(\mathbf{A}, \mathbf{B})$, as defined below, is of full rank, i.e,

$$rank\left(\mathcal{R}(\mathbf{A}, \mathbf{B})\right) = rank\left(\begin{bmatrix} \mathbf{B} & \mathbf{AB} & \mathbf{A}^2\mathbf{B} & \cdots & \mathbf{A}^{n-1}\mathbf{B} \end{bmatrix}\right) = n. \quad (2.5)$$

Definition 2.2.2. Observability: Given the dynamical system $\mathbf{\Sigma}$, the system is called observable if for any initial state $\mathbf{x}(t_0)$, there exists a finite $t_1 > 0$, such that the knowledge of the input $\mathbf{u}(t)$ and the output $\mathbf{y}(t)$ over the interval $[0, t_1]$ suffices to determine uniquely the initial state $\mathbf{x}(t_0)$. In other words, the states can be reconstructed based on the input $\mathbf{u}(t)$ and output $\mathbf{y}(t)$. It can be shown that the LTI dynamical system, $\mathbf{\Sigma}$, defined as in Eq. (2.2), is observable if and only if its reconstructability (observability) matrix, $\mathcal{O}(\mathbf{A}, \mathbf{B})$, as defined below, if of full rank, i.e,

$$rank\left(\mathcal{O}(\mathbf{C}, \mathbf{A})\right) = rank\left(\begin{bmatrix} \mathbf{C}^T & \mathbf{A}^T\mathbf{C}^T & (\mathbf{A}^T)^2\mathbf{C}^T & \cdots & (\mathbf{A}^T)^{n-1}\mathbf{C}^T \end{bmatrix}^T\right) = n. \quad (2.6)$$

An important definition, related to the controllability and observability matrices, is the concept of infinite Gramians and their relation to Lyapunov equations.

Definition 2.2.3. Let $\mathbf{\Sigma}$ be a LTI asymptotically stable system. The so-called infinite reachability gramian $\mathcal{P}$ and the infinite observability gramian $\mathcal{Q}$ are defined as

$$\mathcal{P} := \int_0^\infty e^{\mathbf{A}\tau}\mathbf{B}\mathbf{B}^T e^{\mathbf{A}^T\tau} d\tau \quad \text{and} \quad \mathcal{Q} := \int_0^\infty e^{\mathbf{A}^T\tau}\mathbf{C}^T\mathbf{C} e^{\mathbf{A}\tau} d\tau. \tag{2.7}$$

It readily follows that $\mathcal{P} = \mathcal{P}^T \geq 0$ and $\mathcal{Q} = \mathcal{Q}^T \geq 0$. Moreover, the infinite gramians satisfy the following Lyapunov equations:

$$\mathbf{A}\mathcal{P} + \mathcal{P}\mathbf{A}^T + \mathbf{B}\mathbf{B}^T = \mathbf{0} \quad \text{and} \quad \mathbf{A}^T\mathcal{Q} + \mathcal{Q}\mathbf{A} + \mathbf{C}^T\mathbf{C} = \mathbf{0}. \tag{2.8}$$

2.3 System Norms

Recall the definition of the convolution operator $\mathcal{S}$ for the LTI system $\mathbf{\Sigma}$, as shown in Eq. (2.3). Restricting its domain and co-domain yields the definition of a fundamental operator in model reduction, the so-called *Hankel* operator.

Definition 2.3.1. Given the asymptotically stable LTI system $\mathbf{\Sigma}$, the Hankel operator $\mathcal{H}$ is defined as

$$\mathcal{H} : \mathbf{u}_-(t) \mapsto \mathbf{y}_+(t) := \mathcal{H}(\mathbf{u}_-) = \int_{-\infty}^0 \mathbf{H}(t-\tau)\mathbf{u}_-(\tau)d\tau, \quad t \geq 0. \tag{2.9}$$

where $\mathbf{u}_-(t)$ and $\mathbf{y}_+(t)$ represent past inputs and future outputs, respectively.

In other words, the Hankel operator maps the past inputs to the future outputs. It turns out that, unlike the convolution operator, $\mathcal{H}$ has finite rank, at most n, and hence a finite set of singular values as defined below:

Definition 2.3.2. The Hankel singular values, denoted by $\sigma_i(\mathbf{\Sigma})$ for $i = 1, \ldots, n$, are the non-zero singular values of the Hankel operator. Moreover, given a controllable, observable and asymptotically stable LTI dynamical system $\mathbf{\Sigma}$ of dimension n, the Hankel singular values are the positive square-roots of the eigenvalues of $\mathcal{P}\mathcal{Q}$ as

$$\sigma_i\left(\mathbf{\Sigma}\right) = \sqrt{\lambda_i\left(\mathcal{P}\mathcal{Q}\right)}, \quad i = 1, \cdots, n, \tag{2.10}$$

where $\mathcal{P}$ and $\mathcal{Q}$ are the reachability and observability gramians of $\mathbf{\Sigma}$.

Finally, one defines three important norms applied to asymptotically stable systems:

Definition 2.3.3. Let $\mathbf{\Sigma}$ be an asymptotically stable system with transfer function $\mathbf{H}(s)$. Its *Hankel* norm, denoted by $\|\mathbf{\Sigma}\|_{\mathcal{H}}$ is defined as its largest singular value, i.e.

$$\|\mathbf{\Sigma}\|_{\mathcal{H}} := \sigma_1(\mathbf{\Sigma}). \tag{2.11}$$

The $\mathcal{H}_\infty$ norm of $\mathbf{\Sigma}$ is defined as

$$\|\mathbf{\Sigma}\|_{\mathcal{H}_\infty} := \sup_{\omega \in \mathbb{R}} \sigma_{max}\left(\mathbf{H}(j\omega)\right), \tag{2.12}$$

where σ_{max} denotes the maximum singular value. Finally, the $\mathcal{H}_2$ norm of $\mathbf{\Sigma}$ is defined as

$$\|\mathbf{\Sigma}\|_{\mathcal{H}_2} := \left(\int_{-\infty}^{\infty} \mathrm{trace}\left(\mathbf{H}^*(j\omega)\mathbf{H}(j\omega)\right) d\omega\right)^{1/2}. \tag{2.13}$$

2.4 The Krylov Subspace

In this section, the definition of the Krylov subspaces is stated, and connections to controllability and observability are presented.

Definition 2.4.1. Given a matrix $\mathbf{A} \in \mathbb{R}^{n\times n}$ and a vector $\mathbf{b} \in \mathbb{R}^n$, the kth Krylov sequence $\mathcal{K}(\mathbf{A}, \mathbf{b}, k)$ is a sequence of k column vectors, constructed recursively,

$$\mathcal{K}(\mathbf{A}, \mathbf{b}, k) \equiv \left(\mathbf{b}, \mathbf{A}\mathbf{b}, \mathbf{A}^2\mathbf{b}, \cdots, \mathbf{A}^{k-1}\mathbf{b}\right)$$

and the corresponding column span is called the kth Krylov space, as

$$\mathcal{K}(\mathbf{A}, \mathbf{b}, k) = span\left\{\mathbf{b}, \mathbf{A}\mathbf{b}, \mathbf{A}^2\mathbf{b}, \cdots, \mathbf{A}^{k-1}\mathbf{b}\right\}.$$

By the Cayley-Hamilton Theorem [14], one can check that $\mathcal{K}(\mathbf{A}, \mathbf{b}, k) = \mathcal{K}(\mathbf{A}, \mathbf{b}, n)$, $\forall k > n$. In this manner, Krylov subspaces can be viewed as generalizations of the controllability and observability matrices. A generalization of these concepts is given by the so-called partial generalized reachability matrix:

$$\mathcal{R}_k\left(\mathbf{A}, \mathbf{B}; \sigma\right) = \left[\begin{array}{cccc} \left(\sigma\mathbf{I}_n - \mathbf{A}\right)^{-1}\mathbf{B} & \left(\sigma\mathbf{I}_n - \mathbf{A}\right)^{-2}\mathbf{B} & \cdots & \left(\sigma\mathbf{I}_n - \mathbf{A}\right)^{-k}\mathbf{B} \end{array}\right]. \tag{2.14}$$

The partial generalized observability follows in the same manner.

2.5 Projectors

A projector $\mathbf{P} \in \mathcal{C}^{n\times n}$ onto a subspace $\mathcal{S} \subseteq \mathcal{C}^n$ is defined as a linear mapping from $\mathcal{C}^n$ to itself, such that it satisfies

$$\mathbf{P}^2 = \mathbf{P},\ \mathbf{P}\mathbf{x} \in \mathcal{S},\ \forall \mathbf{x} \in \mathcal{C}^n. \tag{2.15}$$

From this definition, if $\mathbf{P}$ is a projector, it is idempotent, as is $\mathbf{I} - \mathbf{P}$. The following relation holds,

$$Ker(\mathbf{P}) = Ran(\mathbf{I} - \mathbf{P}), \tag{2.16}$$

where $Ker(\cdot)$ and $Ran(\cdot)$ are the kernel and range spaces, respectively. Every vector $\mathbf{x} \in \mathcal{C}^n$ can be written as

$$\mathbf{x} = \mathbf{P}\mathbf{x} + (\mathbf{I} - \mathbf{P})\mathbf{x}, \tag{2.17}$$

and therefore the space $\mathcal{C}^n$ can be decomposed as the direct sum

$$\mathcal{C}^n = Ker(\mathbf{P}) \oplus Ran(\mathbf{P}). \tag{2.18}$$

From this property, for every pair of subspaces M and S which forms a direct sum of $\mathcal{C}^n$ and for any vector $\mathbf{x}$, the vector $\mathbf{P}\mathbf{x}$ satisfies the conditions,

$$\begin{aligned} \mathbf{P}\mathbf{x} &\in M \\ \mathbf{x} - \mathbf{P}\mathbf{x} &\in S \end{aligned} \tag{2.19}$$

and the linear mapping $\mathbf{P}$ is said to project $\mathbf{x}$ *onto* M *and along or parallel* to the subspace S. An orthogonal projector $\mathbf{P}$ satisfies, in addition to Eq. 2.15, the condition

$$(\mathbf{I} - \mathbf{P})\mathbf{x} \in \mathcal{S}^{\perp}. \tag{2.20}$$

2.5.1 Matrix Representation

According to Eqs. 2.19, two bases are required to obtain a matrix representation of a general projector: a basis $\mathbf{V} = [\mathbf{v}_1, \mathbf{v}_2, \cdots, \mathbf{v}_m]$ for the subspace $M = Ran(P)$ and $\mathbf{W} = [\mathbf{w}_1, \mathbf{w}_2, \cdots, \mathbf{w}_m]$ for the subspace $S^{\perp}$.

If the two bases are biorthogonal, i.e, $\mathbf{W}^*\mathbf{V} = \mathbf{I}$, where $(\cdot)^*$ represents the complex conjugate transpose of a matrix, then it follows that the matrix representation of the projector $\mathbf{P}$ is

$$\mathbf{P} = \mathbf{V}\mathbf{W}^* \tag{2.21}$$

and in case where the bases $\mathbf{V}$ and $\mathbf{W}$ are not biorthogonal, the projector is

$$\mathbf{P} = \mathbf{V}\left(\mathbf{W}^*\mathbf{V}\right)^{-1}\mathbf{W}^*. \tag{2.22}$$

2.5.2 Orthogonal and Oblique Projectors

Two classes of projectors are obtained when one considers the relation between the subspaces M and $S^{\perp}$. When $M = S^{\perp}$, i.e, when

$$Ker(\mathbf{P}) = Ran(\mathbf{P})^{\perp},$$

the projector $\mathbf{P}$ is said to be the *orthogonal projector* onto M and satisfies, in addition to Eq. (2.19), the conditions

$$(\mathbf{I} - \mathbf{P})\mathbf{x} \in \mathcal{S}^{\perp} \tag{2.23}$$

$$\mathbf{P}\mathbf{x} \in M \tag{2.24}$$

$$\mathbf{x} - \mathbf{P}\mathbf{x} \perp M.$$

A projector that is not orthogonal is *oblique*.

2.5.3 Projection Methods Applied to Linear Systems

Consider the linear algebraic system

$$\mathbf{A}\mathbf{x} = \mathbf{b}, \tag{2.25}$$

where $\mathbf{A} \in \mathbb{R}^{n \times n}$ and $\mathbf{b} \in \mathbb{R}^n$. The idea of using projection techniques is to search for an approximation subspace of $\mathbb{R}^{n \times n}$ in order to extract an approximate solution to the above problem. Suppose $\mathcal{K}$ and $\mathcal{L}$ are two m-dimensional subspaces of $\mathbb{R}^n$. In general, in numerical computations one cannot find an approximate solution $\tilde{\mathbf{x}}$ to Eq. (2.25) such that the residual $\mathbf{b} - \mathbf{A}\tilde{\mathbf{x}}$ is zero. Instead, one uses a projection technique onto the subspace $\mathcal{K}$ and orthogonal to $\mathcal{L}$, by imposing a relaxed condition that $\tilde{\mathbf{x}}$ belongs to $\mathcal{K}$ and that the new residual vector is orthogonal to $\mathcal{L}$, as

$$(\mathbf{b} - \mathbf{A}\tilde{\mathbf{x}}) \perp \mathcal{L}. \tag{2.26}$$

This is called the *Petrov-Galerkin Condition.* In order to find a solution based on a initial guess $\mathbf{x}_0$ to the solution, defining the approximate solution as $\tilde{\mathbf{x}} = \mathbf{x}_0 + \delta$ and the initial residual to be $\mathbf{r}_0 = \mathbf{b} - \mathbf{A}\mathbf{x}_0$, the Petrov-Galerkin conditions can be written as

$$\tilde{\mathbf{x}} = \mathbf{x}_o + \delta, \quad \delta \in \mathcal{K} \tag{2.27}$$

$$(\mathbf{r}_o - \mathbf{A}\delta, \mathbf{w}) = \mathbf{0}, \quad \forall \mathbf{w} \in \mathcal{L}, \tag{2.28}$$

where $(\cdot, \cdot)$ represents an inner product. In matrix representation, let $\mathbf{V} = [\mathbf{v}_1, \cdots, \mathbf{v}_m]$ be an $n \times m$ matrix whose column-vectors form a basis of $\mathcal{K}$, and similarly for $\mathcal{L}$, the columns of $\mathbf{W} = [\mathbf{w}_1, \cdots, \mathbf{w}_m]$ form a basis for the subspace. Then, the approximate solution can be written as

$$\tilde{\mathbf{x}} = \mathbf{x}_0 + \mathbf{V}\left(\mathbf{W}^{\mathbf{T}}\mathbf{A}\mathbf{V}\right)^{-\mathbf{1}}\mathbf{W}^{\mathbf{T}}\mathbf{r}_0.$$

2.5.4 Projection Methods for Model Order Reduction

A generalization of the above results can be applied to model reduction. For consistency with the previous section, suppose the following state-space representation of a stable LTI single-input single-output (SISO) system is given,

$$\dot{\mathbf{x}}(t) = \mathbf{A}\mathbf{x}(t) + \mathbf{B}u(t) \tag{2.29}$$

$$y(t) = \mathbf{C}x(t) + \mathbf{D}u(t) \tag{2.30}$$

where the state vector $\mathbf{x}(t) \in \mathbb{R}^n$, and $u(t)$, $y(t)$ are the scalar input and output, respectively. Denoting the transfer function as

$$G(s) = \mathbf{C}\left(s\mathbf{I} - \mathbf{A}\right)^{-1}\mathbf{B} + \mathbf{D}, \tag{2.31}$$

we can rewrite it as

$$G(s) = \mathbf{C}G_B(s) = G_C^T(s)\mathbf{B}, \tag{2.32}$$

where $G_B(s)$ and $G_C(s)$ are the solutions to the linear systems

$$\left(s\mathbf{I_n} - \mathbf{A}\right) G_B(s) \quad = \quad \mathbf{B} \tag{2.33}$$

$$G_C^T(s)\left(s\mathbf{I_n} - \mathbf{A}\right) \quad = \quad \mathbf{C} \tag{2.34}$$

and the model reduction problem becomes the one of finding approximate solutions $G_{B,m}(s)$ and $G_{C,m}^T(s)$ to $G_B(s)$ and $G_C^T(s)$, respectively, such that the following Petrov-Garlekin, as given by Eq. (2.26), conditions are satisfied. In this case one can obtain the reduced-order models as

$$\dot{\mathbf{x}}_\mathbf{r}(t) = \underbrace{\mathbf{W^T A V}}_{:=\mathbf{A_r}}\mathbf{x_r}(t) + \underbrace{\mathbf{W^T B}}_{:=\mathbf{B_r}}\mathbf{u}(t) \quad \mathbf{y_r}(t) = \underbrace{\mathbf{CV}}_{:=\mathbf{C_r}}\mathbf{x_r}(t) + \underbrace{\mathbf{D}}_{:=\mathbf{D_r}}\mathbf{u}(t), \tag{2.35}$$

where $\mathbf{W}$ and $\mathbf{V}$ are the matrices that form the projector $\mathbf{\Pi} = \mathbf{V}\mathbf{W^T}$.

Chapter 3

SVD Methods for Model and Controller Reduction

This chapter presents model and controller reduction methods using SVD-based procedures. The key steps in SVD-based methods are the computation of the so-called Hankel singular values, as described in Chapter 2, and balancing of the system. In general terms, balancing consists of simultaneously diagonalization of two appropriate chosen positive definite matrices [8], according to solutions of Lyapunov equations or Riccati equations.

The most commonly used model reduction scheme is the so-called balanced model reduction, which was first introduced by Mullis and Roberts [83] and then in a systems framework by Moore [82]. The main idea of this technique is a change of the state coordinate basis, called a balancing transformation, such that the controllability and observability grammians are both equal to some diagonal matrix, $\mathbf{\Sigma}_d$, where the magnitudes of the diagonal entries of the gramians reflect the contributions of different entries of the state vector of the system.

Although balanced model reduction and its variants have nice system theoretic properties, such as preservation of stability and computation of an error bound, they become computationally prohibitive for large-scale systems. This drawback stems from the fact that they require dense matrix factorizations, such as solving two Lyapunov equations, and therefore the computational cost on the order $\mathcal{O}(n^3)$ and storage of order $\mathcal{O}(n^2)$ becomes impractical for systems of order $n \gg 1000$.

Lyapunov balancing methods are now explored with applications to model reduction. Extensions to the problem of frequency-weighted balanced reduction will introduced. This discussion will support the application of the concepts to the problem of closed-loop controller reduction by balanced truncation.

3.1 Balanced Model Reduction

Consider a stable LTI system model, $\mathbf{G}(s)$, given by its state-space realization and transfer function as described in Eq. (1.1). Then, the infinite controllability and observability gramians are defined, respectively, as in Definition 2.2.3. The gramians satisfy the **Lyapunov equations** as shown in Definition 2.2.3. The square roots of the eigenvalues of the product $\mathcal{P}\mathcal{Q}$ are the Hankel singular values $\sigma_i(\mathbf{G}(s))$ of the system $\mathbf{G}(s)$, and as described in Definition 2.2.3 are given by

$$\sigma_i\left(\mathbf{G}(s)\right) = \sqrt{\lambda_i\left(\mathcal{P}\mathcal{Q}\right)}.$$

Definition 3.1.1. The reachable, observable and stable system $\mathbf{G}(s)$ is called

Lyapunov-balanced if

$$\mathcal{P} = \mathcal{Q} = \mathbf{\Sigma}_d = diag\left(\sigma_1 \mathbf{I}_{m_1}, \cdots, \sigma_q \mathbf{I}_{m_q}\right), \tag{3.1}$$

where $\mathbf{\Sigma}_d$ is a diagonal matrix with $\sigma_1 > \sigma_2 > \cdots > \sigma_q > 0$, and m_i are the multiplicities of σ_i, so that, $m_1 + \cdots + m_q = n$.

According to [8], given a state $\mathbf{x}$ of a stable linear system, the smallest amount of energy needed to steer the system from $\mathbf{0}$ to $\mathbf{x}$ is given by the square root of

$$\varepsilon_r^2 = \mathbf{x}^T \mathcal{P}^{-1} \mathbf{x},$$

while the energy obtained by observing the output of the system with initial condition $\mathbf{x}$ and no excitation function is given by the square root of

$$\varepsilon_o^2 = \mathbf{x}^T \mathcal{Q} \mathbf{x}.$$

Thus, if one simultaneously diagonalizes $\mathcal{P}$ and $\mathcal{Q}$, one can see the states that are difficult to reach and simultaneously difficult to observe. Hence, the idea of model reduction by truncation is that one can eliminate those states which require a large amount of energy ε_r to be reached and yield small amounts of observation energy ε_o. Mathematically, one finds a similarity transformation applied to the LTI system in Eq. (2.2), such that the gramians are equal and diagonal. The following theorem formally describes the balancing method:

Theorem 3.1.1. *Consider a stable system* $\mathbf{G}(s) \in \mathcal{RH}_\infty$ *and suppose* $\mathbf{G}(s) = \left[\begin{array}{c|c} \mathbf{A} & \mathbf{B} \\ \hline \mathbf{C} & \mathbf{D} \end{array}\right]$ *is a balanced realization, i.e, its controllability and observability* *gramians are equal and diagonal given by* $\mathcal{P} = \mathcal{Q} = \mathbf{\Sigma}_d$*, which satisfy the following Lyapunov equations*

$$\begin{aligned} \mathbf{A}\mathbf{\Sigma}_d + \mathbf{\Sigma}_d\mathbf{A}^* + \mathbf{B}\mathbf{B}^* &= \mathbf{0} \quad (3.2) \\ \mathbf{A}^*\mathbf{\Sigma}_d + \mathbf{\Sigma}_d\mathbf{A} + \mathbf{C}^*\mathbf{C} &= \mathbf{0}, \quad (3.3) \end{aligned}$$

where $(\cdot)^*$ *denotes the complex conjugate transpose of a matrix. Partitioning the balanced gramians as* $\mathbf{\Sigma}_d = \begin{bmatrix} \mathbf{\Sigma}_1 & \mathbf{0} \\ \mathbf{0} & \mathbf{\Sigma}_2 \end{bmatrix}$ *with*

$$\mathbf{\Sigma}_1 = diag\left(\sigma_1\mathbf{I}_{m_1}, \cdots, \sigma_k\mathbf{I}_{m_k}\right) \quad and \quad \mathbf{\Sigma}_2 = diag\left(\sigma_{k+1}\mathbf{I}_{m_{k+1}}, \cdots, \sigma_q\mathbf{I}_{m_q}\right)$$

and partitioning the balanced system accordingly

$$G(s) = \left[\begin{array}{c|c} \mathbf{A}_b & \mathbf{B}_b \\ \hline \mathbf{C}_b & \mathbf{D}_b \end{array}\right] = \left[\begin{array}{c|cc} \mathbf{A}_{11} & \mathbf{A}_{11} & \mathbf{B}_1 \\ \hline \mathbf{A}_{21} & \mathbf{A}_{22} & \mathbf{B}_2 \\ \mathbf{C}_1 & \mathbf{C}_2 & \mathbf{D} \end{array}\right], \quad (3.4)$$

where the dimensions are $\mathbf{A}_{11} \in \mathbb{R}^{k\times k}$, $\mathbf{B}_1 \in \mathbb{R}^{k\times m}$, $\mathbf{C}_1 \in \mathbb{R}^{p\times k}$ *and* $\mathbf{D} \in \mathbb{R}^{p\times m}$. *Then, the reduced-order model* $\mathbf{G}_r(s) = \left[\begin{array}{c|c} \mathbf{A}_{11} & \mathbf{B}_1 \\ \hline \mathbf{C}_1 & \mathbf{D} \end{array}\right]$ *obtained by truncation is asymptotically stable, balanced, minimal (controllable and observable) and satisfies*

$$\|\mathbf{G}(s) - \mathbf{G}_r(s)\|_{\mathcal{H}_\infty} \leq 2\left(\sigma_{k+1} + \cdots + \sigma_q\right). \quad (3.5)$$

Equality holds if $\mathbf{\Sigma}_2 = \sigma_q\mathbf{I}_{m_q}$.

In order to compute the simultaneous diagonalization of $\mathcal{P}$ and $\mathcal{Q}$, several algorithms have been proposed in the literature [8]. Two of the algorithms, possessing the same theoretical properties, but different numerical results, are shown below. Let $\mathcal{P}$ and $\mathcal{Q}$ be the gramians of a reachable, observable and stable system $\mathbf{G}(s)$ of order n. Since the gramians are positive-definite, they have a Cholesky decomposition as

$$\mathcal{P} = \mathbf{U}\mathbf{U}^*, \text{ and } \mathcal{Q} = \mathbf{L}^*\mathbf{L}, \tag{3.6}$$

where $\mathbf{U}, \mathbf{L}$ are upper and lower triangular, respectively. It can be shown that computing the eigenvalue decomposition of $\mathbf{U}^*\mathcal{Q}\mathbf{U}$ as

$$\mathbf{U}^*\mathcal{Q}\mathbf{U} = \mathbf{K}\mathbf{\Omega}^2\mathbf{K}^*, \tag{3.7}$$

the transformation and its inverse, defined as

$$\mathbf{T} = \mathbf{\Omega}^{1/2}\mathbf{K}^*\mathbf{U}^{-1} \text{ and } \mathbf{T}^{-1} = \mathbf{U}\mathbf{K}\mathbf{\Omega}^{-1/2}, \tag{3.8}$$

produce simultaneous diagonalization of the gramians as

$$\mathcal{P} = \mathcal{Q} = \mathbf{\Omega}. \tag{3.9}$$

A variant of this algorithm, the so-called *square-root algorithm*, can be accomplished taking the SVD of the product

$$\mathbf{U}^*\mathbf{L} = \mathbf{W}\mathbf{\Omega}\mathbf{V}^*, \tag{3.10}$$

where $\mathbf{W}$ and $\mathbf{V}$ are orthogonal matrices, and forming the balanced transformation as

$$\mathbf{T} = \mathbf{\Omega}^{-1/2}\mathbf{V}^*\mathbf{L}^* \text{ and } \mathbf{T}^{-1} = \mathbf{U}\mathbf{W}\mathbf{\Omega}^{-1/2}. \tag{3.11}$$

In general, the square-root algorithm leads to a smaller condition number. Enhancements to this method have lead to two other algorithms which yield much smaller condition numbers and the same theoretical results: the *diagonal scaling algorithm* and the *balanced-free square root algorithm* [8].

3.1.1 Other Types of Balancing

Besides the Lyapunov balancing method, there exist other types of balancing that diagonalize two appropriate chosen positive-definite matrices that are either solutions to the Lyapunov equations or Riccati equations [8]. This topic will be further developed when model reduction that preserves passivity is analyzed in Chapter 5.

Stochastic Balancing Method: The stochastic balancing method was first proposed by Desai and Pal [26] for balancing stochastic systems. It requires solving one Lyapunov equation and one Riccati equation, as shown by [44, 45];

Positive Real Balancing: This class of balancing is applied to model reduction of positive real (passive) systems. It can be cast as the stochastic balancing method applied to the spectral factor of the given passive system, and it requires solving two positive real Riccati equations;

Bounded Real Balancing: This class of balancing is applied to bounded real systems, and requires solving two Riccati equations.

3.1.2 Frequency Weighted Balanced Truncation

The Lyapunov balancing method presented here provides an approximation to the full order model $\mathbf{G}(s)$ over all frequencies. However, in many applications, one is interested in matching the reduced order model $\mathbf{G}_r(s)$ over a specific range of frequencies. This problem leads to an extension of the balanced truncation method called *frequency weighted balanced truncation.* In this case, the problem becomes to find a low-order approximation $\mathbf{G}_r(s)$ such that

$$\|\mathbf{W}_o(s)\left(\mathbf{G}(s)-\mathbf{G}_r(s)\right)\mathbf{W}_i(s)\|_{\mathcal{H}_\infty} \tag{3.12}$$

is made as small as possible for a given input weighting $\mathbf{W}_i(s) \in \mathcal{RH}_\infty$ and output weighting $\mathbf{W}_o(s) \in \mathcal{RH}_\infty$. The frequency weighted method, proposed first by Enns [33], and later by Lin and Chiu [76], can be posed as follows: Let $\mathbf{G}(s)$, $\mathbf{W}_i(s)$, and $\mathbf{W}_o(s)$ have the following state-space realizations

$$\mathbf{G}(s) = \left[\begin{array}{c|c} \mathbf{A} & \mathbf{B} \\ \hline \mathbf{C} & \mathbf{D} \end{array}\right], \quad \mathbf{W}_i(s) = \left[\begin{array}{c|c} \mathbf{A}_i & \mathbf{B}_i \\ \hline \mathbf{C}_i & \mathbf{D}_i \end{array}\right], \quad \mathbf{W}_o(s) = \left[\begin{array}{c|c} \mathbf{A}_o & \mathbf{B}_o \\ \hline \mathbf{C}_o & \mathbf{D}_o \end{array}\right]. \tag{3.13}$$

Assuming there are no pole-zero cancellations, then the minimal state space realization of the weighted transfer matrices are given by

$$\mathbf{G}(s)\mathbf{W}_i(s) = \left[\begin{array}{c|c} \bar{\mathbf{A}}_i & \bar{\mathbf{B}}_i \\ \hline \bar{\mathbf{C}}_i & \mathbf{0} \end{array}\right] = \left[\begin{array}{cc|c} \mathbf{A} & \mathbf{B}\mathbf{C}_i & \mathbf{B}\mathbf{D}_i \\ \mathbf{0} & \mathbf{A}_i & \mathbf{B}_i \\ \hline \mathbf{C} & \mathbf{0} & \mathbf{D}\mathbf{D}_i \end{array}\right] \tag{3.14}$$

and

$$\mathbf{W}_o(s)\mathbf{G}(s) = \left[\begin{array}{c|c} \bar{\mathbf{A}}_o & \bar{\mathbf{B}}_o \\ \hline \bar{\mathbf{C}}_o & \mathbf{D}_o \end{array}\right] = \left[\begin{array}{cc|c} \mathbf{A} & \mathbf{0} & \mathbf{B} \\ \mathbf{B}_o\mathbf{C} & \mathbf{A}_o & \mathbf{0} \\ \hline \mathbf{D}_o\mathbf{C} & \mathbf{C}_o & \mathbf{D}_o\mathbf{D} \end{array}\right]. \tag{3.15}$$

Let $\bar{\mathcal{P}} = \left[\begin{array}{c|c} \mathcal{P}_{11} & \mathcal{P}_{12} \\ \hline \mathcal{P}_{12}^T & \mathcal{P}_{22} \end{array}\right]$ and $\bar{\mathcal{Q}} = \left[\begin{array}{c|c} \mathcal{Q}_{11} & \mathcal{Q}_{12} \\ \hline \mathcal{Q}_{12}^T & \mathcal{Q}_{22} \end{array}\right]$ be the solutions to the following Lyapunov equations:

$$\bar{\mathbf{A}}_i\bar{\mathcal{P}} + \bar{\mathcal{P}}\bar{\mathbf{A}}_i^T + \bar{\mathbf{B}}_\mathbf{i}\bar{\mathbf{B}}_i^T = \mathbf{0} \tag{3.16}$$

$$\bar{\mathbf{A}}_o^T\bar{\mathcal{Q}} + \bar{\mathcal{Q}}\bar{\mathbf{A}}_o + \bar{\mathbf{C}}_o^T\bar{\mathbf{C}}_o = \mathbf{0}. \tag{3.17}$$

The following theorem, denoted Enn's method, applies:

Theorem 3.1.2. *Given the asymptotically stable and minimal system* $\mathbf{G}(s)$*, let* $\mathbf{G}_r(s)$ *be obtained by simultaneously diagonalizing* $\mathcal{P}_{11}$ *and* $\mathcal{Q}_{11}$*, with*

$$\mathcal{P}_{11} = \mathcal{Q}_{11} = diag\left(\sigma_1 \mathbf{I}_{n_1}, \cdots, \sigma_k \mathbf{I}_{n_k}, \sigma_{k+1} \mathbf{I}_{n_{k+1}, \cdots, \sigma_q \mathbf{I}_{n_q}}\right)$$

where n_i *are the multiplicities of* σ_1 *with* $n_1 + \cdots + n_q = n$ *and in this balanced basis, let the partitioning of the full order model be given by*

$$\mathbf{G}(s) = \left[\begin{array}{c|cc} \mathbf{A}_{11} & \mathbf{A}_{11} & \mathbf{B}_1 \\ \mathbf{A}_{21} & \mathbf{A}_{22} & \mathbf{B}_2 \\ \hline \mathbf{C}_1 & \mathbf{C}_2 & \mathbf{D} \end{array}\right], \tag{3.18}$$

where the dimensions are $\mathbf{A}_{11} \in \mathbb{R}^{k \times k}$*,* $\mathbf{B}_1 \in \mathbb{R}^{k \times m}$*,* $\mathbf{C}_1 \in \mathbb{R}^{p \times k}$ *and* $\mathbf{D} \in \mathbb{R}^{p \times m}$*. Then the reduced-order model is obtained by truncating the full-order model at the largest* k *weighted singular values* σ_i*, as*

$$\mathbf{G}_r(s) = \left[\begin{array}{c|c} \mathbf{A}_{11} & \mathbf{B}_1 \\ \hline \mathbf{C}_1 & \mathbf{D} \end{array}\right]. \tag{3.19}$$

In this case, the σ_i*'s are no longer the Hankel singular values of* $\mathbf{G}(s)$*. However, they still represent a measure of how controllable and observable the input-output filtered states are. Hence, they are called "frequency weighted Hankel singular values". Unlike the Lyapunov balancing, the reduced-order model is not guaranteed to be stable. A simplification occurs if either* $\mathbf{W}_i(s) = \mathbf{I}$ *or* $\mathbf{W}_o(s) = \mathbf{I}$*. In this case* $\mathbf{G}_r(s)$ *is guaranteed to be asymptotically stable and the following error bound is derived*

$$\|\mathbf{W}_o(s)\left(\mathbf{G}(s) - \mathbf{G}_r(s)\right)\mathbf{W}_i(s)\|_{\mathcal{H}_\infty} \leq 2 \sum_{i=k+1}^{q} \sqrt{\sigma_k^2 + (\alpha_k + \beta_k)\sigma_k^{3/2} + \alpha_k \beta_k \sigma_k}, \tag{3.20}$$

where α_k and β_k denote the $\mathcal{H}_\infty$ norms of the transfer function which depend on $\mathbf{W}_o(s)$, $\mathbf{W}_i(s)$, and $\mathbf{G}_{r_j}(s), j = 1, \cdots, k$.

A variant of Enn's method, which overcomes the stability issues for the double sided weights, was developed by Lin and Chiu [76]. The balancing is performed with respect to two matrices derived by a Schur complement operation, i.e, based on simultaneous diagonalization of

$$\tilde{\mathcal{P}} := \mathbf{P}_{11} - \mathbf{P}_{12}\mathbf{P}_{22}^{-1}\mathbf{P}_{12}^T, \quad \tilde{\mathcal{Q}} := \mathbf{Q}_{11} - \mathbf{Q}_{12}^T\mathbf{Q}_{22}^{-1}\mathbf{Q}_{12}^T \tag{3.21}$$

so that if

$$\tilde{\mathcal{P}} = \tilde{\mathcal{Q}} = diag\left(\tilde{\sigma}_1\mathbf{I}_{n_1}, \cdots, \tilde{\sigma}_k\mathbf{I}_{n_k}, \tilde{\sigma}_{k+1}\mathbf{I}_{n_{k+1}}, \cdots, \tilde{\sigma}_q\mathbf{I}_{n_q}\right)$$

are the balanced gramians, then the reduced order model can be obtained as in the Lyapunov balanced method by truncation. This method also satisfies an error equation [76]. Recently, Wang *et al.* [118] introduced a new frequency weighted balancing method as a modification to Enns's method, which guarantees stability and yields a simple *a priori* error bound.

In many cases, the input and output weightings are not given. Thus, the problem becomes the approximation of $\mathbf{G}(s)$ over a given range of frequencies $[\omega_1, \omega_2]$. This problem can be solved by using the frequency domain representation of the gramians, with the limits of the integration restricted according to the frequency range considered [40]

$$\mathcal{P}(\omega) = \frac{1}{2\pi}\int_{-\omega}^{\omega} (i\omega\mathbf{I} - \mathbf{A})^{-1}\mathbf{B}\mathbf{B}^*(-i\omega\mathbf{I} - \mathbf{A}^*)^{-1}\,d\omega \tag{3.22}$$

$$\mathcal{Q}(\omega) = \frac{1}{2\pi}\int_{-\omega}^{\omega} (-i\omega\mathbf{I} - \mathbf{A}^*)^{-1}\mathbf{C}^*\mathbf{C}\,(i\omega\mathbf{I} - \mathbf{A})^{-1}\,d\omega \tag{3.23}$$

and balancing involving the simultaneous diagonalization of the gramians $\mathcal{P}(\omega_1, \omega_2)$ and $\mathcal{Q}(\omega_1, \omega_2)$, using the methods discussed in the previous section. It should be pointed out that the representation of the gramians in the frequency domain allow one to compute the balanced realization for an unstable system [8, 124], and to generalize the balancing methods for the case of second-order systems. This will be further developed in Chapter 7.

3.2 Controller Reduction

Controller reduction problems are often formulated as special frequency-weighted model reduction problems, where the frequency weights are chosen to enforce closed-loop stability and an acceptable performance degradation, when the low-order controller is used in the original closed-loop system [3].

Let $\mathbf{G}(s)$ be the transfer of an n^{th} order time-invariant, continuous-time plant with state-space realization $G(s) = \left[\begin{array}{c|c} \mathbf{A} & \mathbf{B} \\ \hline \mathbf{C} & \mathbf{D} \end{array}\right]$ and let $\mathbf{K}(s)$ be a stabilizing high-order (n_k^{th} order) controller with state-space realization $\mathbf{K}(s) = \left[\begin{array}{c|c} \mathbf{A_K} & \mathbf{B_K} \\ \hline \mathbf{C_K} & \mathbf{D_K} \end{array}\right]$. The controller reduction problem is to seek a low order controller $\mathbf{K}_r(s)$ of order $r \ll n_k$ to replace $\mathbf{K}(s)$ such that the closed-loop stability and performance are preserved.

The controller reduction problem can be recast as a frequency weighted model reduction if one regards the closed-loop system with $\mathbf{K}_r(s)$ replacing $\mathbf{K}(s)$ as being equivalent to that of Fig. 3.1 It is known from [124] that $\mathbf{K}_r(s)$ is a stabilizing controller if

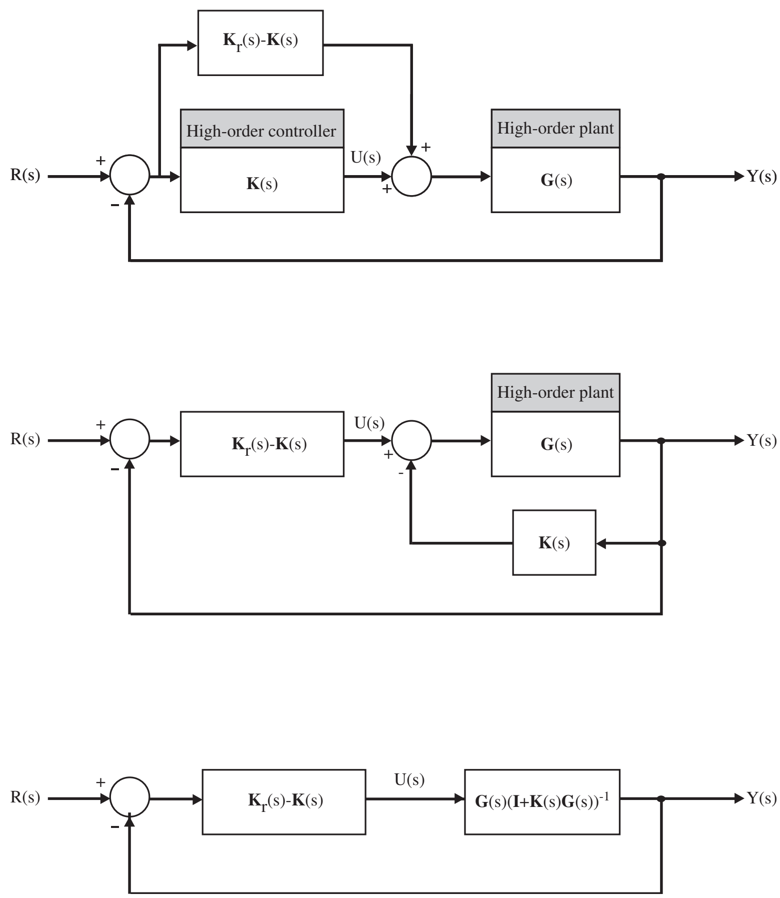

Figure 3.1: Modified Feedback Configurations.

i. $\mathbf{K}(s)$ and $\mathbf{K}_r(s)$ have the same number of unstable poles and no poles on the imaginary axis; and

ii. Either

$$\begin{aligned} \| \left[\mathbf{K}(s) - \mathbf{K}_r(s)\right] \mathbf{G}(s) \left[\mathbf{I} + \mathbf{K}(s)\mathbf{G}(s)\right]^{-1} \|_{\mathcal{H}_\infty} &< 1, \text{ or} \quad (3.24) \\ \| \left[\mathbf{I} + \mathbf{G}(s)\mathbf{K}(s)\right]^{-1} \mathbf{G}(s) \left[\mathbf{K}(s) - \mathbf{K}_r(s)\right] \|_{\mathcal{H}_\infty} &< 1 \quad (3.25) \end{aligned}$$

This can be thought as of a minimization of the weighted error given by

$$\|\mathbf{W}_o(s) \left(\mathbf{K}(s) - \mathbf{K}_r(s)\right) \mathbf{W}_i(s)\|_{\mathcal{H}_\infty} \quad (3.26)$$

where, to ensure closed-loop stability, one can choose the input and output weights as

$$\mathbf{W}_i(s) = \mathbf{I} \quad , \quad \mathbf{W}_o(s) = \left[\mathbf{I} + \mathbf{G}(s)\mathbf{K}(s)\right]^{-1} \mathbf{G}(s), \text{ or} \quad (3.27)$$

$$\mathbf{W}_o(s) = \mathbf{I} \quad , \quad \mathbf{W}_i(s) = \mathbf{G}(s) \left[\mathbf{I} + \mathbf{G}(s)\mathbf{K}(s)\right]^{-1}. \quad (3.28)$$

On the other hand, to preserve closed-loop performance, one can use a two-sided weighting of the form

$$\begin{aligned} \mathbf{W}_o(s) &= \left[\mathbf{I} + \mathbf{G}(s)\mathbf{K}(s)\right]^{-1} \mathbf{G}(s), \text{ and} \quad (3.29) \\ \mathbf{W}_i(s) &= \left[\mathbf{I} + \mathbf{G}(s)\mathbf{K}(s)\right]^{-1}. \quad (3.30) \end{aligned}$$

Following the same structure as the Enns's frequency-weighted balanced reduction method, the reduced order controller can be obtained as in Theorem 3.1.1.

Other representations of the controller lead to different frequency-weighted problems, as in [3], where matrix fractional representation can be used to define the system to be reduced instead of using rational transfer functions. Also, the controller does not need to be stable. In the case of instability, the approach suggested in [3] can be used. In this case, one may decompose $\mathbf{K}(s)$ as

$$\mathbf{K}(s) = \mathbf{K}_{-}(s) + \mathbf{K}_{+}(s) \tag{3.31}$$

where $\mathbf{K}_{-}(s)$ and $\mathbf{K}_{+}(s)$ denote the stable and anti-stable parts of $\mathbf{K}(s)$, respectively. Thus, the model reduction method can be applied to to the stable part $\mathbf{K}_{-}(s)$ with $\mathbf{K}_{+}(s)$ unaltered and copied into the reduced order controller $\mathbf{K}_r(s) = \mathbf{K}_{-r}(s) + \mathbf{K}_{+}(s)$.

3.3 Examples

In order to understand the various options of balanced model reduction and controller reduction, two examples used as benchmarks in model reduction [86] are analyzed: (1) the dynamics of portable CD player, and (2) the dynamics of spinning disks.

3.3.1 The CD player

The full-order model of the CD player describes the dynamics between the lens actuator and the radial arm position, as shown in Fig. 3.2. Traditionally, the behavior of the lens position is represented by a third-order set of differential equations [122]. However, controllers designed from these simple, low-order systems experience difficulties when employed in newer, portable CD players [110]. To obtain a higher-order controller for the CD player, a better model of its dynamics was obtained using finite element approximation, yielding a model that has 120 states with 2 inputs and 2 outputs. Its frequency response (magnitude) is shown in Fig. 3.3.

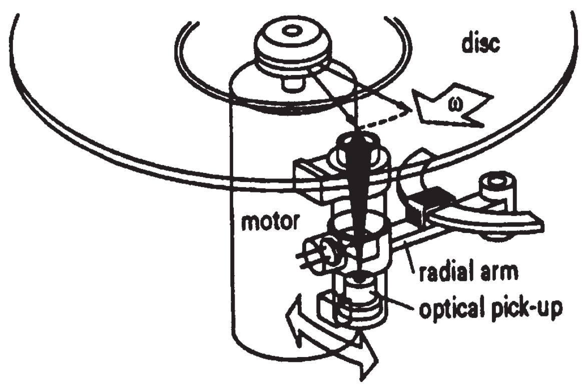

Figure 3.2: CD player model. Source: [110]

Analyzing the eigenvalues of the system matrix of the higher-order model of the CD player, as depicted in Fig. 3.4, one realizes that it contains both very high and very low real and imaginary parts. Also, observing the decay rates of the normalized Hankel singular value (HSV)[1] plot as in Fig. 3.5, one notices that a very rapid decay occurs, indicating that the full-order model might be approximated well with a reduced-order model of very low dimension. Using balanced truncation to approximate the full-order model, one obtains the reduced-order models as described in Table 3.1.

[1]The highest HSV is set to 1 and plotted in a logarithmic scale

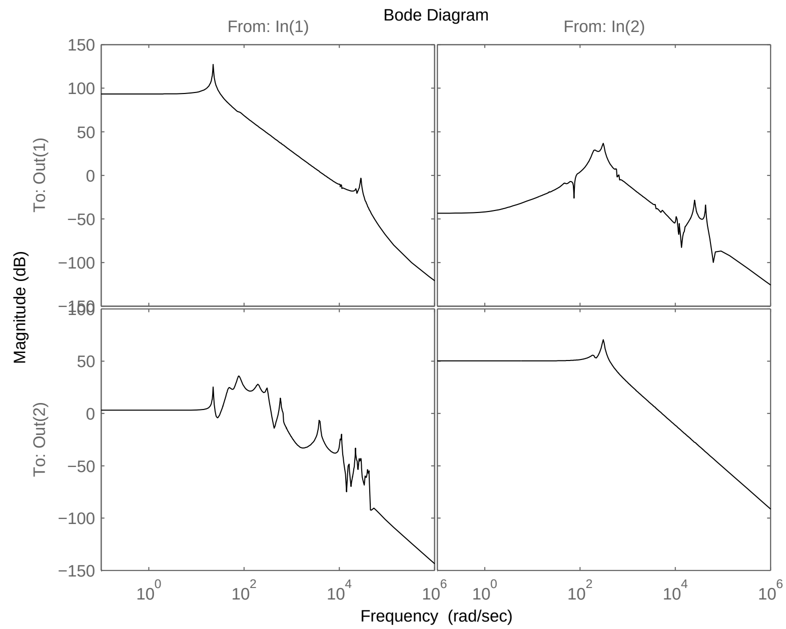

Figure 3.3: MIMO frequency response of the CD player model.

The calculation of the *a priori* error bounds for the balanced truncation technique uses Eq. 3.5. For comparison purposes, the relative errors between the full-order model (FOM) and reduced-order model (ROM) will be computed as follows:

$$\frac{\|\mathbf{G}(j\omega) - \mathbf{G}_r(j\omega)\|_{\mathcal{H}_2,\mathcal{H}_\infty}}{\|\mathbf{G}(j\omega)\|_{\mathcal{H}_2,\mathcal{H}_\infty}}. \tag{3.32}$$

Since the CD player is a multi-input, multi-output model, the frequency response representation is given by the so-called sigma plots, that is, the maximum singular values of the frequency response. The sigma plots of the reduced and error systems are depicted in Fig. 3.6 and Fig. 3.7, respectively.

As can be seen from Figs. 3.6 and 3.7, balanced truncation allows

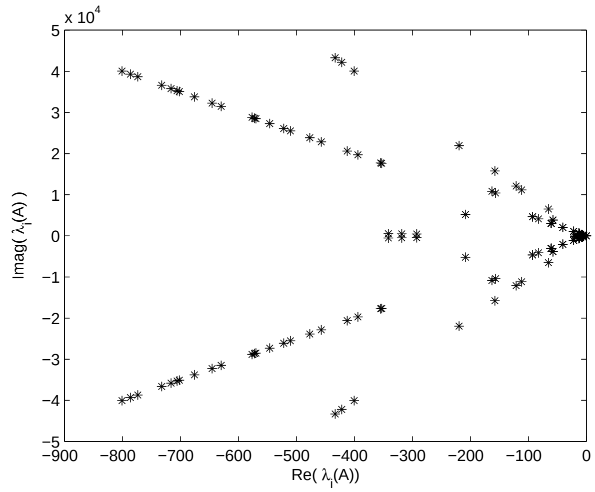

Figure 3.4: Eigenvalues of the higher-order CD player.

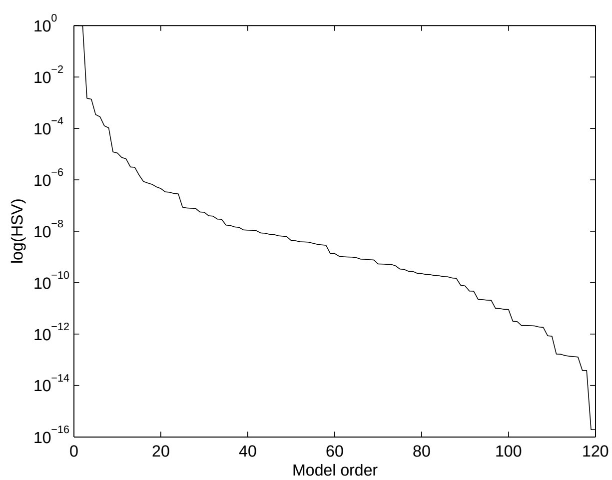

Figure 3.5: Hankel singular values (logarithmic scale) of the higher-order CD player.

one to obtain a good low-order approximation of the high order model. The reduced-order models of order higher than 30 match the full order model at all

Order	H_2 norm	H_∞ norm	H_∞ error bound
50	$2.6558e-007$	$4.1979e-009$	$2.2754e-008$
30	$2.0814e-006$	$3.9388e-008$	$1.7402e-007$
20	$1.5977e-005$	$3.2885e-007$	$1.0221e-006$

Table 3.1: Reduced-order models and error bounds for the CD player.

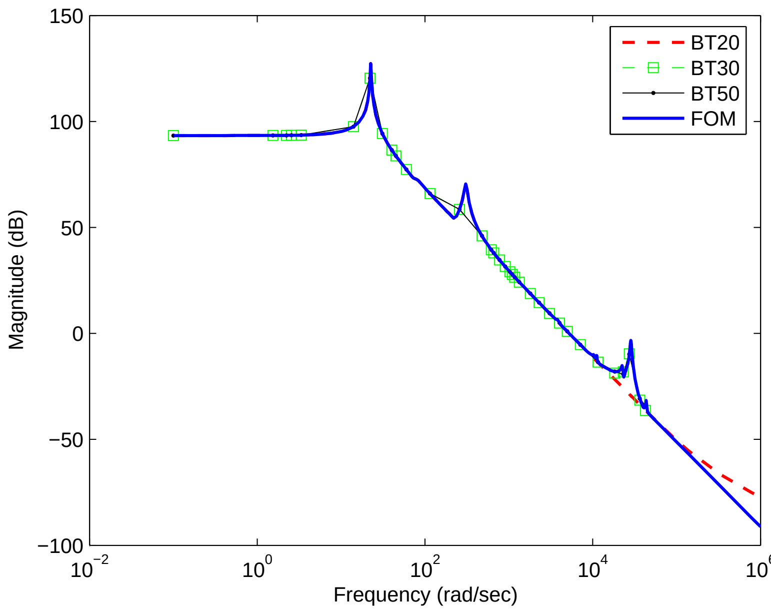

Figure 3.6: Sigma plots of the full-order and reduced-order models.

frequencies of interest. The reduced-order model of size 20 misses a resonant peak between the frequencies 10^4 and 10^5 rad/sec. From the error sigma plots, one can verify that indeed, reduced-order models of order 30 yield low mismatch errors at all frequencies. The reduced-order model of size 20 yields low error except at the resonant peaks of the full-order model.

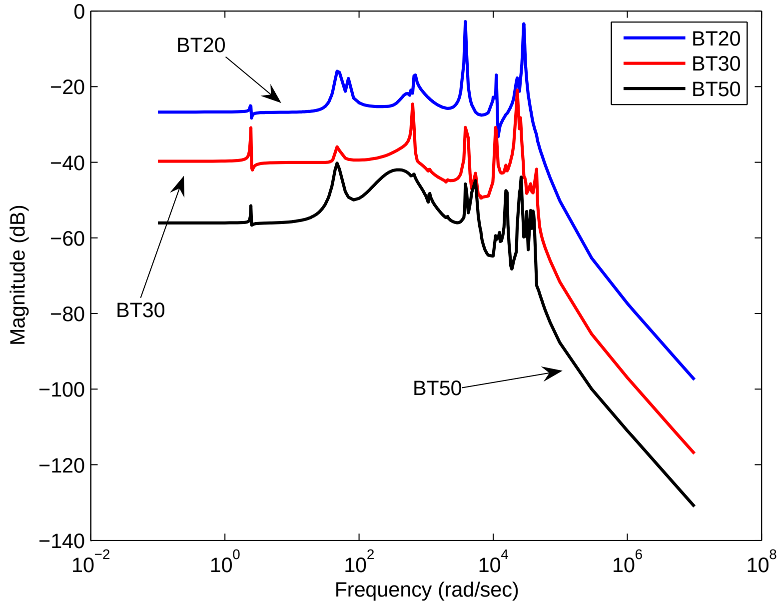

Figure 3.7: Sigma plots of error $(\mathbf{G}(j\omega) - \mathbf{G}_r(j\omega))$ for several reduced-order models.

3.3.2 The Spinning Disks

Consider the well-studied problem of controlling four spinning disks [33, 34, 86], connected by a flexible rod, with torque applied to the third disk, and the angular displacement of the first disk being the control objective. The plant schematic is depicted in Fig. 3.8.

A controller is designed for the full-order model. Consider the controller $\mathbf{K}(s)$ designed by loop shaping $\mathbf{G}(s)\mathbf{K}(s)$. The design specification is given by constraints on the loop gain $|\mathbf{G}(s)\mathbf{K}(s)|$ as shown in Fig. 3.10. For the closed-loop performance specification, a lower bound on the loop gain is assigned.

For robustness against nonstructured uncertainties, an upper bound on the loop gain is determined. The high-order controller is obtained using LQG design techniques by means of tuning the weightings for the linear quadratic performance index and covariance matrices of the noise disturbance [86].

In order to compare the controller reduction techniques, a balanced truncation is first used to approximate the full-order model of size $n = 8$ with a lower-order model. The frequency response of the full-order model is depicted in Fig. 3.9 together with a fourth-order reduced order model. Using the same controller specifications as for the full-order model, a low-order controller is designed based on the fourth-order model.

The closed loop system is then considered for the controller reduction process. A reduction is carried out on the controller by frequency-weighted balanced truncation considering the frequency weighted index $J = \|(\mathbf{K}(s) - \mathbf{K}_r(s))\mathbf{G}(s)(\mathbf{I} + \mathbf{GK}(s))^{-1}\|$ where $\mathbf{K}(s)$ is the high-order controller designed for the original plant. The results are compared in Fig. 3.10.

As can be seen in Figures 3.9 and 3.10, controller reduction in a closed-loop framework using frequency weighted balanced truncation outperforms the design of low-order controllers using low-order models, i.e, open-loop controller reduction. Even though both designs match well the full-order loop gain in the low frequency region, they violate the high-frequency constraint around 1.5 rad/s. In this case, one can fine tune the weights of the controller design in order to achieve good robustness properties. It was observed that in both cases, the reduced-order controller stabilizes the full-order system.

In this example, the one-sided frequency weighted controller reduction was used. However, one can work with a two-sided frequency weighted as shown in Eqs. (3.24) and (3.26) in order to guarantee similar performance of the reduced-order system and the full-order closed-loop system. The results with the fourth-order controller in this case are almost the same as those with the one-sided frequency weighted approach.

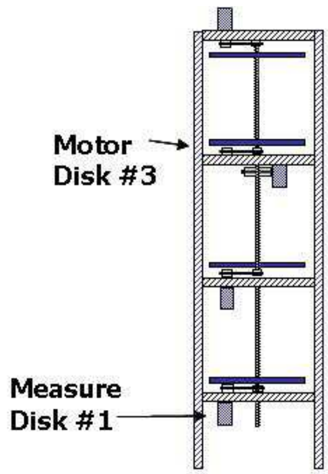

Figure 3.8: Model of the spinning disks.

3.4 Concluding Remarks

This chapter introduced model and controller reduction by balanced truncation methods. It was shown that good reduced-order models can be achieved and that error bounds can be computed using Lyapunov balanced truncation. Also, frequency-weighted balanced truncation was introduced in order to approximate the low-order model at specific frequencies. The con-

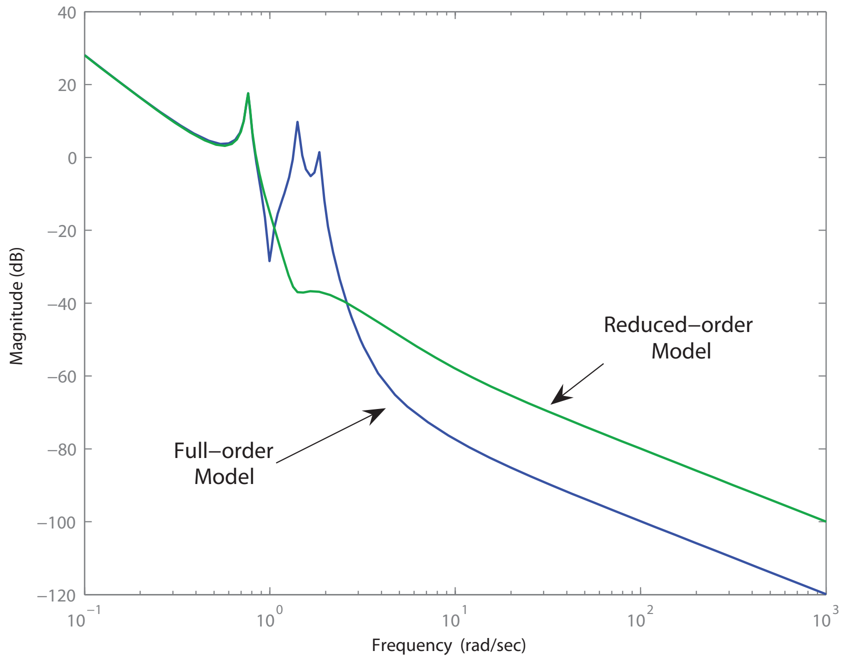

Figure 3.9: Comparison of the frequency response of the full order model and a reduced order model.

troller reduction problem was posed as a frequency-weighted controller reduction, where weights were chosen to take into account the system closed-loop behavior. It was shown that good low-order controllers can be obtained by balancing methods. However, using frequency-weighted balanced truncation, one loses the important issue of stability of the closed-loop system, i.e, the reduced-order controller is not guaranteed to stabilize the full-order model.

Despite the nice system theoretical properties, such as stability and error bounds, and the computational improvements of the balanced system, the

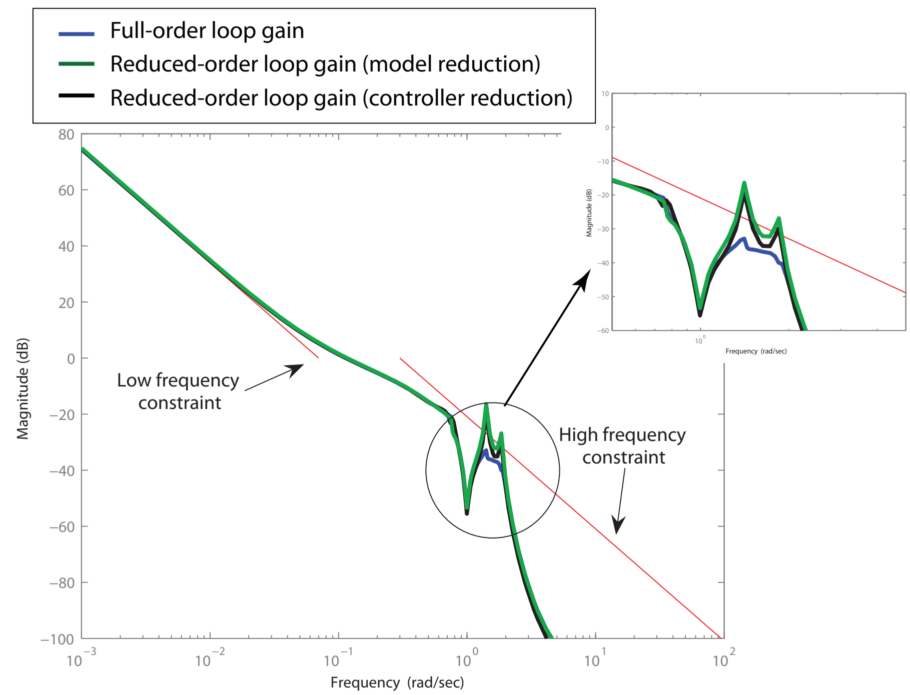

Figure 3.10: Loop gain design constraint.

SVD-based methods become expensive and impractical for large-scale system. They require dense matrix factorizations, yielding computational costs of order $\mathcal{O}(n^3)$ and storage requirements of order $\mathcal{O}(n^2)$. This is mainly due to the need to solve two large-scale Lyapunov or Riccati equations in order to compute the required system gramians. In the next chapter, the notion model reduction by moment matching is introduced. It will be shown that model and controller reduction for large-scale systems can be achieved using efficient algorithms.

Chapter 4

Krylov-Based Model Reduction

SVD-based methods are not suitable for large-scale systems due to the use of dense matrix factorizations of $\mathcal{O}(n^3)$ and storage of $\mathcal{O}(n^2)$. As an alternative, model reduction techniques that rely on matrix-vector multiplication and that can be implemented iteratively in a numerically efficient manner become good choices for large-scale systems. Krylov subspace techniques provide this alternative [8].

The key ingredient of Krylov-based methods is *moment matching*. The idea is to match moments of the original higher-order model $\mathbf{\Sigma} = \left[\begin{array}{c|c} \mathbf{A} & \mathbf{B} \\ \hline \mathbf{C} & \mathbf{D} \end{array}\right]$, by the moments of a lower-order model. This is achieved by iteratively constructing matrices that span certain (generalized) Krylov subspaces of $\mathbf{A}$ and $\mathbf{B}$ (controllability susbspace) and/or $\mathbf{A}^T$ and $\mathbf{C}^T$ (observability subspace).

This chapter begins by introducing the notion of moments of a dynamical system and their relation to model reduction. Then, two important algorithms for moment matching, Arnoldi and Lanczos procedures, which are suitable for single interpolation point, are examined. Also, a generalization of the multi-point rational interpolation will be given and the Rational Krylov (Arnoldi) algorithm for SISO systems will be explored. As will be seen, some modifications are required for applications to MIMO systems. Finally, the problem of closed-loop controller reduction using Krylov techniques will be presented. Numerical examples follow to illustrate moment matching at different frequencies and its relation to the reduced-order model behavior.

4.1 System Representation and Moments

In order to describe the general form of model reduction, it is assumed that the original system is described by the SISO generalized (descriptor) state-space equations

$$\mathbf{E}\dot{\mathbf{x}}(t) = \mathbf{A}\mathbf{x}(t) + \mathbf{B}u(t) \tag{4.1}$$

$$y(t) = \mathbf{C}\mathbf{x}(t) + \mathbf{D}u(t) \tag{4.2}$$

where $\mathbf{E}, \mathbf{A} \in \mathbb{R}^{n\times n}$, $\mathbf{B} \in \mathbb{R}^{n\times 1}$, $\mathbf{C} \in \mathbb{R}^{1\times n}$, and $\mathbf{D}$ is a scalar. Also, as in the case of large-scale problems, it is assumed that the system matrix $\mathbf{A}$ and the descriptor matrix $\mathbf{E}$ are large, sparse and nonsingular. Without loss of generality, the system given by Eq. (4.1) and (4.2) will be assumed to be strictly proper, i.e, the feedforward term $\mathbf{D}$ is assumed to be zero.

The model reduction problem is the one that finds a reduced-order approximation to Eq. (4.1) and (4.2) in the form

$$\mathbf{E}_r\dot{\mathbf{x}}_r(t) = \mathbf{A}_r\mathbf{x}_r(t) + \mathbf{B}_r u(t) \tag{4.3}$$

$$y_r(t) = \mathbf{C}_r\mathbf{x}_r(t) \tag{4.4}$$

where the dimension of the reduced-order model is $r \ll n$, and the behavior of the reduced-order system approximates the original model in certain aspects with the desired accuracy. A good approximation would require the output $y_r(t)$ to be a good representation of the true output $y(t)$ for all inputs $u(t)$. Therefore, a good measure of the accuracy of the approximation could be evaluated in terms of a system norm, in which one tries to bound the $\mathcal{H}_\infty$ or $\mathcal{H}_2$ norms of the difference $y(t) - y_r(t)$. Another method for evaluating the accuracy of the approximation takes into account the assessment of which properties of the original model are preserved in the reduction process (invariant properties). This will be important for controller design, where one has to guarantee stability of the reduced-order closed-loop system.

Model reduction by Krylov techniques is not based on minimization, as with the SVD-based reduction methods. Instead Krylov techniques are based on moment matching, where one attempts to match the coefficients of a power series expansion of the transfer function for the original and reduced-order models. The definition of moments is as follows:

Definition 4.1.1. Given the transfer function of the original and reduced-order systems, respectively

$$G(s) = \mathbf{C}\left(s\mathbf{E} - \mathbf{A}\right)^{-1}\mathbf{B}; \quad G_r(s) = \mathbf{C}_r\left(s\mathbf{E}_r - \mathbf{A}_r\right)^{-1}\mathbf{B}_r, \tag{4.5}$$

if the transfer functions in Eq. 4.5 are expanded in a Laurent series around a given point in the complex plane, $\sigma \in \mathbb{C}$, then

$$\begin{aligned} G(s) &= \mathbf{C}\left(s\mathbf{E}-\mathbf{A}\right)^{-1}\mathbf{B} = \mathbf{C}\left(s\mathbf{E}+\sigma\mathbf{E}-\sigma\mathbf{E}-\mathbf{A}\right)^{-1}\mathbf{B} \\ &= \mathbf{C}\left(\mathbf{I}-(\sigma\mathbf{E}-\mathbf{A})^{-1}\mathbf{E}(\sigma-s)\right)^{-1}(\sigma\mathbf{E}-\mathbf{A})^{-1}\mathbf{B} \\ &= m_o + m_1(\sigma-s) + m_2(\sigma-s)^2 + m_3(\sigma-s)^3 + \cdots \\ &= \sum_{i=0}^{\infty} m_i(\sigma-s)^i. \end{aligned} \tag{4.6}$$

The coefficients denoted by m_i are called *moments* of the system at a point σ. It can be shown that the moments of the system are the values of the transfer function and its derivatives evaluated at the expansion point σ [8]. Similarly, one obtains the moments of the reduced-order model as m_{r_i}.

The main idea of model-order reduction by moment matching is to match a given number of moments as

$$m_i = m_{r_i}, \quad i = 1\cdots, l, \qquad \text{and} \quad l \ll n,$$

of the original and reduced-order transfer functions.

Several special cases of the moments can be determined depending on the location of the expansion points in the complex plane. In the case of $\sigma = \infty$, the moments are the well-known Markov parameters of the system. Assuming $\mathbf{E}$ to be nonsingular, the expansion of Eq. (4.5) around $\sigma = \infty$ is obtained as in Eq. 4.6 using the Laurent series expansion of the transfer function:

$$G(s) = \mathbf{C}\mathbf{E}^{-1}\mathbf{B}s^{-1} + \mathbf{C}\left(\mathbf{E}^{-1}\mathbf{A}\right)\mathbf{E}^{-1}\mathbf{B}s^{-2} + \cdots + \mathbf{C}\left(\mathbf{E}^{-1}\mathbf{A}\right)^{i-1}\mathbf{E}^{-1}\mathbf{B}s^{-i}\cdots \tag{4.7}$$

yielding the Markov parameters $m_i = \mathbf{C}\left(\mathbf{E}^{-1}\mathbf{A}\right)^{i-1}\mathbf{E}^{-1}\mathbf{B}$. The Markov parameters represent the values of the zero-state impulse response, or transfer function $\mathbf{G}(s)$, and subsequent derivatives of the impulse response at $t = 0$. Since matching the Markov parameters emphasizes the behavior at $t = 0$, the reduced-order model may be dominated by rapid decaying dynamics, not representing accurately the behavior at later time. In the frequency domain, once can show good matching of the frequency response of the system at high frequencies.

A power series expansion can also be performed about $\sigma = 0$. By assuming $\mathbf{A}$ is nonsingular, one has

$$G(s) = -\mathbf{C}\mathbf{A}^{-1}\mathbf{B} - \mathbf{C}\left(\mathbf{A}^{-1}\mathbf{E}\right)\mathbf{A}^{-1}\mathbf{B}s - \cdots - \mathbf{C}\left(\mathbf{A}^{-1}\mathbf{E}\right)^{i-1}\mathbf{A}^{-1}\mathbf{B}s^{i-1}\cdots \tag{4.8}$$

and thus, the moments are given by $m_{i-1} = -\mathbf{C}\left(\mathbf{A}^{-1}\mathbf{E}\right)^{i-1}\mathbf{A}^{-1}\mathbf{B}$, and the reduced-order model whose moments match the original moments up to $2r$, where r is the order of the reduced-order model, is known as *Padé* approximation. In this case, since moments are being matched at $\sigma = 0$, the reduced-order model will be a good approximation to the steady-state response of the original system.

In general, one may be interested in matching moments at a particular frequency, σ. By replacing s in the expansion in Eq. (4.6) with the shifted variable $s - \sigma$ yields

$$G(s) = \sum_{i=1}^{\infty} (s - \sigma)^{i-1} m_{i-1},$$

producing the shifted moments $m_{i-1} = -\mathbf{C}\left\{(\sigma\mathbf{E}-\mathbf{A})^{-1}\mathbf{E}\right\}^{i-1}(\sigma\mathbf{E}-\mathbf{A})^{-1}\mathbf{B}$. Beyond single-point moment matching, one may be interested in matching the moments of the transfer function at selected frequencies, i.e., one may be interested in a reduced-order model that interpolates the frequency response and its derivatives at multiple points $\{\sigma_1, \sigma_2, \ldots, \sigma_k\}$. This is called rational interpolation and will be explored in Section 4.3. As a summary, Table 4.1 is constructed based on Eq. (4.6).

Frequency to be Approximated	Power Series Expansion of the TF	i^{th} Moment
About $\sigma = \infty$ Partial Realization	$\sum_{i=1}^{\infty} m_{-i}s^{-i}$	$\mathbf{C}\left(\mathbf{E}^{-1}\mathbf{A}\right)^{i-1}\mathbf{E}^{-1}\mathbf{B}$
About $\sigma = 0$ or Padé	$\sum_{i=1}^{\infty} m_{i-1}s^{i-1}$	$-\mathbf{C}\left(\mathbf{A}^{-1}\mathbf{E}\right)^{i-1}\mathbf{A}^{-1}\mathbf{B}$
About $s = \sigma$ or Shifted Padé	$\sum_{i=1}^{\infty} m_{i-1}(s-\sigma)^{i-1}$	$\mathbf{C}\left\{(\sigma\mathbf{E}-\mathbf{A})^{-1}\mathbf{E}\right\}^{i-1}\times$ $\times(\sigma\mathbf{E}-\mathbf{A})^{-1}\mathbf{B}$

Table 4.1: Expansions and moments to be matched.

4.2 Approximations by Moment Matching

A straightforward approach to constructing reduced-order models can be obtained by explicitly computing $2r$ moments of the original system as in Table 4.1, where r is the size of the reduced-order model. Then, the frequency response of the reduced-order system is forced to correspond to the selected moments. This can be viewed as a selection of the coefficients for the numerator and denominator of the reduced-order transfer function through the solution of a linear system involving Hankel matrices. Unfortunately, numerical drawbacks of the explicit moment-matching can occur, such as ill-conditioned Hankel matrices, sensitivity of the partial realization, moment scaling, and the stability of the approximation [36].

Numerically reliable algorithms have been reported in the literature for moment matching without explicit moment computations [48]. The main Krylov subspace methods for nonsymmetric problems, that is when $\mathbf{A}, \mathbf{E}$ are nonsymmetric, rely on the Arnoldi algorithm and the nonsymmetric Lanczos algorithm. While the Arnoldi algorithm constructs an orthonormal base for a Krylov subspace of dimension r, leading to an $r \times r$ Hessenberg matrix, the nonsymmetric Lanczos algorithms constructs biorthogonal bases for two Krylov subspaces, resulting in a $r \times r$ tridiagonal matrix. One of the first connections between the Lanczos algorithm and model reduction was shown in [43].

In this section, the Lanczos and Arnoldi algorithms will be derived in a system-theoretical framework [8] and its numerical algorithms will be given. Without loss of generality, it will be assumed that $\mathbf{E} = \mathbf{I}$.

4.2.1 Lanczos and Arnoldi Methods

Recall the definitions of the controllability and observability matrices, given in Chapter 2. Based on the moments expansion as in Eq. (4.6), one can define the Hankel matrix $\mathcal{H}_k$ and the shifted Hankel matrix $\sigma\mathcal{H}_k$, respectively, as:

$$\mathcal{H}_k = \begin{bmatrix} m_1 & m_2 & \cdots & m_k \\ m_2 & m_3 & \cdots & m_{k+1} \\ \vdots & & \ddots & \\ m_k & m_{k+1} & \cdots & m_{2k-1} \end{bmatrix}, \ \sigma\mathcal{H}_k = \begin{bmatrix} m_2 & m_3 & \cdots & m_{k+1} \\ m_3 & m_4 & \cdots & m_{k+2} \\ \vdots & & \ddots & \\ m_{k+1} & m_{k+2} & \cdots & m_{2k} \end{bmatrix} \tag{4.9}$$

It can be shown that [17], $\mathcal{H}_k = \mathcal{O}_k\mathcal{R}_k$ and $\sigma\mathcal{H}_k = \mathcal{O}_k\mathbf{A}\mathcal{R}_k$.

4.2.1.1 Lanczos Method

For the Lanczos procedure, assuming that $\det(\mathcal{H}_i) \neq 0, i = 1, \cdots, k$, the LU factorization of $\mathcal{H}_k$ can be computed as

$$\mathcal{H}_k = \mathbf{LU},\ \mathbf{L}(i,j) = 0, i < j \text{ and } \mathbf{U}(i,j) = 0, i > j, \tag{4.10}$$

where $\mathbf{L}$ and $\mathbf{U}$ can be chosen such that

$$\mathbf{L}(i,i) = \pm\mathbf{U}(i,i).$$

Define the maps:

$$\mathbf{W}^T := \mathbf{L}^{-1}\mathcal{O}_k \text{ and } \mathbf{V} := \mathcal{R}_k\mathbf{U}^{-1}.$$

With the definitions of $\mathbf{V}$ and $\mathbf{W}$, it follows that $\mathbf{W}^T\mathbf{V} = \mathbf{I}$. Thus $\mathbf{V}\mathbf{W}^T$ is an oblique projection. Therefore, one can define the reduced-order system $\mathbf{\Sigma}_k$ obtained by projection as:

$$\mathbf{A}_k := \mathbf{W^T A V},\ \mathbf{B_k} := \mathbf{W^T B},\ \mathbf{C}_k := \mathbf{CV}. \tag{4.11}$$

The following theorem holds:

Theorem 4.2.1 (Lanczos Procedure)**.** *Given the full-order model as in Eq. (4.5), the reduced-order model* $\mathbf{\Sigma}_k$ *defined as above matches* $2k$ *Markov parameters, i.e,* $\mathbf{C}\mathbf{A}^{i-1}\mathbf{B} = \mathbf{C}_k\mathbf{A}_k^{i-1}\mathbf{B}_k$*, for* $i = 1, \cdots, 2k$*. Furthermore,* $\mathbf{A}_k$ *is tridiagonal, and* $\mathbf{B}_k, \mathbf{C}_k^T$ *are multiples of the unit vector* $\mathbf{e}_1$*, where* $\mathbf{e}_1$ *is a vector of one at the position* 1 *and zeros elsewhere.*

Proof. The complete proof is found in [8] □

4.2.1.2 The Non-Symmetric Lanczos Algorithm

The Lanczos algorithm was originally proposed by Lanczos [75] as a method for computation of eigenvalues of symmetric and nonsymmetric matrices. The algorithm can also be used to construct all of the subspaces associated with the controllability and observability decomposition of a system [15]. The nonsymmetric Lanczos algorithm presented here follows [8] and references therein.

Consider a model as in Eq. (4.1) and (4.2) with $\mathbf{E} = \mathbf{I}$ and $\mathbf{D} = \mathbf{0}$. Also, assume that $\mathbf{A}$ is of large dimension and sparse. The algorithm depicted in Table 4.2 can be employed to determine the projection matrices $\mathbf{V}_k$ and $\mathbf{W}_k$. In this case, the following relationships hold:

$$\mathbf{V}_m = \begin{pmatrix} \mathbf{v}_1 & \mathbf{v}_2 & \cdots & \mathbf{v}_m \end{pmatrix} \tag{4.12}$$

$$\mathbf{W}_m = \begin{pmatrix} \mathbf{w}_1 & \mathbf{w}_2 & \cdots & \mathbf{w}_m \end{pmatrix} \tag{4.13}$$

$$\mathbf{A}\mathbf{V}_m = \mathbf{V}_m\mathbf{A}_m + \tilde{\mathbf{v}}_{m+1}\tilde{\mathbf{a}}_{mV}^T, \quad \mathbf{B} = \mathbf{V}_m\mathbf{B}_m \tag{4.14}$$

$$\mathbf{A}^T\mathbf{W}_m = \mathbf{W}_m\mathbf{A}_m^T + \tilde{\mathbf{w}}_{m+1}\tilde{\mathbf{a}}_{mW}^T, \quad \mathbf{C} = \mathbf{W}_m\mathbf{C}_m \tag{4.15}$$

1. $\beta_1 = \sqrt{\mathbf{C}^T\mathbf{B}}; \quad \delta_1 = \beta_1 \cdot sign\left(\mathbf{C}^T\mathbf{B}\right);$

2. $\mathbf{v}_1 = \mathbf{B}/\delta_1; \mathbf{w}_1 = \mathbf{C}/\beta_1; \mathbf{v}_0 = 0; \mathbf{w}_0 = 0;$

3. **for** $j = 1$ **to** m

   $\alpha_j = \mathbf{w}_j^T\mathbf{A}\mathbf{v}_j;$

   $\hat{\mathbf{v}}_{j+1} = \mathbf{A}\mathbf{v}_j - \alpha_j\mathbf{v}_j - \beta_j\mathbf{v}_{j-1}; \hat{\mathbf{v}}_{j+1} = \hat{\mathbf{v}}_{j+1} - \mathbf{V}_j\left(\mathbf{W}_j^T\hat{\mathbf{v}}_{j+1}\right)$

   $\hat{\mathbf{w}}_{j+1} = \mathbf{A}^T\mathbf{w}_j - \alpha_j\mathbf{w}_j - \delta_j\mathbf{w}_{j-1}; \hat{\mathbf{w}}_{j+1} = \hat{\mathbf{w}}_{j+1} - \mathbf{W}_j\left(\mathbf{V}_j^T\hat{\mathbf{w}}_{j+1}\right)$

   $\beta_{j+1} = \sqrt{\left|\hat{\mathbf{w}}_{j+1}^T\hat{\mathbf{v}}_{j+1}\right|}$

   if $\beta_{j+1} \le \epsilon$

   stop

   end

4. $\delta_{j+1} = \beta_{j+1} \cdot sign\left(\hat{\mathbf{w}}_{j+1}^T\hat{\mathbf{v}}_{j+1}\right)$

5. $\mathbf{v}_{j+1} = \hat{\mathbf{v}}_{j+1}/\delta_{j+1}; \mathbf{w}_{j+1} = \hat{\mathbf{w}}_{j+1}/\beta_{j+1}$

Table 4.2: The non-symmetric Lanczos algorithm.

$$\mathbf{A}_m = \mathbf{W}_m^T\mathbf{A}\mathbf{V}_m = \begin{bmatrix} \alpha_1 & \beta_2 & & 0 \\ \delta_2 & \alpha_2 & \ddots & \\ & \ddots & \ddots & \beta_m \\ 0 & & \delta_m & \alpha_m \end{bmatrix} \in \mathbb{R}^{m\times m} \tag{4.16}$$

and

$$\tilde{\mathbf{a}}_{mV}^T = \delta_{m+1}\mathbf{e}_m^T, \quad \mathbf{B}_m = \mathbf{e}_1\delta_1, \tag{4.17}$$

$$\tilde{\mathbf{a}}_{mW}^T = \beta_{m+1}\mathbf{e}_m^T, \quad \mathbf{C}_m = \mathbf{e}_1\beta_1, \tag{4.18}$$

where the vector $\mathbf{e}_i$ denotes the i^{th} unit vector. In a pictorial manner, the algorithm can be depicted in Fig. 4.1.

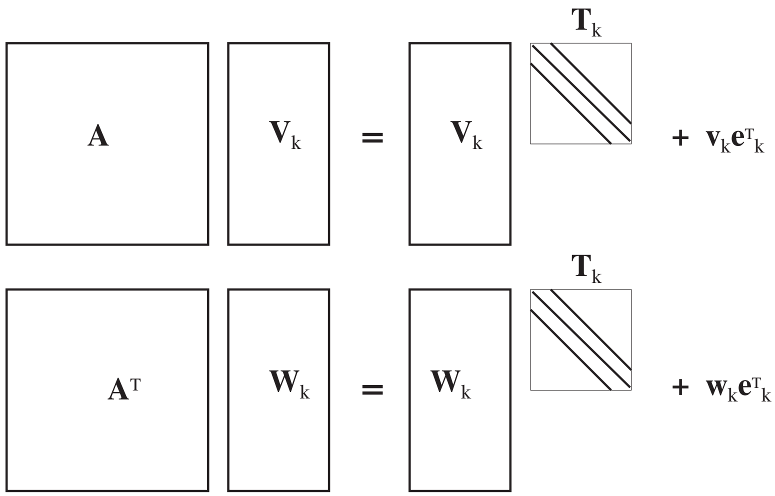

Figure 4.1: The kth step of the Lanczos algorithm.

4.2.1.3 Arnoldi Procedure

As in the Lanczos procedure, the Arnoldi procedure can be developed as follows: Let the controllability matrix of $G(s)$ in Eq. (4.5) be given as in Eq. (2.7). Then, one can write

$$\mathbf{A}\mathcal{R}_k = \mathcal{R}_k\mathbf{F}, \text{where } \mathbf{F} = \begin{bmatrix} 0 & 0 & \cdots & 0 & -\alpha_0 \\ 1 & 0 & \cdots & 0 & -\alpha_1 \\ 0 & 1 & \cdots & 0 & -\alpha_2 \\ & & \ddots & & \\ 0 & 0 & \cdots & 1 & -\alpha_{k-1} \end{bmatrix} \tag{4.19}$$

and $\chi_A(s) = \det(s\mathbf{I} - \mathbf{A}) = s^n + \alpha_{n-1}s^{n-1} + \cdots + \alpha_1 s + \alpha_0$ is the characteristic polynomial of $\mathbf{A}$. Unlike the computation of a LU factorization of $\mathcal{H}_k$ in the Lanczos algorithm, the core of the Arnoldi algorithm is the computation of the QR factorization of $\mathcal{R}_k$ as

$$\mathcal{R}_k = \mathbf{W}\mathbf{R}_A \tag{4.20}$$

where $\mathbf{W}$ is orthogonal and $\mathbf{R}_A$ is upper triangular. Using Eq. (4.19), one can write

$$\mathbf{AWR}_A = \mathbf{WR}_A\mathbf{F} \Rightarrow \mathbf{AW} = \mathbf{WR}_A\mathbf{FR}_A^{-1} \Rightarrow \mathbf{AW} = \mathbf{W\bar{F}}$$

where $\mathbf{\bar{F}} = \mathbf{R}_A\mathbf{FR}_A^{-1}$. Since $\mathbf{R}_A$ and $\mathbf{R}_A^{-1}$ are upper triangular, $\mathbf{\bar{F}}$ is *upper Hessenberg*. Consequently the projection can be formed, recalling that $\mathcal{H}_k = \mathcal{O}_k\mathcal{R}_k$, and defining the map $\mathbf{V}$ based of the QR factorization of $\mathcal{R}_k$ as:

$$\mathbf{V} = \mathcal{R}_k\mathbf{R}_A^{-1} \in \mathbb{R}^{n\times k}, \tag{4.21}$$

where $\mathbf{V}^T\mathbf{V} = \mathbf{I}_k$ and $\mathbf{R}_A$ is upper triangular. Then $\mathbf{VV}^T$ is an orthogonal projection. Therefore, the reduced order system $\mathbf{\Sigma}_k$ is defined as:

$$\mathbf{A}_k := \mathbf{V^TAV},\ \mathbf{B}_k := \mathbf{V^TB},\ \mathbf{C}_k := \mathbf{CV}. \tag{4.22}$$

The following theorem summarizes the results:

Theorem 4.2.2. *Given the full-order model as in Eq. (4.5), the reduced-order model $\mathbf{\Sigma}_k$ defined as above matches k Markov parameters, i.e, $\mathbf{CA}^{i-1}\mathbf{B} = \mathbf{C}_k\mathbf{A}_k^{i-1}\mathbf{B}_k$, for $i = 1,\cdots,k$. Furthermore, $\mathbf{A}_k$ is upper Hessenberg, and $\mathbf{B}_k, \mathbf{C}_k^T$ are multiples of the unit vector $\mathbf{e}_1$, where $\mathbf{e}_1$ is a vector of one at the position 1 and zeros elsewhere.*

Proof. The complete proof is found in [8] □

4.2.1.4 The Arnoldi Algorithm

The Arnoldi method [10] was introduced as a means of reducing a dense matrix into Hessenberg form. The standard Arnoldi algorithm, in exact arithmetic, is given by the algorithm depicted in Table 4.3 for the single-input, single-output case.

---

1. Set $\mathbf{v}_1 = \frac{\mathbf{B}}{\|\mathbf{B}\|}$
2. **for** $j = 1, 2, \ldots k$
   (a) Compute $h_{ij} = \mathbf{v}_i^T \mathbf{A} \mathbf{v}_j$, for $i = 1, 2, \ldots j$
   (b) $\mathbf{w}_j = \mathbf{A}\mathbf{v}_j - \sum_{i=1}^{j} h_{ij} \mathbf{v}_i$
   (c) $h_{j+1,j} = \|\mathbf{w}_j\|_2$
   (d) **If** $h_{j+1,j} = 0$ **Stop**
   (e) $\mathbf{v}_{j+1} = \mathbf{w}_j / h_{j+1,j}$
3. **end**

Table 4.3: The Arnoldi algorithm.

At each step, the algorithm multiplies the previous Arnoldi vector $\mathbf{v}_j$ by $\mathbf{A}$ and then orthonormalizes the resulting vector $\mathbf{w}_j$ against all previous $\mathbf{v}_j$'s by standard Gram-Schmidt orthogonalization. However, in practice, the more stable Modified Gram-Schmidt algorithm [41, 98] is used. For each step of the Arnoldi algorithm, the following relationship holds

$$\mathbf{A}\mathbf{V}_k = \mathbf{V}_k \mathbf{H}_k + \mathbf{w}_k \mathbf{e}_k^T, \tag{4.23}$$

where

$$\mathbf{H}_k = \mathbf{V}_k^T \mathbf{A} \mathbf{V}_k = \begin{bmatrix} h_{11} & h_{12} & h_{13} & \cdots & h_{1k} \\ h_{21} & h_{22} & h_{23} & \cdots & h_{2k} \\ & \ddots & \ddots & \ddots & \vdots \\ & & h_{k-1,k-2} & h_{k-1,k-1} & h_{k-1,k} \\ & \mathbf{0} & & h_{k,k-1} & h_{kk} \end{bmatrix} \in \mathbb{R}^{k \times k} \tag{4.24}$$

and $\mathbf{e}_k$ denotes the k^{th} unit vector and $\mathbf{V}_k^T\mathbf{V}_k = \mathbf{I}_k$. Schematically, the Arnoldi steps can be illustrated as shown in Fig. 4.2.

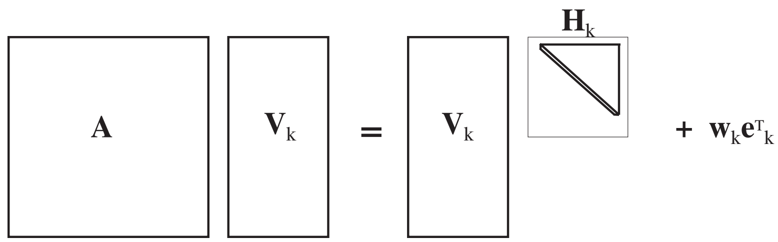

Figure 4.2: The kth step of the Arnoldi algorithm.

Remarks: **(a)** The above procedures apply in the same manner for descriptor systems;

(b) Due to the fact that in the Lanczos procedure, two-sided oblique projection is employed, the reduced-order model obtained by k steps of the Lanczos Algorithm matches $2k$ Markov parameters, whereas, using a one-side orthogonal projection in the Arnoldi Algorithm, one matches only k Markov parameters.

(c) One of the disadvantages of the Lanczos and Arnoldi procedures is the possibility of the algorithm breakdown. In exact arithmetic, Lanczos breaks down if $\det \mathcal{H}_i = 0$, for some $1 \leq i \leq n$. The breakdown occurs because the tridiagonal structure is forced in the reduced-order model. However, one can match $2k$ Markov parameters without the condition $\det \mathcal{H}_i \neq 0$, for $i = 1, \cdots, k$ and therefore this restriction is not required for model reduction. Arnoldi breaks down if $\mathcal{R}_i$, for some $1 \leq i \leq n$, does not have full rank;

However this restriction is not necessary for model reduction, as long as $\mathbf{V}$ has full rank.

(d) Unlike the SVD methods of Chapter 3, the reduced-order model obtained from Arnoldi or Lanczos algorithms might not be stable for a stable full-order model. The remedy is *the implicit restart* of Lanczos and Arnoldi proposed by Sorensen [47, 102]. However, there will be a trade-off between guaranteed stability and exact moment matching.

(e) In general, for matching moments at arbitrary interpolation points $\sigma_i \in \mathbb{C}$, the problem can be solved using *rational interpolation* which will be discussed in detail in the next sections.

4.3 Multi-point Rational Interpolation

Recall the definitions of moments at a point $s = \sigma$, and the concepts of the (generalized) reachability and observability matrices. In the case of moment matching at several points in the complex plane, one can use the Rational Krylov algorithm. The following theorem is presented in [48] for the SISO case. It shows how to construct the projection matrices $\mathbf{V}$ and $\mathbf{W}$, in a numerically efficient way so that multi-point rational interpolation is solved by extending the concepts of Krylov subspaces to the generalized controllability and observability matrices [8].

Theorem 4.3.1. *If*

$$\bigcup_{k=1}^{K} \mathcal{K}_{b_k}\left((\sigma_k \mathbf{I} - \mathbf{A})^{-1}, (\sigma_k \mathbf{I} - \mathbf{A})^{-1}\mathbf{B}\right) \subseteq \mathcal{V} = Im(\mathbf{V}) \tag{4.25}$$

and

$$\bigcup_{k=1}^{K} \mathcal{K}_{c_k}\left((\sigma_k \mathbf{I}-\mathbf{A})^{-T}, ((\sigma_k \mathbf{I}-\mathbf{A})^{-T}\mathbf{C}^T\right) \subseteq \mathbf{W} = Im(\mathbf{W}) \tag{4.26}$$

where $\mathbf{W}^T\mathbf{V} = \mathbf{I}$ *and* σ_k *are chosen such that the matrices* $\sigma_k\mathbf{I}-\mathbf{A}$ *are invertible* $\forall k \in \{1, \cdots, K\}$*, then the moments of* $\mathbf{\Sigma}$ *and* $\hat{\mathbf{\Sigma}}$ *satisfy*

$$\eta_{\sigma_k}^{(j_k)} = \hat{\eta}_{\sigma_k}^{(j_k)},\ for\, j_k = 0, 1, 2, \cdots, b_k + c_k - 1 \quad and \quad k = 1, 2, \cdots, K \tag{4.27}$$

provided the matrices $\sigma_k\mathbf{I} - \mathbf{A}_r$ *are invertible.*

Remarks:

1. Theorem 4.3.1 states that for moment-matching, one has to construct full-rank matrices $\mathbf{V}$ and $\mathbf{W}$ with $Im(\mathbf{V})$ and $Im(\mathbf{W})$ satisfying Eq. (4.25) and (4.26), respectively.

2. Several algorithms have been implemented in the literature (see [48] and referenced therein): Lanczos algorithm and Arnodi algorithm and its variants. In general, they follow the Rational Krylov methods of [94]. As pointed out before, they can suffer from numerical breakdowns as well. A reliable implementation of the Arnoldi algorithm is give in the next section.

4.3.1 The Dual Rational Arnoldi for SISO Systems

The best way to avoid the numerical breakdowns in the construction of $\mathbf{V}$ and $\mathbf{W}$ is to construct them as orthogonal matrices. A simple, yet

1. Initialize parameters: $\rightarrow m = 0$;
   $\mathbf{V} = [\,]$; $\mathbf{Z} = [\,]$

2. **for** $j = 1, \cdots, J$

   (a) **for** $k = 1, \cdots, K$

      i. **If** $j = 1$

      $$\tilde{\mathbf{v}}_m = (\mathbf{A} - \sigma_k \mathbf{I})^{-1} \mathbf{B}, \; and \; \tilde{\mathbf{z}}_m = (\mathbf{A} - \sigma_k \mathbf{I})^{-T} \mathbf{C}^T;$$

      else

      $$\tilde{\mathbf{v}}_m = (\mathbf{A} - \sigma_k \mathbf{I})^{-1} \mathbf{v}_{m-k}, \; and \; \tilde{\mathbf{z}}_m = (\mathbf{A} - \sigma_k \mathbf{I})^{-T} \mathbf{z}_{m-k};$$

      end

      ii. $\hat{\mathbf{v}}_m = \tilde{\mathbf{v}}_m - \mathbf{V}\mathbf{V}^T \tilde{\mathbf{v}}_m \quad and \quad \hat{\mathbf{z}}_m = \tilde{\mathbf{z}}_m - \mathbf{Z}\mathbf{Z}^T \tilde{\mathbf{z}}_m$;

      iii. $\mathbf{V} = \left[\begin{array}{cc} \mathbf{V} & \hat{\mathbf{v}}_m / \|\hat{\mathbf{v}}_m\| \end{array}\right] \quad and \quad \mathbf{Z} = \left[\begin{array}{cc} \mathbf{Z} & \hat{\mathbf{z}}_m / \|\hat{\mathbf{z}}_m\| \end{array}\right]$;

      iv. $m = m + 1$;

3. $\mathbf{Z} \leftarrow \mathbf{Z} \left(\mathbf{V}^T \mathbf{Z}\right)^{-1}$;

Table 4.4: The Dual Rational Arnoldi algorithm for interpolation points $\sigma_i, i = 1, \cdots, K$ and J *moments* to be matched per point.

reliable, implementation of this method is called *Dual Rational Arnoldi* [48]. In this case, $\mathbf{V}$ and $\mathbf{W}$ are constructed independently using steps of the Arnoldi procedure. The basic algorithm is shown in the Table 4.4.

Remarks:

1. In the multi-input, multi-output (MIMO) case, one cannot be sure that the *block* Krylov space will be of full-rank as for SISO systems. This adds complexity to the algorithm, so that deflation has to occur in the construction of $\mathbf{V}$ and $\mathbf{W}$ in order to achieve linearly independent vectors (or blocks) for the corresponding Krylov subspaces.

2. Extensions of the Arnoldi and Lanczos algorithms for the MIMO case have been proposed in the literature [14, 49]. A neat and clear version of the Arnoldi procedure has been suggested by Boley [14]. In this case, the deflation is achieved by the use of a rank-revealing QR algorithm. This is discussed in the next section.

4.3.2 Rational Krylov Methods for MIMO Systems

As discussed in Section 4.3, in order to solve the multi-point rational interpolation by Krylov techniques, one has to construct *full rank* matrices $\mathbf{V}$ and $\mathbf{W}$ which span the required Krylov subspaces for interpolation points σ_i, for $i = 1, \cdots, K$. In the SISO case, due to the minimality of the system $\mathbf{\Sigma}$, the controllability ($\mathcal{R}_r$) and observability ($\mathcal{O}_r$) are guaranteed to be full-rank, and therefore constructing $\mathbf{V}$ and $\mathbf{W}$ based on the images of the $\mathcal{R}_r$ and $\mathcal{O}_r$ yields the required full-rank Krylov projection. However, for MIMO systems, the construction of a full-rank projection is more difficult since one cannot guarantee generation of linearly independent vectors from the corresponding Krylov subspaces. To overcome this problem in the MIMO case, one has to search for an orthogonal basis for $\mathbf{V}$ and $\mathbf{W}$ by means of *deflating* linearly dependent vectors.

Extensions of both Lanczos and Arnoldi algorithms for the MIMO case have been proposed in the literature [14, 35]. One of the suggestions for the MIMO version of Arnoldi, is the use of a rank-revealing QR algorithm as a deflation technique. This algorithm, introduced by [14] will be further explored.

It is interesting to note, see for instance [49], that deflation in this case has an interpretation as the selection of nice indices for the controllability matrix [7].

4.3.3 The Algorithms for Rational Krylov in the MIMO case

In this section, the construction of the projection matrix $\mathbf{V}$ will be considered. The construction of the dual matrix $\mathbf{W}$ follows similarly. In this manner, the so-called *block-wise construction with deflation* will be used [14, 49]. This algorithm adds, at the i^{th} step, m columns to $\mathbf{V}$ if the i^{th} block has full-rank. Otherwise, the block will be deflated and $m_i < m$ columns will be added to $\mathbf{V}$. The procedure will continue until the required Krylov subspace is spanned or m_i becomes zero.

Consider the LTI system given by Eq. (2.2), and K interpolation points σ_i with multiplicities b_i, where $i \in \{1, \cdots, K\}$. Also consider the following definitions

$$\begin{aligned} \mathbf{F}_i : &= (\sigma_i \mathbf{I} - \mathbf{A})^{-1}, \quad \mathbf{G}_i := (\sigma_i \mathbf{I} - \mathbf{A})^{-1}\mathbf{B} \quad \text{if} \quad \sigma_i \neq \infty \\ \mathbf{F}_i : &= \mathbf{A}, \quad \mathbf{G}_i := \mathbf{B} \qquad\qquad\qquad\qquad\qquad \text{if} \quad \sigma_i = \infty \end{aligned}$$

where for $i = 1, \cdots, K$, let

$$\mathbf{G}_i = \left[\begin{array}{cccc} \mathbf{g}_{i_1} & \mathbf{g}_{i_2} & \cdots & \mathbf{g}_{i_m} \end{array} \right], \quad \mathbf{V}_i = \mathcal{K}_{b_i}\left(\mathbf{F}_i, \mathbf{G}_i\right), \quad \mathbf{V} = \left[\begin{array}{cccc} \mathbf{V}_1 & \mathbf{V}_2 & \cdots & \mathbf{V}_K \end{array} \right]$$

The algorithm in Table 4.3.3 computes a full-rank orthogonal $\mathbf{V}$ such that $Im(\mathbf{V}) = Im(\mathbf{V}_1, \cdots, \mathbf{V}_K)$. It can be shown that, since all $\mathbf{V}_i$'s, for $i = 1, \cdots, K$ satisfy $Im(\mathbf{V}_i) = \mathcal{K}_{b_i}\left(\mathbf{F}_i, \mathbf{G}_i\right)$ by construction, then it is guaranteed that

$$\bigcup_{k=1}^{K} \mathcal{K}_{b_i}\left((\sigma_i \mathbf{I} - \mathbf{A})^{-1}, (\sigma_i \mathbf{I} - \mathbf{A})^{-1}B\right) \subseteq \mathcal{V} = Im(\mathbf{V})$$

and therefore $\mathbf{V}$ is the appropriate choice for the Krylov subspace.

A version of this algorithm, the so-called *vector-wise construction with deflation* has also been proposed in the literature. In this case, the algorithm will add only one column to $\mathbf{V}$ at each step until the required Krylov subspace is spanned. The reader is referred to [35, 49] for details.

4.4 $\mathcal{H}_2$ Expression for the Lanczos procedure (SISO case)

The $\mathcal{H}_2$-norm of a continuous-time system $\mathbf{\Sigma} = \left[\begin{array}{c|c} \mathbf{A} & \mathbf{B} \\ \hline \mathbf{C} & \mathbf{D} \end{array}\right]$ is defined as the $\mathcal{L}_2$-norm of the impulse response in the time-domain, so that

$$\|\mathbf{\Sigma}\|_{\mathcal{H}_2} = \|h(t)\|_{\mathcal{L}_2} \tag{4.28}$$

Using Parseval's theorem and the properties of the trace of a matrix, one obtains

$$\|\mathbf{\Sigma}\|_{\mathcal{H}_2} = \sqrt{trace\,[\mathbf{B}^T \mathcal{Q} \mathbf{B}]} = \sqrt{trace\,[\mathbf{C} \mathcal{P} \mathbf{C}^T]}. \tag{4.29}$$

where $\mathcal{P}$ and $\mathcal{Q}$ are the controllability and observability gramians of $\mathbf{\Sigma}$. Antoulas [8] showed that for a continuous-time system $\mathbf{\Sigma}$, with a stable transfer function $\mathbf{H}(s)$, the following result holds

$$\|\mathbf{\Sigma}\|^2_{\mathcal{H}_2} = \sum_{i=1}^{n} c_i \mathbf{H}(s)^*|_{s=\lambda_i^*} = \sum_{i=1}^{n} c_i \mathbf{H}(-\lambda_i^*)^*|_{s=\lambda_i^*} \tag{4.30}$$

where $\lambda_i, i = 1, \cdots, n$ are distinct poles of $\mathbf{H}(s)$ and c_i is the corresponding residue: $c_i = \mathbf{H}(s)(s - \lambda_i)|_{s=\lambda_i}\, i = 1, \cdots, n$. This result can be generalized

1. **for** $= 1, \cdots, K$

   (a) **if** $\sigma_i \neq \infty$

   $$\mathbf{F}_i = (\sigma_i \mathbf{I} - \mathbf{A})^{-1} \quad and \quad \mathbf{G}_i = (\sigma_i \mathbf{I} - \mathbf{A})^{-1}\mathbf{B}$$

   else

   $$\mathbf{F}_i = \mathbf{A} \qquad and \qquad \mathbf{G}_i = \mathbf{B}$$

   (b) $\mathbf{Q}_0\mathbf{R} = qr(\mathbf{G}_i)$ (*Rank revealing qr decomposition*)

   (c) **For** $k = 1, 2, \cdots, b_k - 1$

      i. $\mathbf{Q}_k = \mathbf{F}_i \mathbf{Q}_{k-1}$

      ii. *Apply Gram-Schmidt to ortogonalize* $\mathbf{Q}_k$ *to previous* $\mathbf{Q}_j'$*s where* $j = 1 : k - 1$

      iii. $\mathbf{Q}_k\mathbf{R} = qr(\mathbf{Q}_k)$ (*Rank revealing qr decomposition*)

      iv. $r_k = rank(\mathbf{Q}_k)$

      v. **if** $r_k \neq 0$

      $$\mathbf{V}_i = [\mathbf{V}_i \quad \mathbf{Q}_k]$$

      else

      $k = b_k - 1$ (*the* k^{th} *block is complete*)

2. **for** $i = 1 : K$ (*If* $\mathbf{V}_i$ *not assumed to be linearly independent*)

   (a) *Apply Gram-Schmidt on* $\{\mathbf{V}1, \cdots, \mathbf{V}_K\}$ *to get* $\mathbf{V}$

3. $\mathbf{V}$ *is the required full-rank projection matrix*

Table 4.5: MIMO Rational Krylov (Arnoldi) with blockwise construction.

for the case of poles with multiplicity greater than one [8]. Inspired by the above results and the work of Antoulas and Sorensen [104], where an exact expression for the $\mathcal{H}_2$ norm of the error system obtained by truncation is presented, Gugercin [51] showed a similar result considering model reduction by the Lanczos process. Consider a system $\mathbf{\Sigma}$ with transfer function $\mathbf{H}(s)$ and the reduced-order model $\mathbf{\Sigma}_r = \hat{\mathbf{H}}(s)$. Let also ϕ_i and $\hat{\phi}$ denote the residues of the transfer function $\mathbf{H}(s)$ and $\hat{\mathbf{H}}(s)$ at λ_i and $\hat{\lambda}_i$ respectively, i.e.,

$$\phi_i = \mathbf{H}(s)(s-\lambda_i)|_{s=\lambda_i}, \; i = 1, \cdots, n \text{ and} \tag{4.31}$$

$$\hat{\phi}_j = \hat{\mathbf{H}}(s)(s-\hat{\lambda}_j)|_{s=\hat{\lambda}_j}, \; j = 1, \cdots, r \tag{4.32}$$

The following lemma holds [51]:

Lemma 4.4.1. Exact expression for the $\mathcal{H}_2$ norm error system. *Let $\mathbf{\Sigma}_r$ be obtained by the r step Lanczos reduction of $\mathbf{\Sigma}$. Then the norm of the error system, defined as, $\mathbf{\Sigma}_e := \mathbf{\Sigma} - \mathbf{\Sigma}_r$ is given by*

$$\|\mathbf{\Sigma}_e\|^2_{\mathcal{H}_2} = \sum_{i=1}^{n} \phi_i \left(\mathbf{H}(-\lambda_i^*) - \hat{\mathbf{H}}(-\lambda_i^*)\right) + \sum_{j=1}^{r} \hat{\phi}_i \left(\hat{\mathbf{H}}(-\hat{\lambda}_j^*) - \mathbf{H}(-\hat{\lambda}_j^*)\right) \tag{4.33}$$

Lemma 4.4.1 shows that the $\mathcal{H}_2$-norm of the error is due to the mismatch of the full-order model and reduced-order model at the mirror images of the full-order poles and reduced-order poles.

Based on the $\mathcal{H}_2$ error analysis, Gugercin and Antoulas [50] proposed to choose as interpolation points (for the SISO case) a subset of the mirror images of the full-order poles, i.e., one can choose

$$\sigma_i = -\lambda_i^*(\mathbf{A}), \tag{4.34}$$

where the subset can be chosen based on the highest residues of the transfer function. By means of an iterative process, Gugercin [53] showed how one can achieve the minimization.

4.5 Rational Krylov for Controller Reduction

Computing a reduced-order controller by simply using an open-loop strategy, such as reducing the controller $\mathbf{K}(s)$ to some $\mathbf{K}_r(s)$ by one of the methods mentioned above, is often not enough to preserve the desired closed-loop performance. The controller reduction problem benefits when the plant dynamics are taken into account. The SVD-methods (presented in Chapter 3) achieve this through frequency weighting. However, this requires solving two large-scale Lyapunov equations on order n_K or $n + n_K$, which becomes a difficult task for large-scale systems.

In order to have a more efficient controller reduction Gugercin, *et al.* [12, 54] proposed to use the Rational Krylov method to reduce the large-scale controller. It was shown that a reduced-order controller, obtained through a rational Krylov model reduction scheme, is *guaranteed* to yield closed-loop behavior which approximates the full-order closed-loop system as described in the following proposition:

Proposition 4.5.1. *[12] For a given plant $\mathbf{G}(s)$ and full-order controller $\mathbf{K}(s)$, let $\mathbf{T}(s)$ denote the full-order closed-loop system as*

$$\mathbf{T}(s) = [\mathbf{I} + \mathbf{G}(s)\mathbf{K}(s)]^{-1}\,\mathbf{G}(s).$$

Given a set of interpolation points $\sigma_k,\ k = 1, \cdots, 2K$, and the number of moments j_k to be matched at each σ_k, let $\mathbf{K}_r(s)$ be the reduced r^{th}-order controller obtained from $\mathbf{K}(s)$ using a Rational Krylov method of Section 4.3. Denote the closed-loop transfer function using the reduced-order controller as $\mathbf{T}_r(s)$, then

$$\mathbf{T}_r(s) = \left[\mathbf{I} + \mathbf{G}(s)\mathbf{K}_r(s)\right]^{-1} \mathbf{G}(s).$$

Therefore, $\mathbf{T}_r(s)$ interpolates the full-order closed-loop system $\mathbf{T}(s)$ and its first $j_k - 1$ derivatives at σ_k for $k = 1, \cdots, 2K$, i.e,

$$\left.\frac{(-1)^j}{j!}\frac{d^j\mathbf{T}(s)}{ds^j}\right|_{s=\sigma_k} = \left.\frac{(-1)^j}{j!}\frac{d^j\mathbf{T}_r(s)}{ds^j}\right|_{s=\sigma_k} \tag{4.35}$$

for $k = 1, \ldots, 2K$ and for $j = 1, \ldots, j_k$.

As with model reduction, the selection of interpolation points is an *ad hoc* procedure. So, for the case of the closed-loop controller reduction, it is suggested to use σ_k from the union of mirror images of the poles of $\mathbf{T}(s)$ and $\mathbf{K}(s)$. Hence this choice is expected to yield a small $\mathcal{H}_2$ error for both error systems $\mathbf{K}(s) - \mathbf{K}_r(s)$ and $\mathbf{T}(s) - \mathbf{T}_r(s)$.

4.6 Numerical Examples

To illustrate the various options of moment matching using the Lanczos Algorithm, two examples used as a benchmark in model reduction are analyzed: (1) the dynamics of portable CD player [110] and (2) the dynamics of the flex modes of the 1R (Russian Service Module) for the International Space Station (ISS) [8].

4.6.1 Model Reduction: The CD Player

The frequency response corresponding to this system is shown as a solid line in Figure 4.3. Based on Figures 3.4 and 3.5, we reduce the order of the full model to $r = 14$. The frequency responses of a partial realization, i.e, expansion about $\sigma = \infty$ (dotted line), a Padé approximation, i.e, expansion about $\sigma = 0$ (dashed line), and a shifted Padé approximation, i.e, expansion about $\sigma = 10^4$ (dashed-dot line) are also represented for comparison. This exam-

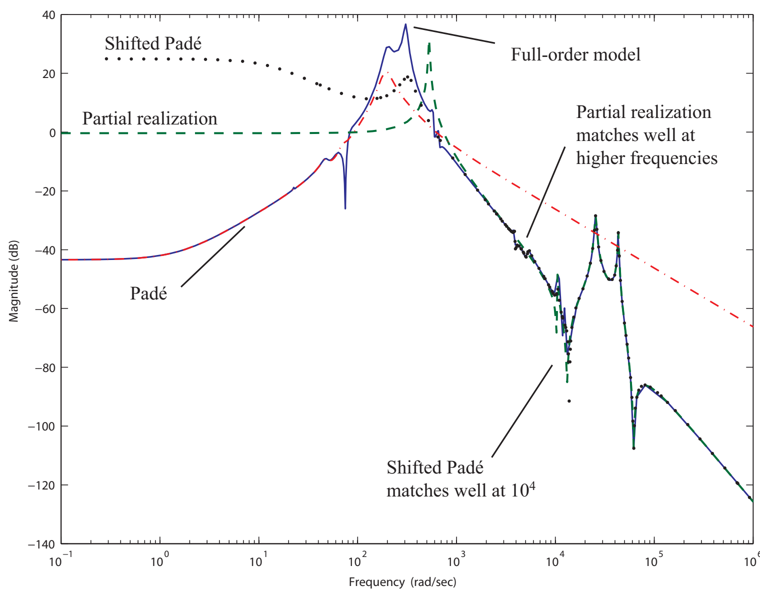

Figure 4.3: Frequency responses of a full-order model of the CD player and frequency responses for reduced-order models based on partial realization, Padé and shifted Padé approximations.

ple shows the behavior expected from each of the moment-matching methods, as described in the previous sections. The partial realization captures only higher frequency behavior. The two single-point Padé approximations are related to the choice of σ. While choosing $\sigma = 0$, the behavior matches of the reduced-order model matches the full-order model at lower frequencies, choosing $\sigma = 10^4$ makes the reduced order model approximately equal at this frequency.

4.6.2 Model Reduction: The Russian Service Module of the Space Station

The full-order model represents the component 1R (Russian Service Module) for the International Space Station. It is comprised of 270 states, 3 inputs and 3 outputs. The frequency response of the MIMO system is depicted in the Figure 4.4.

In order to verify the model reduction methods, MIMO Krylov methods are employed and compared with the balanced reduction techniques of the previous chapter. The normalized Hankel singular values are depicted in Fig. 4.5. It appears from the decay rate of its Hankel singular values that a reduced-order model of $r = 20$ should give a good approximation. The frequency responses of the reduced-order models for balanced truncation and Krylov techniques are shown in Figure 4.6.

As seen in the development of the rational Krylov algorithms, the order of the reduced-order model using MIMO rational Krylov is restricted by the size of the input and output matrices, i.e, the number of sensors and actuators, and the linear dependency of the columns of the projection matrices. In this case, one cannot choose directly the size of the reduced-order model. One can, however, experiment with the choice of interpolation points together with the number of derivatives to be matched per point to yield the size of the reduced-order model.

For the Russian Service example, it was chosen to work with two scenarios: (1) interpolation points at frequencies $0.1, 10, 80$ rad/sec, evaluated in the imaginary axis matching only the value of the transfer function, and (2) interpolation points at frequencies $0.1, 2, 10, 20, 80$ rad/sec, evaluated in the imaginary axis matching only the value of the transfer function. The rationale regarding this choice is that the former gives a reduced-order model of size $r = 18$ and matches some of the peaks in the frequency response of the full-order model, whereas the later yields a reduced-order model of size $r = 30$ and tries to match all peaks of the frequency response of the full-order model. Figures 4.6 and 4.7 illustrate those choices.

As observed in Fig. 4.7, all three of the reduced-order models match well the full-order model in the frequency range under consideration. Even though balanced truncation seems to perform better for reduced-order models of approximately the same size, its computational efforts are much higher than Krylov techniques, as seen in the Table 4.6.

4.6.3 Controller Reduction Examples

Two examples are considered for the case of controller reduction by the Krylov method: (1) the rotational disks and (2) the CD player. For the case of

Model Reduction	Size	Time
Balanced Truncation	$r = 20$	3.7260 sec
MIMO Krylov	$r = 18$	0.3700 sec
MIMO Krylov	$r = 30$	0.5910 sec

Table 4.6: Computational time for the reduced-order models of the Russian Module of the ISS (full-order model: $n = 270$ states) based on computations performed in Matlab

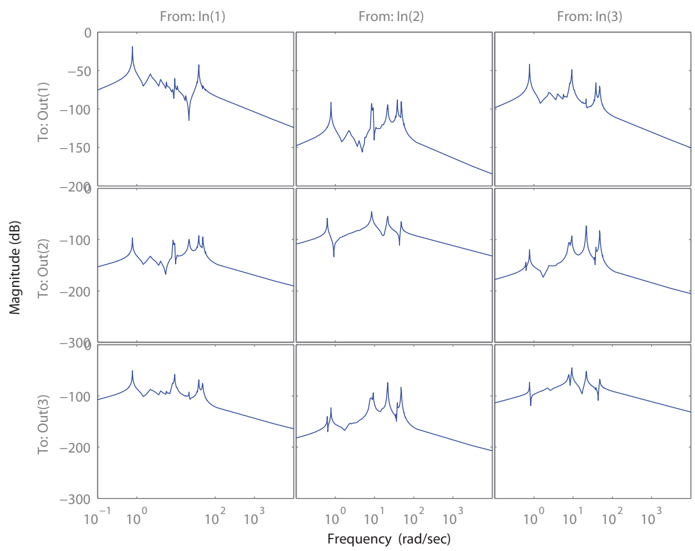

Figure 4.4: MIMO frequency responses of the 1R Module of the ISS.

the spinning disks, a fourth-order reduced controller is obtained and compared with the case of frequency weighted balanced reduction. For the CD player, a 14^{th} order controller is obtained from the full-order controller by the Rational Krylov procedure.

Consider first the spinning disks example. As seen in the previous chapter, an eighth-order LQG controller is obtained by loop shape design. The

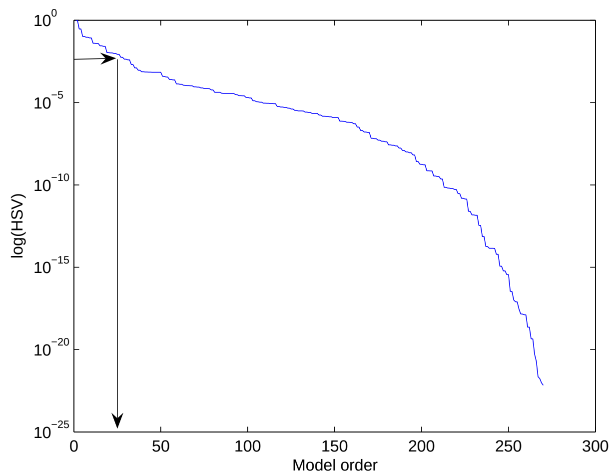

Figure 4.5: Normalized Hankel Singular Values of the ISS.

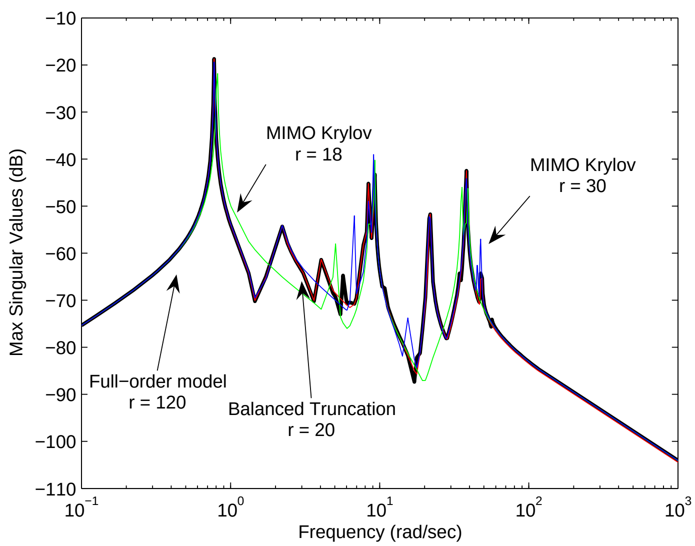

Figure 4.6: Frequency responses the reduced-order model for the 1R module of the ISS (black: FOM; red: balanced truncation; green: Krylov; blue: Krylov).

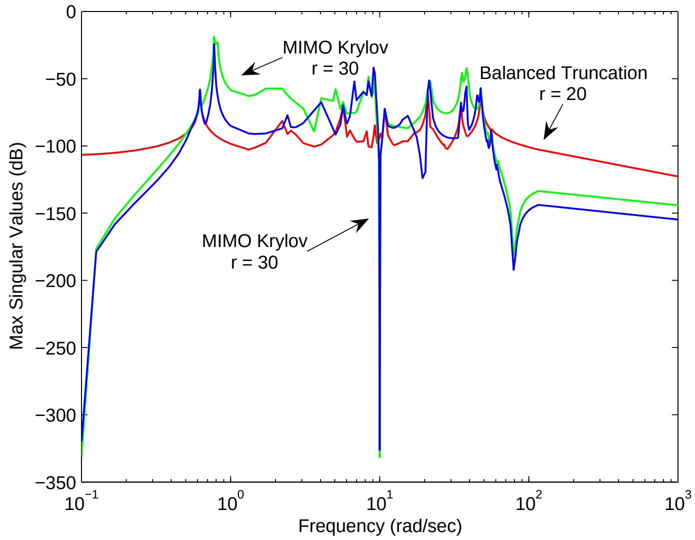

Figure 4.7: Frequency responses of the systems error of the reduced-order models for the 1R module of the ISS.

rational Krylov technique is applied here to obtain a fourth-order controller. In order to determine the interpolation points to be matched by the reduced-order controller, the procedure shown in Section 4.4 is used. Hence, the interpolation points were chosen to be the mirror images of some of the closed-loop and full-order controller poles. As seen in Fig. 4.8, the reduced-order controller obtained by rational Krylov performs as well as the one obtained by frequency weighted balanced truncation. The closed-loop system, in this case, is stable as well.

Consider now the CD player example. A SISO model was considered for the controller design in order to perform model reduction using the choice of the interpolation points as in Section 4.5. A LQG controller was designed

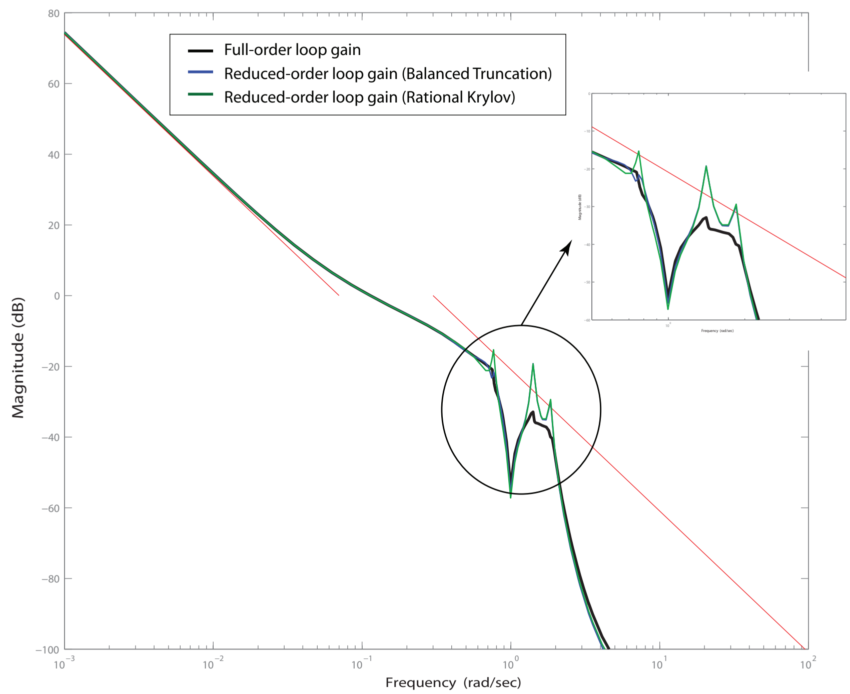

Figure 4.8: Frequency responses of the loop gain for the spinning disks examples comparing balanced truncation and rational Krylov for a fourth-order reduced-order controller.

based on the SISO model to reduce the oscillations as can be seen in Fig. 4.9, where the impulse response of the uncompensated and the compensated systems are shown. The oscillations represent the lens position due to an impulse disturbance on the lens actuator.

Two approaches were taken to obtain the reduced-order controller. First, as suggested in Section 4.5, the union of some mirror images of the poles of the closed-loop and full-order controller were chosen to obtain a $14th$ reduced-order controller. The choice of the interpolants among all poles were based on the poles with the highest residues. Simulation was performed in order to arrive to a 14^{th} order controller yielding good response and closed-loop stability.

Secondly, the interpolation points were chosen to match some of the peaks of the frequency response of the full-order system loop gain. In this case, choosing 14 frequencies, based on the frequency response plot, evaluated in the imaginary axis yielded unstabilizable reduced-order controllers. Thus, a stabilizing reduced-order controller was obtained by randomly choosing frequencies between $[10^1 \quad 10^5]$ rad/s.

The impulse response of the reduced-order closed-loop systems are depicted in Fig. 4.10. As can be observed, both reduced-order controllers match well the closed-loop behavior of the full-order controller. Furthermore, as illustrated in Fig. 4.11, both reduced-order controllers yield good matching in the frequency range under consideration.

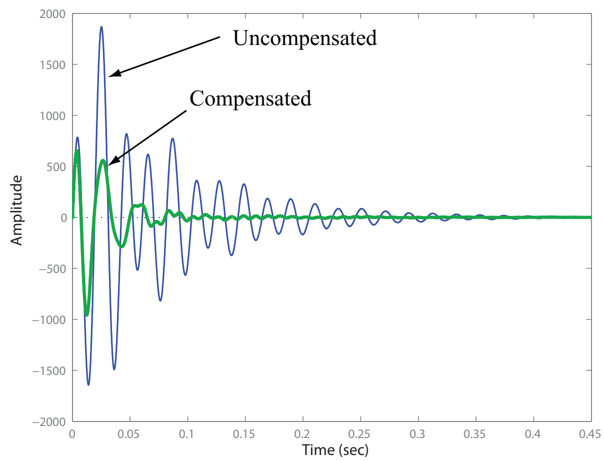

Figure 4.9: Impulse response of the uncompensated and the LQG-compensated systems for the CD player.

4.7 Concluding Remarks

This chapter introduced moment matching techniques for model reduction of large-scale systems. It was shown how to construct, in a numerically efficient way, full-rank projection matrices to be applied to the large-scale system. Unlike the SVD-based methods, reduced-order models are not guaranteed to be stable from a stable full-order model.

Also, the problem of controller reduction in a closed-loop framework was presented using Krylov techniques. It was shown that one can obtain reduced-order controllers that approximate well the full-order controller and the full-order closed-loop systems in the neighborhood of specific frequencies or points in the complex plane. Those frequencies are determined by *ad hoc*

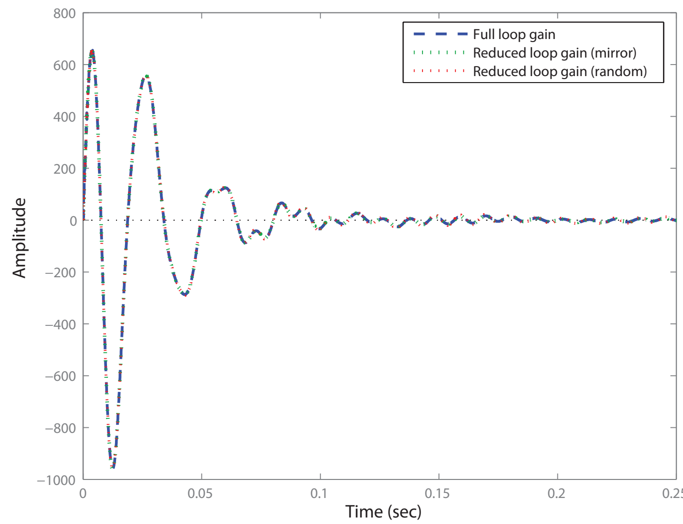

Figure 4.10: Impulse response of the reduced-order closed-loop systems for the CD player.

procedures such as the mirror images of the poles of the full closed-loop system. In order to fully apply these efficient procedures for controller reduction of large-scale systems, methods that guarantee closed-loop stability need to be addressed. This will be covered in the next chapter.

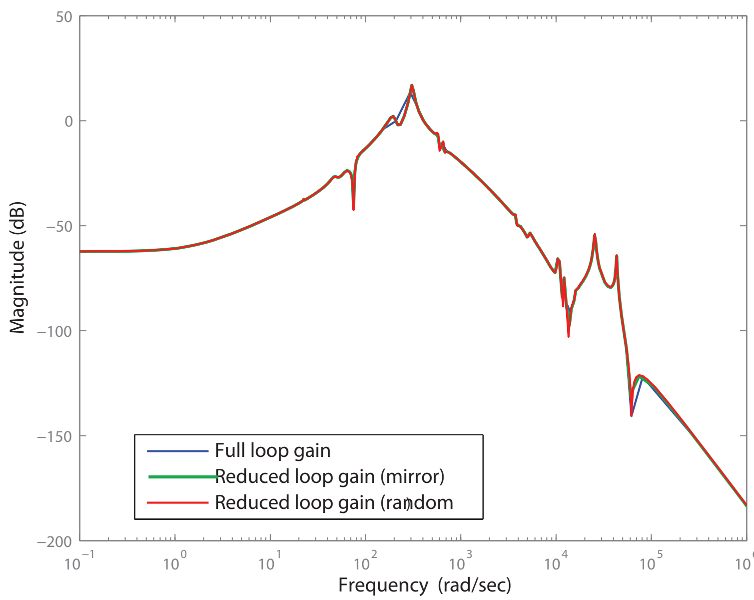

Figure 4.11: Frequency response of the reduced-order closed-loop systems for the CD player.

Chapter 5

Passivity Preserving Model and Controller Reduction

This chapter deals with the reduced-order controller design that guarantees closed-loop stability. An approach to model reduction will be proposed based on the "dissipativity" property of linear systems. In a broad sense, this property reveals that some external energy put into the system gets dissipated. The term energy will be defined in a general sense, and some simplifications will be made to arrive at the concept of passivity of a linear time invariant system.

By means of a well-known characterization of passive systems, the Positive Real Lemma, it will be shown how one can obtain closed-loop stability by feedback interconnection of two passive systems. Also, the development of such concepts for flexible structures will be achieved. In what follows, passivity preserving model reduction will be developed and its connection to the systems spectral zeros will be made.

5.1 System Dissipativity

A generalization of the Lyapunov stability criterion useful for the analysis of feedback systems is called *system dissipativity* or *system passivity* [121]. Broadly speaking, a system is said to be dissipative (or passive) if it does not generate energy internally, and strictly dissipative if it dissipates or consumes input energy [9, 71, 103]. As will be seen in the following sections, the main advantage of dissipative systems is that they can be robustly stabilized by a controller that itself satisfies a certain dissipativity condition.

5.1.1 System Dissipativity, Passivity and Positive Real Lemma

Mathematically, system dissipativity is defined as follows [8, 121]. Given the dynamical system $\dot{\mathbf{x}} = f(\mathbf{x}, \mathbf{u}), \quad \mathbf{y} = g(\mathbf{x}, \mathbf{u})$, with inputs $\mathbf{u} \in \mathbb{U}$, outputs $\mathbf{y} \in \mathbb{Y}$ and state-space $\mathbf{x} \in \mathbb{X}$, one can define a *supply function* to the system

$$\mathbf{s} : \mathbb{U} \times \mathbb{Y} \to \mathbb{R},\ (\mathbf{u}, \mathbf{y}) \mapsto \mathbf{s}(\mathbf{u}, \mathbf{y})$$

which may represent the power delivered to the system. The system is called *dissipative*, with respect to the supply function $\mathbf{s}$, if there exists a non-negative function $\mathbf{\Theta} : \mathbb{X} \mapsto \mathbb{R}$ such that the following dissipation inequality holds for all $t_0 \leq t_1$ and all trajectories $(\mathbf{u}, \mathbf{x}, \mathbf{y})$ which satisfy the system equations.

$$\mathbf{\Theta}\left(\mathbf{x}(t_1)\right) - \mathbf{\Theta}\left(\mathbf{x}(t_0)\right) \leq \int_{t_0}^{t_1} \mathbf{s}\left(\mathbf{u}(t), \mathbf{y}(t)\right) dt \tag{5.1}$$

In the case of a stable and square LTI dynamical system $\mathbf{\Sigma}$, one can define the supply function as a quadratic "power function" [67]

$$p(\mathbf{u}, \mathbf{y}) = \begin{bmatrix} \mathbf{y}^T & \mathbf{u}^T \end{bmatrix} \begin{bmatrix} \mathbf{Q} & \mathbf{N} \\ \mathbf{N}^T & \mathbf{R} \end{bmatrix} \begin{bmatrix} \mathbf{y} \\ \mathbf{u} \end{bmatrix} \tag{5.2}$$

where $\mathbf{Q}$, $\mathbf{N}$ and $\mathbf{R}$ have the appropriate dimensions. Several important special cases of dissipative linear systems are defined below

Definition 5.1.1. A linear system which is dissipative with respect to the power function $p(\mathbf{u}, \mathbf{y})$ in Eq. (5.2) is said to be

- *Passive* if $\mathbf{Q} = \mathbf{0}$, $\mathbf{R} = \mathbf{0}$ and $\mathbf{N} = \mathbf{I}$;
- *Norm-bounded* if $\mathbf{Q} = -\mathbf{I}$, $\mathbf{R} = -\gamma^2\mathbf{I}$, and $\mathbf{N} = \mathbf{0}$ for some finite $\gamma > 0$. In this case, $\gamma > \mathcal{H}_\infty$-norm of the system;
- *Sector-bounded* inside the sector $[a\, b]\,, a < 0 < b$ if $\mathbf{Q} = -\mathbf{I}$, $\mathbf{R} = -ab\mathbf{I}$, and $\mathbf{N} = \alpha\mathbf{I}$ with $\alpha = (a+b)/2$.

In this dissertation, only passive systems will be discussed. A large class of dynamical systems can qualify to be passive systems [42]. An important class of passive systems is an RLC circuit consisting only of resistors, inductors and capacitors. Also, some examples include large flexible space structures with collocated sensors and actuators [69]. It turns out that for linear systems, passivity is equivalent to the concept of *positive realness* of a transfer function [8].

Definition 5.1.2. An square $m \times m$ rational matrix $\mathbf{G}(s)$, with $\mathbf{G}^*(s) = \mathbf{G}^T(-s)$, is said to be *positive real* (PR) if

1. all elements of $\mathbf{G}(s)$ are analytic in $\Re e(s) > 0$;

2. $\mathbf{G}(s)$ maps the right-half of the complex plane $\mathbb{C}$ onto itself, i.e.,

$$s \in \mathbb{C}, \Re e(s) \geq 0 \Rightarrow \Re e(\mathbf{G}(s)) \geq 0, \quad s \text{ not a pole of } \mathbf{G}$$

3. $\mathbf{G}(s) + \mathbf{G}^*(s) \geq 0$ in $\Re e(s) > 0$ or equivalently

   (a) pole (in the Smith-McMillan sense) on the imaginary axis are simple and have non-negative definite residues, and

   (b) $\mathbf{G}(j\omega) + \mathbf{G}^*(j\omega) \geq 0$ for $\omega \in (-\infty, \infty)$

The time-domain equivalence of a positive real transfer function is given by the well known Kalman-Yacubovich-Popov (KYP) Lemma which is stated below without proof (see [71, 121] for proofs).

Lemma 5.1.1. *[8]* **(a) Positive Real Lemma** *The minimal system* $\mathbf{\Sigma} = \left[\begin{array}{c|c} \mathbf{A} & \mathbf{B} \\ \hline \mathbf{C} & \mathbf{D} \end{array}\right]$ *is dissipative with respect to the supply rate* $\mathbf{s} = \mathbf{y}^*\mathbf{u} + \mathbf{y}^*\mathbf{y}$, *if, and only if, there exists* $\mathbf{X} = \mathbf{X}^* \geq 0$, $\tilde{\mathbf{K}}$ *and* $\mathbf{L}$ *such that*

$$\begin{aligned} &\mathbf{A}^*\mathbf{X} + \mathbf{X}\mathbf{A} + \tilde{\mathbf{K}}^*\tilde{\mathbf{K}} = \mathbf{0} \\ &\mathbf{X}\mathbf{B} + \tilde{\mathbf{K}}^*\mathbf{L} = \mathbf{C}^* \\ &\mathbf{D} + \mathbf{D}^* = \mathbf{L}^*\mathbf{L} \end{aligned} \tag{5.3}$$

(b) *Let* $\mathbf{D} + \mathbf{D}^*$ *be non-singular and define* $\mathbf{\Delta} = (\mathbf{D} + \mathbf{D}^*)^{-1}$. *The system* $\mathbf{\Sigma}$ *is positive real if, and only if, there exists a positive semi-definite solution* $\mathbf{X} = \mathbf{X}^* \geq 0$ *to the Riccati equation*

$$(\mathbf{A}^* - \mathbf{C}^*\mathbf{\Delta}\mathbf{B}^*)\,\mathbf{X} + \mathbf{X}\,(\mathbf{A} - \mathbf{B}\mathbf{\Delta}\mathbf{C}) + \mathbf{X}\mathbf{B}\mathbf{\Delta}\mathbf{B}^*\mathbf{X} + \mathbf{C}^*\mathbf{\Delta}\mathbf{C} = \mathbf{0} \tag{5.4}$$

The above definitions imply the existence of a stable rational matrix function $\mathbf{W}(s)$, the so-called *spectral factor of* $\mathbf{G}$, such that: (1) $\mathbf{W}(s)$ has a stable inverse, and (2) $\mathbf{G}(s)+\mathbf{G}^{\mathbf{T}}(-s)=\mathbf{W}(s)\mathbf{W}^{T}(-s)$. This is the *spectral factorization* of $\mathbf{G}(s)$. Also, the zeros of $\mathbf{W}(s)$, i.e, $\lambda_i, i=1,\cdots,n$, such that $\det \mathbf{W}(\lambda_i)=0$, are the so-called *spectral zeros* of $\mathbf{G}(s)$. It turns out that the spectral zeros can be determined using the following generalized eigenvalue problem $\mathcal{A}\mathbf{\Lambda}=\mathcal{E}\mathbf{\Lambda}\mathbf{Z}$, where [103]

$$\mathcal{A} := \begin{bmatrix} \mathbf{A} & \mathbf{0} & \mathbf{B} \\ \mathbf{0} & -\mathbf{A}^T & -\mathbf{C}^T \\ \mathbf{C} & \mathbf{B}^T & \mathbf{D}+\mathbf{D}^T \end{bmatrix}, \quad \text{and} \quad \mathcal{E} := \begin{bmatrix} \mathbf{I} & & \\ & \mathbf{I} & \\ & & \mathbf{0} \end{bmatrix}, \tag{5.5}$$

and $\mathbf{Z}$ is a diagonal matrix which contains the spectral zeros. Finally, there is one extension of the positive real lemma to systems that are stable and bounded by one on the imaginary axis. It is called *bounded real systems.* One can show [8] that a condition for a system to be bounded real is given by the *Bounded Real Lemma* as follows

Lemma 5.1.2. *[8]* **(a) Bounded Real Lemma** *The minimal system* $\mathbf{\Sigma} = \left[\begin{array}{c|c} \mathbf{A} & \mathbf{B} \\ \hline \mathbf{C} & \mathbf{D} \end{array}\right]$*, with* $\mathbf{D}\neq\mathbf{0}$*, is bounded real, i.e, the* $\mathcal{H}_\infty$ *norm of* $\mathbf{\Sigma}$ *is at most one, if, and only if there exists* $\mathbf{X}\geq 0$*,* $\tilde{\mathbf{K}}$ *and* $\mathbf{L}$ *such that*

$$\begin{aligned} &\mathbf{A}^*\mathbf{X}+\mathbf{X}\mathbf{A}+\mathbf{C}^*\mathbf{C}\tilde{\mathbf{K}}^*\tilde{\mathbf{K}}=\mathbf{0} \\ &\mathbf{X}\mathbf{B}+\mathbf{C}^*\mathbf{D}+\tilde{\mathbf{K}}^*\mathbf{L}=\mathbf{0} \\ &\mathbf{I}-\mathbf{D}^*\mathbf{D}=\mathbf{L}^*\mathbf{L} \end{aligned} \tag{5.6}$$

The main passivity result is related to the feedback connection of two passive systems. It is based on a fundamental theorem of passivity which states that a *negative* feedback interconnection of two passive system is passive, and also, the negative feedback interconnection of any passive and strictly passive system is asymptotically stable. This property will be developed further and will be the basis for the passive controller reduction scheme. Next, the stability theorem is given without proof for the feedback interconnection of passive systems.

5.1.2 Stabilization by a Passive System

The main result of feedback interconnection of passivity system is given by the following theorem.

Theorem 5.1.3. *[71, 79] Consider the system of Fig. 5.1. Then, it follows that the negative feedback interconnection of* $\mathbf{G}_1(s)$ *and* $\mathbf{G}_2(s)$ *is globally asymptotically stable if* $\mathbf{G}_1(s)$ *is positive real (PR),* $\mathbf{G}_2(s)$ *is strictly positive real (SPR), and none of the purely imaginary poles of* $\mathbf{G}_2(s)$ *is a transmission zero of* $\mathbf{G}_1(s)$*. Mathematically, one can write*

$$\int_0^T u_1^T y_1 + \beta \geq 0, \quad \textit{for all} \quad T > 0$$

where β *is a positive constant and therefore, the signal* u_2 *can be shown to be* $u_2 \in \mathfrak{L}_2$*.*

This theorem shows that if one obtains a passive system, $\mathbf{G}_1$, and designs a strictly passive controller $\mathbf{G}_2$, the closed-loop feedback system of $\mathbf{G}_1$ and $\mathbf{G}_2$ is guaranteed to be asymptotically stable. Moreover, if one obtains either a passive reduced-order plant $\mathbf{G}_{r_1}$ from $\mathbf{G}_1$ or a passive reduced-order

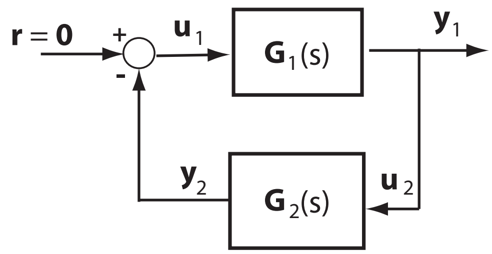

Figure 5.1: A PR connected via negative Feedback with SPR system.

controller $\mathbf{G}_{r_2}$, the reduced-order closed-loop system is still guaranteed to be stable. The problem, thus, becomes the one of seeking passivity preserving model reduction schemes and the design of passive controllers. These issues will be treated in the next sections and chapters.

5.2 Passivity Preserving Model Reduction

In order to use the stability of a passive feedback system with a reduced-order model or controller, one has to guarantee that the reduced model or controller preserves the passivity of the original system. This section deals with such algorithms. First, using the same framework as Chapters 3 and 4, an SVD-based model reduction is presented using concepts of PR systems. They have already been mentioned on Chapter 3, but here their algorithms are further developed. Next, using the framework of Krylov methods, it is shown how one can use a Rational Krylov algorithm in order to produce a passive reduced-order model based on a passive original model.

5.2.1 Bounded Real Balancing

One important class of dynamical systems is the class of bounded real systems [8, 52]. They are stable systems whose transfer function is bounded by one on the imaginary axis, i.e., its transfer function $\mathbf{G}(s)$ satisfies: $\mathbf{I} - \mathbf{G}^*(-i\omega)\mathbf{G}(i\omega) \geq 0, \omega \in \mathbb{R}$. It is called strictly bounded if this inequality is strict. Recall the bounded real lemma. If one defines $\mathbf{R_C} := \mathbf{I} - \mathbf{D}^*\mathbf{D}$, then $\mathbf{G}(s)$ is bounded real if and only if there exists $\mathcal{Y} = \mathcal{Y}^* > 0$ such that the following Riccati equations holds

$$\mathbf{A}^*\mathcal{Y} + \mathcal{Y}\mathbf{A} + \mathbf{C}^*\mathbf{C} + (\mathcal{Y}\mathbf{B} + \mathbf{C}^*\mathbf{D})\,\mathbf{R_C}^{-1}\,(\mathcal{Y}\mathbf{B} + \mathbf{C}^*\mathbf{D})^* = \mathbf{0}. \tag{5.7}$$

Any solution $\mathcal{Y}$ lies between two extremal solutions, i.e, $0 < \mathcal{Y}_{min} \leq \mathcal{Y} \leq \mathcal{Y}_{max}$. $\mathcal{Y}_{min}$ is a unique solution to Eq. (5.7). Also, one can define a dual Riccati equation

$$\mathbf{A}\mathcal{Z} + \mathcal{Z}\mathbf{A}^* + \mathbf{B}\mathbf{B}^* + (\mathcal{Z}\mathbf{C}^* + \mathbf{B}\mathbf{D}^*)\,\mathbf{R_B}^{-1}\,(\mathcal{Z}\mathbf{C}^* + \mathbf{B}\mathbf{D}^*)^* = \mathbf{0}, \tag{5.8}$$

where $\mathbf{R_B} := \mathbf{I} - \mathbf{D}\mathbf{D}^*$ and the solution lies in between two extremal solutions: $0 < \mathcal{Z}_{min} \leq \mathcal{Z} \leq \mathcal{Z}_{max}$.

Lemma 5.2.1. *[84, 85] If $\mathcal{Y} = \mathcal{Y}^* > 0$ is a solution to Eq. (5.7), then $\mathcal{Z} = \mathcal{Y}^{-1}$ is a solution to 5.8. Hence $\mathcal{Z}_{min} = \mathcal{Y}_{max}^{-1}$ and $\mathcal{Z}_{max} = \mathcal{Y}_{min}^{-1}$.*

Based on this fact, one can define a bounded real balanced representation of the system $\mathbf{\Sigma}$ by means of simultaneously diagonalizing $\mathcal{Y}_{min}$ and $\mathcal{Z}_{min} = \mathcal{Y}_{max}^{-1}$.

Definition 5.2.1. [8, 84]. A bounded real system is called bounded real balanced if

$$\mathcal{Y}_{min} = \mathcal{Z}_{min} = \mathcal{Y}_{max}^{-1} = \mathcal{Z}_{max}^{-1} = \text{diag}\left(\xi_1 \mathbf{I}_{l_1}, \cdots, \xi_q \mathbf{I}_{l_q}\right) \tag{5.9}$$

where $1 > \xi_1 > \xi_2 > \cdots > \xi_q > 0, m_i = 1, \cdots, q$ are the multiplicities of ξ_i, and $m_1 + \cdots + m_q = n$. The $\xi_i' s$ are the bounded real singular values of $\mathbf{\Sigma}$.

Balanced reduction follows as the usual balanced truncation as done in Chapter 3, by simply eliminating the states which correspond to small bounded real singular values. An error bound is derived in [52, 84].

5.2.2 Positive Real Balancing

Following the same procedure as for the bounded real balancing, one can define a reduced-order model based on the positive real lemma. Recall the definition of the positive real Riccati equations as in Eq. (5.4). Then a system $\mathbf{\Sigma}$ with transfer function $\mathbf{G}(s) = \left[\begin{array}{c|c} \mathbf{A} & \mathbf{B} \\ \hline \mathbf{C} & \mathbf{D} \end{array}\right] \in \mathbb{R}^{(n+p)\times(n+m)}, m = p$ is PR if and only if there exists $\mathcal{K} = \mathcal{K}^* > 0$ such that the following Riccati equations hold

$$\mathbf{A}^*\mathcal{K} + \mathcal{K}\mathbf{A} + \left(\mathcal{K}\mathbf{B} - \mathbf{C}^*\right)\left(\mathbf{D} + \mathbf{D}^*\right)^{-1}\left(\mathcal{K}\mathbf{B} + \mathbf{C}^*\right)^* = \mathbf{0} \tag{5.10}$$

Also, one can define a dual Riccati equation

$$\mathbf{A}\mathcal{L} + \mathcal{L}\mathbf{A}^* + \left(\mathcal{L}\mathbf{C}^* - \mathbf{C}\mathbf{B}\right)\left(\mathbf{D} + \mathbf{D}^*\right)^{-1}\left(\mathcal{L}\mathbf{C}^* - \mathbf{C}\mathbf{B}\right)^* = \mathbf{0} \tag{5.11}$$

Lemma 5.2.2. *[84] Any solution $\mathcal{K}_{min}$ and $\mathcal{L}_{min}$, of the positive real Riccati equations, lies between two extremal solutions, i.e, $0 < \mathcal{K}_{min} \leq \mathcal{K} \leq \mathcal{K}_{max}$*

and $0 < \mathcal{L}_{min} \leq \mathcal{L} \leq \mathcal{L}_{max}$. *If* $\mathcal{K} = \mathcal{K}^* > 0$ *is a solution to Eq. (5.10), then* $\mathcal{L} = \mathcal{K}^{-1}$ *is a solution to Eq. (5.11). Hence* $\mathcal{K}_{min} = \mathcal{L}_{max}^{-1}$ *and* $\mathcal{K}_{max} = \mathcal{L}_{min}^{-1}$

Analogous to the bounded real case, a positive real balancing transformation is performed by simultaneously diagonalizing the minimal solutions $\mathcal{K}_{min}$ and $\mathcal{L}_{min}$. Hence, it follows:

Definition 5.2.2. [8, 84]. A positive real system is called positive real balanced if

$$\mathcal{K}_{min} = \mathcal{L}_{min} = \mathcal{K}_{max}^{-1} = \mathcal{L}_{max}^{-1} = \mathrm{diag}\left(\pi_1 \mathbf{I}_{s_1}, \cdots, \pi_q \mathbf{I}_{s_q}\right) \tag{5.12}$$

where $1 > \pi_1 > \pi_2 > \cdots > \pi_q > 0, s_i = 1, \cdots, q$ are the multiplicities of π_i, and $s_1 + \cdots + s_q = n$. The $\pi_i' s$ are the positive real singular values of $\mathbf{\Sigma}$.

Similarly, balanced reduction follows as the usual balanced truncation as done in Chapter 3, by simply eliminating the states which corresponds to small positive real singular values. An error bound is derived in [52, 84]. For the same reasons as the Lyapunov-balanced truncation, theses two algorithms are not suitable for large-scale systems, since one has to solve two large Riccati equations. Methods based on Krylov methods will be derived next.

5.2.3 Passivity Preserving Rational Krylov

As seen in the previous chapters, SVD-based methods for large-scale model reduction rely on solving large-scale Lyapunov or Riccati equations. Therefore, it is interesting to obtain reduced-order models using Krylov techniques that preserve passivity and stability. Antoulas [9] has shown how one can produce a passive reduce-order model based on interpolation of the spectral zeros of the full order system, i.e., a passive reduced-order model will result if certain spectral zeros are preserved (interpolated) in the reduced order model. In this case, rational Krylov methods can be applied for the interpolation problem. The approach taken here follows [8, 9]. The theorems will be stated without proof.

Theorem 5.2.3. *[8] Recall the definitions of the spectral zeros as in Eq. (5.5). Given a stable and passive system $\mathbf{\Sigma}$, let Z denotes its set of spectral zeros. If the projection matrices $\mathbf{V}$ and $\mathbf{W}$ are obtained as follows*

$$\mathbf{V} := \left[(\lambda_1\mathbf{I} - \mathbf{A})^{-1}\mathbf{B} \quad \cdots \quad (\lambda_k\mathbf{I} - \mathbf{A})^{-1}\mathbf{B}\right] \tag{5.13}$$

$$\mathbf{W} := \left[\left(\gamma_1\mathbf{I} - \mathbf{A}^T\right)^{-1}\mathbf{C}^T \quad \cdots \quad \left(\gamma_k\mathbf{I} - \mathbf{A}^T\right)^{-1}\mathbf{C}^T\right] \tag{5.14}$$

where $\lambda_i \neq \gamma_i,\ i, j = 1, \cdots, k,\ \lambda_1, \cdots, \lambda_k \in Z$ and in addition $\gamma_i = -\lambda_i^*$, then the reduced system $\mathbf{\Sigma}_r$ is obtained by projection as

$$\mathbf{A}_r = \tilde{\mathbf{W}}^T\mathbf{A}\mathbf{V}, \quad \mathbf{B}_r = \tilde{\mathbf{W}}^T\mathbf{B}, \quad \mathbf{C}_r = \mathbf{C}\mathbf{V}, \quad \mathbf{D_r} = \mathbf{D}$$

with $\tilde{\mathbf{W}} = \mathbf{W}(\mathbf{V}^*\mathbf{W})^{-1}$ and $\det(\mathbf{W}^*\mathbf{V}) \neq 0$ satisfies: **(i)** $\mathbf{G}(\lambda_i) = \mathbf{G}_r(\lambda_i)$ *and* $\mathbf{G}(\gamma_i) = \mathbf{G}_r(\gamma_i)$, **(ii)** *is stable* **(iii)** *is passive.*

In the context of this dissertation, there remains the question of how to apply the passivity preserving model reduction to the building models. The next section deals with the positive realness of flexible structures.

5.3 Passivity in Flexible Structures

It is known that for flexible structures, the plant transfer function is positive real if the sensors are collocated with the actuators [66, 70, 92]. This property holds, for instance, if force actuators and velocity sensors or torque actuators and angular rate sensors are collocated. In this manner, for a flexible structure with m force inputs and m collocated velocity measurements, one can define its equation of motion as

$$\mathbf{M}\ddot{\mathbf{x}}(t) + \mathbf{D_a}\dot{\mathbf{x}}(t) + \mathbf{K}\mathbf{x}(t) = \mathbf{B}_s\mathbf{u}(t) \tag{5.15}$$

$$\mathbf{y}(t) = \mathbf{B}_s^T\dot{\mathbf{x}}(t) \tag{5.16}$$

and its state-space realization as in Eq. (2.2), where

$$\mathbf{A} = \begin{bmatrix} \mathbf{0} & \mathbf{I} \\ -\mathbf{M}^{-1}\mathbf{K} & -\mathbf{M}^{-1}\mathbf{D_a} \end{bmatrix}; \quad \mathbf{B} = \begin{bmatrix} \mathbf{0} \\ -\mathbf{M}^{-1}\mathbf{B}_s \end{bmatrix}; \tag{5.17}$$

$$\mathbf{C} = \begin{bmatrix} \mathbf{0} & \mathbf{B}_s^T \end{bmatrix}; \quad \mathbf{D} = \mathbf{0}. \tag{5.18}$$

Theorem 5.3.1. *Given the flexible structural model as in Equations (5.15)-(5.17) with symmetric mass, stiffness and damping matrices. One can, thus, define the square roots factors*

$$\mathbf{K} = \mathbf{K}_1^T\mathbf{K}_1; \quad \mathbf{M} = \mathbf{M}_1^T\mathbf{M}_1; \quad \mathbf{D}_a = \mathbf{D}_{a_1}^T\mathbf{D}_{a_1}. \tag{5.19}$$

The positive real lemma 5.1.1 is satisfied if

$$\mathbf{X} = \begin{bmatrix} \mathbf{K} & \mathbf{0} \\ \mathbf{0} & \mathbf{M} \end{bmatrix}; \quad \tilde{\mathbf{K}} = \begin{bmatrix} \mathbf{0} & \sqrt{2}\mathbf{D}_{a_1}^T \end{bmatrix}. \tag{5.20}$$

Proof. By direct substitution of the above equations into the positive real lemma. □

Having found a solution to the positive real lemma, one guarantees that the flexible structure is indeed passive (or positive real), and therefore, one can determine a reduced-order model using passivity preserving model reduction schemes. The solution, $\mathbf{X}$, of the positive real lemma will play an important role in the derivation of a passive optimal controller, as will be seen in Chapter 8.

5.4 Concluding Remarks

This chapter introduced the concept of passivity of a linear systems. Connection to the positive realness property was shown through the used of the well-known positive real lemma (or KYP-lemma). By the fact that a negative interconnection of two passive systems results in a stable closed-loop system, a method of computing reduced-order models and controllers was derived using passivity preserving techniques. Three methods were shown for obtaining the passive reduced-order model: positive-real balancing, bounded-real balancing and passivity preserving Krylov algorithm. Needless to say, the first two reduction schemes are not appropriate for large-scale implementations.

Passivity of flexible structures was shown based on the collocation of sensors and actuators. Thus, using the methods presented in this chapter, one can obtain reduced-order models and controllers that guarantee stability of the closed-loop system. There are some concepts remaining for the full application of passivity preserving controller reduction of large-scale systems: the design of a passive controller. This issue will be dealt with in the next chapters using ideas from the passive-LQG controllers.

Chapter 6

Structural Control in Civil Engineering

Control studies in civil engineering can be divided into two categories: those which address serviceability issues and those whose main concern is safety. When serviceability is the main concern, control is used to reduce structural acceleration in order to increase occupant comfort during relatively mild wind or seismic excitations. However, for those controllers developed for stronger excitations, where occupant safety is the main concern, the goal is to improve structural response by reducing peak interstory drift or by increasing energy dissipation.

For structural control to gain viability in the earthquake engineering community, understanding the role of controllers within the context of performance-based engineering is of primary importance. Design of a structure/controller system should involve a thorough understanding of how various types of controllers enhance structural performance, such that the most effective type of controller is selected for the given structure and seismic hazard. Controllers may be passive, requiring no external energy source, or active, requiring an external power source. Application of certain passive systems, including base isolation and viscous dampers, have become more common, leading to a reasonable understanding of how such systems reduce the dynamic behavior of structures. However, few full-scale applications of active controllers exist and their assessment, either for structural performance or reduced-order controller implementation is less studied.

In this chapter, an introduction to structural control for buildings is presented. First, an overview of the types of energy dissipation system, that is passive, active or semi-active, is presented in a general sense. Then, topics in modeling active and semi-active control are discussed with emphasis on their mathematical models, control interaction, and control techniques applied to vibration mitigation in civil structures. Finally, a family of benchmark problems is introduced to illustrate the application of the model and controller reduction schemes described in the previous chapters.

6.1 Classification of Building Control

Structural control systems can be grouped into four broad areas [19] based on the energy requirements of the control systems and the presence of sensors and the type of control algorithms: (1) base isolation or passive control, (2) active control, (3) semi-active control, and (4) hybrid control. Base isolation can be considered the most widely-used control in building applications. The basic configuration of those systems is shown schematically in Fig. 6.1 and their description is given below.

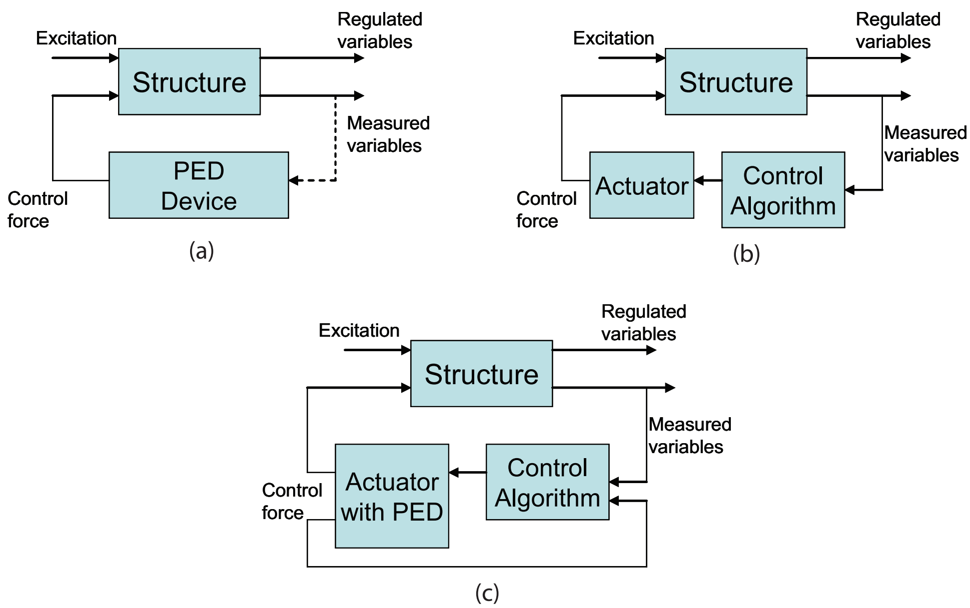

Figure 6.1: Block diagram of various structural control strategies: (a) Passive, (b) Active, and (c) Semi-active [101]

Passive Control Passive control systems do not require external forces. The forces applied to the structural system are functions of the response to the excitation. By simply increasing the dissipated energy capacity of the structure through the use of special damper devices and materials, vibration mitigation can be accomplished.

One of the most successful types of passive systems is called the *base isolation* system, as shown in Fig. 6.2. It is typically placed at the foundation of a structure. The isolation system introduces flexibility and energy absorption capabilities, thereby reducing the level of energy that can be transmitted to the structure. Another example of a passive control system employs passive supplemental damping devices, such as viscous dampers and tuned-mass dampers. Although passive control systems have reached a mature stage in technological development, they have inherent limitations. Usually, passive devices are optimally tuned to protect the structure from a particular dynamic loading or a particular mode of vibration (in general the first mode), and thus the performance of these devices is suboptimal for other loading scenarios and configurations. A comprehensive review of the literature on passive supplemental damping devices for civil engineering structures can be found in [100, 101, 107]. In this dissertation, only active and semi-active types of control systems will be considered for further implementations, due to the passive nature (no feedback control) of those systems.

Active Control A logical extension of the passive control system is its en-

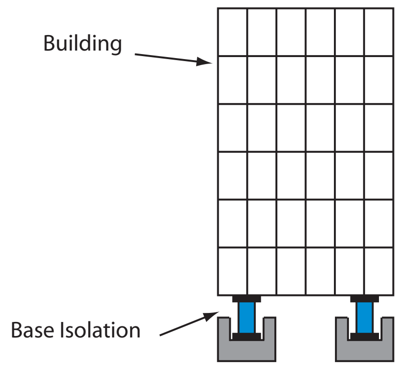

Figure 6.2: Base isolation schematic

hancement with the addition of external inputs to the structure. Active control systems contain external powered actuators that apply forces in a pre-determined manner. They both add and dissipate energy in the structure. A computer-based control algorithm uses information from sensors to command the actuator system. The main advantage of active control systems is that they act simultaneously with the hazard excitation to provide enhanced structural behavior for improved service and safety [19]. The main drawback of such systems stems from the fact that external power (actuators, motors) has to be added to the system, thus, increasing its complexity.

Active control systems can be implemented in several configurations: active bracing, active tendon, and active mass drivers, among others. The differences are only on the type and direction of forces and torques applied to the structure. They all need an external power supply and a computer for the control implementation.

Semi-Active Control A semi-active control system can be considered as a passive device whose properties can be actively controlled. For example, a fluid viscous damper whose damping constant can be controlled. These systems require power inputs that are significantly reduced from a fully active system. They can be implemented in a variety of schemes: variable-orifice dampers, variable-friction dampers, electrorheological devices, and magnetorheological devices.

The main advantages of semi-active control devices stem from the fact that they operate on battery power and they do not destabilize the structure.

Hybrid Control

Lastly, by combining features of both passive and active control systems, a hybrid system can be used. Generally, a passive device is utilized to control the larger portion of the response, while the active device is utilized to optimize the response to the given excitation and maintain the passive system within desired parameters.

6.2 Actuator Systems for Active and Semi-Active Building Control

Many different actuation systems have been implemented for applications in active and semi-active control of civil structures. The actuation schemes differ only in the type of force applied to the structure. In this dissertation, a few actuation systems are illustrated and only the active bracing system is used in the subsequent analysis.

6.2.1 Hydraulic Actuation and Active Bracing

The active bracing actuation system is usually placed across a single story level using a chevron or V-shape configuration. In large structures, they can span several story levels. There are other variations, such as X-braces. The system is comprised of a hydraulic actuator attached to the structure in order to create horizontal forces between floor diaphragm levels. For a hydraulic actuator system, the equation of motion describing the fluid flow rate in an actuator can be linearized about the origin yielding [27]

$$\dot{f}(t) = \frac{2\beta}{V}\left(Ak_q c(t) - k_c f(t) - A^2 \dot{x}_a(t)\right) \tag{6.1}$$

where c is the valve input, f is the force generated by the actuator, A is the cross-sectional area of the actuator, β is the bulk modulus of the fluid, V is the characteristic hydraulic fluid volume for the actuator, x_a is the actuator displacement, and (k_q, k_c), are system constants.

In general, the open-loop system in Eq. (6.1) is unstable. Closed-loop is essential for stabilization of the actuator. Also, the dynamics of the force applied by the actuator are dependent on the velocity response of the actuator, i.e., the feedback interaction path is intrinsic to the dynamical response of a hydraulic actuator. Incorporating unity gain displacement feedback into the hydraulic actuator model yields

$$\dot{f}(t) = \frac{2\beta}{V}\left(Ak_q\gamma(u(t) - x_a(t)) - k_c f(t) - A^2\dot{x}_a(t)\right) \tag{6.2}$$

where u is the is the control command, and γ is a proportional feedback gain of the stabilizing controller for the actuator. Eq. (6.2) can be rewritten as

$$\dot{f}(t) = a_1 u(t) - a_1 x_a(t) - a_2 \dot{x}_a(t) - a_3 f(t) \tag{6.3}$$

where $a_1 = \frac{2\beta k_q \gamma}{V}$, $a_2 = \frac{2\beta A^2}{V}$ and $a_3 = \frac{2\beta k_c}{V}$. Eq. (6.3) can be written in a state-space form (useful later for its implementation) as

$$\dot{\mathbf{x}}_a = \mathbf{A}_a \mathbf{x}_a + \mathbf{B}_a \mathbf{u} \tag{6.4}$$

$$\mathbf{y}_a = \mathbf{C}_a \mathbf{x}_a + \mathbf{D}_a u = \mathbf{f} \tag{6.5}$$

For the case of a single actuator, it follows that

$$\mathbf{A}_a = [-a_3], \quad \mathbf{B}_a = [a_1 \quad -a_1 \quad -a_2], \quad \mathbf{C}_a = 1, \quad \mathbf{D}_a = [0 \quad 0 \quad 0] \tag{6.6}$$

The generalization to the case of several actuators readily follows from the state-space equations in Eq. (6.4) and (6.5).

6.2.2 Hydraulic Actuation and Active Tendons

The actuation system using an active tendon configuration is similar to the active bracing system, except that the forces generated by the hydraulic system are transmitted to the structure through a set of tendons or two pre-tensioned cables spanning the inter-story space at angles in an X-pattern. A single degree-of-freedom structure is shown in Fig. 6.2.2. The mathematical model of system is given by

$$m\ddot{x}(t) + c\dot{x}(t) + kx(t) = -m\ddot{x}_g(t) + (4k_c \cos\alpha)f(t) \tag{6.7}$$

where m, c, k are the mass, damping and stiffness of the structure, respectively, k_c is the tendon stiffness, α is the tendon inclination angle and f is the hydraulic actuator force as given by Eq. (6.2). The state-space equations follow the same ideas as for the active bracing system and will not be discussed here.

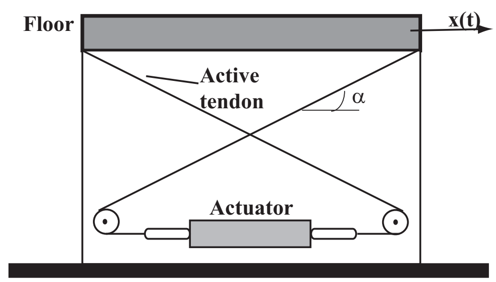

Figure 6.3: Hydraulic actuation and active tendon configuration. Adapted from [29]

6.2.3 Hydraulic Actuation and the Active Mass Driver

The active mass driver actuation system is based on the base-excitation principle of structural systems [24, 61], or what is called tuned mass damper. The idea is to incorporate a second spring-mass-damper into the system to change from a single-degree-of-freedom to a multi-degree-of-freedom in order to tune the motion of the original system. As an example, consider the spring-mass system shown in Fig. 6.4. The equations of motion of the tuned-mass are given by

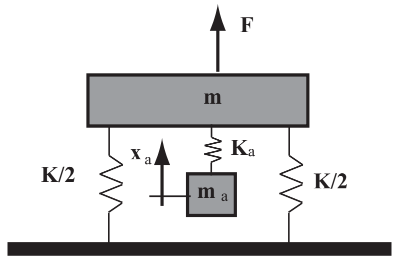

Figure 6.4: Tuned Mass-Damper

$$\begin{bmatrix} m & 0 \\ 0 & m_a \end{bmatrix} \begin{bmatrix} \ddot{x} \\ \ddot{x}_a \end{bmatrix} + \begin{bmatrix} K + K_a & -K_a \\ -K_a & K_a \end{bmatrix} \begin{bmatrix} x \\ x_a \end{bmatrix} = \begin{bmatrix} F_o \sin \omega t \\ 0 \end{bmatrix} \tag{6.8}$$

One chooses the parameters of the added system (m_a, K_a) such that in the steady-state, the displacement of the original system is minimized. In this case, one can write the solution in the steady-state for the displacement of the structure and the added mass as

$$x_{ss}(t) = X \sin \omega t \tag{6.9}$$

$$x_{a_{ss}}(t) = X_a \sin \omega t \tag{6.10}$$

Substituting Eqs. (6.9) and (6.10) into Eq. (6.8), yields

$$X = \frac{(K_a - m_a \omega^2) F_0}{(K + K_a - m\omega^2)(K_a - m_a \omega^2) - K_a^2} \tag{6.11}$$

$$X_a = \frac{K_a F_0}{(K + K_a - m\omega^2)(K_a - m_a \omega^2) - K_a^2} \tag{6.12}$$

So, to minimize X, select ω according to

$$\omega^2 = \frac{K_a}{m_a} \tag{6.13}$$

One of the drawbacks of this approach is the lack of tuning in multiple frequencies, as shown by the tuning condition given in Eq. (6.13). For tuning the system at several frequencies, hydraulic actuators together with dampers can be added and feedback control techniques can be applied to enhance the performance of the entire system. In this case, a hybrid system is used and, hence, the system is called active-mass-driver.

6.2.3.1 Magneto-Rheological Actuators

According to Dyke [31, 32], semi-active control strategies using, for example, magneto-rheological (MR) actuators, provide a promising solution for several challenges in seismic control. Semi-active control devices offer the reliability of passive devices while maintaining the versatility of active control together with a decrease in size and power requirements.

MR fluids are the magnetic analogs of electro-rheological (ER) fluids and typically consist of micron-sized, magnetically polarizable particles dispersed in a carrier medium, such as mineral or silicone oil [32]. When a magnetic field is applied to the fluid, particle chains form and the fluid becomes a semi-solid. The fluid then exhibits viscoplastic behavior similar to that of ER fluids. Transition to rheological equilibrium can be achieved in a few milliseconds, allowing construction of devices with high bandwidth. Also, a wider choice of additives (surfactants, dispersants, friction modifiers, anti-wear agents, etc.) can generally be used with MR fluids to enhance stability, seal life, and bearing life. The MR fluid can be readily controlled with a low voltage $(12 - 24V)$, current-driven power supply outputting only $1 - 2$ amps. The schematic of an MR damper is shown in Fig. 6.5.

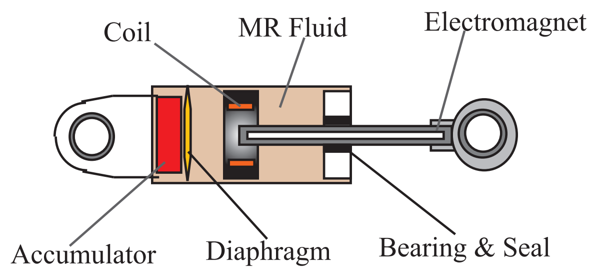

Figure 6.5: Magneto-rheological Dampers. Adapted from [109].

Due to its promising characteristics, several studies have been undertaken in the past decade and several commercially available dampers have been developed [22]. The mathematical model of an MR is very complex due to its nonlinear nature. Several models have been developed and tested in an experimental framework [109]. One of the mechanical idealizations of the MR damped force that is numerically tractable uses the Bouc-Wen model [120] for hysteretic systems. The most effective model for predicting the behavior of an MR damper was proposed by Spencer [109], as shown in Fig. 6.6 and can be mathematically modeled as follows:

$$F = \alpha z + c_0(\dot{x} - \dot{y}) + k_0(x - y) + k_1(x - x_0) = c_1\dot{y} + k_1(x - x_0) \tag{6.14}$$

with

$$\dot{z} = \gamma|\dot{x} - \dot{y}|z|z|^{n-1} - \beta(\dot{x} - \dot{y})|z|^n + A(\dot{x} - \dot{y}) \tag{6.15}$$

$$\dot{y} = \frac{1}{c_0 + c_1}\left[\alpha z + c_0\dot{x} + k_0(x - y)\right] \tag{6.16}$$

where F is the applied force of the damper, k_1 is the accumulator stiffness, c_0 is the viscous damping observed at larger velocities, c_1 is the damping introduced to model the nonlinear roll-off in the force-velocity at low velocities, k_0 is present to control the stiffness at higher velocities, and x_0 is the initial displacement of the spring k_1. The mathematical model can be determined by adjusting the parameters γ, β, A using system identification procedures.

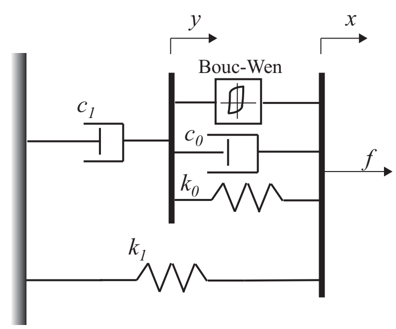

Figure 6.6: Schematic model of magneto-rheological dampers. Adapted from [109].

To account for the dependence of the force on the voltage applied to the current driver and the resulting magnetic current, one can use [109]

$$\alpha = \alpha(u) = \alpha_a u + \alpha_b u \tag{6.17}$$

$$c_1 = c_1(u) = c_{1_a} u + c_{1_b} u \tag{6.18}$$

$$c_0 = c_0(u) = c_{0_a} u + c_{0_b} u \tag{6.19}$$

where, due to the dynamics in reaching rheological equilibrium and in driving the electromagnet in the MR damper, u is given as a first-order system as a function of the commanded voltage to the current driver, ν, such that

$$\dot{u} = \eta(u - \nu) \tag{6.20}$$

In order to show the effectiveness of the proposed MR damper model, a simulation was performed in Matlab-Simulink using the same parameters as in [109]. The MR block diagram is depicted in the Appendix A and the results due to a sinusoidal displacement input and several input voltages are given in Fig. 6.7 and Fig. 6.8.

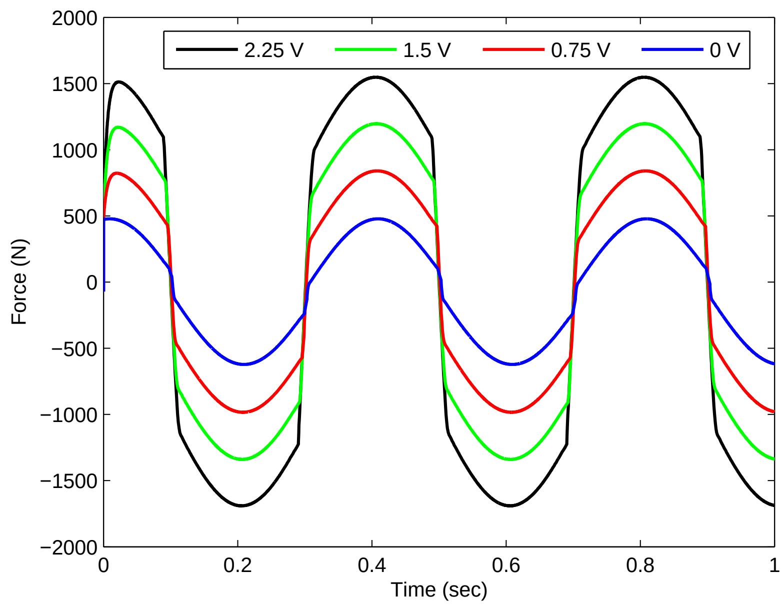

Figure 6.7: MR force due to a sinusoidal displacement and varying input voltages.

From Figure 6.7, it can be seen that the force produced by the damper is not centered at zero. This effect is due to the presence of the accumulator in

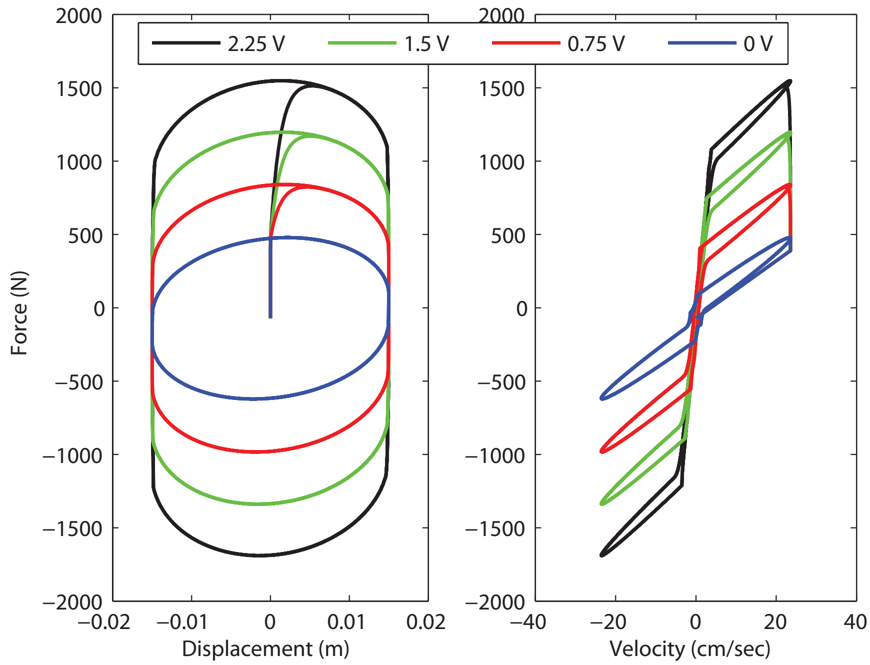

Figure 6.8: MR force due to a sinusoidal displacement and varying input voltages.

the MR damper. The enhancement on the MR output force can be observed in Fig 6.7, as voltage is increased from $0\,V$ to $2.25\,V$. Also, the effects of changing the magnetic field are readily observed from Fig. 6.8. At $0\,V$ the MR damper function as a purely viscous device. As the voltage increases, the damper force also increase and produces behavior associated with a plastic material in parallel with a viscous damper as shown by the hysteretic behavior of the MR force and velocity. In the following sections, the effectiveness of the MR damper will be shown for seismic response reduction.

6.3 Models of Civil Structures for Control Design

In general, civil structures are modeled as multi-story shear buildings [91], that is, structures in which there is no rotation of a horizontal section at the level of the floors [24, 91]. In order to consider this simplification, several key assumptions have to be made:

1. The total mass of the structure is concentrated at the level of the floors;
2. The girders on the floor are infinitely rigid as compared to the columns; and
3. The deformation of the structure is independent of the axial forces in the columns.

These assumptions transform the problem from a structure with an infinite number of degrees of freedom to a structure that has only as many degrees as it has lumped masses at the floor levels. Also, in some cases, the problem of a building comprised of several bays can be considered as a single bay, due to the rigidity of the floors. The mathematical model of a building subjected to an earthquake excitation is usually considered as a response of a shear building to a base or foundation displacement. This can be accomplished if one considers the floor displacements relative to the base motion [24, 91]. Therefore, the equation of motion for the shear building can be written as

$$[\mathbf{M}]\,\ddot{\mathbf{x}}(t) + [\mathbf{D}]\,\dot{\mathbf{x}}(t) + [\mathbf{K}]\,\mathbf{x}(t) = \mathbf{B_s}\mathbf{F}(t) - [\mathbf{M}]\,\boldsymbol{\Gamma}\ddot{\mathbf{x}}_g(t) \tag{6.21}$$

where $\mathbf{x}(t)$ is the floor displacements relative to the base motion, $\mathbf{M}, \mathbf{D}, \mathbf{K}$ are, respectively, the mass, damping and stiffness of the building, $\mathbf{B_s}$ is a matrix of input selection, $\mathbf{F}(t)$ is a matrix of external input forces from the control system, $\ddot{\mathbf{x}}_g(t)$ is the earthquake excitation and finally, $\mathbf{\Gamma}$ is a matrix of ones on the respectively earthquake directions.

For control design problem, the building model can be rewritten in a state-space framework as

$$\begin{aligned}
\dot{\mathbf{x}}(t) &= \mathbf{A}\mathbf{x}(t) + \mathbf{B}\mathbf{F}(t) + \mathbf{E}\ddot{\mathbf{x}}_g(t) && (6.22)\\
\mathbf{y}_m(t) &= \mathbf{C}_m\mathbf{x}(t) + \mathbf{D}_m\mathbf{F}(t) + \mathbf{F}_m\ddot{\mathbf{x}}_g(t) + \mathbf{v} && (6.23)\\
\mathbf{z}(t) &= \mathbf{C}_z\mathbf{x}(t) + \mathbf{D}_z\mathbf{F}(t) + \mathbf{F}_z\ddot{\mathbf{x}}_g(t) && (6.24)\\
\mathbf{y}_c(t) &= \mathbf{C}_c\mathbf{x}(t) + \mathbf{D}_c\mathbf{F}(t) + \mathbf{F}_c\ddot{\mathbf{x}}_g(t) && (6.25)
\end{aligned}$$

where $\mathbf{x}$ is the state vector, $\mathbf{y}_m$ is the measured output vector, $\mathbf{z}$ is the regulated output vector, $\mathbf{y}_c$ is the feedback vector for the control devices, that is, the actuator connections due to the actuator-structure interactions [30], and $\mathbf{v}$ is the measurement noise. Also, the matrices $\mathbf{D}_m, \mathbf{D}_z, \mathbf{D}_c$ represent the contribution of the input vector on the respective output of the system (for instance, in the case of acceleration feedback), and the matrices $\mathbf{F}_m, \mathbf{F}_z, \mathbf{F}_c$ represent the contribution of the external disturbances (earthquake) to the respective output of the system. The state-space matrices are

$$\mathbf{A} = \begin{bmatrix} \mathbf{0} & \mathbf{I} \\ -\mathbf{M}^{-1}\mathbf{K} & -\mathbf{M}^{-1}\mathbf{D} \end{bmatrix}; \quad \mathbf{B} = \begin{bmatrix} \mathbf{0} \\ \mathbf{M}^{-1}\mathbf{B}_s \end{bmatrix}; \quad \mathbf{E} = \begin{bmatrix} \mathbf{0} \\ -\mathbf{\Gamma} \end{bmatrix}. \quad (6.26)$$

For the case of position, velocity and acceleration measurements one can derive the following output matrices:

$$\mathbf{C}_m = \begin{bmatrix} \mathbf{I} & \mathbf{0} \\ \mathbf{0} & \mathbf{I} \\ -\mathbf{M}^{-1}\mathbf{K} & -\mathbf{M}^{-1}\mathbf{D} \end{bmatrix}, \quad \mathbf{D}_m = \begin{bmatrix} \mathbf{0} \\ \mathbf{0} \\ \mathbf{M}^{-1}\mathbf{B}_s \end{bmatrix}. \tag{6.27}$$

Similar expressions can be derived for the regulated and the connections output matrices. In this dissertation, it will be assumed that

$$\mathbf{F}_m = \mathbf{F}_z = \mathbf{F}_c = \mathbf{0}. \tag{6.28}$$

The state-space formulation can be modified in a way to include dynamics of the actuator and sensors (possibly a gain matrix). In this respect the actuators and sensor can be represented by their state-space form as

$$\mathbf{\Sigma}_s \; : \; \mathbf{y}_{sensor}(t) = \mathbf{D}_{sensor}\mathbf{y}_m(t) \tag{6.29}$$

$$\mathbf{\Sigma}_a \; : \; \begin{cases} \dot{\mathbf{x}}_a(t) = \mathbf{A}_a\mathbf{x}_a(t) + \mathbf{B}_a \begin{bmatrix} \mathbf{u}(t) \\ \mathbf{y}_c(t) \end{bmatrix} \\ \\ \mathbf{f}_a(t) = \mathbf{C}_a\mathbf{x}_a(t) + \mathbf{D}_a \begin{bmatrix} \mathbf{u}(t) \\ \mathbf{y}_c(t) \end{bmatrix} \end{cases} \tag{6.30}$$

$$\tag{6.31}$$

The actuator input matrix can be partitioned according to the type of its inputs, i.e., $\mathbf{B}_a = \begin{bmatrix} \mathbf{B}_{a1} & \mathbf{B}_{a2} \end{bmatrix}$. In order to enhance performance of the control design, the actuator and structure models are lumped together forming only one design state-space system as

$$\dot{\mathbf{x}}_d = \mathbf{A}_d\mathbf{x} + \mathbf{B}_d\mathbf{F} + \mathbf{E}_d\ddot{\mathbf{x}}_g \tag{6.32}$$

$$\mathbf{y}_m = \mathbf{C}_{md}\mathbf{x} + \mathbf{D}_{md}\mathbf{F} + \mathbf{F}_{md}\ddot{\mathbf{x}}_g + \mathbf{v} \tag{6.33}$$

$$\mathbf{z}_d = \mathbf{C}_{zd}\mathbf{x} + \mathbf{D}_{zd}\mathbf{F} + \mathbf{F}_{zd}\ddot{\mathbf{x}}_g + \mathbf{v} \tag{6.34}$$

where

$$
\begin{aligned}
\mathbf{A}_d &= \left[\begin{array}{c|c} \mathbf{A} & \mathbf{B}\mathbf{C}_a \\ \hline \mathbf{B}_{a2}\mathbf{C}_c & \mathbf{A}+\mathbf{B}_{a2}\mathbf{D}_c\mathbf{C}_a \end{array}\right], \quad \mathbf{B}_d = \begin{bmatrix} \mathbf{0} \\ \mathbf{B}_{a1} \end{bmatrix}, \qquad (6.35) \\
\mathbf{E}_d &= \begin{bmatrix} \mathbf{E}_r \\ \mathbf{B}_{a2}\mathbf{F}_c \end{bmatrix} \\
\mathbf{C}_{md} &= \begin{bmatrix} \mathbf{C}_m & \mathbf{D}_m\mathbf{C}_a \end{bmatrix}, \quad \mathbf{C}_{zd} = \begin{bmatrix} \mathbf{C}_z & \mathbf{D}_z\mathbf{C}_a \end{bmatrix} \\
\mathbf{D}_{md} &= \mathbf{D}_{zd} = 0, \quad \mathbf{F}_{md} = \mathbf{F}_m, \quad \mathbf{F}_{md} = \mathbf{F}_z
\end{aligned}
$$

6.3.1 Active Control Systems: The LQG Approach

Several control algorithms have been developed for the active control system as discussed in Section 6.2.1. The most common approach for building control uses the LQG/$\mathcal{H}_2$ methods associated with linear controller design [4, 111, 124]. In this manner the control design problem can be formulated as follows: Given the design model in state-space as in Eqs. (6.35), $\mathbf{\Sigma} = \left[\begin{array}{c|c} \mathbf{A}_d & \mathbf{B}_d \\ \hline \mathbf{C}_{md} & \mathbf{D}_{md} \end{array}\right]$, design a linear quadratic Gaussian (LQG) control algorithm for vibration reduction due to external inputs, such as earthquakes. The LQG solution minimizes the following performance index:

$$
\mathrm{J} = \lim_{\tau\to\infty} \mathrm{E}\left[\int_0^{\tau} \left\{\mathbf{z}_d^T\mathbf{Q}\mathbf{z}_d + \mathbf{F}^T\mathbf{R}\mathbf{F}\right\} dt\right], \qquad (6.36)
$$

where E is the expectation operator. It is known that [4, 111], an LQG controller is given by the following state-space equations:

$$
\begin{aligned}
\dot{\mathbf{x}}_C(t) &= (\mathbf{A}_d - \mathbf{B}_d\mathbf{K} - \mathbf{L}\mathbf{C}_{md} + \mathbf{L}\mathbf{D}_{md}\mathbf{K})\mathbf{x}_C(t) + \mathbf{L}\mathbf{u}(t) \qquad (6.37) \\
\mathbf{F}(t) &= -\mathbf{K}\mathbf{x}_C(t) \qquad (6.38)
\end{aligned}
$$

where $\mathbf{K}, \mathbf{L}$ are the regulator and estimator gains determined by the solution of two particular Riccati equations.

6.3.2 Semi-Active Control Systems: The Clipped Optimal Control Approach

Several control algorithms have been developed for semi-active systems [65]. One algorithm that has been shown to be effective when used with MR dampers is the clipped-optimal control approach proposed by Dyke *et al.* [31, 32]. The idea of the clipped-optimal control is to design a linear optimal controller $\mathbf{K}_c(s)$, using a variety of synthesis methods (H_2/LQG, for instance) to generate a vector of desired control forces $\mathbf{f}_c$ that would be achieved by the actuator if it could apply an active force to the system. Due to the dissipative nature of the semi-active device, this linear force cannot be achieved at all times. Thus, a logic has to be implemented in order to take into account the direction of the relative velocity of the control device.

The design of the linear optimal controller is based on the measured structural responses, i.e, $\mathbf{y}_m$ and the measured control force vector $\mathbf{F}$ applied to the structure, that is

$$\mathbf{f}_c = \mathcal{L}^{-1}\left\{\mathbf{K}_c(s)\mathcal{L}\left\{\begin{array}{c}\mathbf{y}_{md}\\ \mathbf{F}\end{array}\right\}\right\} \tag{6.39}$$

where $\mathcal{L}\{\cdot\}$ denotes the Laplace transform.

In order to generate the desired optimal control force, a force feedback loop is added to induce the MR damper to generate approximately the desired optimal control force, such that the command voltage $\mathbf{v}$ is selected as follows.

When the MR damper provides the desired optimal force (i.e., $\mathbf{F} = \mathbf{f}_c$), the voltage applied to the damper should remain at the present level. If the magnitude of the force produced by the damper is smaller than the magnitude of the desired optimal force and both have the same sign, the voltage applied to the current driver is increased to the maximum level in order to increase the force produced by the damper to match the desired control force. Otherwise, the commanded voltage is set to zero. Mathematically, the above algorithm can be stated as

$$\mathbf{v} = V_{max}\mathcal{H}\left[(\mathbf{f}_c - \mathbf{F})\mathbf{F}\right] \tag{6.40}$$

where $\mathcal{H}[\cdot]$ is the Heaviside step function and V_{max} is the voltage of the current driver associated with saturation of the magnetic field in the MR damper.

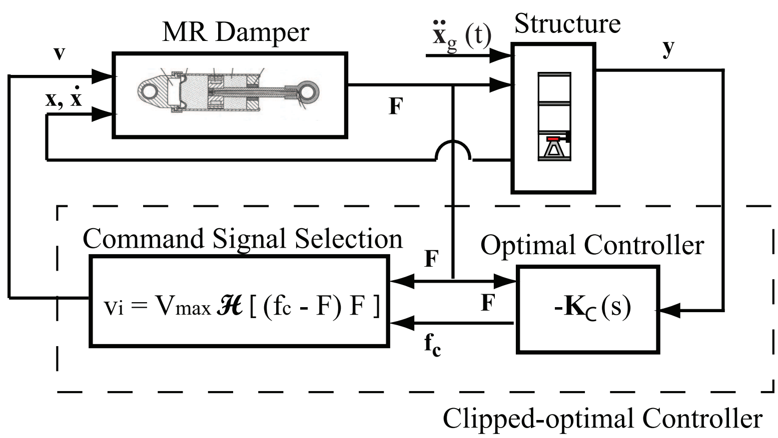

Figure 6.9: Clipped-Optimal Control Strategy

It should be pointed out that some modification of the LQG control law is necessary to take into account the clipped-optimal control strategy. Since the output of the controller is not anymore a direct input to the plant, one needs to write

$$\dot{\mathbf{x}}_C(t) = \mathbf{A}_d\mathbf{x}_C(t) + \mathbf{B}_d\mathbf{F}(t) + \mathbf{L}\left[\mathbf{y}_{md} - (\mathbf{C}_{md}\mathbf{x}_c(t) + \mathbf{D}_{md}\mathbf{F}(t))\right] \quad (6.41)$$

$$\mathbf{f}_C(t) = -\mathbf{K}\mathbf{x}_C(t) \quad (6.42)$$

In this manner, the clipped-optimal controller becomes

$$\dot{\mathbf{x}}_C(t) = (\mathbf{A}_d - \mathbf{L}\mathbf{C}_{md})\mathbf{x}_C(t) + \begin{bmatrix} \mathbf{L} & \mathbf{B}_d - \mathbf{L}\mathbf{D}_{md} \end{bmatrix} \begin{bmatrix} \mathbf{y}_m(t) \\ \mathbf{F}(t) \end{bmatrix} \quad (6.43)$$

$$\mathbf{f}_C(t) = -\mathbf{K}\mathbf{x}_C(t) \quad (6.44)$$

6.4 Numerical Example: Three-Story Building

A three story building is used to illustrate the active and semi-active controller implementations. The building is depicted in Fig 6.10. A hydraulic actuator (active bracing system) is placed at the first floor of the building and attached to the ground on the structure. For this system, the actuator displacement is equivalent to the displacement of the first floor. A position sensor is used to measure the displacement of the first floor and provide feedback for the control actuator. Also, accelerometers were placed on each floor for measurement of absolute accelerations. For comparison purposes a MR device is placed on the first floor using the same configuration as the active bracing system, and its controller is redesigned for the same building.

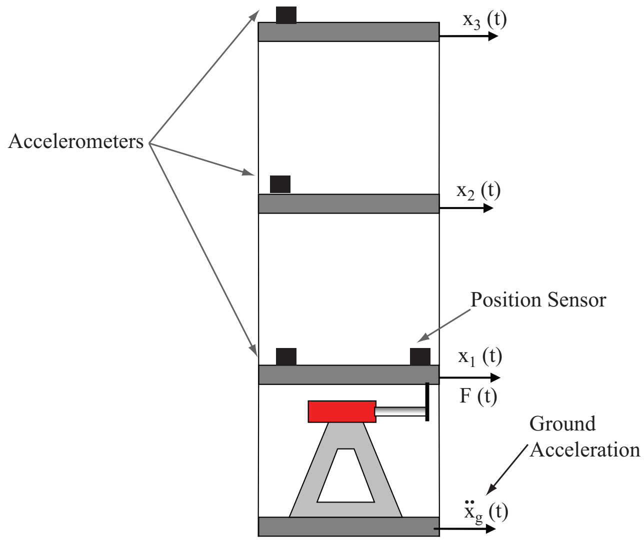

Figure 6.10: Three-story building schematic

6.4.1 Active Bracing System

The mathematical model used here is taken from [20, 21]. The model consists of lumped masses at each floor with respective stiffness and damping effects. A hydraulic actuator is placed at the first floor. Numerically, the model is given by

$$[\mathbf{M}]\,\ddot{\mathbf{x}}(t) + [\mathbf{C}]\,\dot{\mathbf{x}}(t) + [\mathbf{K}]\,\dot{\mathbf{x}}(t) = \mathbf{B_s}F(t) - [\mathbf{M}]\,\mathbf{\Gamma}\ddot{\mathbf{x}}_g(t) \tag{6.45}$$

where

$$\mathbf{M} = 175.2\begin{bmatrix} 5.6 & 0 & 0 \\ 0 & 5.6 & 0 \\ 0 & 0 & 5.6 \end{bmatrix}; \quad \mathbf{K} = 175.2\begin{bmatrix} 15649 & -9370 & 2107 \\ -9370 & 17250 & -9274 \\ 2107 & -9274 & 7612 \end{bmatrix};$$

$$\mathbf{C} = 175.2\begin{bmatrix} 2.185 & -0.327 & 0.352 \\ -0.327 & 2.608 & -0.015 \\ 0.352 & -0.015 & 2.497 \end{bmatrix}; \quad \mathbf{\Gamma} = \begin{bmatrix} 1 \\ 1 \\ 1 \end{bmatrix}; \quad \mathbf{B}_s = \begin{bmatrix} 1 \\ 0 \\ 0 \end{bmatrix}$$

with the following units: $M \rightarrow [kg]$, $K \rightarrow [N/m]$, $C \rightarrow [N*m/sec]$. The hydraulic actuator is modeled as in 6.3 and its parameters are given by [30]:

$$a_1 = 6.08e5\,[kN/m*s]; \quad a_2 = 6.567e5\,[kN/m]; \quad a_3 = 29.6\,[1/s]$$

Using the acceleration of the all floors together with the displacement of the actuator as a regulated output vector, i.e, $\mathbf{z} = \begin{bmatrix} \ddot{x}_1 & \ddot{x}_2 & \ddot{x}_3 & x_1 \end{bmatrix}$ the results for an actual earthquake input (El Centro [116]) is given in Figures 6.11-6.4.1.

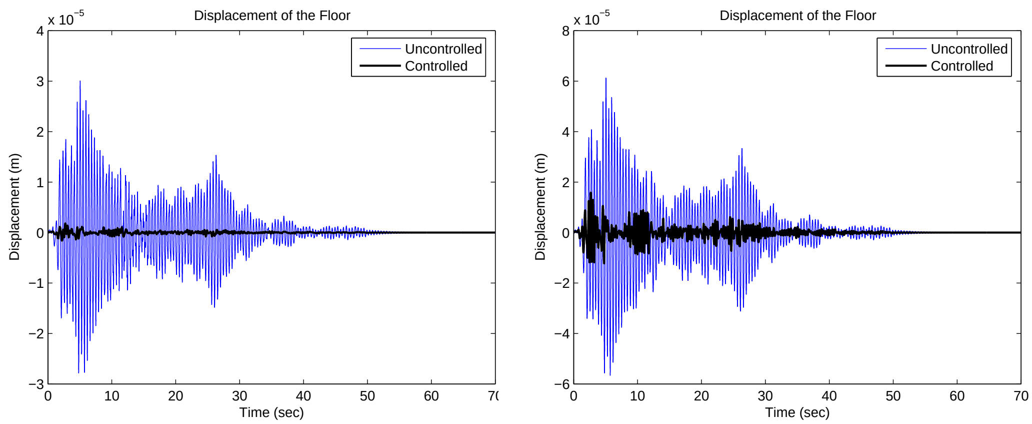

(a) (b)

6.4.2 Magneto-Rheological System

For illustration of semi-active control, the same mathematical model of a three-story building was used as in the previous section. The MR model was taken from Section 6.2.3.1. For the controller design, it is not possible to directly command the MR damper to generate a specified force to be applied to the structure as in Section 6.4.1. Only the control voltage can be directly commanded to increase or decrease the force produced by MR the device.

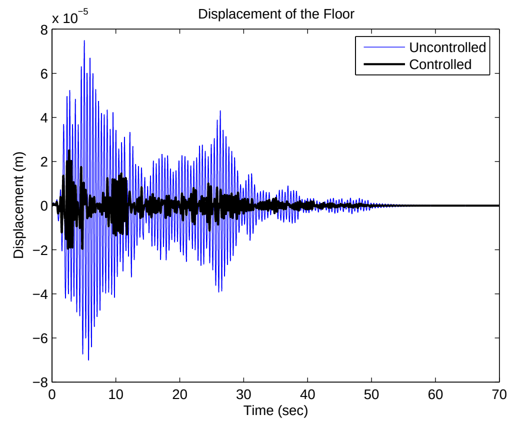

(c)

Figure 6.11: With active bracing: displacement of the (a) first, (b) second, and (c) third floors.

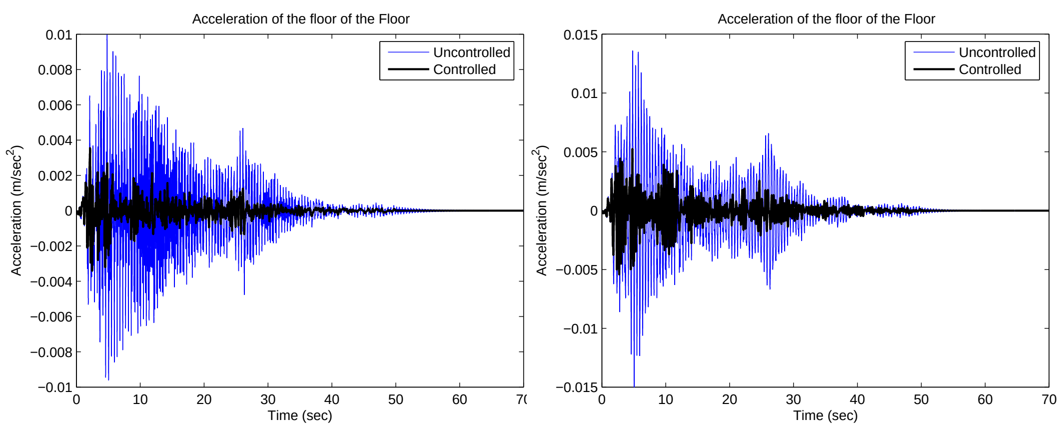

(a) (b)

The application of the MR damper to a three-story building can be modeled using the block diagram depicted in Fig. 6.9. The effectiveness of the semi-active control for seismic mitigation, can be seen in Figures 6.13-6.16.

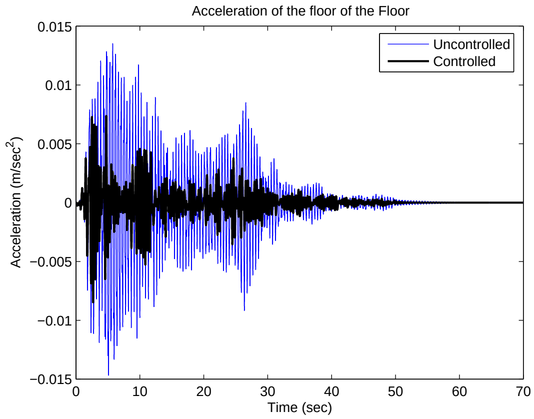

(c)

Figure 6.12: With active bracing: acceleration of the (a) first, (b) second, and (c) third floors.

The input to the system is given by the same El-Centro earthquake [116] data as the previous section.

Comparing the outputs of the active bracing system with the MR actuation scheme, one observes that the MR outperforms the active control scheme in terms of input efforts and actual displacement and acceleration reduction.

6.5 A Family of Benchmark Problems

In an effort to develop a common basis for comparison of the various algorithms and devices for seismic control, the American Society of Civil Engineers (ASCE) Committee on Structural Control has developed a benchmark for structural control design [87, 106, 108]. The benchmark problems are comprised of three generations: **(1) First Generation** Three-story linear build-

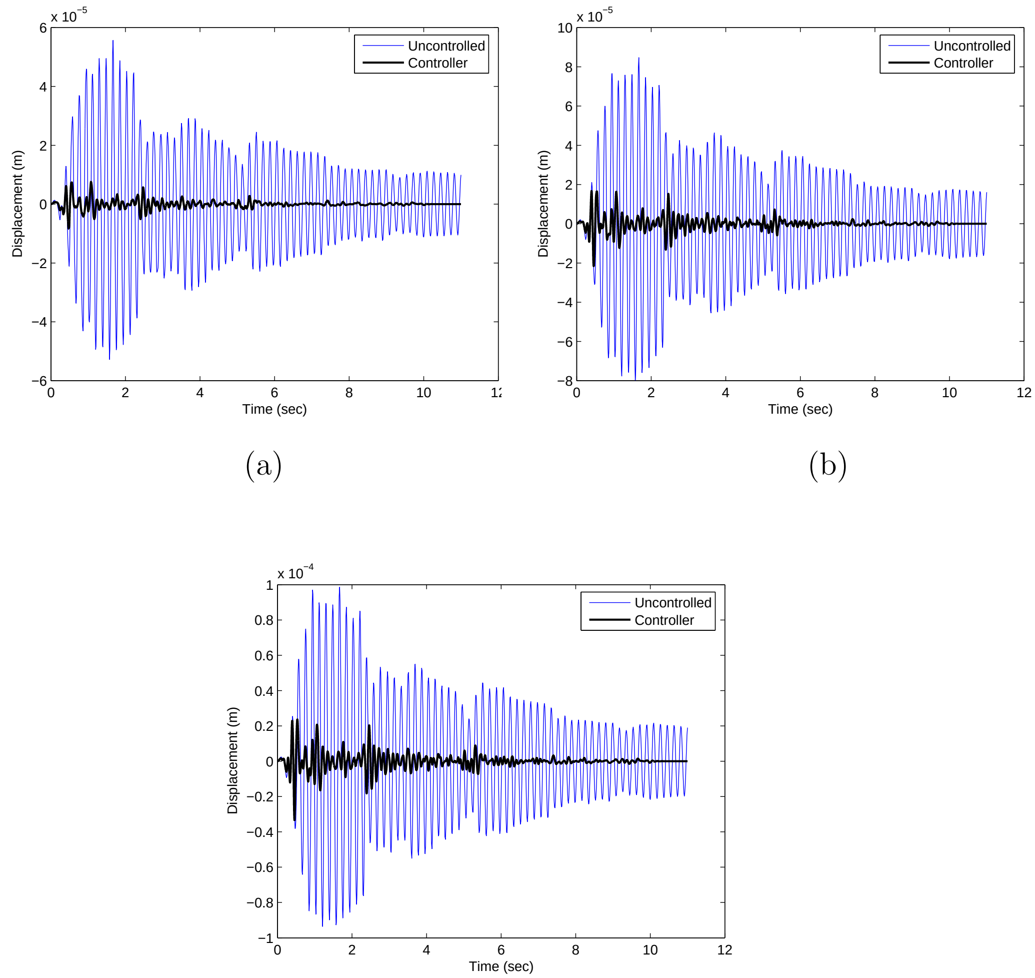

(a) (b) (c)

Figure 6.13: With MR device: displacement of the (a) first, (b) second, and (c) third floors.

ing; **(2) Second Generation**: Twenty-story linear building, and **(3) Third Generation**: Three-, nine-, and twenty-story non-linear building models.

As reported in the 1997 ASCE Structures Congress [100], several suc-

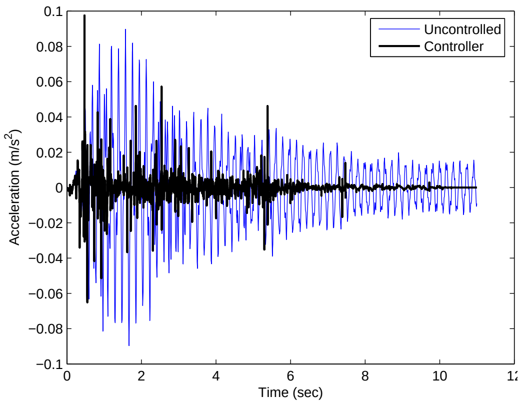

(a)

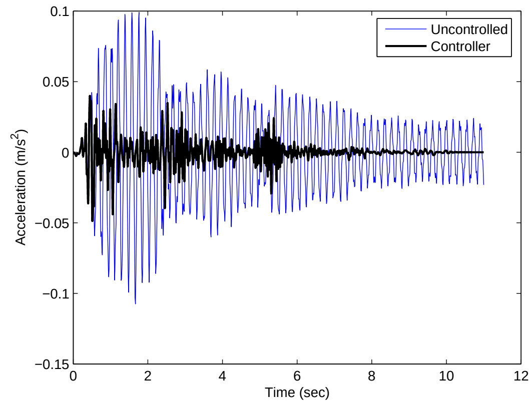

(b)

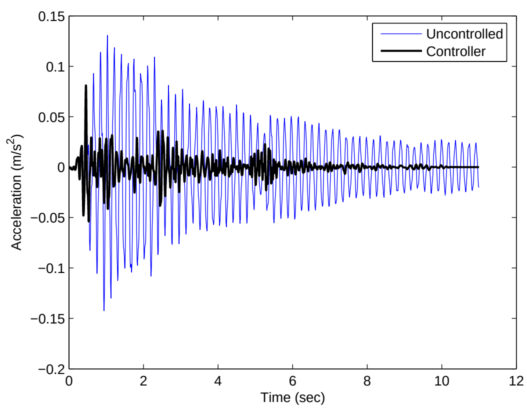

(c)

Figure 6.14: With MR device: acceleration of the (a) first, (b) second, and (c) third floors.

cessful control algorithms have been implemented in simulation and experimentally verified for the three-story building model. However, during the Second International Workshop on Structural Control in 1996, it was recog-

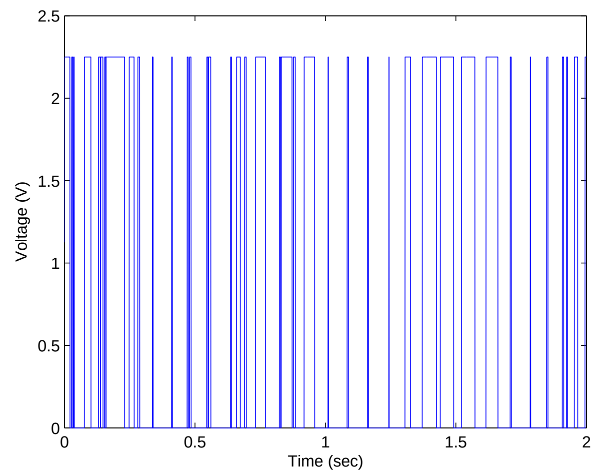

Figure 6.15: Voltage applied to the current driver.

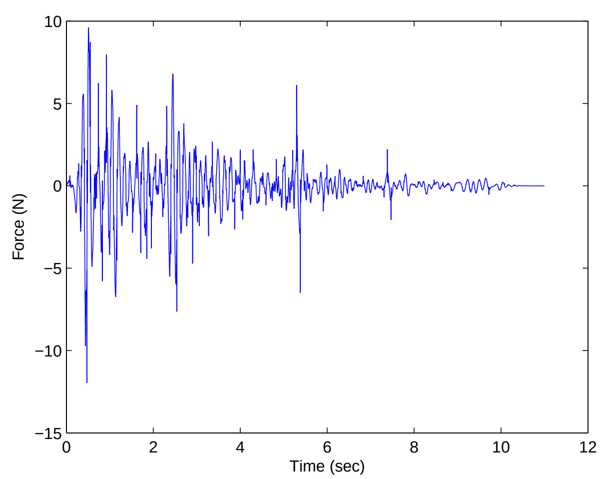

Figure 6.16: Force output from the MR damper.

nized that developing a family of benchmark building models was important to provide systematic and standardized means by which competing control strategies, including devices, algorithms, and sensors, could be evaluated.

Following the suggestions of the Working Group on Building Control (ASCE), two benchmark problems were proposed during 2nd World Conference on Structural Control held in 1998. The first, a benchmark problem considered wind excited buildings (see Yang, *et al.* [123]). The second benchmark problem was the next generation benchmark control problem for seismically excited buildings (see Spencer, *et al.* [108]). Both benchmark problems assumed that the structural models remained perfectly elastic during the disturbance inputs.

Finally, due to the fact that large magnitude earthquakes can cause material yielding in the structural elements, a nonlinear building model was proposed. High-fidelity nonlinear models were developed as extensions to the second generation of benchmark problem addressing other heights [87, 88]. The nonlinear building model benchmark problem will not be pursued in this dissertation.

In order to verify the consequences of model order reduction applied to the benchmark problem, it was decided to work with the seismically excited next generation benchmark problem [108]. Moreover, due to its systematic model construction approach, it allows one to readily perform changes in the model, such as the number of floors and bays. In this manner, a smaller six-story building was developed for the evaluation of the model reduction procedures. Finally, in order to assess the effectiveness of model reduction for large-scale structures, a larger problem was considered. An actual structure located at Purdue University, called the Bowen Model, was modeled by finite element techniques and used as the third structure evaluated.

6.5.1 Twenty-Story Building Model

The twenty-story building is shown in Fig. 6.17. It was developed as a benchmark study for structural control strategies comparison. Although the building was designed by a construction firm to meet seismic code for the Los Angeles region, it was not constructed. The Los Angeles twenty-story (known here as the LA 20-story) structure is 30.48 m by 36.58 m in plan, and 80.77 m in elevation. The bays are 6.10 m on center, in both directions, with five bays in the north-south (N-S) direction and six bays in the east-west (E-W) direction. The buildings lateral load-resisting system is comprised of steel perimeter moment-resisting frames (MRFs). The interior bays of the structure contain simple framing with composite floors. Refer to [108] for more design details.

A high-fidelity linear time-invariant state-space model was developed and was designated the *evaluation model* [108]. The LA 20-story structure is modeled using finite element techniques resulting in 180 nodes interconnected by 284 elements, as seen in Fig. 6.17. The nodes are located at beam-to-column joints and column splices. Each node has three degrees-of-freedom (DOFs): horizontal, vertical and rotational. The entire structure has 540 DOFs prior to application of boundary conditions/constraints and subsequent model reduction. Global mass and stiffness matrices are assembled from the elemental mass and stiffness matrices by summing the mass and stiffness associated with each DOF for each element of the entire structure.

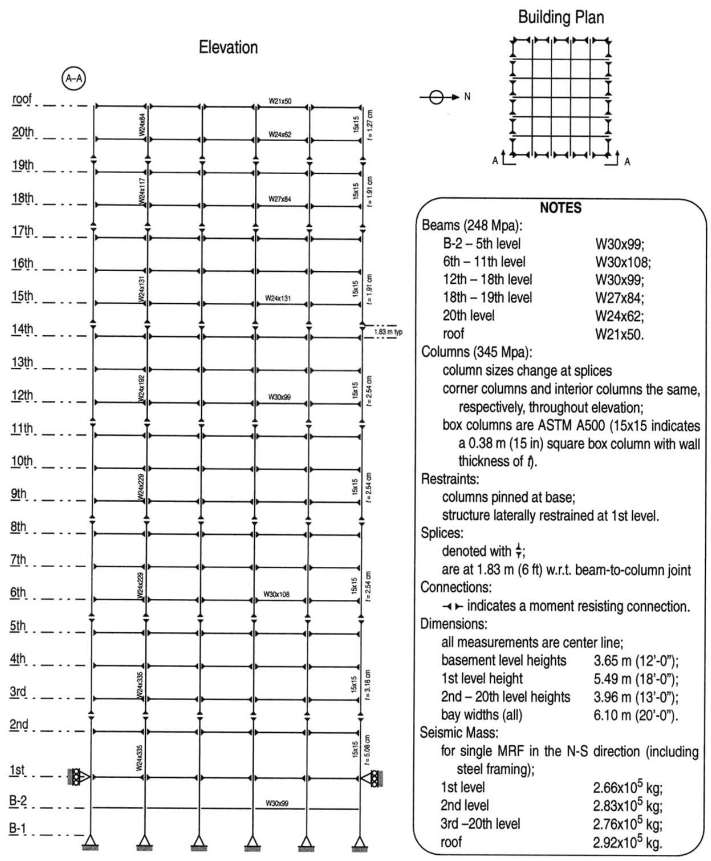

Figure 6.17: Twenty-story benchmark building model. Source [108].

6.5.2 Six-Story Building Model

A less complex version of the twenty-story building was constructed in order to investigate the mathematical model of the structure for the controller design and eventually to use to illustrate the model reduction techniques. Removing floors of the twenty-story structure, a **six-story** building was developed. The building is illustrated in Fig. 6.18. The same material properties and structure types were used for the six-story building as for the twenty-story building. However, several modifications were made to the finite element program to suit the six-story model, such as the connections between columns and floors.

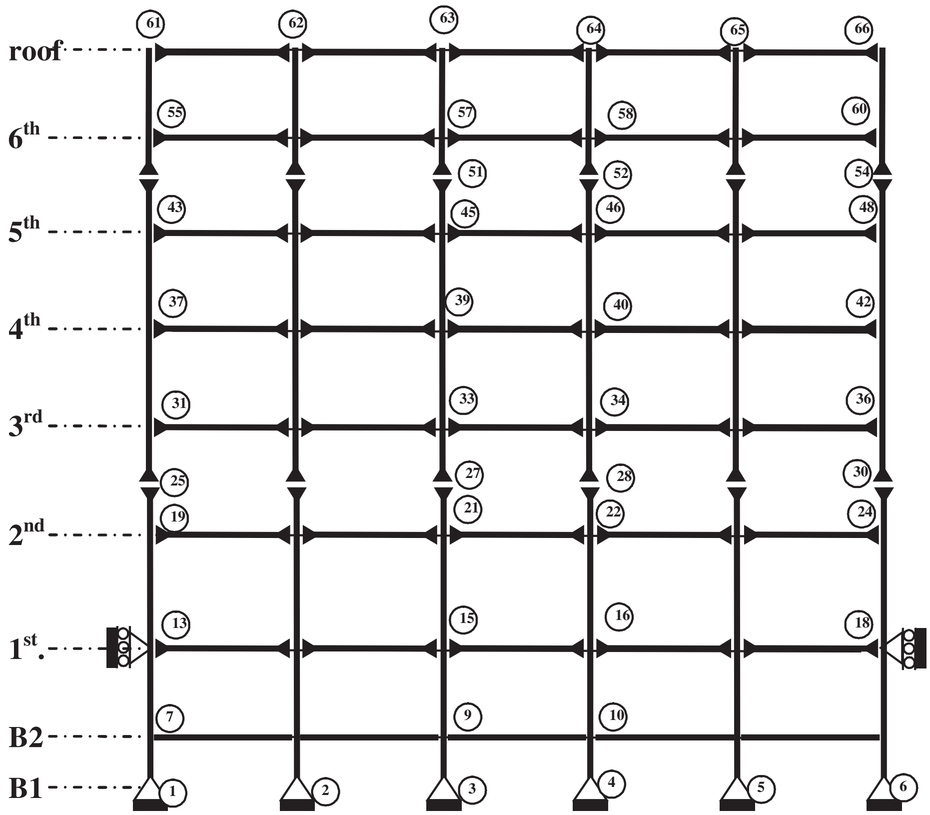

Figure 6.18: 6-Story building model

6.5.3 The Bowen Building Model

The Bowen building is an actual structure built in the Large Scale Research Laboratory in the Department of Civil Engineering at Purdue University. Even though it is comprised of only three floors, the finite element model system matrices are on order of $\mathbf{M} \in \mathbb{R}^{4950\times 4950}$ and $\mathbf{K} \in \mathbb{R}^{4950\times 4950}$. Moreover, the model is well-suited for testing the model reduction techniques for large-scale structures since there are some freedom on the choice of actuator and sensor locations, and on the type of actuation (active, semi-active, or hybrid) to be used.

Figure 6.19: Bowen Building at Purdue University. Source [113].

6.6 Actuator and Sensor Placement

It is known that actuator and sensor placement, i.e., determination of the total number of actuator control and sensors together with their physical location on the structure, have great influence of the closed-loop performance

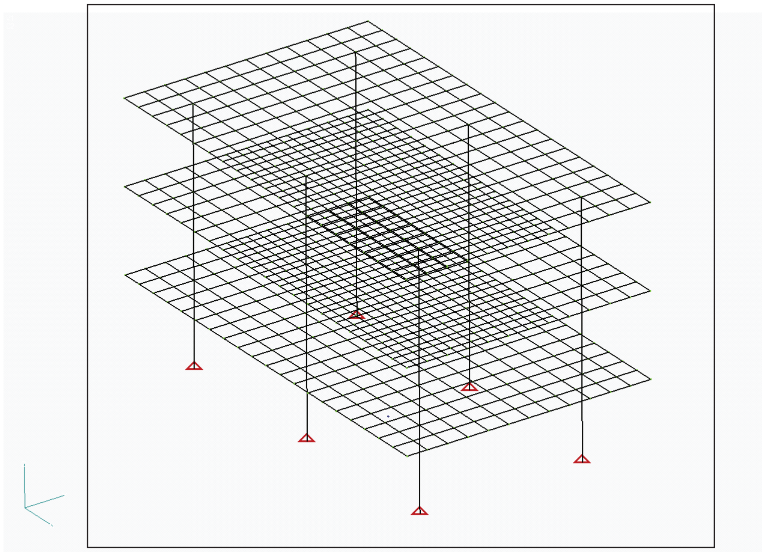

Figure 6.20: Bowen Building at Purdue University - The Finite Element Model obtained in NASTRAN. Source [72].

of the structure [81]. This becomes more important for 3D multi-story civil structures with lateral-torsional behavior. The vertical distribution of sensors and actuators across the building height is critical to structural performance, as well as the horizontal distribution at floor levels [119]. This section discusses the placement issues associated with actuators and sensors for flexible structures.

The actuator and sensor placement issue has been investigated since the introduction of the concept of structural control [78]. Many techniques for the optimal placement of sensors and actuators in vibration control systems have been developed in recent years based on the concepts of controllability and observability. It is known that the controllability and observability are closely related to an optimal placement of actuators and sensors. Chang and Soong [16] placed a limited number of active devices in a structure for modal control by minimizing a particular performance index. In [77], an appropriate number and placement of devices based on independent modal space control was analyzed. Cheng and Pantiledes [18] computed the controllability index associated with each story of a building, from which the actuator locations were provided.

In practice, the actuator and sensor placement procedure should be simple and efficient and require a limited computational effort. Also, the procedure should take into account the fact that, for technical and economical reasons, the number of sensors significantly exceeds the number of actuators, so that the actuator placement is done first, and once fixed, the sensor placement is established. This dissertation focuses on a different controllability-observability approach proposed by [89] and described in detail in [38, 39]. This approach involves the computation of the system norms of each device location for selected modes, and then grades them according to their participation in the total system norm giving rise to the concept of placement indices. First, the concepts of modal representations is presented and it is shown how one can compute in a straightforward manner the system norms and therefore the placement indices.

6.6.1 Nodal and Modal Representations

The state-space representation is not unique. Usually, the state equations are written using displacement and velocity at structural locations yielding the nodal coordinates. By means of a similarity transformation, the nodal state-space representation can be converted to modal displacements and their derivatives as states yielding the modal state-space representation.

However, modal coordinates are not unique either. They can be transformed to convenient representations such that the state matrix $\mathbf{A}$ is expressed in diagonal or block diagonal forms [38, 39]. Given the modal state-space representation

$$\dot{\mathbf{x}} = \mathbf{A}\mathbf{x} + \mathbf{B}\mathbf{u} \tag{6.46}$$

$$\mathbf{y} = \mathbf{C}\mathbf{x} + \mathbf{D}\mathbf{u} \tag{6.47}$$

it can be transformed to the modal model as

$$\mathbf{A}_m = \mathrm{diag}(\mathbf{A}_{m_i}), \quad \mathbf{B}_m = \begin{bmatrix} \mathbf{B}_{m_1} \\ \mathbf{B}_{m_2} \\ \vdots \\ \mathbf{B}_{m_n} \end{bmatrix}, \quad \mathbf{C}_m = \begin{bmatrix} \mathbf{C}_{m_1} & \mathbf{C}_{m_2} & \cdots & \mathbf{C}^T_{m_n} \end{bmatrix}. \tag{6.48}$$

for $i = 1, 2, \cdots, n$ modes. In this case, $\mathbf{A}_{m_i}$ are 2×2 blocks, $\mathbf{B}_{m_i}$ and $\mathbf{C}_{m_i}$ are $2 \times s$ and $r \times 2$ blocks, for s actuators and r sensors respectively.

According to [38, 39], three modal representations have important properties that will be used in the actuator and sensor placement context. They are:

- Modal Model 1:

$$\mathbf{A}_{mi} = \begin{bmatrix} 0 & \omega_i \\ -\omega_i & -2\zeta_i\omega_i \end{bmatrix}, \quad \mathbf{B}_{mi} = \begin{bmatrix} 0 \\ b_{mi} \end{bmatrix}, \quad \mathbf{C}_{mi} = \begin{bmatrix} \frac{c_{mqi}}{\omega_i} & c_{mvi} \end{bmatrix}; \tag{6.49}$$

- Modal Model 2:

$$\mathbf{A}_{mi} = \begin{bmatrix} -\zeta\omega_i & \omega_i \\ -\omega_i & -\zeta_i\omega_i \end{bmatrix}, \quad \mathbf{B}_{mi} = \begin{bmatrix} 0 \\ b_{mi} \end{bmatrix}, \mathbf{C}_{mi} = \begin{bmatrix} \frac{c_{mqi}}{\omega_i} - c_{mvi}\zeta_i & c_{mvi} \end{bmatrix}; \tag{6.50}$$

- Modal Model 3:

$$\mathbf{A}_{mi} = \begin{bmatrix} 0 & 1 \\ -\omega_i^2 & -2\zeta_i\omega_i \end{bmatrix}, \quad \mathbf{B}_{mi} = \begin{bmatrix} 0 \\ b_{mi} \end{bmatrix}, \quad \mathbf{C}_{mi} = \begin{bmatrix} c_{mqi} & c_{mvi} \end{bmatrix}; \tag{6.51}$$

Consider a modal state-space representation as in Eq. (6.48) and its transfer function representation $\mathbf{G}_m(s) = \mathbf{C}_m(s\mathbf{I} - \mathbf{A}_m)^{-1}\mathbf{B}_m$. It readily follows [38, 39] that the H_2, H_∞ and Hankel norms for each mode are approximated by

$$\begin{aligned} \|G_i\|_2 &\cong \frac{\|\mathbf{B}_{m,i}\|_2\|\mathbf{C}_{m,i}\|_2}{2\sqrt{\zeta_i\omega_i}}, \quad \|G_i\|_\infty \cong \frac{\|\mathbf{B}_{m,i}\|_2\|\mathbf{C}_{m,i}\|_2}{2\zeta_i\omega_i}, \\ \|G_i\|_h &\cong \frac{\|\mathbf{B}_{m,i}\|_2\|\mathbf{C}_{m,i}\|_2}{4\zeta_i\omega_i}. \end{aligned} \tag{6.52}$$

Also, an additive property of the modal norms yield the norm of the entire structure as

$$\|G\|_2 \cong \sqrt{\sum_{i=1}^{n} \|G_i\|_2^2}, \tag{6.53}$$

$$\|G\|_\infty \cong \max\|G_i\|_\infty, \quad i = 1, \cdots, n \tag{6.54}$$

$$\|G\|_h \cong \max\|G_i\|_h = \gamma_{max}, \quad i = 1, \cdots, n \tag{6.55}$$

where γ_{max} is the largest singular value of the system.

6.6.2 Placement Indices and Strategies

The method used in this dissertation for the actuator and sensor placement uses the Hankel norms for construction of the placement indices. The reason is that measures of controllability and observability are captured by the Hankel singular values of the system and are system invariants. Using the concepts from the previous section, in particular, the Eq. (6.55), one can define the placement index, σ_{ij}, that evaluates the jth actuator at the ith mode in terms of Hankel norm as

$$\sigma_{ij} = \frac{\|G_{ij}\|_h}{\|G\|_h}. \tag{6.56}$$

Similarly, for the sensor placement, one can define

$$\sigma_{ik} = \frac{\|G_{ik}\|_h}{\|G\|_h}. \tag{6.57}$$

where σ_{ik} evaluates the kth sensor at the ith mode of the structure. It is convenient to to represent the placement indices in a matrix form, having r actuators and s sensors and n modes, as follows:

$$\Sigma_h \;=\; \begin{array}{cc} \begin{bmatrix} \sigma_{11} & \sigma_{12} & \cdots & \sigma_{11} & \cdots & \sigma_{1r} \\ \sigma_{21} & \sigma_{22} & \cdots & \sigma_{2j} & \cdots & \sigma_{2r} \\ \vdots & \vdots & \cdots & \vdots & \vdots & \vdots \\ \sigma_{i1} & \sigma_{i2} & \cdots & \sigma_{ij} & \cdots & \sigma_{ir} \\ \vdots & \vdots & \cdots & \vdots & \vdots & \vdots \\ \sigma_{n1} & \sigma_{n2} & \cdots & \sigma_{nj} & \cdots & \sigma_{nr} \end{bmatrix} & \begin{array}{l} \\ \\ \\ \Leftarrow ith\, mode \\ \\ \\ \end{array} \\ \Uparrow jth\, actuator & \end{array} \tag{6.58}$$

Similarly, the sensor placement matrix is

$$\Sigma_h = \begin{array}{ll} \left[\begin{array}{cccccc} \sigma_{11} & \sigma_{12} & \cdots & \sigma_{11} & \cdots & \sigma_{1s} \\ \sigma_{21} & \sigma_{22} & \cdots & \sigma_{2k} & \cdots & \sigma_{2s} \\ \vdots & \vdots & \cdots & \vdots & \vdots & \vdots \\ \sigma_{i1} & \sigma_{i2} & \cdots & \sigma_{ik} & \cdots & \sigma_{is} \\ \vdots & \vdots & \cdots & \vdots & \vdots & \vdots \\ \sigma_{n1} & \sigma_{n2} & \cdots & \sigma_{nk} & \cdots & \sigma_{ns} \end{array}\right] & \begin{array}{l} \\ \\ \\ \Leftarrow ith\, mode \\ \\ \\ \end{array} \\ \qquad\qquad\qquad\quad \Uparrow kth\, sensor & \end{array} \tag{6.59}$$

The placement matrices give information about each actuator/sensor with respect to each mode. However, it can be studied from two different points of view: (1) one may examine the importance of a single actuator/sensor over all modes, i.e., compute the rms of the rows of the placement matrix, or (2) one may examine the importance of all control devices/sensors to a single mode, i.e., compute the rms of the columns of the placement matrix. Since the former method can possibly result in large indices for higher modes, it does not agree with the building models, where the first few (lower) modes dominate the response, and thus will not be considered here. In this manner one can compute

$$\sigma_{Am} = \left[\begin{array}{cccc} \sigma_{Am1} & \sigma_{Am2} & \cdots & \sigma_{Amn} \end{array} \right] \tag{6.60}$$

$$\sigma_{Sm} = \left[\begin{array}{cccc} \sigma_{Sm1} & \sigma_{Sm2} & \cdots & \sigma_{Smn} \end{array} \right] \tag{6.61}$$

where σ_{Am} and σ_{Sm} are the actuator and sensor index vectors respectively, and

$$\sigma_{Ami} = \sqrt{\sum_{j=1}^{s} \sigma_{ij}^2}, \qquad \sigma_{Smi} = \sqrt{\sum_{k=1}^{r} \sigma_{ik}^2}. \tag{6.62}$$

Therefore, it is possible to readily eliminate locations with small indices for lower modes.

The above criteria works well for small to medium sizes structures [39]. However, for large-scale structures, this criteria might not be enough. Suppose for a specific sensor location with high placement index, locations close to it will have high indices as well. The neighboring locations to the original sensor might not be the best choice for placement since by adjusting sensors gains, one can eliminate the location's redundancies [38, 39]. In this manner, correlation coefficients are used to remove highly correlated locations. This procedure is explained in [38, 39].

6.6.3 Twenty-Story Building Model: Actuator and Sensor Placement

Due to the simplicity of the actuator and sensor placement for this structure (rigid floors and shear building model), a different approach will be taken. Hydraulic actuators are employed as the active control device. The actuators are placed on each floor of the structure, and a total of fifty hydraulic actuators are used to control the twenty-story benchmark problem. The actuators are distributed as follows: eight actuators are located on the first floor, four are located on both the second and third floors, and two actuators on each of the remaining floors of the structure [108]. For this benchmark, the actuators are implemented on the structure using a chevron brace configuration, in which the actuator is horizontal and rigidly attached between two consecutive floors.

Due to the *Action and Reaction Law* [99, 108], the forces caused by the hydraulic actuators have to be taken into account for the two floor in between the actuator. The force distribution can be seen in Fig. 6.21 for actuators in every floor. In this picture, the *red* forces are due to the application of the actuation, and the *blue* are the reaction of the actuation. For simplification, the forces are considered at nodal locations.

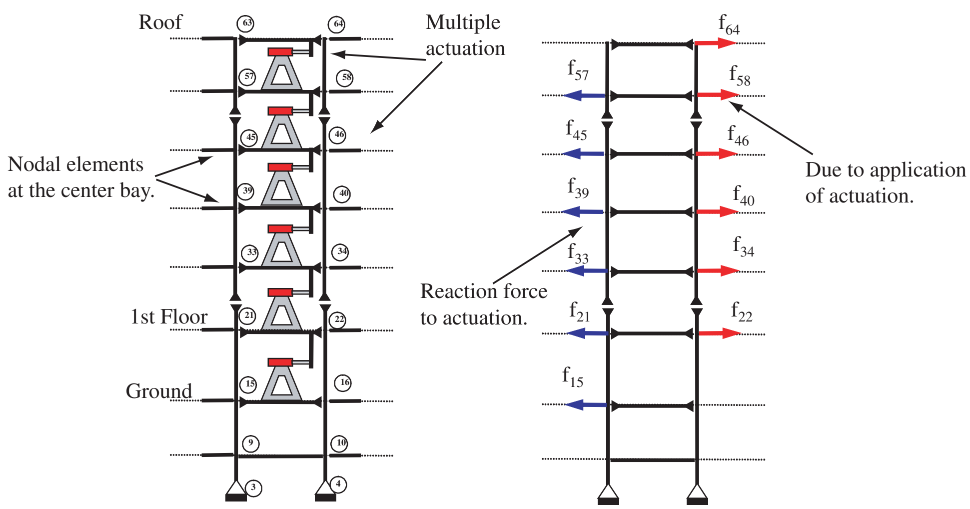

Figure 6.21: Actuation Placement and Forces Diagram

Assigning the nodal coordinates of the actuator locations allow the formation of the input matrix $\mathbf{B}_s$. Since the actuator nodal coordinates are referenced to the global coordinate system (that is, before any constraints have been applied), a transformation has to be performed on the coordinates after boundary conditions. It should be pointed out that new coordinate translations have to be taken into account when model reduction is performed.

Acceleration feedback will be considered for the controller design. A total of five accelerometers were selected for feedback in the control system (on floors 5, 9, 13, 17 and the roof). In this case, there is no need to compute the sensor placement matrix, since rigidity of the floors was considered.

6.6.4 Six-Story Building Model: Actuator and Sensor Placement

The placement strategy for this smaller building follows the same procedure as the twenty-story building model. A first attempt to control the structure is to place several actuators on every floor, with some known distribution on the number of actuators in each floor. We are considering the floors to be rigid, hence it is assumed that all the actuators on a single floor undergo the same inputs, and in turn, responds in the same way. Therefore, only six independent actuators are used for the control calculations. For simulation purposes, thus, a matrix gain is used to take into account the actuator distribution in all floors. Based on Fig. 6.18 and 6.21, the nodal coordinates of the actuator placement was chosen as:

$$\begin{aligned} \text{Actual forces} \Rightarrow &= \begin{bmatrix} 22 & 34 & 40 & 46 & 58 & 64 \end{bmatrix} \\ \text{Reaction forces} \Rightarrow &= \begin{bmatrix} 15 & 21 & 33 & 39 & 45 & 57 \end{bmatrix} \end{aligned}$$

which represents forces applied in every floor at the center bay. The sensor placement follows the same structure as the twenty-story building model. In this case, a total of six accelerometers were placed in every floor of the building.

6.6.5 Bowen Building: Actuator and Sensor Placement Strategy

Based on the above analysis, the placement strategy is established. For the Bowen building model, sensor placement is more flexible, so actuator locations are accomplished first. The placement procedure is described as follows:

- Place the control devices in order at the allowed locations, one in the x-direction and one in the y-direction. Assume each admissible sensor location has two sensors, one in the x- and one in the y-direction, so that the $\mathbf{C}_m$ matrix is fixed. For each location, compute the modal $\mathbf{B}_m$ matrix and then the Hankel placement indices for all modes, until the placement index matrix is formed.

- Choose 40 to 45 locations with the largest placement indices in the lower modes.

- Check the correlation coefficients for the selected locations. Reject actuators with high correlation. The resulting values (≈ 30) are the final locations. Fix the $\mathbf{B}_m$ matrix for the resulting set of actuator locations.

- Compute the floor sensor placement indices, assuming sensors are put at all allowable locations for each floor while none are on other floors to determine $\mathbf{C}_m$ matrix. Repeat for each floor until the the sensor placement index matrix is formed.

- Reject insignificant floors that have very low sensor placement indices.
- For the remaining floors, compute the placement indices one by one. Retain the non-correlated ones.
- Once this procedure is accomplished all control device and sensor locations are determined for the entire building.

In this manner, analyzing the placement indices as depicted in Figures 6.22 and 6.23, one can see that the actuator locations circled in the Figure 6.22 represent the locations with the highest contribution on all modes of the structure. The final selected actuator locations is shown in the Appendix B. Even though a procedure is given for the sensor placement, it was decided to use in the final sensors placement, a collocated actuator/sensor strategy (i.e., actuators and sensors in the same location). This is due to the fact that actuators and sensors collocation is an important issue for the passivity-based model reduction of flexible structures, as will be seen in the next chapters.

6.7 Concluding Remarks

This chapter illustrated the techniques involved in the process of designing controllers for seismically excited building models. First, different actuation schemes were shown. The differences between active and semi-active control strategies were illustrated with a three-story building model.

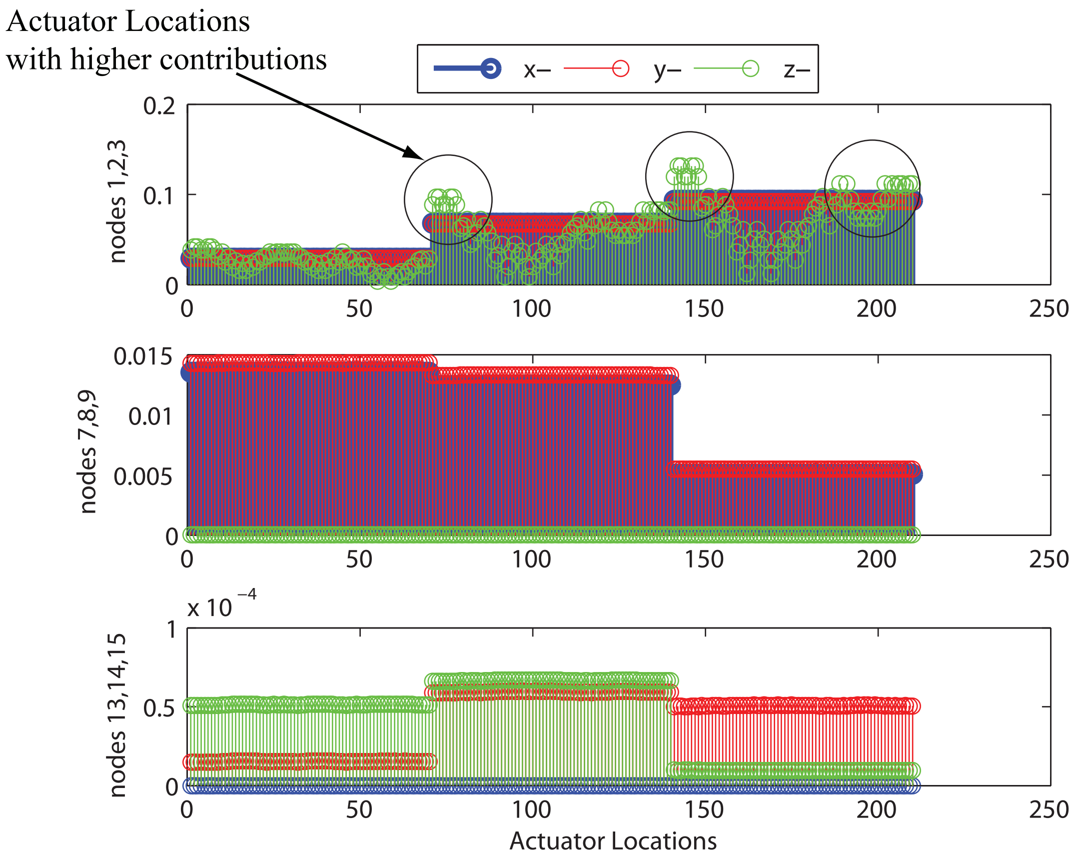

Figure 6.22: Control Device Placement Indices vs. Control Device Locations for the Bowen Building - displacement modes.

In order to apply the model and controller reduction techniques to real building structures, a family of benchmark building problems was introduced together with actuator and sensor placement techniques. Based on such schemes, the building models were constructed using Matlab/Simulink. Controller design and controller reduction for the benchmark problems become the next steps to be seen in the next chapters.

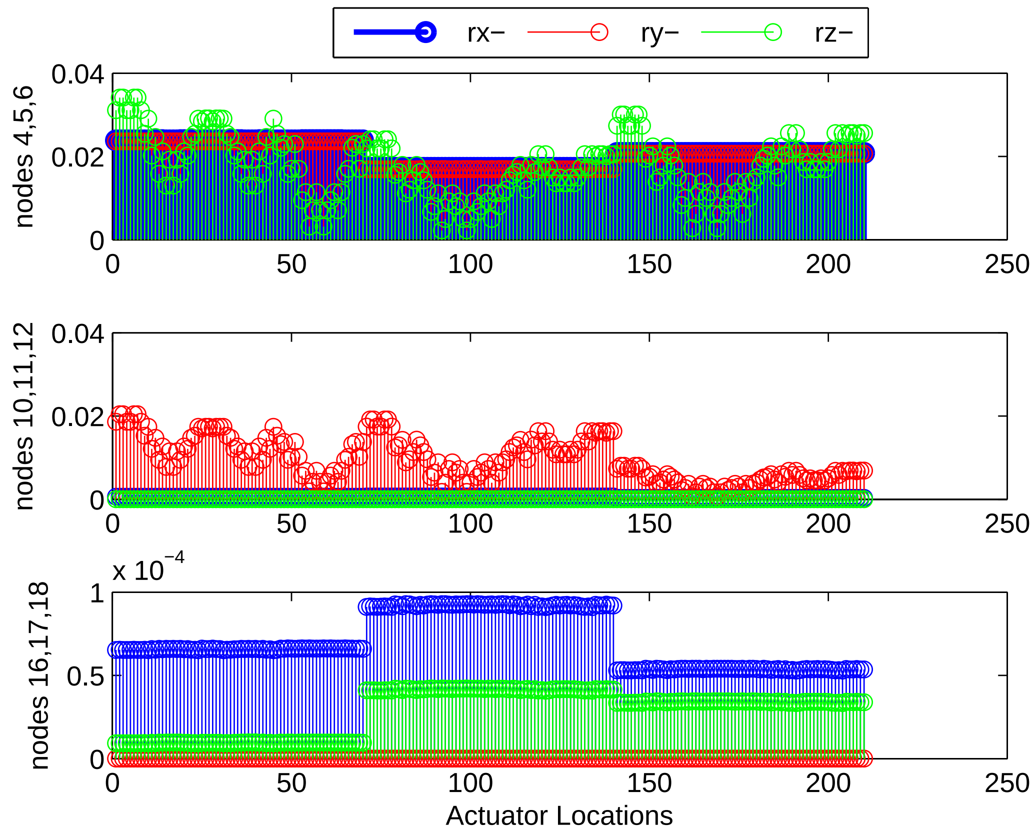

Figure 6.23: Control Device Placement Indices vs. Control Device Locations for the Bowen Building - rotational modes.

Chapter 7

Model Reduction in Structural Dynamics

Great improvements have been reported in the theory and application of Finite Element Modeling (FEM) during the past several decades. Many commercial software packages exist in the field of structural dynamics analysis, including NASTRAN [23], ANSYS [59], and SAP2000 [60], among others. However, the models obtained are usually of large dimensions due to a fine grid on the finite element modeling. In general, the output of such software are the equivalent of the mass, spring and dampers matrices as

$$\mathbf{M}\ddot{\mathbf{x}}(t) + \mathbf{D}\dot{\mathbf{x}}(t) + \mathbf{K}\mathbf{x}(t) = \mathbf{B}\mathbf{u}(t) \tag{7.1}$$

$$\mathbf{y}(t) = \mathbf{C}_0\mathbf{x}(t) + \mathbf{C}_1\dot{\mathbf{x}}(t). \tag{7.2}$$

As seen in the previous chapters, model reduction can be used to lower the order of such large-scale systems using balanced truncation and Krylov techniques. However, before the reduction procedure, the system has to be represented in the conventional state-space formulation as

$$\mathbf{\Sigma} : \begin{cases} \dot{\mathbf{x}}(t) = \mathbf{A}\mathbf{x}(t) + \mathbf{B}\mathbf{u}(t) \\ \mathbf{y}(t) = \mathbf{C}\mathbf{x}(t) + \mathbf{D}\mathbf{u}(t) \end{cases} \Leftrightarrow \mathbf{\Sigma} = \left[\begin{array}{c|c} \mathbf{A} & \mathbf{B} \\ \hline \mathbf{C} & \mathbf{D} \end{array}\right] \in \mathbb{R}^{(n+p)\times(n+m)} \tag{7.3}$$

As noted by several authors [105, 114], this leads to a mixture of states and there is no guarantee that the reduced-order model would have the same mass, spring and dampers structure, thereby losing its physical meaning. Therefore, methods that preserve the second-order structure are of great importance.

This chapter introduces model reduction that preserves the second-order structure. In the context of aeroelasticity, Guyan Reduction, is an approximate dynamical analog of static condensation, and is a popular method of structural model reduction. It is based on a rather rough approximation, but is very simple, involves almost no computational cost, and often yields satisfactory aeroelastic solutions. Another standard procedure in structural dynamics is modal truncation, where modal decomposition is performed, and only limited number of the eigenmodes with the lowest frequencies are retained to represent the structure, whereas the high-frequency modes are truncated. A recently developed method that provide extensions to the gramians of a second-order structure in the frequency domain is explored for model reduction for second-order structure preservation.

7.1 Nodal Approach

7.1.1 Constraints Reduction - Ritz Reduction

Although constraint reduction is not considered a technique of model order reduction, it will be treated here for completeness. Usually, one has to enforce certain constraints or boundary conditions on the finite element model (zero displacements, prescribed forces), prior to solving the associated matrix equations, since the system matrices $\mathbf{K}$ and $\mathbf{M}$ were assembled as though all joints of the structure were unrestrained [24]. This could lead to singular stiffness matrix $\mathbf{K}$, and therefore, free rigid-body motion.

One of the most straight-forward procedures for enforcing zero displacements, in the case of restrained joints, is the partition of the system into *active* degrees-of-freedom and *constrained* degrees-of-freedom. Mathematically, one can write

$$\begin{bmatrix} \mathbf{M}_{aa} & \mathbf{M}_{ac} \\ \mathbf{M}_{ca} & \mathbf{M}_{cc} \end{bmatrix} \begin{bmatrix} \ddot{\mathbf{x}}_a \\ \ddot{\mathbf{x}}_c \end{bmatrix} + \begin{bmatrix} \mathbf{K}_{aa} & \mathbf{K}_{ac} \\ \mathbf{K}_{ca} & \mathbf{K}_{cc} \end{bmatrix} \begin{bmatrix} \mathbf{x}_a \\ \mathbf{x}_c \end{bmatrix} = \begin{bmatrix} \mathbf{P}_a \\ \mathbf{P}_c \end{bmatrix} \tag{7.4}$$

In the case where $\mathbf{x}_c = 0$, Eq. (7.4) can be written as

$$\mathbf{M}_{aa}\ddot{\mathbf{x}}_a + \mathbf{K}_{aa}\mathbf{x}_a = \mathbf{P}_a \tag{7.5}$$

$$\mathbf{M}_{ca}\ddot{\mathbf{x}}_a + \mathbf{K}_{ca}\mathbf{x}_a = \mathbf{P}_c \tag{7.6}$$

It should be pointed out that since only $\mathbf{M}_{aa}$ and $\mathbf{K}_{aa}$ are required in the solution of the active displacement vector $\mathbf{x}_a$, there is no need assemble the entire matrices $\mathbf{M}$ and $\mathbf{K}$.

In Eq. (7.4), the constraints were imposed as boundary conditions on the structure. However, in general, one can write relationships among system displacement coordinates, which can be enforced by using a transformation of coordinates called *Ritz Transformation* [24] as

$$\mathbf{x} = \mathbf{T}\hat{\mathbf{x}} \tag{7.7}$$

where $\hat{\mathbf{x}}$ is a vector of generalized coordinates and the transformation $\mathbf{T}$ arises from the relationships among the displacement coordinates, as

$$\mathbf{R}\mathbf{x} = \begin{bmatrix} \mathbf{R}_{da} & \mathbf{R}_{dd} \end{bmatrix} \begin{bmatrix} \mathbf{x}_a \\ \mathbf{x}_d \end{bmatrix} = \mathbf{0} \tag{7.8}$$

In this case, $\mathbf{x}_d$ is the vector on n_d $d$ependent coordinates and $\mathbf{x}_a$ is the vector of independent or $a$ctive coordinates. From Eq. (7.8), one can write

$$\mathbf{x}_d = -\mathbf{R}_{dd}^{-1}\mathbf{R}_{da}\mathbf{x}_a$$

and, the entire coordinates can be related to only the active coordinates as

$$\mathbf{x} = \mathbf{T}\hat{\mathbf{x}}_a = \begin{bmatrix} \mathbf{I}_{aa} \\ -\mathbf{R}_{dd}^{-1}\mathbf{R}_{da} \end{bmatrix} \mathbf{x}_a.$$

Using energy equivalence, it can be shown [24] that the reduced model obtained by imposing the constraints equations is given by

$$\hat{\mathbf{M}}\ddot{\mathbf{x}}_a + \hat{\mathbf{D}}\ddot{\mathbf{x}}_a + \hat{\mathbf{K}}\mathbf{x}_a = \hat{\mathbf{P}}_a \tag{7.9}$$

where

$$\hat{\mathbf{M}} = \mathbf{T}^T\mathbf{M}\mathbf{T}, \quad \hat{\mathbf{K}} = \mathbf{T}^T\mathbf{K}\mathbf{T}, \quad \hat{\mathbf{D}} = \mathbf{T}^T\mathbf{D}\mathbf{T} \quad \text{and} \quad \hat{\mathbf{P}}_a = \mathbf{T}^T\mathbf{P}_a.$$

7.1.2 Guyan Reduction - Static Condensation

The simplest and the most straightforward approach for reducing the stiffness (mass) matrix is the static condensation method, first proposed by Guyan [57] and Irons [62]. It consists of a selection of DOFs to be eliminated by means of a partition of the displacement vector into *primary degrees of freedom* to be kept and the *secondary degrees of freedom* to be eliminated. The principal assumption of this technique is that the inertia terms associated with the omitted DOFs are negligible compared to the elastic forces transmitted to the omitted DOFs by the motion of the active DOFs. Mathematically, one writes a set of static conditions based on the eigenvalue problem from Eq. (7.1), as

$$\mathbf{K}\mathbf{x} = \omega^2 \mathbf{M}\mathbf{x} \tag{7.10}$$

which can be represented in partitioned form as

$$\begin{bmatrix} \mathbf{K}_{rr} & \mathbf{K}_{rc} \\ \mathbf{K}_{cr} & \mathbf{K}_{cc} \end{bmatrix} \begin{bmatrix} \mathbf{x}_r \\ \mathbf{x}_c \end{bmatrix} = \omega^2 \begin{bmatrix} \mathbf{M}_{rr} & \mathbf{M}_{rc} \\ \mathbf{M}_{cr} & \mathbf{M}_{cc} \end{bmatrix} \begin{bmatrix} \mathbf{x}_r \\ \mathbf{x}_c \end{bmatrix} \tag{7.11}$$

where $\mathbf{x}_r$ refers to the active coordinates to be kept and $\mathbf{x}_c$ are the coordinates to be condensed out. Expanding Eq. (7.11) yields

$$\mathbf{K}_{rr}\mathbf{x}_r + \mathbf{K}_{rc}\mathbf{x}_c = \omega^2 \left(\mathbf{M}_{rr}\mathbf{x}_r + \mathbf{M}_{rc}\mathbf{x}_c \right) \tag{7.12}$$

$$\mathbf{K}_{cr}\mathbf{x}_r + \mathbf{K}_{cc}\mathbf{x}_c = \omega^2 \left(\mathbf{M}_{cr}\mathbf{x}_r + \mathbf{M}_{cc}\mathbf{x}_c \right). \tag{7.13}$$

Assuming that the secondary coordinates have two components, static and dynamic, $\mathbf{x}_c = \mathbf{x}_s + \mathbf{x}_d$, the static coordinate can be defined as the solution of the static problem

$$\begin{bmatrix} \mathbf{K}_{rr} & \mathbf{K}_{rc} \\ \mathbf{K}_{cr} & \mathbf{K}_{cc} \end{bmatrix} \begin{bmatrix} \mathbf{x}_r \\ \mathbf{x}_c \end{bmatrix} = \begin{bmatrix} \mathbf{P}_1 \\ \mathbf{0} \end{bmatrix} \tag{7.14}$$

Therefore, it follows that

$$\mathbf{x}_s = -\mathbf{K}_{cc}^{-1}\mathbf{K}_{cr}\mathbf{x}_r. \tag{7.15}$$

Substituting Eq. (7.15) into Eq. (7.12), yields

$$\begin{aligned} \mathbf{K}_{cr}\mathbf{x}_r + \mathbf{K}_{cc}\left(-\mathbf{K}_{cc}^{-1}\mathbf{K}_{cr}\mathbf{x}_r + \mathbf{x}_d\right) &= \omega^2 \left(\mathbf{M}_{cr}\mathbf{x}_r + \mathbf{M}_{cc}(-\mathbf{K}_{cc}^{-1}\mathbf{K}_{cr}\mathbf{x}_r + \mathbf{x}_d)\right) \\ \left[\mathbf{K}_{cc} - \omega^2\mathbf{M}_{cc}\right] &= \omega^2 \left[\mathbf{M}_{cr} - \mathbf{M}_{cc}\mathbf{K}_{cc}^{-1}\mathbf{K}_{cr}\right]\mathbf{x}_r \end{aligned}$$

and therefore

$$\left[\mathbf{K}_{cc} - \omega^2\mathbf{M}_{cc}\right]\mathbf{x}_d = \omega^2 \left[\bar{\mathbf{M}}_{cr}\right]\mathbf{x}_r \tag{7.16}$$

where $\bar{\mathbf{M}}_{cr} = \mathbf{M}_{cr} - \mathbf{M}_{cc}\mathbf{K}_{cc}^{-1}\mathbf{K}_{cr}$.

The above condensation technique is termed as *Dynamic Condensation*. Several improvements of this technique have been developed [91], [93], mainly in the area of Iterative Methods. A simplification of this method, known as *Static Condensation*, has been developed such that the dynamic displacement vector $\mathbf{x}_d$ is neglected and thus $\mathbf{x}_c = \mathbf{x}_s$. In this manner

$$\mathbf{x} = \begin{bmatrix} \mathbf{x}_r \\ \mathbf{x}_c \end{bmatrix} = \mathbf{T}\mathbf{x}_r = \begin{bmatrix} \mathbf{I}_{rr} \\ -\mathbf{K}_{cc}^{-1}\mathbf{K}_{cr} \end{bmatrix} \mathbf{x}_r$$

and therefore, it can be used to produce the equation of motion for the active coordinates only. In this case, the reduced mass and stiffness matrices are determined by

$$\begin{aligned} \bar{\mathbf{M}}_{rr} &= \mathbf{T}^T\mathbf{M}\mathbf{T} = \mathbf{M}_{rr} - \mathbf{M}_{rc}\mathbf{K}_{cc}^{-1}\mathbf{K}_{cr} - \mathbf{K}_{rc}\mathbf{K}_{cc}^{-1}\mathbf{M}_{cr} + \\ &\quad \mathbf{K}_{rc}\mathbf{K}_{cc}^{-1}\mathbf{M}_{cc}\mathbf{K}_{cc}^{-1}\mathbf{K}_{cr} \qquad (7.17) \\ \bar{\mathbf{K}}_{rr} &= \mathbf{K}_{rr} - \mathbf{K}_{rc}\mathbf{K}_{cc}^{-1}\mathbf{K}_{cr}. \qquad (7.18) \end{aligned}$$

Several remarks are in order:

1. The major advantages of the Guyan/Irons reduction technique are that it is computationally efficient and easy to implement. It is a standard option in many commercial finite element software packages.

2. The major disadvantage of the Guyan/Irons method is that it does not explicitly account for the inertia effects associated with the omitted DOFs, and that the validity of static condensation depends on the extent to which the vector $\mathbf{x}_d$ is negligible.

3. Since the total DOFs of the full-order model is partitioned, the selection of the active DOFs plays an important role in the reduction process;

4. One can use dynamic condensation to remedy the negligible inertia. However, dynamic condensation is frequency dependent and nonlinear with respect to the unknown eigenvalue. Several techniques have been introduced in the literature to approximate and improve the dynamic condensation. They include: first order condensation, second order dynamic condensation and iterative dynamic condensation [93].

7.1.3 CMS: Craig-Bampton

The standard reduction approach used in the industry for structural dynamic problems is modal truncation. The justification is that higher modes have much lower influence in the total response of the system. However, computational cost of modal truncation becomes prohibitive for large-scale systems due to the costly computation of its eigensolutions. In order to solve this large-scale eigenvalue computation, it is common to represent the structure as an assembly of smaller finite element models grouped together as substructures, or superelements [24, 93].

Component mode synthesis (CMS) is one of the well-established superelement analysis methods frequently employed in structural dynamics analysis. It is a model reduction process for partitioning a large complex structure into several components, modeling each component by a set of Ritz basis vectors, describing the physical coordinates of each component in terms of both reduced physical coordinates and generalized modal coordinates, and assembling the basis coordinates of components into global coordinates. One can then solve the approximate problem, and recover the required data. The advantage of subdividing a single large problem into several reduced-order problems follows due to the behavior of each component that is approximated by a superposition of Ritz basis vectors with greatly reduced size compared with the original finite element model. CMS is a much more efficient method for the process of design and analysis, particularly when the components of structural systems are designed and analyzed separately.

The Craig-Bampton method [24, 25] is a type of CMS, that relies on two mode sets: (1) fixed substructure interface normal modes, and (2) constraint modes. The fixed-interface normal modes are calculated by assuming that the substructure interface DOFs are fully fixed. The constraint modes are influence coefficients describing the static deformation of the substructure due to interface displacement. They can be thought of as the structural deformation resulting from successive unit displacements of the interface DOFs while the other interface DOFs are held to zero. Consider first the undamped equation of motion for a single substructure, that is divided in two substructures for convenience The first step of the Craig-Bampton method is to reorder the matrices $\mathbf{K}, \mathbf{M}$ and $\mathbf{D}$, such that they become divided with the following sparsity pattern

$$\mathbf{K} = \begin{bmatrix} \mathbf{K}_1 & \mathbf{0} & \mathbf{K}_{1,3} \\ \mathbf{0} & \mathbf{K}_2 & \mathbf{K}_{2,3} \\ \mathbf{K}_{1,3}^T & \mathbf{K}_{2,3}^T & \mathbf{K}_3 \end{bmatrix}; \quad \mathbf{M} = \begin{bmatrix} \mathbf{M}_1 & \mathbf{0} & \mathbf{M}_{1,3} \\ \mathbf{0} & \mathbf{M}_2 & \mathbf{M}_{2,3} \\ \mathbf{M}_{1,3}^T & \mathbf{M}_{2,3}^T & \mathbf{M}_3 \end{bmatrix} \tag{7.19}$$

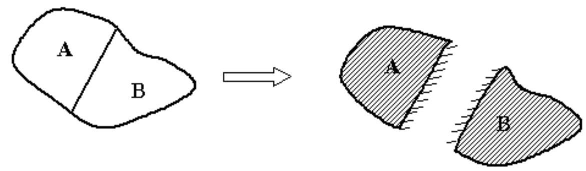

Figure 7.1: Division of a structure into two components with fixed interface.

Applications of the Guyan reduction and modal truncation results in the reduced-order model. A generalization of classical component mode synthesis has been proposed by Bennighof [13] and it is called the Automated Multilevel Substructuring Method (AMLS), in which the structure is recursively divided into thousands of subdomains and Craig-Bampton techniques are applied to those subdomains. The AMLS matured in 2001 to a commercially available software in the industry, and today is the largest eigensolver software used in the automotive industry. The CMS approach and its variants will not be pursued in this dissertation.

7.2 SVD-based Approach

7.2.1 Second-order Balanced Truncation

The first-order reduction presented previously using balanced reduction techniques, in general, destroys the second-order structure of the dynamical equations. However, it is important in structural dynamical problems to keep the second-order structure with mass, stiffness and damping matrices as the parameters. Several techniques have been developed in the literature to perform a balanced truncation preserving the second-order structure (see [8], and references therein).

First, two pairs of “second order gramians” are defined. The first pair $(\mathcal{P}_{pos}, \mathcal{L}_{pos})$ will correspond to an energy optimization problem depending only on the positions $\mathbf{x}(t)$ and not on the velocities $\dot{\mathbf{x}}(t)$. Analogously, the second pair $(\mathcal{P}_{vel}, \mathcal{L}_{vel})$ will represent the optimization problem depending only on the velocities $\dot{\mathbf{x}}(t)$ and not on the positions $\mathbf{x}(t)$. The second step follows from the balancing method. A coordinate transformation is applied to the gramians in such a way that the second-order gramians are equal and diagonal: $\bar{\mathcal{P}}_{pos} = \bar{\mathcal{L}}_{pos} = \mathbf{\Sigma}_{pos}$ and $\bar{\mathcal{P}}_{vel} = \bar{\mathcal{L}}_{vel} = \mathbf{\Sigma}_{vel}$.

In order to compute the balancing transformation, the following Lyapunov equations are defined based on the state-space as given in Eqs. (7.3):

$$\mathcal{A}\mathcal{P} + \mathcal{P}\mathcal{A}^T + \mathcal{B}\mathcal{B}^T = 0, \quad \mathcal{A}^T\mathcal{L} + \mathcal{L}\mathcal{A} + \mathcal{C}^T\mathcal{C} = 0. \tag{7.20}$$

It can be shown [8], that $(\mathcal{P}_{pos}, \mathcal{L}_{pos}) = (\mathcal{P}_{11}, \mathcal{L}_{11})$, that is, the $n \times n$ left upper block of $\mathcal{P}$ and $\mathcal{L}$ as in Eq. (7.20) and $(\mathcal{P}_{vel}, \mathcal{L}_{vel}) = (\mathcal{P}_{22}, \mathcal{L}_{22})$, where $(\mathcal{P}_{22}, \mathcal{L}_{22})$ are the $n \times n$ right lower block of $\mathcal{P}$ and $\mathcal{L}$, respectively.

7.2.2 Structured Eigenvalue Reduction

Using a structured version of the gramians, called *second-order gramians*, a reduction scheme for truncation of the eigenvalues of the second-order gramians written in the frequency domain was developed in [105]. This special version of the gramian provides a measure of the error bound for the reduction process. The following definition is in order:

Definition 7.2.1. Given a second-order structure as

$$\mathbf{M}\ddot{\mathbf{x}}(t) + \mathbf{D}\dot{\mathbf{x}}(t) + \mathbf{K}\mathbf{x}(t) = \mathbf{B}\mathbf{u}(t)$$
$$\mathbf{y}(t) = \mathbf{C}_0\mathbf{x}(t) + \mathbf{C}_1\dot{\mathbf{x}}(t),$$

a second-order gramian in the frequency domain is defined as

$$\mathcal{P}_2 := \frac{1}{2\pi}\int_{-\infty}^{\infty} \left(-\omega^2\mathbf{M} + i\omega\mathbf{D} + \mathbf{K}\right)^{-1} \mathbf{B}\mathbf{B}^* \left(-\omega^2\mathbf{M}^* - i\omega\mathbf{D}^* + \mathbf{K}^*\right)^{-1} d\omega \tag{7.21}$$

The model reduction can be accomplished using the following theorem [105]:

Theorem 7.2.1. *Let* $\mathcal{P}_2 = \mathbf{V}\mathbf{\Lambda}\mathbf{V}^*$ *with* $\mathbf{V} = [\mathbf{V}_1 \quad \mathbf{V}_2]$ *and* $\mathbf{\Lambda} = diag\,[\mathbf{\Lambda}_1 \quad \mathbf{\Lambda}_2]$, *the reduced-order model can be written as*

$$\hat{\mathbf{M}} = \mathbf{V}_1^*\mathbf{M}\mathbf{V}_1; \quad \hat{\mathbf{D}} = \mathbf{V}_1^*\mathbf{D}\mathbf{V}_1; \quad \hat{\mathbf{K}} = \mathbf{V}_1^*\mathbf{K}\mathbf{V}_1; \quad \hat{\mathbf{B}} = \mathbf{V}_1^*\mathbf{B}; \quad \hat{\mathbf{C}} = \mathbf{C}\mathbf{V}_1 \tag{7.22}$$

In this case, the reduction error bound is given as

$$\|\mathbf{\Sigma} - \hat{\mathbf{\Sigma}}\|^2_{\mathcal{H}_2} \leq \; trace\,\{\mathbf{C_2}\mathbf{\Lambda_2}\mathbf{C_2^*}\} + \kappa \; trace\,\{\mathbf{\Lambda_2}\} \tag{7.23}$$

where $\kappa = \sup_\omega \|(\mathbf{C_1}\mathbf{L}(i\omega))^*(\mathbf{C_1}\mathbf{L}(i\omega) - 2\mathbf{C_2})\|_2$.

7.2.2.1 Gramian Computation

In order to use Theorem 7.2.1, the controllability gramian must be computed. In the general case, the second-order gramian needs to be integrated in the frequency domain as in Eq. (7.21).

The gramian can be computed by "brute-force" integration of Eq. (7.21). If one defines a grid for $\omega = [\omega_1 : \Delta\omega : \omega_2]$ and the integrand being the function

$$f(\omega) = \left(-\omega^2\mathbf{M} + i\omega\mathbf{D} + \mathbf{K}\right)^{-1}\mathbf{B}\mathbf{B}^*\left(-\omega^2\mathbf{M}^* - i\omega\mathbf{D}^* + \mathbf{K}^*\right)^{-1}, \qquad (7.24)$$

the approximated gramian can be writen as

$$\mathcal{P}_{approx} = \int_{-\omega}^{\omega} f(\omega)d\omega \approx \sum_{k=1}^{length(\omega)} f(\omega)\Delta\omega \qquad (7.25)$$

A simplification for the gramian computation is achieved for structures with proportional damping, i.e., $\mathbf{D} = \alpha\mathbf{M} + \beta\mathbf{K}$. The proportional damping can now be diagonalized together with the mass and stiffness matrices using modal analysis. In this manner, given $\mathbf{M}, \mathbf{D}$ and $\mathbf{K}$, a generalized eigenvalue decomposition can be performed on $\mathbf{M}$ and $\mathbf{K}$ and the matrices can be written as

$$\begin{aligned}
[\mathbf{V}, \mathbf{E}] &= eig(\mathbf{K}, \mathbf{M}) \rightarrow \mathbf{KV} = \mathbf{MVE} \\
\mathbf{M} &\leftarrow \mathbf{V}^{\mathbf{T}}\mathbf{MV} = \mathbf{I} \\
\mathbf{K} &\leftarrow \mathbf{V}^{\mathbf{T}}\mathbf{KV} = \mathbf{E} = diag(k_1, \cdots, k_n) \\
\mathbf{D} &\leftarrow \mathbf{V}^{\mathbf{T}}\mathbf{DV} = diag(d_1, \cdots, d_n);
\end{aligned}$$

Using the above definitions, it can be shown that each element of the second-order gramian matrix can be computed as

$$\mathcal{P}_{ij} = \frac{1}{2\pi}\int_{-\infty}^{\infty}\left(-\omega^2 + i\omega d_i + k_i\right)^{-1} B(i,:)B^*(:,j)\left(-\omega^2 - i\omega d_j^* + k_j^*\right)^{-1} d\omega \qquad (7.26)$$

Making use of partial fraction expansions, this integral can be evaluated [105] and, thus one explicitly constructs the required gramian. It should be pointed out that the gramian obtained has to be transformed back to the coordinates given prior to the modal transformations.

7.3 Model Reduction Applied to the Benchmark Building Problems

The application of the aforementioned model-order reduction methods for the family of benchmark building problems is now considered. The approach taken here will follow two different pathways, as depicted in Fig. 7.2. Starting with the **full-order model (FOM)**, boundary conditions are applied to the structure and constraint nodal coordinates are removed yielding the so-called **Model_BC**. Based on this model, one way to compare the various model reduction methods is to apply Ritz transformations and Guyan model reduction and then to form the basis for a smaller model called the *evaluation model*. The idea here is that for large-scale systems, balanced truncation and modal truncation should be considered from a small to medium size model, so that it can be computed with a reasonable amount of computational effort. The second path is to consider reductions based directly on the model after boundary conditions have been applied. In this case, model reduction is performed on a larger model, and one should be careful to use the proper techniques.

Four techniques will be evaluated for the benchmark problems presented in Chapter 6: balanced truncation, modal truncation, second-order structure preserving and Krylov subspaces. According to the pathway chosen they will be named as:

- balanced truncation from Guyan model $\Longrightarrow$ **Model_BT_G**
- balanced truncation from **Model_BC** $\Longrightarrow$ **Model_BT_BC**
- second-order structure preserving from Guyan model $\Longrightarrow$ **Model_SOSR_G**
- second-order structure preserving from **Model_BC** $\Longrightarrow$ **Model_SOSR_BC**
- Krylov from Guyan model $\Longrightarrow$ **Model_K_G**
- Krylov from **Model_BC** $\Longrightarrow$ **Model_K_BC**

7.3.1 Model Reduction for the Six-Story Building Model

Guyan Reduction After eliminating all rotational DOFs and some of the vertical DOFs, a reduced-order model of size 34, i.e., a state-space of order 68, is obtained for the building model. In this case, for the partition of the system, all the active horizontal DOFs (after boundary conditions have been applied), as well as the vertical DOFs for levels 1-6 located on the second and fifth columns, are chosen as active DOFs to be kept after the reduction.

Balanced Truncation A balanced truncation is performed using the square-root algorithm for the balanced-realization. The order of the reduced order model was varied from 60 to 20.

Structured Eigenvalue Reduction The structured eigenvalue reduction is also obtained using a reduced model of the same size as the models obtained by balanced truncation.

In order to evaluate the effectiveness of the model reduction techniques presented above, the frequency response plots or sigma plots, i.e., the maximum singular value of the transfer function matrix of the reduced-order models, are obtained. Also, the the error sigma plots, i.e., the sigma plots of the error between the full-order and reduced-order models are obtained. They are depicted in Fig. 7.3-7.18. Reduced-order models of size $r = 60, 50, 40, 30,$ and 20 were obtained.

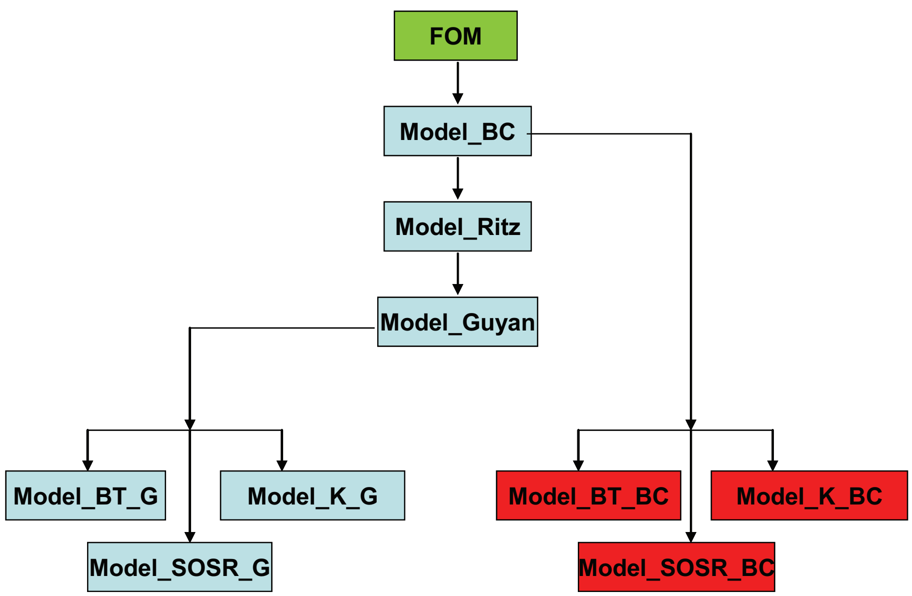

Figure 7.2: Model-order reduction sequence.

7.3.2 Model Reduction for the Twenty-Story Building Model

Following the same procedures as for the six-story building model, several reduced-order models were obtained applying the techniques described in the previous sections. Since this is a bigger building, reduced order models were chosen to be of size $r = 100, 80, 60, 50,$ and 20.

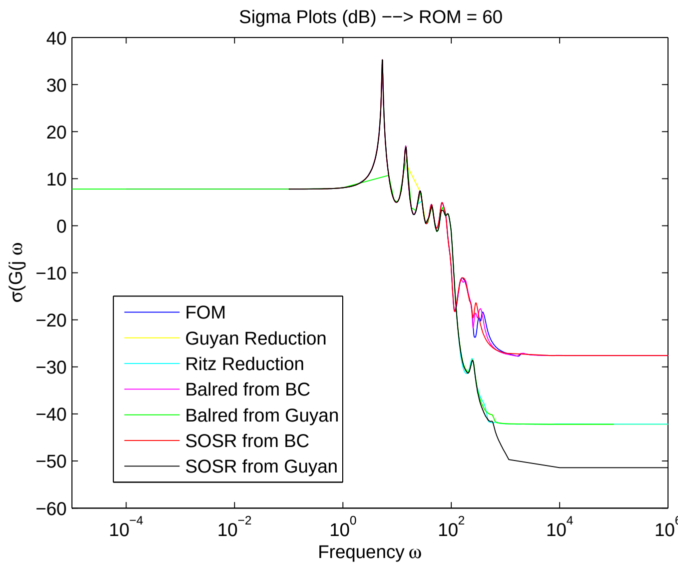

(a)

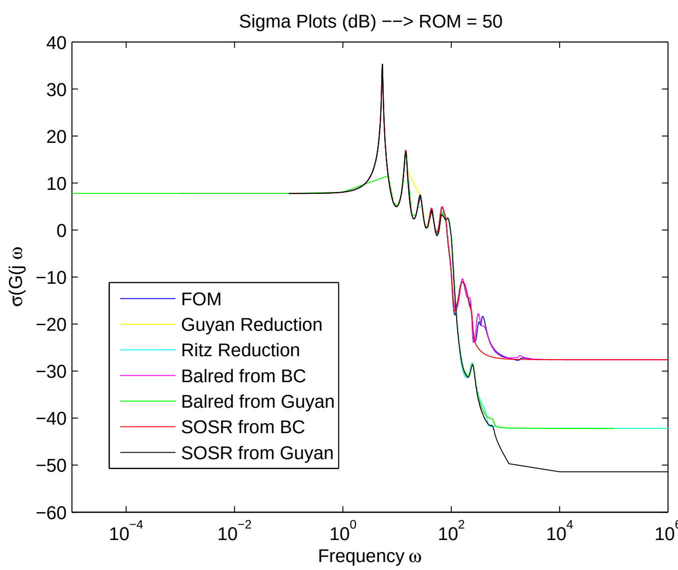

(b)

Figure 7.3: Six-story building sigma plots of the reduced-order model for the sizes (a) $r = 60$, (b) $r = 50$

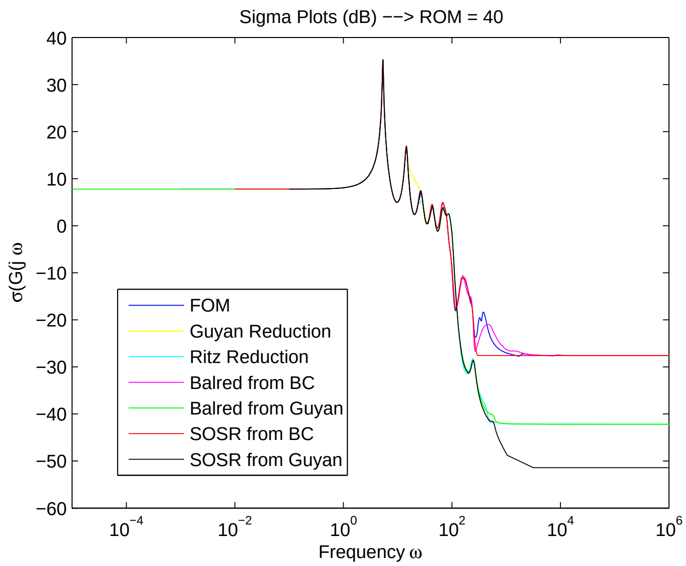

(a)

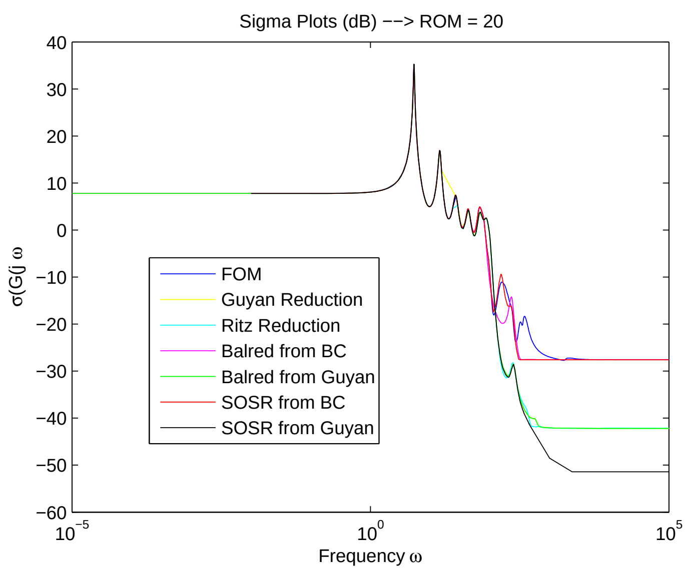

(b)

Figure 7.4: Six-story building sigma plots of the reduced-order model for the sizes (a) $r = 40$, (b) $r = 20$

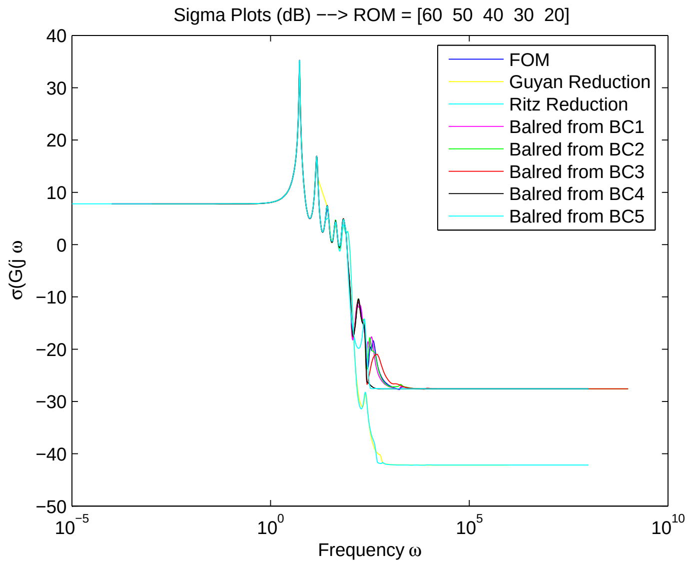

(a)

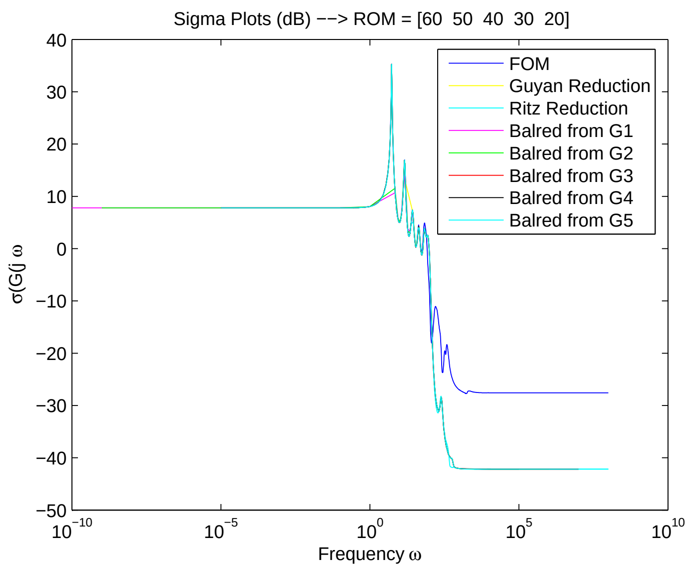

(b)

Figure 7.5: Six-story building sigma plots of the reduced-order model different model-order reduction techniques. (a) Balanced Truncation reduced-order model full model, (b) Balanced Truncation reduced-order model Guyan model.

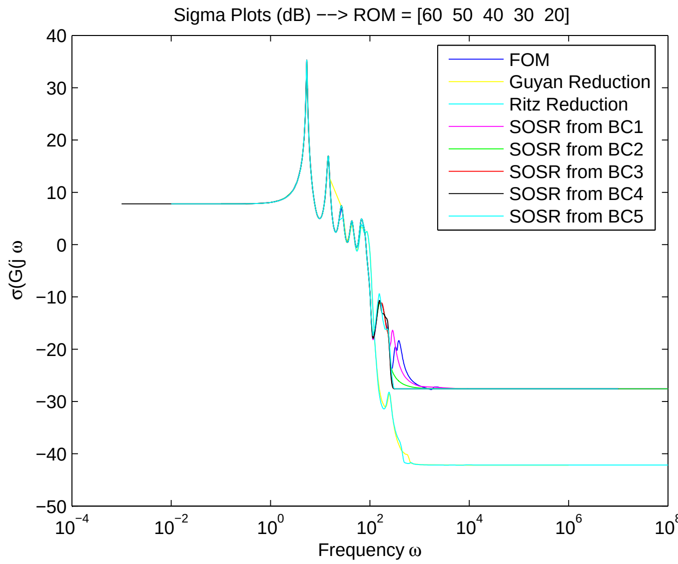

(a)

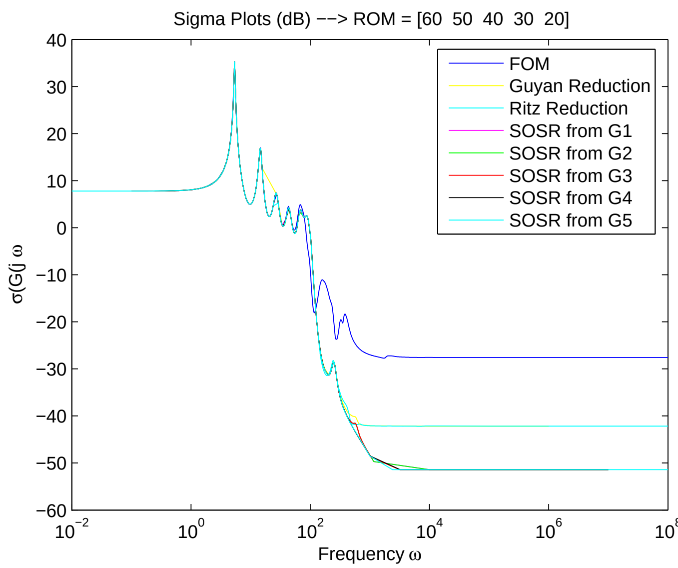

(b)

Figure 7.6: Six-story building sigma plots of the reduced-order model different model-order reduction techniques. (a) second-order structured reduction(SOSR) from full model, (b) SOSR from Guyan model.

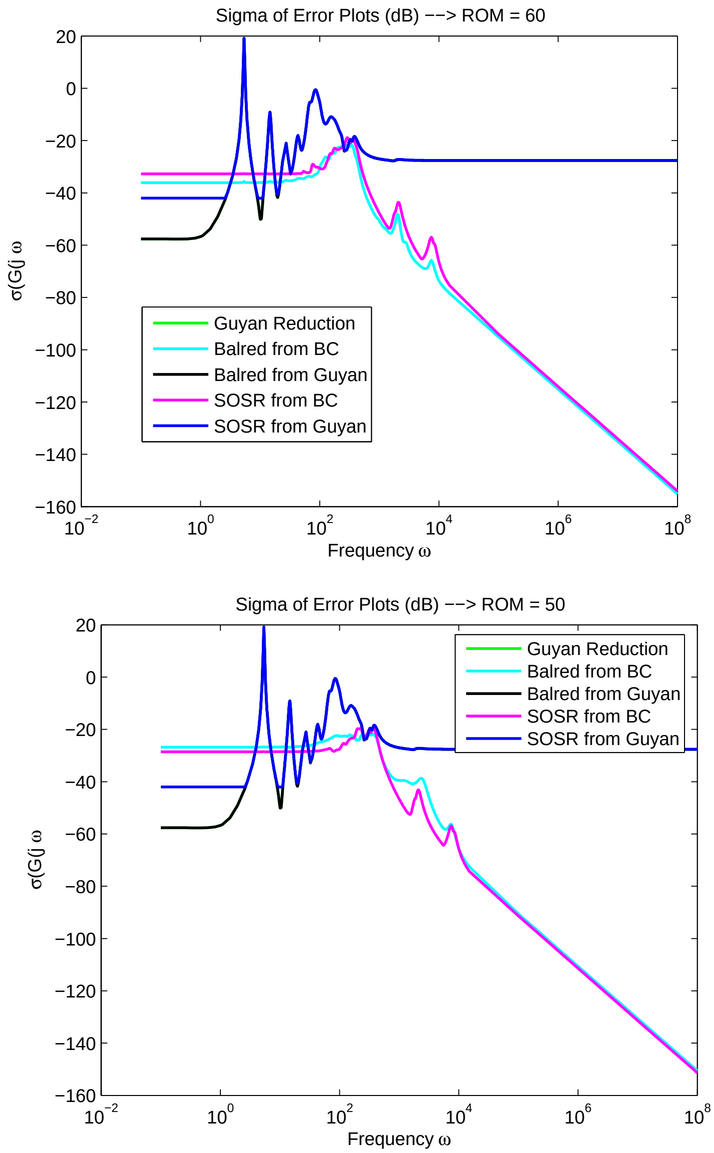

(a)

(b)

Figure 7.7: Six-story building error sigma plots of the reduced-order model for the sizes (a) $r = 60$, $r = (b)50$.

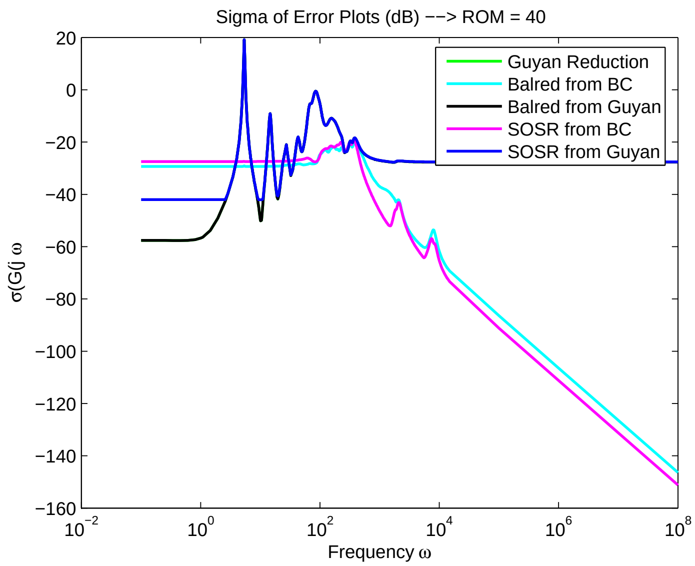

(a)

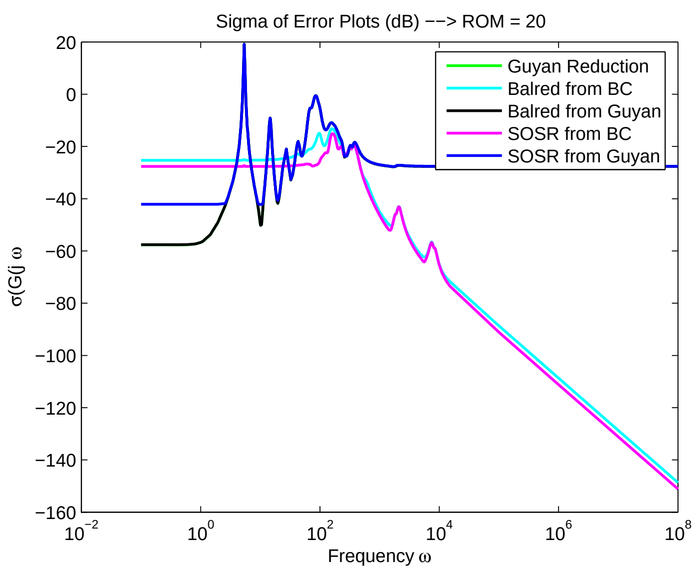

(b)

Figure 7.8: Six-story building error sigma plots of the reduced-order model for the sizes (a) $r = 40$ (b) $r = 20$.

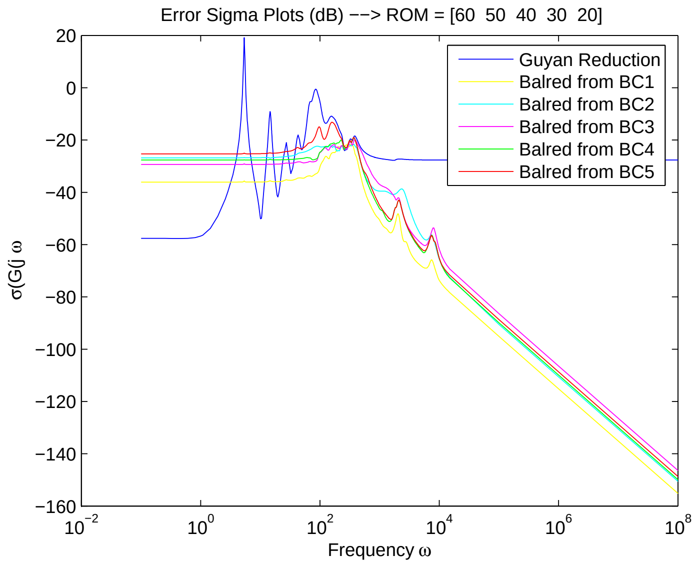

(a)

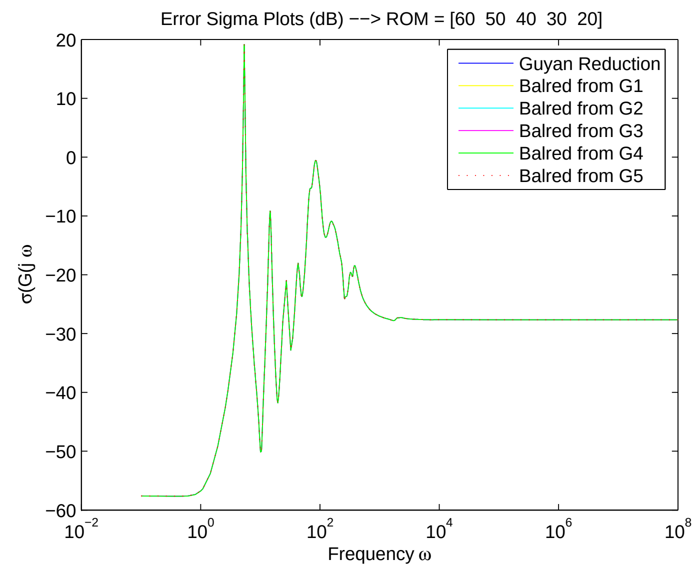

(b)

Figure 7.9: Six-story building error sigma plots of the reduced-order model from different model reduction techniques. (a) Balanced Truncation reduced-order model from full model, (b) Balanced Truncation reduced-order model from Guyan model.

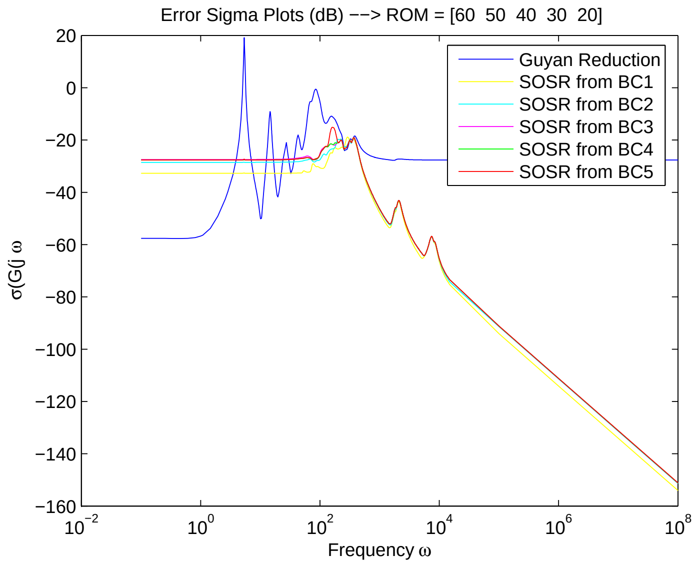

(a)

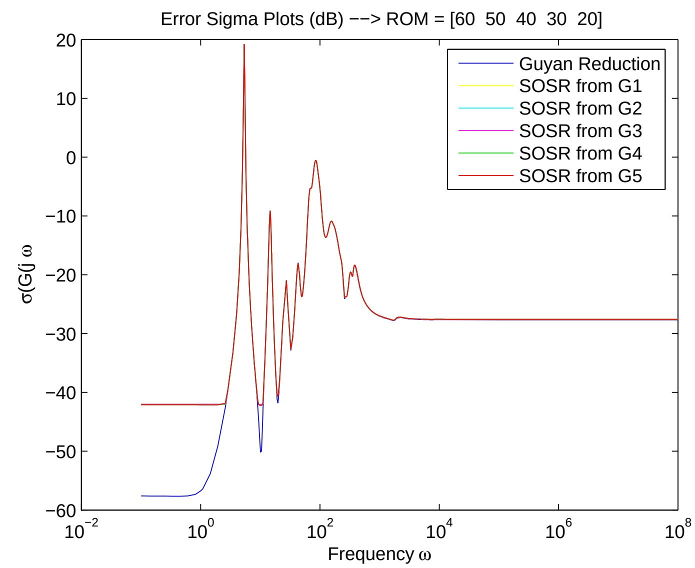

(b)

Figure 7.10: Six-story building sigma plots of the reduced-order model from different model reduction techniques. (a) Second-order structured reduction (SOSR) from full model, (b) SOSR reduced-order model from Guyan model.

7.3.3 Model Reduction for the Bowen Building Model

For the case of the Bowen building model, a different approach was pursued. The Bowen building finite element model is comprised of system matrices of order $n = 4950$. However, the mass matrix is singular due to the fact that rotational inertia was neglected during the modeling process. Thus, direct application of techniques involving the state-space realization would fail, since the inverse of the mass matrix is required. Hence, Guyan reduction was performed first on the system, in order to condense out the rotational degrees-of-freedom. Other techniques of model reduction were performed using the reduced-order model.

It should be pointed out that even with the reduction of the full-order model to a smaller version using Guyan (2439 DOFs), balanced truncation is impractical for such large systems. In this manner, modal truncation was performed to obtain reduced-order models of reasonable sizes.

7.4 Concluding Remarks

Figures 7.3-7.18 show two important aspects of the model reduction techniques presented. If one starts the reduction process based on the Guyan model, the high frequency content of the model is removed. Guyan reduction eliminates those high-order modes due to vertical and rotational degrees-of-freedom. The frequency response closely match the full-order models in the lower region frequencies. However, for large-scale buildings, it might lead to structures rather stiffer than the original model (shear building model) and therefore reduced-order controller design based on those reduced-models might lead to spillover effects.

Furthermore, structure preserving model reduction leads to reduced-order models that perform worse than the other reduction techniques. This can readily be observed reduced-order model the error sigma plots. The error of the second-order structure preserving model reduction is always higher than other techniques. Balanced reduction is the one that performs the best.

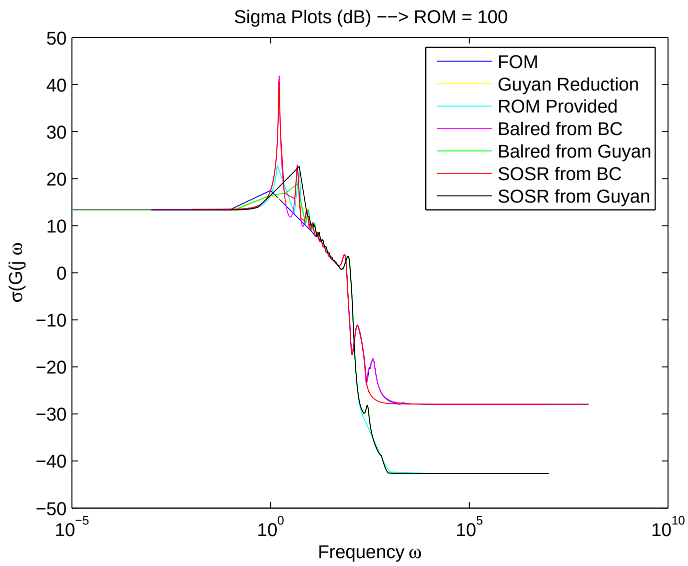

(a)

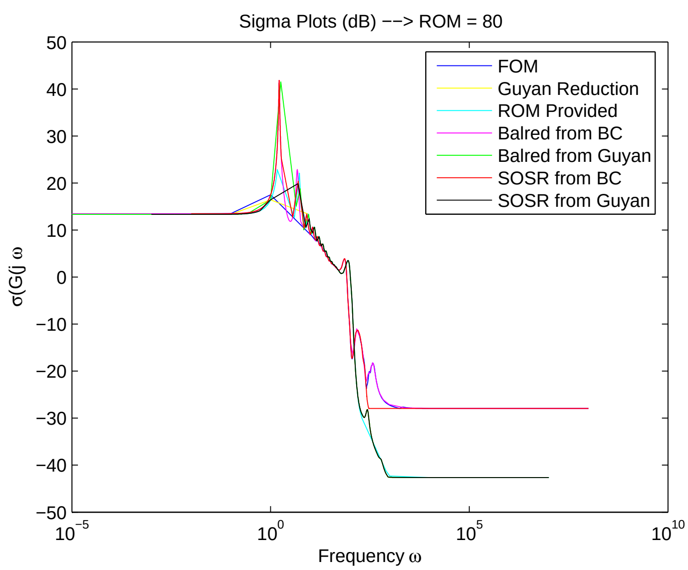

(b)

Figure 7.11: Twenty-story building: Sigma plots of the reduced-order model for the sizes (a) 100 (b) 80

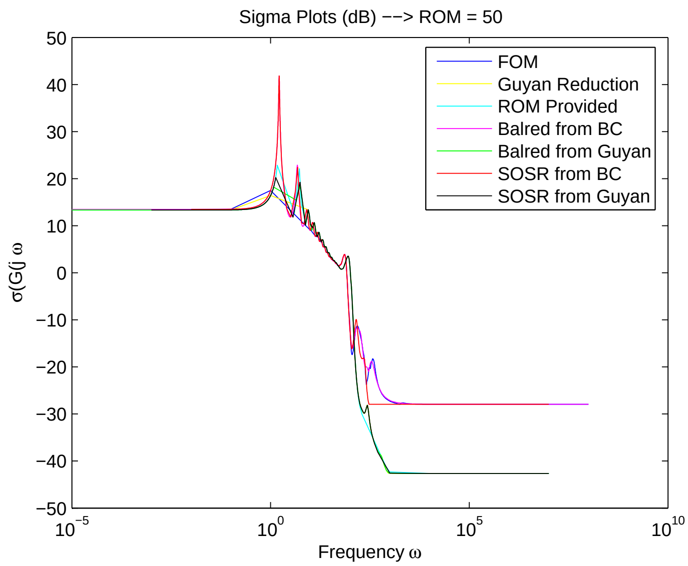

(a)

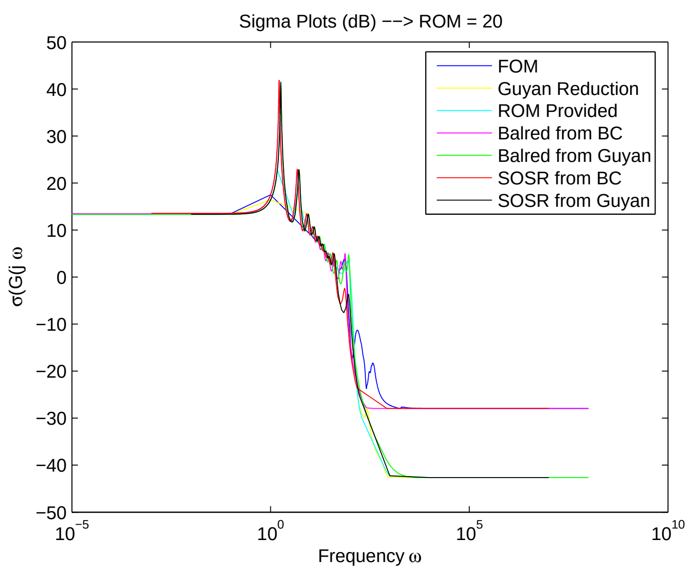

(b)

Figure 7.12: Twenty-story building sigma plots of the reduced-order model for the sizes. (a) $r = 50$, (b) $r = 20$.

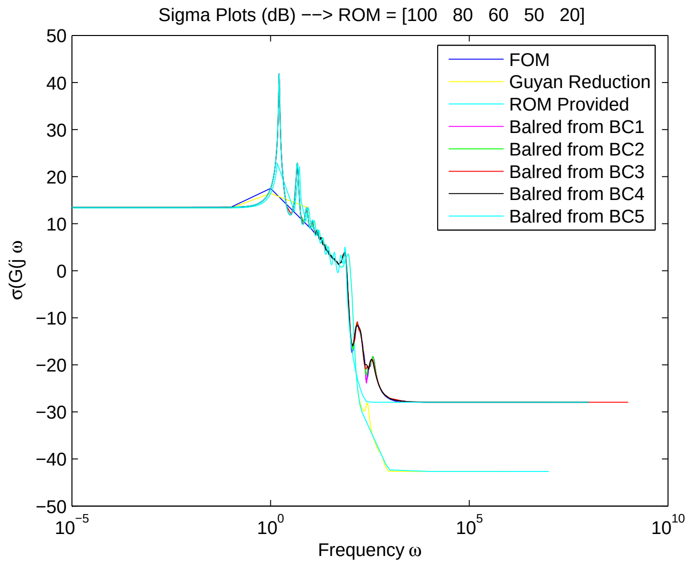

(a)

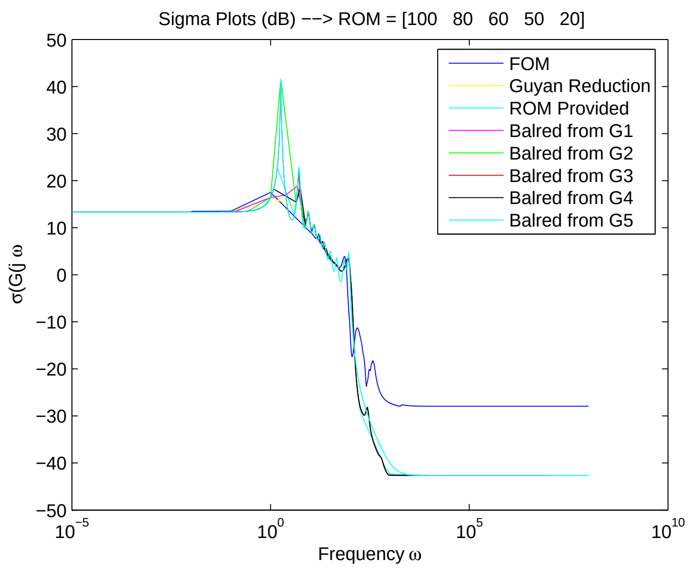

(b)

Figure 7.13: Twenty-story building sigma plots of the reduced-order model for different model reduction techniques. (a) Balanced Truncation from full model, (b) Balanced Truncation from Guyan model.

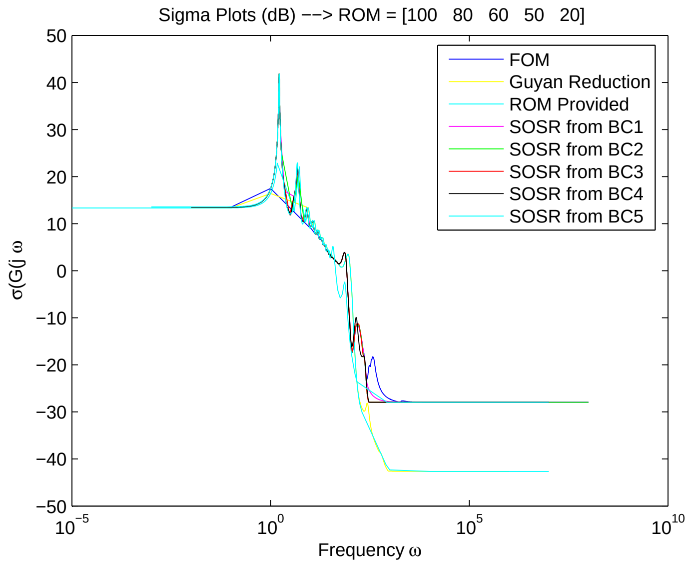

(a)

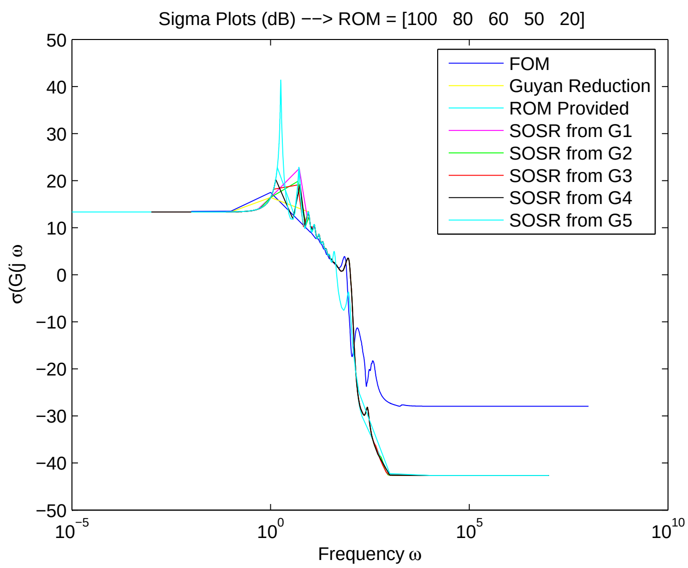

(b)

Figure 7.14: Twenty-story building sigma plots of the reduced-order model foe different model reduction techniques. (a) Second-order structure reduction (SOSR) from full model, (b) SOSR from Guyan model.

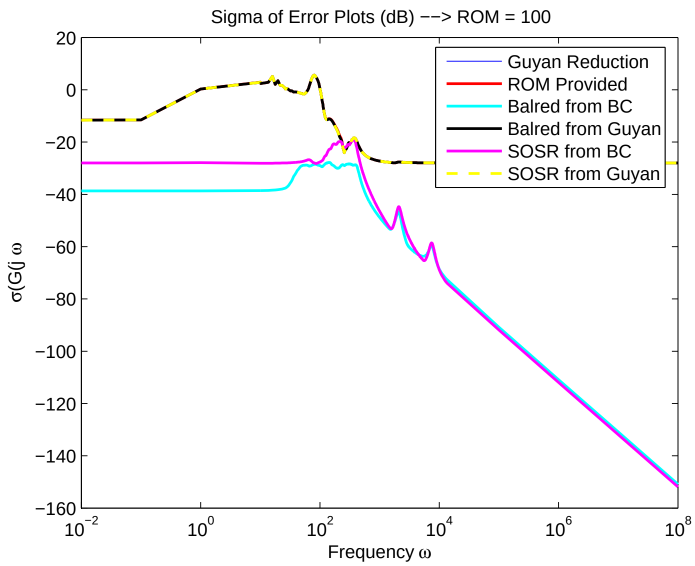

(a)

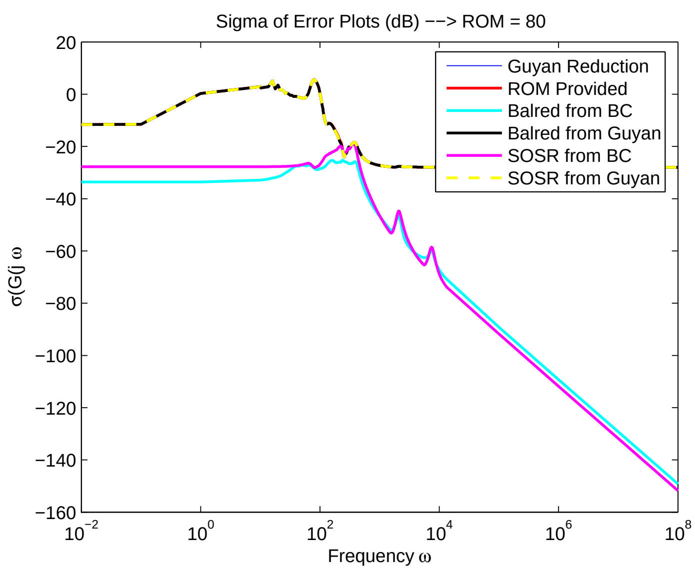

(b)

Figure 7.15: Twenty-story building error sigma plots of the reduced-order model for the sizes (a) $r = 60$, (b) $r = 50$.

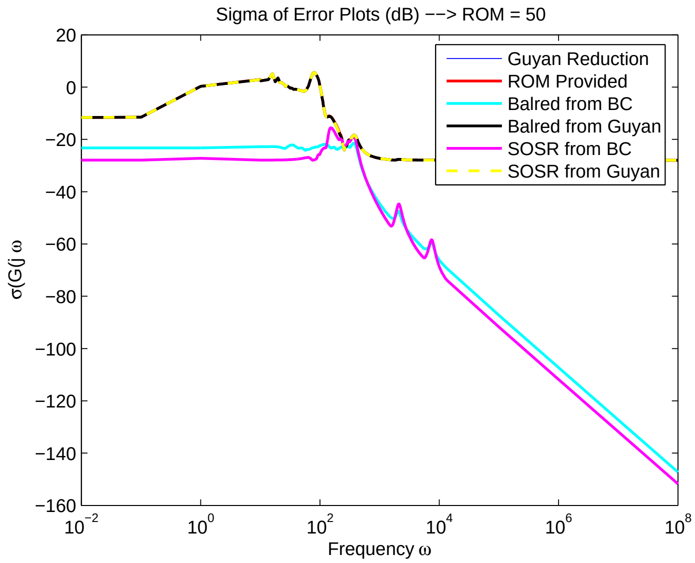

(a)

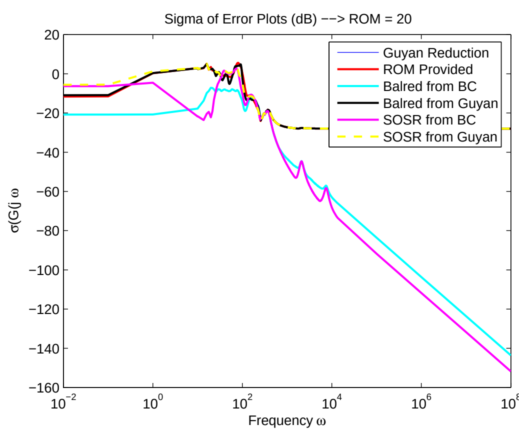

(b)

Figure 7.16: Twenty-story building error sigma plots of the reduced-order model for the sizes (a) $r = 40$, (b) $r = 20$.

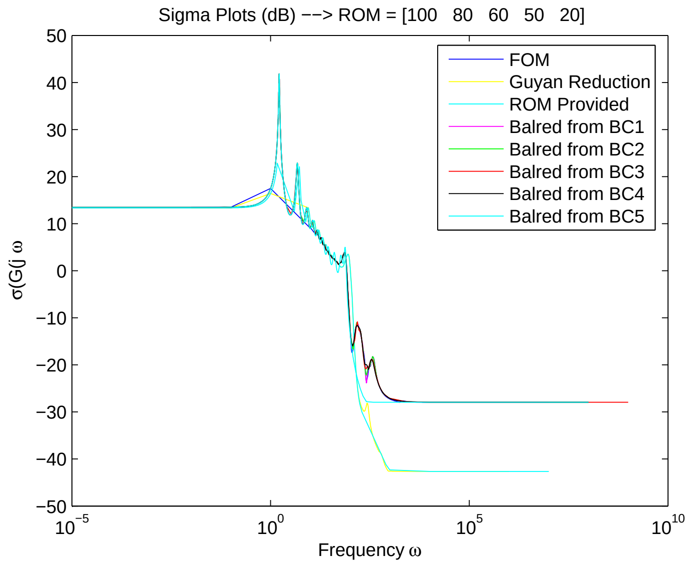

(a)

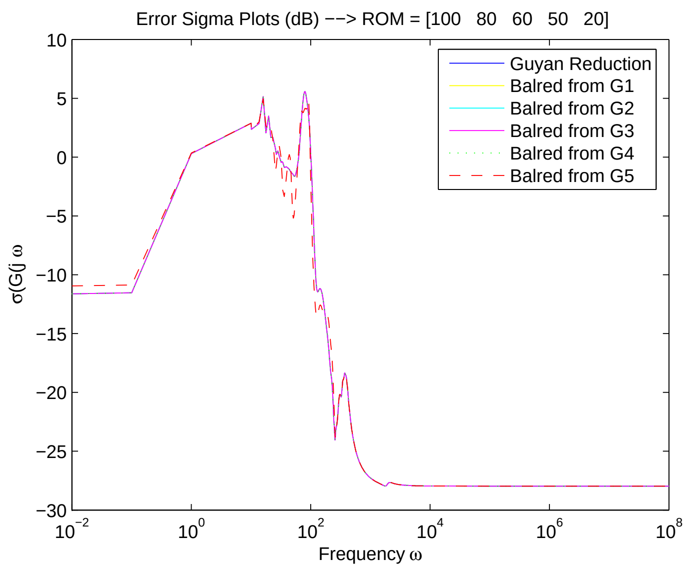

(b)

Figure 7.17: Twenty-story building error sigma plots of the reduced-order model for different model reduction techniques. (a) Balanced Truncation from full model, (b) Balanced Truncation from Guyan model

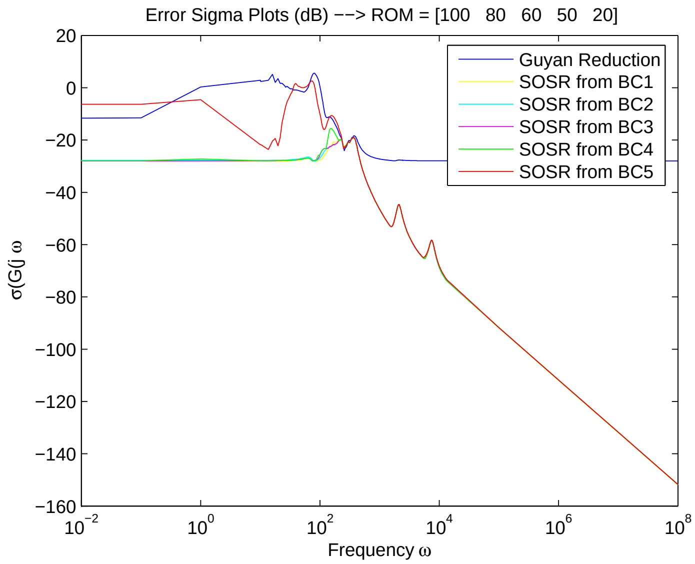

(a)

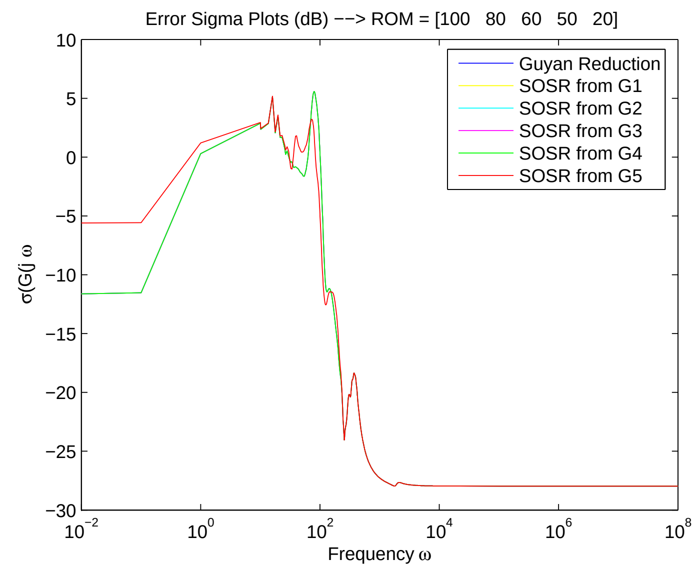

(b)

Figure 7.18: Twenty-story building sigma plots of the reduced-order model for different model reduction techniques. (a) Second-order structure reduction (SOSR) from full model, (b) SOSR from Guyan model

Chapter 8

Low-order Controller Design for the Building Problems

This chapter deals with the reduced-order controller design for the benchmark problems described in previous chapters. In a first approach, reduced-order controllers will be obtained by means of model reduction on the building model. As will be seen, this approach leads to good responses, but no guarantees on the closed-loop stability. As a second approach, controller reduction based on SVD and Krylov methods will be performed directly on the full-order controller, which was designed based on the full-order building model. Again, closed-loop stability will be shown to be not always guaranteed. Finally, a third approach will be proposed, based on the "dissipativity" property of linear systems. The term energy will be defined in a general sense, and some simplifications will be made to arrive at the concept of passivity of a linear time-invariant system.

In what follows, LQG controller design will be performed for the benchmark building problems, and several performance indices will be defined for assessing the response of the closed-loop system to seismic inputs. Also, details about the controller implementation will be given and results for the low-order controller will be compared. The passivity preserving model reduction is explained and dissipative-LQG-controllers will be designed such that closed-loop stability is guaranteed. It should be pointed out that in this chapter, stability of the closed-loop system will be the main issue studied, even though performance will be assessed by means of evaluation criteria formulated for seismic excited buildings.

8.1 Controller Design for the Benchmark

In order to evaluate different control strategies, a criteria based on maximum response quantities [108], defined in Table 8.1, together with the number of sensors and control devices used in the implemented solution is proposed for the benchmark building problems. This criteria involves the evaluation of the closed-loop control system for four different inputs excitation (ground acceleration) of four historical earthquake records [108]: (i) *El Centro*, (ii) *Hachinohe*, (iii) *Northridge* and (iv) *Kobe*. Smaller values of these evaluation criteria are generally more desirable.

A summary of the fifteen evaluation criteria is given in Table 8.1. A detailed description of the meaning of each quantity is given in [108]. Essentially, Table 8.1 provides indices for the evaluation of the effectiveness of the control algorithm with the optimal number of sensors and actuators.

In order to make the benchmark control problem as representative of the full-scale implementation as possible, several specifications regarding the controllers and implementation are given [108]:

Floor Displacement $J_1 = \max\limits_{\substack{\text{El Centro}\\ \text{Hachinohe}\\ \text{Northridge}\\ \text{Kobe}}} \left\{ \dfrac{\max\limits_{\substack{t\\ i \in \boldsymbol{\eta}}} \lvert x_i(t) \rvert}{x^{\max}} \right\}$	Normed Floor Displacement $J_5 = \max\limits_{\substack{\text{El Centro}\\ \text{Hachinohe}\\ \text{Northridge}\\ \text{Kobe}}} \left\{ \dfrac{\max\limits_{i \in \boldsymbol{\eta}} \lVert x_i(t) \rVert}{\lVert x^{\max} \rVert} \right\}$	Control Force $J_9 = \max\limits_{\substack{\text{El Centro}\\ \text{Hachinohe}\\ \text{Northridge}\\ \text{Kobe}}} \left\{ \dfrac{\max\limits_{t,\,i} \lvert f^i(t) \rvert}{W} \right\}$	Control Devices J_{13} = number of control devices required
Interstory Drift $J_2 = \max\limits_{\substack{\text{El Centro}\\ \text{Hachinohe}\\ \text{Northridge}\\ \text{Kobe}}} \left\{ \dfrac{\max\limits_{t,\,i} \left(\dfrac{\lvert d_i(t) \rvert}{h_i} \right)}{d_{\text{n}}^{\max}} \right\}$	Normed Interstory Drift $J_6 = \max\limits_{\substack{\text{El Centro}\\ \text{Hachinohe}\\ \text{Northridge}\\ \text{Kobe}}} \left\{ \dfrac{\max\limits_{t,\,i} \left(\dfrac{\lVert d_i(t) \rVert}{h_i} \right)}{\lVert d_{\text{n}}^{\max} \rVert} \right\}$	Control Device Stroke $J_{10} = \max\limits_{\substack{\text{El Centro}\\ \text{Hachinohe}\\ \text{Northridge}\\ \text{Kobe}}} \left\{ \dfrac{\max\limits_{t,\,i} \lvert y_i^{\text{a}}(t) \rvert}{x^{\max}} \right\}$	Sensors J_{14} = number of sensors required
Floor Acceleration $J_3 = \max\limits_{\substack{\text{El Centro}\\ \text{Hachinohe}\\ \text{Northridge}\\ \text{Kobe}}} \left\{ \dfrac{\max\limits_{\substack{t\\ i \in \boldsymbol{\eta}}} \lvert \ddot{x}_{\text{a}i}(t) \rvert}{\dot{x}_{\text{a}}^{\max}} \right\}$	Normed Floor Acceleration $J_7 = \max\limits_{\substack{\text{El Centro}\\ \text{Hachinohe}\\ \text{Northridge}\\ \text{Kobe}}} \left\{ \dfrac{\max\limits_{i \in \boldsymbol{\eta}} \lVert \ddot{x}_{\text{a}i}(t) \rVert}{\lVert \dot{x}_{\text{a}}^{\max} \rVert} \right\}$	Control Power $J_{11} = \max\limits_{\substack{\text{El Centro}\\ \text{Hachinohe}\\ \text{Northridge}\\ \text{Kobe}}} \left\{ \dfrac{\max\limits_{t} \left[\sum\limits_i \mathcal{P}_i(t) \right]}{\dot{x}^{\max} W} \right\}$	Computational Resources $J_{15} = \dim(\mathbf{x}_k^{\text{c}})$
Base Shear $J_4 = \max\limits_{\substack{\text{El Centro}\\ \text{Hachinohe}\\ \text{Northridge}\\ \text{Kobe}}} \left\{ \dfrac{\max\limits_{t} \left\lvert \sum\limits_{i=1}^{20} m_i \ddot{x}_{\text{a}\eta_i}(t) \right\rvert}{F_b^{\max}} \right\}$	Normed Base Shear $J_8 = \max\limits_{\substack{\text{El Centro}\\ \text{Hachinohe}\\ \text{Northridge}\\ \text{Kobe}}} \left\{ \dfrac{\left\lVert \sum\limits_{i=1}^{20} m_i \ddot{x}_{\text{a}\eta_i}(t) \right\rVert}{\lVert F_b^{\max} \rVert} \right\}$	Normed Control Power $J_{12} = \max\limits_{\substack{\text{El Centro}\\ \text{Hachinohe}\\ \text{Northridge}\\ \text{Kobe}}} \left\{ \dfrac{\sum\limits_i \lVert \mathcal{P}_i(t) \rVert}{x^{\max} W} \right\}$	

Table 8.1: Summary of evaluation criteria for the benchmark problem. Source [108].

1. Digital control systems are implemented with a sampling time of $T = 0.005$ seconds.

2. Each of the measured responses contains an RMS noise of 0.03V, which is approximately 0.3% of the full span of the A/D converters. The measurement noises are modeled as Gaussian rectangular pulse processes with a pulse width of 0.001 seconds.

3. The control algorithm is required to be stable.

4. Sensors are modeled as having constant magnitude and phase. The sensitivity of the accelerometers is given by $10\,V/g$ where $1g = 9.81\,m/sec^2$.

5. Active control is employed using hydraulic actuators in a chevron bracing configuration, in which the actuator is horizontal and rigidly attached between the two consecutive floors of the building. Thus, in the analysis, the compliance of the bracing is neglected.

Based on the above specifications, LQG controllers are designed for the benchmark control problems. The following LQG performance is used

$$\mathcal{J} = \lim_{\tau\to\infty} \frac{1}{\tau}\mathrm{E}\left[\int_0^{\tau} \left\{\mathbf{y}_{wd}^T\mathbf{Q}\mathbf{y}_{wd} + \mathbf{u}^T\mathbf{R}\mathbf{u}\right\} dt\right] \tag{8.1}$$

where $\mathbf{y}_{wd}$ is the regulated output and the LQR parameters, $\mathbf{Q}$ and $\mathbf{R}$ were chosen according to the RMS value of the output signals.

Several controller design strategies are applied to the twenty-story building used in the Second Generation Benchmark Control Problem for Seismically

Excited Buildings. In order to remain consistent in the comparative study, the same LQG criteria and the same number of sensors and actuators are used for all the model and controller reduction processes. In this manner, the LQG parameters were chosen as $\mathbf{Q} = 3 \times 10^{-3}\mathbf{I}_{20\times 20}$; $\mathbf{R} = \mathbf{I}_{20\times 20}$ and $S_{\ddot{x}_g\ddot{x}_g}/S_{v_i v_i} = 25$.

First, model reduction is performed. The frequency response plots of the full-order model (FOM) and reduced-order models (ROM), for a fixed reduced-order size ($r = 20$), are depicted in Fig. 8.1. The benchmark problem used the model obtained by Guyan reduction as the evaluation model. In this manner, all of the reduction techniques were applied to the evaluation model. A reduced-order model obtained by balanced truncation was selected for the low-order controller design.

As can be seen in Fig. 8.1, model reduction based on static condensation can be used to eliminate high-order modes due to vertical and rotational degrees-of-freedom. The frequency response closely matches the full-order model in the lower region frequencies. However, for large-scale buildings, it might lead to structures rather stiffer than the original model (shear building model).

In the second approach, controller reduction is performed based on a LQG controller designed using the evaluation model. The same evaluation criteria, as shown in Table 8.2, is used for the twenty-story building as in the benchmark. Controller reduction was performed using the methods presented in the previous chapters. It was chosen to work with the frequency-weighted controller reduction scheme as the controller reduction method for performance

$Index$	Original Benchmark $r = 62$	Red. Model $r = 40$	Red. Controller $r = 20$
J_1	0.84169	0.83478	0.84207
J_2	0.89064	0.91473	0.89061
J_3	0.90873	0.90204	0.90288
J_4	0.92953	0.93459	0.92933
J_5	0.69826	0.69546	0.69788
J_6	0.73189	0.75206	0.73303
J_7	0.62149	0.60536	0.62255
J_8	0.70146	0.70404	0.7010
J_9	1.3881×10^{-2}	1.554×10^{-2}	1.402×10^{-2}
J_{10}	1.0050×10^{-1}	1.027×10^{-1}	1.0068×10^{-1}
J_{11}	1.9699×10^{-1}	2.0963×10^{-1}	2.0041×10^{-1}
J_{12}	6.6554×10^{-2}	6.8608×10^{-2}	6.6984×10^{-2}
J_{13}	50	50	50
J_{14}	5	5	5
J_{15}	62	40	20

Table 8.2: Pre-Earthquake Evaluation Criteria for the Full-order and Reduced-order Models.

evaluation. As can be seen in Fig. 8.1 and Table 8.2, low-order controllers can be obtained without compromising the response of the system. However, several simulations were performed in order to obtain a good reduced-order controller which stabilized the original building model.

8.2 Dissipative LQG-Optimal Controller

Dissipative LQG controllers are presented here based on the Positive Real Lemma applied to a special realization of a positive real plant system [28, 42, 58, 67, 80]. This section follows the work in [67, 80]. The following theorem holds.

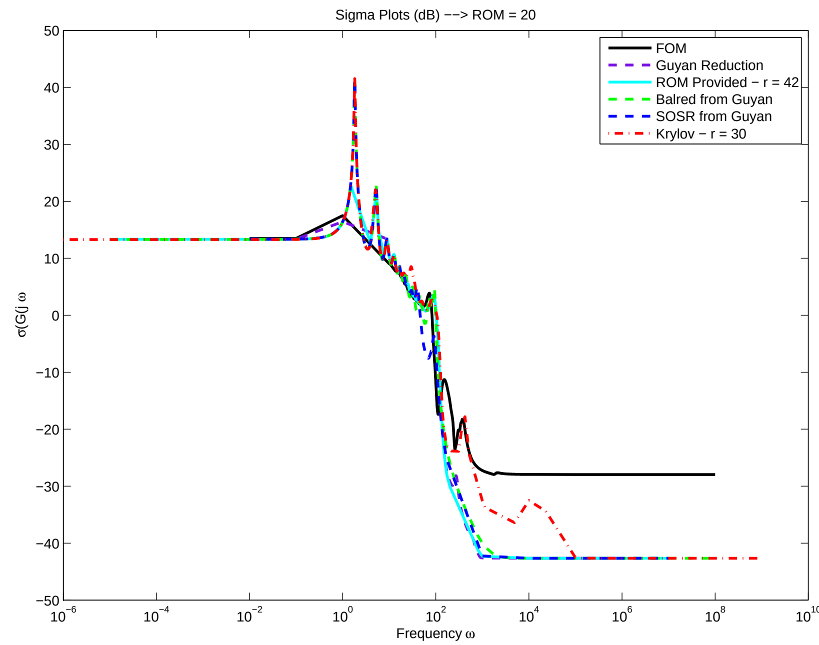

Figure 8.1: Frequency response of the full-order model and reduced-order models ($r = 20$).

Theorem 8.2.1. *Given the positive real dynamical system* $\mathbf{\Sigma}$ *and* $\mathbf{X}$ *that satisfy the positive real lemma, one can obtain the so-called self-dual realization by means of a coordinate transformation of the form* $\zeta = \mathbf{X}_1\mathbf{x}$*, where* $\mathbf{X}_1$ *is the square root factor (or Cholesky factor) of* $\mathbf{X}$*, i.e.,* $\mathbf{X} = \mathbf{X}_1^T\mathbf{X}_1$*. The self-dual realization of* $\mathbf{\Sigma}$ *is the one that satisfies the positive real lemma with*

$$\mathbf{X} = \mathbf{I}; \quad \tilde{\mathbf{K}} = -(\mathbf{A} + \mathbf{A}^T); \quad \mathbf{B} = \mathbf{C}^T. \tag{8.2}$$

Therefore, without loss of generality, it will be assumed that the dynamical system considered in this section is a self-dual realization. To this

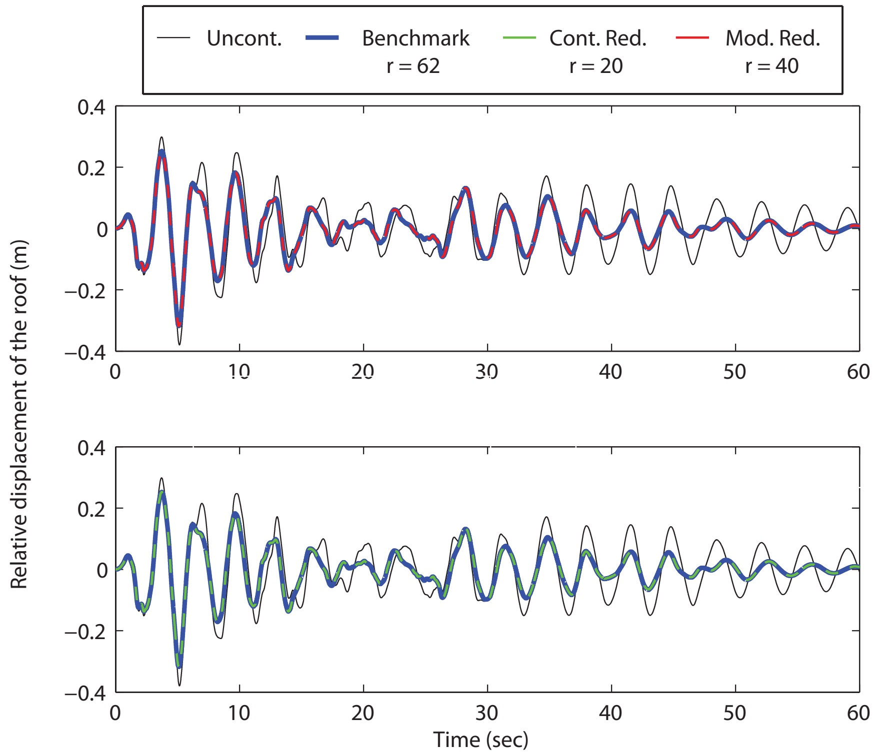

Figure 8.2: Uncontrolled and controlled responses for the pre-Earthquake due to El Centro.

end, consider an LQG controller designed based on this self-dual realization plant. It is known that the controller which minimizes the LQG performance index is given by

$$\dot{\mathbf{x}}_c = \mathbf{A}_c\mathbf{x}_c + \mathbf{B}_c\mathbf{y} \tag{8.3}$$

$$\mathbf{y}_c = \mathbf{C}_c\mathbf{x}_c; \quad \mathbf{u} = -\mathbf{y}_c \tag{8.4}$$

where

$$\mathbf{A}_c = \mathbf{A} - \mathbf{B}\mathbf{R}_r^{-1}\mathbf{B}^T\mathbf{P}_r - \mathbf{P}_f\mathbf{C}^T\mathbf{R}_f^{-1}\mathbf{C}; \quad \mathbf{B}_c = \mathbf{P}_f\mathbf{C}^T\mathbf{R}_f^{-1}; \quad \mathbf{C}_c = \mathbf{R}_r^{-1}\mathbf{B}^T\mathbf{P}_r \tag{8.5}$$

and $\mathbf{P}_r$ and $\mathbf{P}_f$ satisfy the controller and filter algebraic Riccati equations

$$\mathbf{P}_r\mathbf{A} + \mathbf{A}^T\mathbf{P}_r - \mathbf{P}_r\mathbf{B}\mathbf{R}_r^{-1}\mathbf{B}^T\mathbf{P}_r + \mathbf{Q}_r = \mathbf{0} \tag{8.6}$$

$$\mathbf{P}_f\mathbf{A}^T + \mathbf{A}\mathbf{P}_f - \mathbf{P}_c\mathbf{C}^T\mathbf{R}_f^{-1}\mathbf{C}\mathbf{P}_f + \mathbf{Q}_f = \mathbf{0} \tag{8.7}$$

The following theorem due to [80] will be stated without proof. For a complete proof see [67, 80].

Theorem 8.2.2. *Consider the positive real system as in Theorem 8.2.1 and the LQG-type controller as in Eqs. 8.5. If $\mathbf{Q}_r$, $\mathbf{Q}_f$, $\mathbf{R}_r$ and $\mathbf{R}_f$ are chosen such that*

$$\mathbf{Q}_r > \mathbf{B}\mathbf{R}_r^{-1}\mathbf{B}^T \Rightarrow \mathbf{Q}_r = \mathbf{Q}_B + \mathbf{B}\mathbf{R}_r^{-1}\mathbf{B}^T, \textit{ for } \mathbf{Q}_B > 0 \tag{8.8}$$

$$\mathbf{R}_f = \mathbf{R}_r \tag{8.9}$$

$$\mathbf{Q}_f = -(\mathbf{A} + \mathbf{A}^T) + \mathbf{B}\mathbf{R}_r^{-1}\mathbf{B}^T \tag{8.10}$$

then the LQG controller defined in Eq. (8.5) is strictly positive real.

8.3 Passivity Preserving Controller Reduction Applied to the Building Problems

In this section, the concepts of dissipative-LQG controller design and the passivity preserving model reduction will be applied to the three-story building model and to the twenty-story benchmark problem. For the three-story problem, due to the simplicity of its model, all the steps related to the controller design and model and controller reduction process are shown. Performance of the full-order and reduced-order controllers are compared through the use of the evaluation criteria as in Table 8.1. The fifteen evaluation criteria will not be the main issue in assessing the performance of the reduced-order controllers. Guaranteed stability and the order of the reduced-order controllers are used as a main arguments supporting this new passivity-based technique.

8.3.1 Three-Story Building Problem

For the three-story building model, the following procedure is used:

1. Determine the state-space model using collocated actuators and sensors;
2. Using a coordinate transformation, take the state-space model to a self-dual realization using:

$$\begin{aligned} \mathbf{X} &= \begin{bmatrix} \mathbf{K} & \mathbf{0} \\ \mathbf{0} & \mathbf{M} \end{bmatrix}; && (8.11) \\ \mathbf{X} &= \mathbf{X}_1^T \mathbf{X}_1 && (8.12) \\ \mathbf{A}_p &= \mathbf{X}_1 \mathbf{A} \mathbf{X}_1^{-1}; \quad \mathbf{B}_p = \mathbf{B}\mathbf{X}_1^{-1}; \quad \mathbf{C}_p = \mathbf{X}_1 \mathbf{C}. && (8.13) \end{aligned}$$

3. Design a passive LQG controller using:

$$R = 25; \quad \mathbf{Q}_r = \mathbf{B}_p R^{-1} \mathbf{B}_p^T; \quad \mathbf{Q} = \mathbf{Q}_r + \alpha \mathbf{I}.$$

4. Vary α and obtain the spectral zeros (SZ) of the controller. In this case, with $\alpha = 1 \times 10^{-1}$, it follows that

$$SZ = \begin{bmatrix} Inf \\ Inf \\ 14.3927 + 62.6032i \\ 14.3927 - 62.6032i \\ -14.3927 + 62.6032i \\ -14.3927 - 62.6032i \\ 40.9569 \\ -40.9569 \\ 8.3190 + 15.4617i \\ 8.3190 - 15.4617i \\ -8.3190 + 15.4617i \\ -8.3190 - 15.4617i \\ Inf \end{bmatrix}$$

5. Select the spectral zeros of the controller. In this case, the first four complex spectral zeros were chosen, yielding a reduced-order controller of size 2.

6. Perform controller reduction using passivity preserving methods. Numerical simulation were performed and depicted in Fig. 8.4. One can check that the reduced-order controller is indeed passive and, therefore, stabilizes the closed-loop system.

As can be seen in Fig. 8.4, a reduced-order controller based on passivity preserving model reduction guarantees closed-loop stability, since it is itself passive. Even though the performance of the closed-loop system deteriorates with the choice of the LQG passive controller, fine-tuning of its gain can be used to obtain better results.

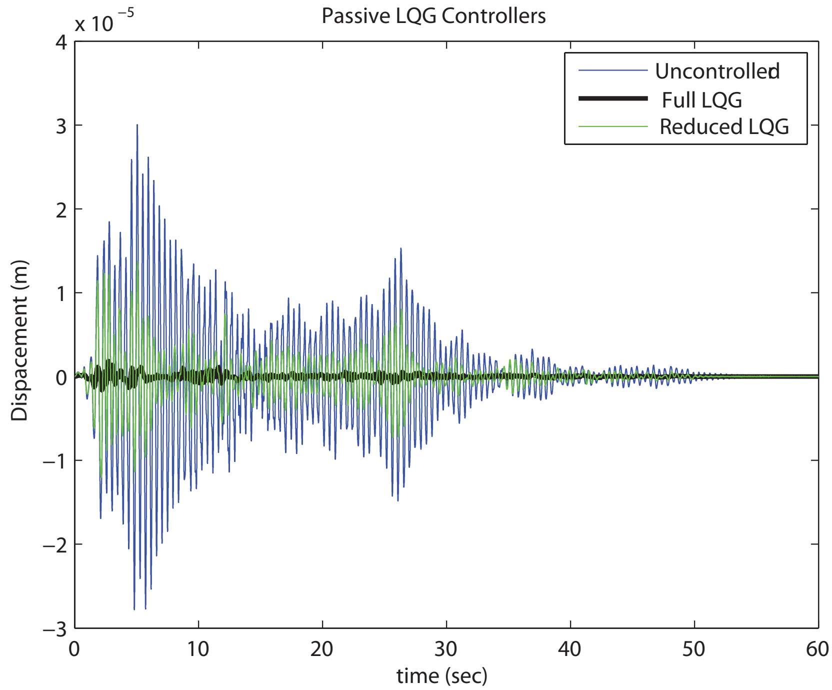

Figure 8.3: Uncontrolled and Controlled Three-Story Building Model.

8.3.2 Twenty-Story Building Problem

Applying the same procedure as for the three-story building model, dissipative LQG controllers are obtained for the twenty-story building. Simulations were performed to tune the gains of the controller. In this case, in order to obtain a square system, i.e., the same number of inputs and outputs, twenty actuators and sensors are placed on each floor. The passivity preserving controller reduction scheme was then applied to the full-order LQG controller.

Unlike the three-story building model, the MIMO rational Krylov was used to perform the reductions. As seen in previous chapters, one cannot directly choose the order of the reduced-order model. In this case, one can perform simulations taking into account the number of spectral zeros to be matched in order to find the size of the reduced-order controller. Choosing four spectral zeros, a reduced-order controller of size 80 was obtained. On the other hand, choosing three spectral zeros, a controller of size 40 was obtained. In both cases, the selection of the spectral zeros to be interpolated was arbitrary. There is no known theoretical basis for this selection. The results of the LQG design are depicted in Figures 8.4 and 8.5 and summarized in Table 8.3.

Figure 8.4 shows the displacement of the first floor for the twenty-story building model. Even though the full-order passive-LQG controller yield responses with higher noise content, the reduced-order controller performs approximately in the same manner as the original LQG controller designed for the benchmark problem. The only remaining differences are in the value of some of the evaluation criteria performances. As seen in Table 8.3, the LQG passive controller yields closed-loop systems with some performance indeces better than the original model, but some that are worse than the original, as in the case of the maximum stroke force for the actuators. It should be pointed out that stability is always guaranteed for the passive-LQG reduced controller. However performance of the closed-loop system, even though assessed by the evaluation criteria design, should be further investigated. As seen in Table 8.3, some of the performances were better for the reduced-order controller than the original controller. Also, some of performance measures exceeded the maximum limits allowed for this particular benchmark. This issue should be

Index	Original Benchmark $r = 62$	Full passive LQG $r = 212$	Reduced passive LQG $r = 80$
J_1	0.84169	0.81745	1.015
J_2	0.89064	1.0376	0.9938
J_3	0.90873	14.464	1.0693
J_4	0.92953	1.6706	0.9587
J_5	0.69826	0.81904	0.9131
J_6	0.73189	–	0.8682
J_7	0.62149	0.60536	2.5358
J_8	0.70146	1.4448	0.8863
J_9	1.3881×10^{-2}	3.546×10^{-2}	9.132×10^{-4}
J_{10}	1.0050×10^{-1}	1.167×10^{-1}	1.0608×10^{-1}
J_{11}	1.9699×10^{-1}	–	1.5421
J_{12}	6.6554×10^{-2}	–	–
J_{13}	50	50	50
J_{14}	5	20	20
J_{15}	62	212	80

Table 8.3: Earthquake evaluation criteria for the full-order and reduced-order models using passive LQG Controller.

resolved by fine tuning the gains of the controller.

8.4 Concluding Remarks

In this chapter, low-order controllers were obtained for the seismically excited building control problems. It was shown that by performing model and controller reduction using the standard SVD-based and Krylov-based approaches, one cannot guarantee the stability of the closed-loop system. On the other hand, by means of passivity properties and the passive preserving model reduction scheme, one can obtain an efficient algorithm that performs controller reduction and guarantees closed-loop stability. Even though closed-

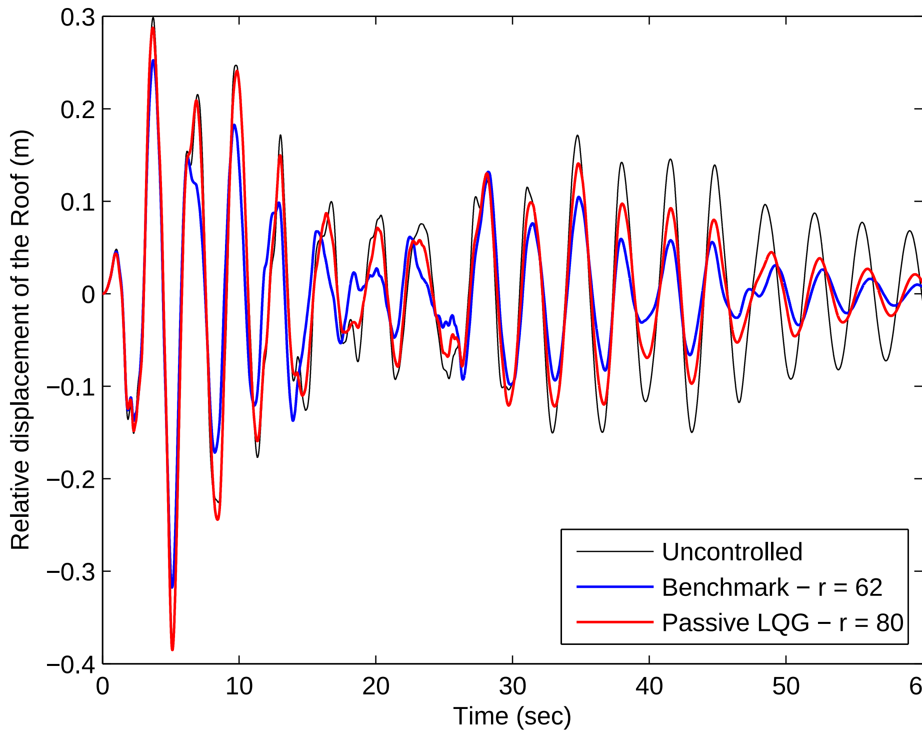

Figure 8.4: A comparison of the original benchmark controller and PR LQG controllers for the twenty-story building Model - displacement of the first floor.

loop performance was assessed by means of seismic evaluation criteria, one cannot evaluate the effectiveness of the passive LQG controllers as developed in this chapter. Further investigations should be performed in order to properly determine a good set of controller gains and number of sensors and actuators to be used in the assessment of the evaluation criteria.

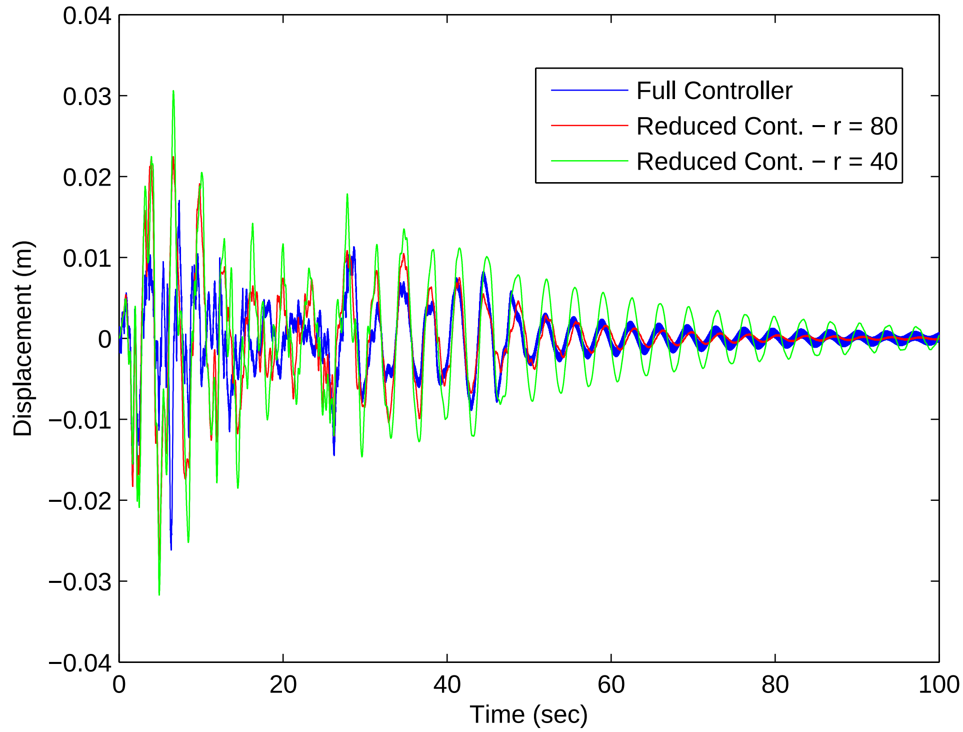

Figure 8.5: Passive LQG reduced-order controllers for the twenty-story building model - displacement of the first floor.

Chapter 9

Conclusions and Future Directions

This chapter provides a summary of the results on model and controller reduction applied to building control as developed in the previous chapters. Moreover, suggestions for future directions on the improvements of the aforementioned techniques will be stated.

9.1 Concluding Remarks

This dissertation focused on the development of efficient techniques for model and controller reduction applied to structural control, emphasizing the importance of such procedures for the case of building control for hazard mitigation. A procedure for effectively constructing reduced-order controllers based on large-scale systems, such that the reduced-order controller is guaranteed to yield closed-loop stability when connected to the full-order large-scale plant, has been developed. The effectiveness of such procedure has been evaluated using a family of benchmark problems for building control. Upon considering models of different order, from a small three degrees-of-freedom building model to a more complex model with almost five thousand degrees-of-freedom, reduced-order models and controllers have been successfully implemented.

Several model and controller reduction approaches were investigated using a projection framework. Two different pathways were used: model reduction followed by low-order controller design, and controller reduction directly from a high-order controller model. First, SVD-based methods, such as Lyapunov balanced truncation, were used to determine low-order models for control design purposes. It was shown that even though good reduced-order models can be obtained, there is no guarantees on the reduced-order closed-loop stability. Secondly, controller reduction based on the frequency-weighted balanced truncation has been used to determine low-order controllers. For the same reasons, closed-loop stability was not guaranteed. Furthermore, it has been shown that SVD-based methods are suited for small to medium size models, due to the two Lyapunov equations to be solved. A remedy for this issue is the application of approximate balancing, which is part of an ongoing research and thus will be left for future work.

For large-scale systems, Krylov-based methods were presented. It was shown that reduced-order models can be achieved through the use of moment matching techniques. Depending on the location of the interpolation points in the complex plane, several special cases can be obtained: Markov parameters ($s = \infty$), Padé approximation ($s = 0$), and rational interpolation ($s = \sigma$). It was shown that such techniques are suited for large-scale systems due to the fact that they depend only on matrix-vector multiplications. The problem of controller reduction by Krylov methods has also been addressed. It was shown that the low-order closed-loop system is guaranteed to interpolate the full-order closed-loop system at the chosen interpolation points, which were suggested to be given by the mirror images of the poles of the full-order controller and full-order closed-loop system. As in the case of SVD methods, closed-loop stability is not guaranteed.

For structural models, i.e., models written as a second-order dynamical systems, several model reduction methods were presented. Instead of collapsing the second-order equations into a set of first-order differential equations to work in a state-space framework, one can directly use model reduction methods on the second-order equations. The rationale of this approach is that once the state-space is obtained, the physical meaning of mass, stiffness and damping on the structure is lost, and there is no guarantee that the reduced-order models could be realized again as a set of mass, stiffness and damping matrices. In this manner, several approaches were discussed: static (Guyan) and dynamic condensation, modal truncation, component mode synthesis and the structure preserving eigenvalue reduction. Even though Guyan reduction is one of the most widely used model reduction techniques for structural dynamic problems, in the building control framework, it is only used to eliminate those high-order modes due to vertical and rotational degrees-of-freedom. Its frequency response closely matches the full-order model in the lower region frequencies. However, for large-scale buildings, it might lead to structures rather stiffer than the original model (shear building model). Modal truncation is also widely used for model reduction. However, it lacks error bounds and generalizations for the problem of controller reduction. Also, it is costly in the application of large-scale systems.

The main contribution of this dissertation belongs to the area of dissipative systems. In a broad sense, dissipative systems have the property that some of the energy put into the system is dissipated. A particular case of the definition of the "energy" of the system are the so-called passive systems. For LTI systems, passivity is connected to the well-known positive realness of dynamical systems and hence to the Positive Real Lemma. A major advantage of passive systems is that they can be robustly stabilized by a controller that is itself passive. In this case, a method was proposed based on the passivity preserving model reduction through interpolation of the spectral zeros of the large-scale system. The design method of a passive LQG yielded controllers that were easy to design and implement, and at the same time guaranteed closed-loop stability. The effectiveness of the proposed control strategies was demonstrated and evaluated through application to the twenty-story benchmark problem.

9.2 Future Directions

The goal of this dissertation was to provide an efficient controller reduction procedure suited for large-scale systems, such that, one could guarantee closed-loop stability. Some recommendations for future studies related to this work are presented below:

9.2.1 Large-scale Building Problems

In this dissertation, reduced-order models were obtained for relatively small to medium systems. Even though the procedures presented for obtaining reduced-order controllers can be used for large-scale systems, its effectiveness should be assessed. Building models comprised of fifty-thousand to several million states have already been obtained using finite element methods. Therefore, application of the passive-LQG design approach together with controller reduction should be investigated.

9.2.2 Rational Krylov

Rational Krylov has been shown to be very effective for large-scale systems. In this dissertation, methods based upon the state-space equations have been investigated. However, as is the case of structural models, Krylov methods based on the second-order equations can be used. Several second-order preserving methods have been proposed in the literature. Thus, investigation of such methods for the case of large-scale building models could be addressed. Furthermore, investigation of the selection of the interpolation points specific to structural models might introduce optimality to the reduction process. In this dissertation, the algorithms for moment matching were based on extensions of the SISO rational Krylov to the case of multi-input, multi-output (MIMO) systems through the use of a deflation technique. One of the disadvantages of this technique is that the full-rank projection matrices, and in turn, the size of the reduced-order models, are constrained by the number of inputs and outputs in the system. Thus, for the case of the building problems where a large number of actuators and sensors are used, model reduction by moment matching using tangential interpolation should be investigated.

9.2.3 MR Dampers

Magneto-rheological (MR) dampers have been successfully implemented in several fields of semi-active structural control: building control, car suspensions, bridge-control, and seat vibration, among others. Control strategies based on semi-active devices combine the best features of both passive and active control systems. In this dissertation, active control was considered for the controller reduction problem. It would therefore be interesting to apply the model and controller reduction procedures of this research to the case of semi-active control. Semi-active control strategies are based on nonlinear control methodologies. Thus, extensions to the problem of nonlinear control strategies should also be addressed.

9.2.4 Nonlinear Building Models

Even though several important model reduction problems are still being investigated for linear systems, it is considered a mature field. The next major challenge in the field of model and controller reduction is the application of such concepts to nonlinear systems. Several methods have been devised for model and controller reduction using the so-called proper orthogonal decomposition and its variants. However, there is not a general theory as in the linear case, and usually, the model reduction procedures are problem dependent. In the case of building models, large magnitude earthquakes can cause material yielding in the structural elements, and therefore, nonlinearities are present. The applications of linear model/controller reduction together with the nonlinear model reduction can be addressed using the third generation of benchmark problems.

9.2.5 Passivity Preserving Model and Controller Reduction

Dissipative-LQG controller design was shown to be very effective for large-scale seismic building control. Passivity-based design, which was optimized for the LQG performance index, guaranteed closed-loop stability. Improvements in the design could be addressed since the passivity conditions make the controller design conservative. With respect to passivity preserving model reduction, one has to interpolate the reduced-order model at some of the spectral zeros of the full-order model. In this manner, methods for the selection of spectral zeros in order to guarantee, besides passivity, optimality of the error between the full-order model and the reduced-order model should be addressed. Also, the issue of selection as mirror images could be generalized for structural models.

Appendices

Appendix A

Simulink Block Diagrams

In this section, two Simulink block diagrams will be shown: Building Control and MR damper.

A.1 Building Control

The building control problem, used for simulation of the benchmark problems, is given by the following block diagram.

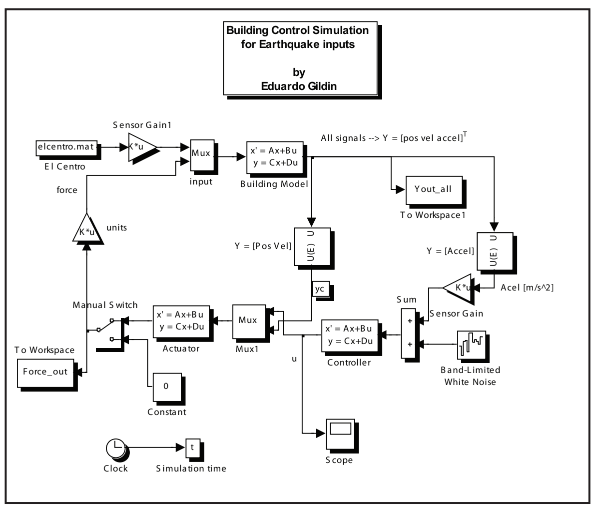

Figure A.1: Building Block Diagram.

A.2 MR damper

As described in detail in Chapter 6, the following equations represent the equations of motion of a MR damper. Its block diagram used for simulation is given by Fig. A.2

$$F = \alpha z + c_0(\dot{x} - \dot{y}) + k_0(x - y) + k_1(x - x_0) = c_1\dot{y} + k_1(x - x_0) \tag{A.1}$$

with

$$\begin{aligned} \dot{z} &= \gamma\left(|\dot{x} - \dot{y}|\right) z|z|^{n-1} - \beta(\dot{x} - \dot{y})|z|^n + A(\dot{x} - \dot{y}) && \text{(A.2)} \\ \dot{y} &= \frac{1}{c_0 + c_1}\left[\alpha z + c_0\dot{x} + k_0(x - y)\right] && \text{(A.3)} \end{aligned}$$

$$\begin{aligned} \alpha &= \alpha(u) = \alpha_a u + \alpha_b u && \text{(A.4)} \\ c_1 &= c_1(u) = c_{1_a} u + c_{1_b} u && \text{(A.5)} \\ c_0 &= c_0(u) = c_{0_a} u + c_{0_b} u && \text{(A.6)} \end{aligned}$$

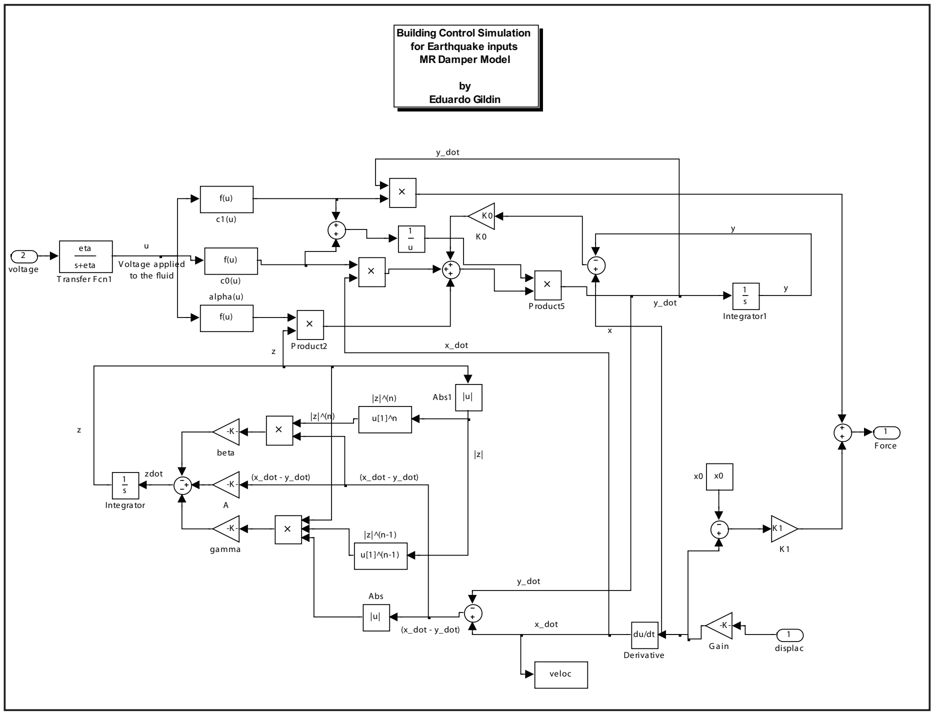

Figure A.2: MR Block Diagram

Appendix B

Actuator Placement for the Bowen Model

B.1 Actuator Locations

Based on the method presented in Chapter 6, actuator locations were determined for the Bowen building model. Its finite element model is comprised of 825 nodes, or 4950 degrees-of-freedom. Two actuators were placed in each location, in the x-direction and y-direction. It should be noted that the procedure used to determine the actuator locations did not yield any locations in the first floor. The actuator locations are given in the following diagrams.

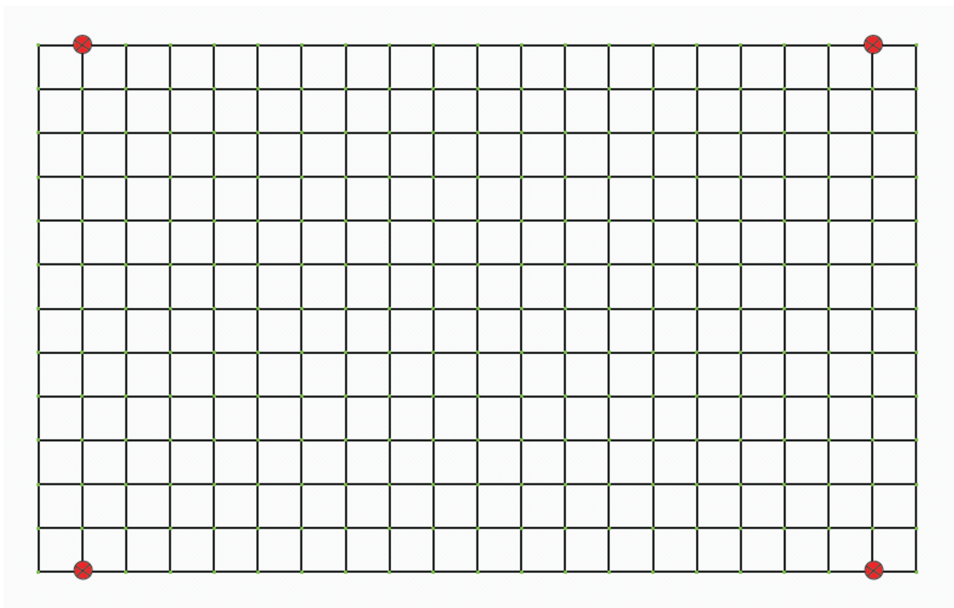

Figure B.1: Actuator Locations for the Second Floor.

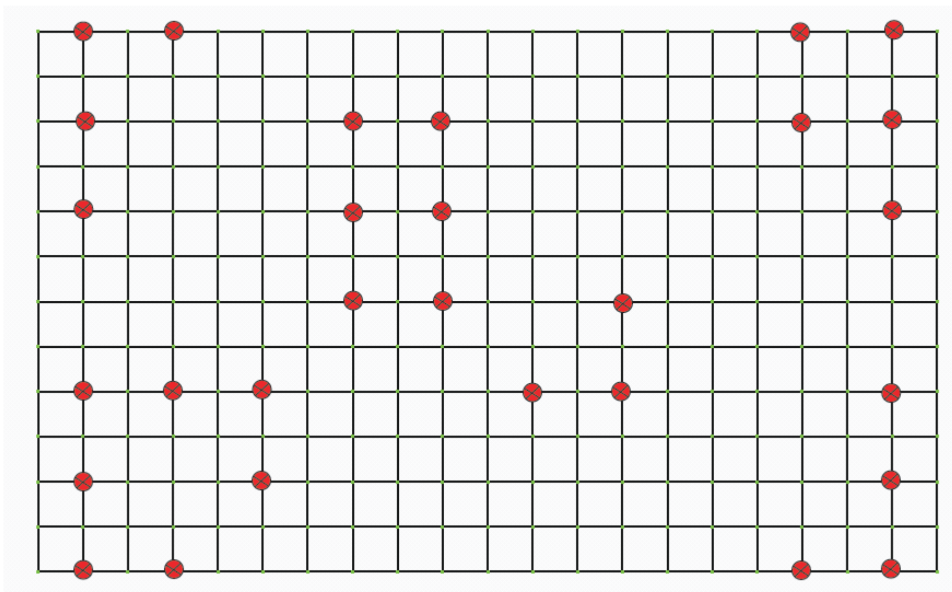

Figure B.2: Actuator Locations for the Third Floor.

Bibliography

[1] B.D.O. Anderson and A. C. Antoulas. Rational approximation and state space variable realizations. *Linear Algebra and Appl.*, 138:479–509, 1990.

[2] B.D.O. Anderson and Y. Liu. Controller reduction: Concepts and approaches. *IEEE Transactions of Automatic Control*, 34:802–812, 1989.

[3] B.D.O Anderson and Y. Liu. Controller reduction: Concepts and approaches. *IEEE Trans. On Automatic Control*, AC-34(8):802–812, 1989.

[4] B.D.O. Anderson and J.B. Moore. *Optimal control: linear quadratic methods*. Prentice Hall, 1990.

[5] A. Antoulas, D. Sorensen, K.A. Gallivan, P. Van Dooren, A. Grama, C. Hoffmann, and A. Sameh. Model reduction and real-time control for dynamic data driven systems. *Dynamic data driven simulation, Ed. F. Darema, Kluwer Publication*, 2005.

[6] A. C. Antoulas, J. A. Ball, J. Kang, and J.C. Willens. On the solution of the minimal rational interpolation problem. *Linear Algebra and Appl., Special Issue on Matrix Problems*, 138:511–573, 1990.

[7] A.C. Antoulas. On recursiveness and related topics in linear systems. *IEEE Trans. on Automatic Control*, AC-31:1121–1135, 1986.

[8] A.C. Antoulas. *Approximation of Large-Scale Dynamical Systems*. Philadelphia: SIAM, 2005.

[9] A.C. Antoulas. A new result on positive real interpolation and model reduction. *Systems and Control Letters*, 54:361–374, 2005.

[10] W.E. Arnoldi. The principle of minimized iteration in the solution of the matrix eigenvalue problem. *Quart Appl Math*, 9:17–29, 1951.

[11] Z. Bai, J. Demmel, J. Dongarra, A. Ruhe, and editors H. van der Vorst. *Templates for the Solution of Algebraic Eigenvalue Problems: A Practical Guide*. SIAM, Philadelphia, 2000.

[12] C.A. Beattie, S. Gugercin, A.C. Antoulas, and E. Gildin. Controller reduction by Krylov projection methods. In *Proceeding of the Mathematical Theory, Network and Systems - MTNS*, July 2004.

[13] J.K. Bennighof and R.B. Lehoucq. An automated multilevel substructuring method for eigenspace computation in linear elastodynamics. *SIAM. J. Sci. Comput.*, 25(6), 2004.

[14] D. Boley. Krylov subspace methods on state-space control models. *Circuits, Systems, Signal Process* , 13(6):733–758, 1994.

[15] D. Boley and G. Golub. The nonsymmetric Lanczos algorithm and controllability. *Systems & Control Letters*, 16:97–105, 1991.

[16] C.C. Chang and P.N. Roschke. Neural network modeling of a magnetorheological damper. *Journal of Intelligent Material Systems and Structures*, 9(9), 1999.

[17] Chi-Tsong Chen. *Linear System Theory and Design*. Oxford University Press, 3rd ed., 1999.

[18] F.Y. Cheng and C.P. Pantelides. Optimal placement of actuators for structural control. *Technical Report NCEER-88-0037, Multidisciplinary Center for Earthquake Engineering Research, Buffalo, New York.*, 1988.

[19] S.Y. Chu, Soong T.T., and A.M. Reinhorn. *Active, Hybrid and Semi-Active Structural Control: A Design and Implementation Handbook*. Wiley, 2005.

[20] L.L. Chung, R.C. Lin, T.T. Soong, and A.M. Reinhorn. Experimental Study of Active Control of MDOF Seismic Structures. *ASCE J. Eng. Mech.*, 115:1609–1627, 1989.

[21] L.L. Chung, A.M. Reinhorn, and T.T. Soong. Experiments on active control of seismic structures. *ASCE J. Eng. Mech.*, 114:241–256, 1988.

[22] Lord Coorporation. *http://www.lord.com/*.

[23] MSC Software Corp. *http://www.mscsoftware.com/*. Nastran Software.

[24] R.R. Craig Jr. *Structural Dynamics: An Introduction to Computer Methods*. Wiley, 1981.

[25] R.R. Craig Jr. and M.C.C. Bampton. Coupling of substructures for dynamic analysis. *AIAA Journal*, 6:1313–1319, 1968.

[26] U.B. Desai and D. Pal. A transformation approach to stochastic model reduction. *IEEE Trans. on Automatic Control*, AC-29:1097–1110, 1984.

[27] C.W. deSilva. *Control Sensors and Actuators*. Prentice Hall, 1989.

[28] R. Drai. H_2 Dissipative Controllers for Non-Positive Systems. In *IEEE International Conference on Control Applications*, Hatford, CT, October 1997.

[29] S.J. Dyke. *Acceleration Feedback Control Strategies for Active and Semi-active Control Systems: Modeling, Algorithm Development, and Experimental Verification*. PhD thesis, University of Notre Dame. Notre Dame, Indiana, 1996.

[30] S.J. Dyke, B.F. Spencer Jr., P. Quast, and M.K. Sain. Role of control-structure interaction in protective system design. *ASCE Journal of Engineering Mechanics*, 121(2):322–338, 1995.

[31] S.J. Dyke, B.F Spencer Jr., M.K. Sain, and J.D. Carlson. Modeling and control of magnetorheological dampers for seismic response reduction. *Smart Mat. and Struct.*, 5:565–575, 1996.

[32] S.J. Dyke, B.F Spencer Jr., M.K. Sain, and J.D. Carlson. Seismic response reduction using magnetorheological dampers. In *IFAC World Congress*, pages 145–150, 1996.

[33] D.F. Enns. *Model reduction for control systems design*. PhD thesis, Dep. Aeronaut. Astronaut., Stanford University, Stanford, C.A., 1984.

[34] D.F. Enns. Model reduction with balanced realizations: An error bound and frequency weighted generalizations. *Proceedings of the IEEE Conference on Decisions & Control*, pages 127–132, 1984.

[35] R.W. Freund. Model reduction methods based on Krylov subspaces. *Acta Numerica*, 12:267–319, 2003.

[36] K. Gallivan, E. Grimme, D. Sorensen, and P. Van Dooren. On some modifications of the Lanczos algorithm and the relation with Padé approximations. *Mathematical Research Series, Akademie Verlag, Berlin*, 7:87–116, 1996.

[37] K.A. Gallivan, E.J. Grimme, and P. Van Dooren. A Rational Lanczos Algorithm for Model Reduction. *Numerical Algorithms*, 12:33–63, 1996.

[38] W. Gawronski. *Balanced control of flexible structures*. New York: Springer Verlag, 1996.

[39] W. Gawronski. *Advanced structural dynamics and active control of structures*. New York: Springer Verlag, 2004.

[40] W. Gawronski and J.-N. Juang. Model reduction in limited time and frequency intervals. *Int. J. Systems Science*, 21:349–376, 1990.

[41] G.H. Golub and C.F. Van Loan. *Matrix Computations*. The John Hopkins University Press, Baltimore and London, 1996.

[42] S.V. Gosavi and A.G. Kelkar. Modeling, indentification, and passivity-based robust control of piezo-actuated flexible beam. *Journal of Vibration and Accoustics*, 126:260–271, 2004.

[43] W.B. Gragg and A. Lindquist. On the Partial Realization Problem. *Linear Algebra and its Applications*, 50:277–319, 1983.

[44] M. Green. Balanced stochastic realizations. *Linear Algebra and Its Applications*, 98:211–247, 1988.

[45] M. Green and D.J.N. Limembeer. *Linear Robust Control*. Englewood Cliffs, NJ: Prentice Hall, 1995.

[46] E. Grimme and K. Gallivan. A Rational Lanczos Algorithm for Model Reduction II: Interpolation Point Selection. *Technical report, University of Illinois at Urbana Champaign*, 1998.

[47] E. Grimme, D.C. Sorensen, and P. Van Dooren. Model reduction of state-space systems via an implicitly restarted Lanczos method. *Numerical Algorithms*, 12:1–31, 1995.

[48] E. J. Grimme. *Krylov projection methods for model reduction.* PhD thesis, ECE Dept., University of Illinois, Urbana-Champaign.

[49] S. Gugercin. Projection methods for model reduction of large-scale dynamical systems. *Ph.D. Thesis, ECE Dept. Rice University, Houston*, 2003.

[50] S. Gugercin and A.C. Antoulas. On model reduction by the Lanczos and the rational Krylov methods, ECE Dep., Rice University. Technical report, 2002.

[51] S. Gugercin and A.C. Antoulas. An H_2 error expression for the Lanczos procedure. In *Proceedings of the 42nd IEEE Conference on Decision and Control*, December 2003.

[52] S. Gugercin and A.C. Antoulas. A survey of model reduction by balanced truncation and some new results. *International Journal of Control*, 77(8):748–766, 2004.

[53] S. Gugercin, A.C. Antoulas, and C.A. Beattie. A rational Krylov iteration for optimal H_2 model reduction. In *Mathematical Theory, Network and Systems - MTNS2006*, July 2006.

[54] S. Gugercin, A.C. Antoulas, C.A. Beattie, and E. Gildin. Krylov-based controller reduction for large-scale systems. In *43rd IEE Conference on Decision and Control*, December 2004.

[55] M.H. Gutknecht. A completed theory of the unsymmetric Lanczos process and related algorithms, Part I. *SIAM J. Matrix Anal. Appl.*, 13:594–639, 1992.

[56] M.H. Gutknecht. A completed theory of the unsymmetric Lanczos process and related algorithms, Part II. *SIAM J. Matrix Anal. Appl.*, 15:15–58, 1994.

[57] R.J. Guyan. Reduction of stiffness and mass matrices. *AIAA Journal*, 2(3):380, 1965.

[58] W.M. Haddad, D.S. Bernstein, and Y.W. Wang. Dissipative H_2/H_∞ Controller Synthesis. *IEEE Trans. Automatic Control*, 39(4):827–831, 1994.

[59] Ansys Inc. *http://www.ansys.com/*. ANSYS.

[60] CSI Computers & Structures Inc. *http://www.csiberkeley.com/products_SAP.html*. SAP2000.

[61] D.J. Inman. *Engineering Vibration*. Prentice-Hall, 2nd. Ed., 2001.

[62] B.M. Irons. Structural eigenvalue problems - elimination of unwanted variables. *AIAA Journal*, 5(3):961–962, 1965.

[63] I.M. Jaimoukha and E.M. Kasenally. Krylov subspace methods for solving large Lyapunov equations. *SIAM J. Numer. Anal.*, 31:227–251, 1994.

[64] I.M. Jaimoukha and E.M. Kasenally. Implicitly restarted Krylov subspace methods for stable partial realizations. *SIAM J. Matrix Anal. Appl.*, 18:633–652, 1997.

[65] L.M. Jansen and S.J. Dyke. Semiactive Control Strategies for MR Dampers: Comparative Study. *ASCE J. Eng. Mech.*, 126(8):795–803, 2000.

[66] S.M. Joshi. *Control of Large Flexible Space Structures.* Lecture Notes in Control and Information Sciences, Springer Verlag, 1989.

[67] S.M. Joshi. Robust Control of Uncertain Systems via Dissipative LQG-Type Controllers. *NASA, Technical Report, NASA/TM-2000-209866*, 2000.

[68] T. Kailath. *Linear Systems.* NJ: Prentice Hall, 1990.

[69] A.G. Kelkar and S.M. Joshi. *Control of Nonlinear Multibody Flexible Space Structures.* Vol 221 of Lecture Notes in Control and Information Sciences, Spring Verlag, 1996.

[70] A.G. Kelkar and S.M. Joshi. Robust control of non-passive systems via passification. In *American Control Conference*, Albuquerque, NM, June 1997.

[71] H.K. Khalil. *Nonlinear Systems.* Prentice Hall, 3rd. Ed., 2002.

[72] S.A. Kilic. *Personal communications.*

[73] H.M. Kim and R.R. Craig Jr. Structural dynamics analysis using an unsymmetric block Lanczos algorithms. *Internat. J. Numer. Methods Engrg*, 26:2305–2318, 1988.

[74] H.M. Kim and R.R. Craig Jr. Computational enhancement of an unsymmetric block Lanczos algorithms. *Internat. J. Numer. Methods Engrg*, 30:1083–1089, 1990.

[75] C. Lanczos. An iteration method for the solution of the eigenvalue problem of linear differential and integral operators. *J. Res. Nat. Bur. Stand.*, 45:255–282, 1950.

[76] C.-A. Lin and T.-Y. Chiu. Model reduction via frequency weighted balanced realization. *Control Theory and Advanced Technology*, 8:341–351, 1992.

[77] R.E. Lindberg Jr. and R.W. Longman. On the number and placement of actuators for independent modal space control. *AIAA Journal of Guidance, Control and Dynamics*, 7(2):215221, 1984.

[78] R.W. Longman, S.W. Siilin, T. Li, and G. Sevaston. The fundamental structure of the degree of observability. *AIAA/AAS*, 82:1434, 1982.

[79] R.-L. Lozano. Strictly positive real transfer functions revisted. *IEEE Trans. Automatic Control*, 35(11):1243–1245, 1990.

[80] R.-L. Lozano and S.M. Joshi. On the Design of Dissipative LQG-Type Controllers. In *27th Conference on Decision and Control*, Austin, TX, December 1988.

[81] L. Meirovitch. *Fundamentals of Vibration*. Mc Graw Hill, 2001.

[82] B.C. Moore. Principal component analysis in linear systems: controllability, observability and model reduction. *IEEE Trans. Automat. Control*, AC-26:17–32, 1981.

[83] C.T. Mullis and R.A. Roberts. Roundoff noise in digital filters: Frequency transformations and invariants. *IEEE Trans. Acoust. Speec. Signal Process.*, 24(6):538–550, 1976.

[84] R. Ober. Balanced parametrizations of classes of linear systems. *SIAM J. Cont. Optim.*, 29:1251–1287, 1991.

[85] R. Ober and D. McFarlane. Balanced canonical forms for minimal systems: A normalized coprime factorization approach. *Linear Algebra and Its Appl.*, 122-124:23–64, 1989.

[86] G. Obinata and B.D.O Anderson. *Model Reduction for Control System Design*. Springer, 2000.

[87] Y. Ohtori, R.E. Christenson, B.F. Spencer Jr., and S.J. Dyke. Benchmark control problems for seismically excited nonlinear buildings. In *Second European Conference on Structural Control*, Paris, France, July 2000.

[88] Y. Ohtori, R.E. Christenson, B.F. Spencer Jr., and S.J. Dyke. Nonlinear benchmark control problem for seismically excited buildings. *ASCE Journal of Engineering Mechanics*, 130(4):366–385, 2004.

[89] H. Panossian, W. Gawronski, and J. Ossman. Balanced shaker and sensor placement for modal testing of large flexible structures. *IMAC-XVI, Santa Barbara, CA*, 1998.

[90] V. Papakos. *Restarted Lanczos algorithms for model reduction.* PhD thesis, Imperial College of Science, Technology and Medicine, University of London, 2002.

[91] M. Paz. *Structural Dynamics: Theory and Computation, 4th. ed.* 1997.

[92] A. Preumont. *Vibration Control of Active Structures: An Introduction.* Kluwer Academic, 2nd Ed., 2002.

[93] Zu-Qing Qu. *Model Order Reduction Techniques with Applications in Finite Element Analysis.* Springer, 2004.

[94] A. Ruhe. Rational Krylov sequence methods for eigenvalue computations. *Linear Algebra and Appl.*, 58:391–405, 1984.

[95] A. Ruhe. Rational Krylov algorithms for nonsymmetric eigenvalue problems II: Matrix pairs. *Linear Algebra and Appl.*, 197:283–295, 1994.

[96] A. Ruhe. Rational Krylov algorithms for nonsymmetric eigenvalue problems III: Complex shifts for real matrices. *BIT*, 34:165–176, 1994.

[97] Y. Saad. *Iterative Methods for Sparse Linear Systems*. PWS Publishing Company, 1996.

[98] Y. Saad. *Iterative Methods for Sparse Linear Systems*. SIAM, 2nd. ed., 2003.

[99] R.A. Serway and Jerry S.F. *College physics*. Fort Worth : Saunders College Pub., 5th ed., 1999.

[100] T.T. Soong and B.F. Spencer Jr. Controlling buildings: A new frontier in feedback. *IEEE Control Systems Magazine on Engineering Technology*, 17(6):19–35, 1997.

[101] T.T. Soong and B.F. Spencer Jr. Supplemental energy dissipation: state-of-the-art and state-of-the-practice. *Engineering Structures*, 24:243–259, 2002.

[102] D.C. Sorensen. Implicit application of polynomial filters in a k-step arnoldi method. *SIAM J. Matrix Anal. Appl.*, 13:357–385, 1992.

[103] D.C. Sorensen. Passivity Preserving Model Reduction via Interpolation of Spectral Zeros. *Systems and Control Letters*, 54:347–360, 2005.

[104] D.C. Sorensen and A.C. Antoulas. The sylvester equation and approximate balanced reduction. *Fourth Special Issue on Linear Systems and Control, Edited by V. Blondel, D. Hinrichsen, J. Rosenthal, and P.M. van Dooren, Linear Algebra and Its Applications*, 351-352:671–700, 2002.

[105] D.C. Sorensen and A.C. Antoulas. On model reduction of structured systems. *In P. Benner* et al*, eds., Dimension Reduction of Large-Scale Systems, Lecture Notes in Computational Science and Engineering*, 45:117–130, 2005.

[106] B.F. Spencer Jr. *http://sstl.cee.uiuc.edu/Default.html*. University of Illinois Urbana-Champaign.

[107] B.F. Spencer Jr. and S. Nagarajaiah. State of the art of structural control. *Journal of Structural Engineering, ASCE*, 129(7):845–856, 2003.

[108] B.J. Spencer Jr., R.E. Christenson, and S.J. Dyke. Krylov-based controller reduction for large-scale systems. In *Second World Conference on Structural Control*, Kyoto, Japan, June-July 1998.

[109] F. Spencer Jr., B, S.J. Dyke, M.K. Sain, and J.D. Carlson. Phenomenological model of a magnetorheological damper. *Journal of Engineering Mechanics, ASCE*, 123(3):230–238, 1997.

[110] M. Steinbuch, P.J.M. Van Gross, G. Schootsra, P.M.R Wortelboer, and O.H Bosgra. mu-synthesis of a compact disc player. *Int. J. Robust Nonlinear Control, ()*, 8:169–189, 1998.

[111] R.F. Stengel. *Stochastic optimal control : theory and application*. Wiley, 1986.

[112] T.J. Su and R.R. Craig Jr. Model reduction and control of fexible structures using Krylov vectors. *J. Guid. Contr. Dyn.*, 14:260–267, 1991.

[113] Purdue University. *https://engineering.purdue.edu/CE.* Civil Engineering - The Bowen Laboratory.

[114] A. Vandendorpe and P. Van Dooren. Krylov techniques for model reduction of second-order systems. *Université Catholique de Louvain, CESAME, Report TR07-2004*, 2004.

[115] A. Varga and B.D.O. Anderson. Frequency-weighted balancing related controller reduction. In *IFAC2002 congress, Barcelona, Spain*, 2002.

[116] Vibrationdata. *http://www.vibrationdata.com/elcentro.htm.* El Centro Earthquake Page.

[117] C.D. Villemagne and R.E. Skelton. Model reduction using a projection formulation. *Int. J. Contr.*, 46:2141–2169, 1987.

[118] J.M. Wang, V. Sreeram, and W.Q. Liu. A new frequency-weighted balanced truncation method and an error bound. *IEEE Trans. on Automatic Control*, AC-44:1734–1737, 1999.

[119] Y. Wang. *Control Strategies for 3D Smart Base Isolation Systems Using Modal and Nodal Approaches.* PhD thesis, Washington University, The Henry Edwin School, Department of Civil Structure, 2006.

[120] Y.K. Wen. Method of random vibration of hysteretic systems. *Journal of Engineering Mechanics Division, ASCE*, 102(EM2):249263, 1976.

[121] J.C. Willems. Dissipative Dynamical Systems- Part I and II: General Theory. *Arch. Rational Mechanics and Analysis*, 45:321–391, 1972.

[122] P.M.R. Wortelboer, M. Steinbuch, and O.H. Bosgra. Iterative Model and Controller Reduction Using Closed-Loop Balancing, with Application to a Compact Disc Mechanism. *Int. J. Robust and Nonlinear Control*, 9:123–142, 1999.

[123] J.N. Yang, J.C. Wu, B. Samali, and A.K. Agrawal. A benchmark problem for response control of wind-excited tall buildings. In *2nd World Conference on Structural Control*, 1998.

[124] K. Zhou and J.C. Doyle. *Essentials of Robust Control*. Prentice Hall, 1998.

[125] K. Zhou, J.C. Doyle, and K. Glover. *Robust and Optimal Control*. Prentice Hall, 1996.

Vita

Eduardo Gildin was born in Sao Paulo, Brazil, on 26 August 1973, the son of Jacob Gildin and Raquel Gildin. He received the Bachelors Degree in Mechanical Engineering, with emphasis on Automotive Engineering, from Faculdade de Engenharia Industrial in Brazil. After a short passage as a Automotive Consultant, he joined the Masters Program in Mechanical/Mechatronics Engineering at The University of Sao Paulo, Brazil. Eduardo then started the Ph.D. Program at The University of Texas at Austin where he has held several positions as TA and AI. During the Spring of 2000, Eduardo Gildin was awarded the best TA prize of the University.

During the Summer of 2000, Eduardo Gildin went back to Brazil to get married to Suzana Zilber Gildin, who has also taken the Masters Degree in Advertising from The University of Texas at Austin. In July 2003, their first son, Daniel, was born in Austin. After graduating, Eduardo will take a joint Post-doctoral position with the ICES/CSM at the University of Texas at Austin and the ECE Department at Rice University in Houston, TX.

Permanent address: 2600 Gracy Farms Lane #921
Austin, Texas 78758

This dissertation was typeset with LaTeX† by the author.

†LaTeX is a document preparation system developed by Leslie Lamport as a special version of Donald Knuth's TeX Program.